Minéralisation trachéale

Lina Tabcheh

Ecole Doctorale BioSE (Biologie-Santé-Environement)

Thèse

Présentée et soutenue publiquement pour l'obtention du titre de

DOCTEUR DE L'UNIVERSITE DE LORRAINE

Mention : « Sciences de la Vie et de la Santé »

par **Lina TABCHEH**

Tracheal Mineralization:

Cellular and Molecular Mechanisms in Mice.

31/10/2014

Membres de jury:

Rapporteurs :	M. David MAGNE	Professeur, UMR CNRS 5246, Lyon. Président de jury
	M. Laurent BECK	Chargé de recherche, INSERM U791, Nantes.
Membre Invité :	M. Sylvain PROVOT	Chargé de recherche, INSERM U606, Paris.
Examinateurs :	M. Hervé KEMPF	Chargé de recherche, UMR CNRS 7365, Nancy. Co-directeur de thèse.
	M. Jean-Yves JOUZEAU	PUPH, UMR CNRS 7365, Nancy. Co-directeur de thèse.

UMR 7365 CNRS, INGENIERIE MOLECULAIRE ET PHYSIOPATHOLOGIE ARTICULAIRE (IMoPA)
9, Avenue de la Foret de Haye, Biopôle de l'Université de Lorraine, 54500 Vandoeuvre Les Nancy.


بسم الله الرحمن الرحيم

Acknowledgments

First of all, I would like to thank Pr. Magdalou and Pr. Jouzeau to have welcomed me into their lab.

I would like to particularly thank my supervisor Pr. Jouzeau, for his insightful remarks and guidance.

I express my gratitude to my co-director and mentor Dr. Kempf Hervé for his constant support and advice over the last three years, and for never giving up on this project nor on me; even in the darkest days. It was a pleasure to work under your command sir.

My deepest thanks go to Dr. Bianchi Arnaud for his technical help and his kindness.

Besides my advisors, I would like to thank the rest of Jury member; Dr. Magne David, Dr. Laurent Beck and Dr. Provot Sylvain for evaluating this work.

I also want to thank my thesis committee; Dr. Provot Sylvain and Dr. Rossignol Patrick.

Special thanks for the entire member IMOPA-4 group member Pascal, Pascale, Nathalie, Cecile, for their help and constant enthusiasm for science, , a special thank for David for his hospitality. It was a pleasure to work with all of you.

Thank you Melissa and Hongyuan for your friendship, our ice-cream was a must during this long journey.

Thanks for the Badminton team, Yong, superman “Olivier”, Layla,Yueying and the best badminton teacher ever Meriem… I am so grateful that our paths have crossed.

Thanks for all the lab members especially, Jean-Baptiste for the deep deep conversation, Jean-Marc for your cultural feeds, Alexander and Samia for all the non-sens, Gigi for her warm smile , Valerie for teasing me, Nadia for her kindness, Julie for all the tea.

I also want to thank Fredy for being the sweetest and freakish person I ever met (till now), Bea for her loveable presence, and Mathieu for Metz at 3 am, Gerardmer and everything else …it was a real pleasure to share all these adventures with you.

Thank you Micka and Ayria, I really enjoyed your company. Thank you Ishraq for always being around, Patricia for being so special, Irfan for your sweetness, Loic for always poping up with sweet things and for teach me the basics in tortoise world.

I also want to thank my dearest friend Suzy, even when you’re away your flower always made me happy.

At least but not last I want to thank my family;

Fidaa and Ayman for keeping a place for me, even when I am not there…

Zeina, Amal, Maha, Mouhamad, Nour “apfeleyti”, our youngest Khalil and Rym and younger ☺

You give me courage, put me back on the track, give me hope in life, and strength to conquer my fears. Even when nothing goes right being loved by you give life its meaning…

My sweet Dad for making me the person I am…

My lovely Mom for always reminding me of the person I am…

To my dearest,

Those I found

And those I lost

Table of contents

List of Figures

List of tables

Abbreviations

ADP	Adenosine 5’ diphosphate
AMP	Adenosine 5’ monophosphate
ANK	Inorganic pyrophosphate transport regulator
APC	Adenomatous polyposis coli
APs	Alkaline phosphatase
ASM	Airway Smooth Muscle
ATP	Adenosine 5’ triphosphate
BGP	Bone Gla Protein
Bmp	Bone morphogenetic protein
BSP	bone sialoprotein
C6-C7	sixth and seventh cervical vertebra
Cav3.2	Calcium channel, voltage-dependent, T type, alpha 1H subunit
cAMP	cyclic AMP (adenosine monophosphate)
CF	Cystic fibrosis
CFTR	Cystic fibrosis transmembrane regulator
CKD	Chronic kidney disease
Coll I/ II/X	Collagen I/ II and X
CPP	Pyrophosphate dehydrate crystals
CS	Carnegie stage
E	Embryonic day
EA/TEF	Esophageal atresia/ Tracheo esophageal fistula
ECM	Extracellular matrix
E-NPPs	NPP-type ectophosphodiesterases
eNs	5’-nucleotidase
E-NTPDases	Ectonucleoside triphosphate diphosphohydrolases
Erk	Extracellular signal-regulated Kinases
EXIT	Ex-Utero Intrapartum Therapy procedure
FA	Fetuin A (2α-Heremans-Scmid glycoprotein)
Foxf1	Forkhead box F1
Foxj1	Forkhead box J1
FGF9/10/18/23	Fibroblast Growth Factor 9/10/18/23

Fra-1/ FOSL1	FOS-like antigen 1
GAG	Glycosaminoglycan
GATA6	GATA binding protein 6
Gla	γ-carboxyglutamate residues
Gli	GLI-Kruppel family
GRP	Gla Rich protein
GSK3	Glycogen synthase kinase 3
HDAC1/2	Histone desacetylases 1 and 2
Hes	hes family bHLH transcription factor
Hey	hairy ears, Y-linked gene
HH	Halburger and Hamilton stage
Hoxa5	Homeobox A5
K14	Keratin 14
KO	Knock-out
LePS2	(Lycopersicon esculentum) phosphate starvation-induced gene
LRP	Lipoprotein receptor related protein
LYVE1	lymphatic vessel endothelial hyaluronan receptor1
MGP	Matrix Gla Protein
miRNA	micro RNA
MV	Matrix vesicles
NKX2.1/TTF-1	NK2 homeobox 1/ Thyroid transcription factor-1
Nogg	Noggin
OPN	Osteopontin
P38-MAPK	P38- mitogen-activated protein kinases
P63	Transformation related protein 63
PC-1/ENPP1	Plasma cell membrane glycoprotein-1
PDNP	Phosphodiesterase nucleotide pyrophosphatase
PECAM1	platelet endothelial cell adhesion molecule 1
PGs	Proteoglycans
PHOSPHO	phosphatase, orphan 1
Pi	Inorganic phosphate
Pit1/2	Phosphate transporter 1/ 2
PPi	Inorganic pyrophosphate
Ptch-1/-2	Patched-1 /-2

PTH	Parathyroid Hormone
RA (ATRA)	Retinoic acid (All trans retinoic acid)
RAR	Retinoic acid receptor
Rspo2	R-spondin
SHH	Sonic Hedgehog
sFRP-4	secreted frizzled-related protein 4
Sftpa	Surfactant associated protein A
SIBLINGs	The Small Integrin Binding Ligand N-Linked Glycoproteins
SLC17	Solute carrier family 17
SLC20	Solute carrier family 20
SLC34	Solute carrier family 34
SM22α/TAGLN	Transgelin
Snai1	Snail family zinc finger 1
Sox 2/9/17	Sry-related high mobility group (HMG) box 2/9 and 17
SPDEF	SAM pointed domain-containing ETS transcription factor
T4-T5	fourth or fifth thoracic vertebra
TA	Tracheal agenesis
Tbx4	T-box transcription factor genes
TCF/LEF	T cell factor/lymphoid enhancer factor
TGF-β	Transforming growth factor β
Tmem16a	Anoctamin 1, calcium activated chloride channel
TNAP	Tissue non specific alkaline phosphatase
TOF	tracheo-oesophageal fistula
Traf4	Tnf receptor associated factor 4
VACTREL	vertebral anomalies, anal atresia, cardiac malformations, tracheo-esophageal fistula with esophageal atresia, renal anomalies, and limb anomalies.
VSM	Vascular smooth muscle
WNT	Wingless-type MMTV integration site family

AVANT PROPOS

Ce travail de thèse a été initié dans le laboratoire UMR 7561 Physiologie, Pharmacologie et Ingénierie Articulaire, devenu depuis UMR 7365 Ingénierie Moléculaire et Physiopathologie Articulaire (IMoPA) dont les thématiques de recherche principales sont la biologie du cartilage, les pathologies associées et les stratégies réparatrices du tissu lésé par le développement de produits de substitution que sont les biomatériaux.

Si le travail effectué au cours de cette thèse avait bien pour sujet principal le dérèglement anormal du phénotype cartilagineux en conditions anormales, il avait la particularité de s'intéresser à un tissu cartilagineux non étudié jusqu'alors dans le laboratoire, à savoir le cartilage de la trachée.

Tout comme son analogue présent dans l'articulation, c'est un cartilage de type hyalin qui, dans de rares situations, peut se minéraliser. En effet, au cours du vieillissement normal et dans de rares conditions pathologiques, la trachée peut se minéraliser de façon importante. Cette minéralisation des voies aériennes supérieures, dans la majorité des cas asymptomatique, peut toutefois entraîner des problèmes respiratoires allant jusqu'à des dyspnées sévères. Les mécanismes cellulaires et moléculaires responsables de cette minéralisation sont peu, voire pas, connus. L'objectif principal de ma thèse était donc de contribuer à la compréhension de ces mécanismes.

Par une décision délibérée, il n'a pas été choisi, dans ce mémoire, de traiter de manière détaillée des domaines très bien discutés dans d'autres thèses du laboratoire ou dans des revues de la littérature (cartilages, pathologies articulaires). En revanche, étant le premier au laboratoire à aborder le tissu trachéal, ce mémoire propose dans un premier chapitre de dresser un large "portrait" de la trachée en précisant son histoire évolutive, sa fonction et sa place dans l'organisme, en décrivant dans le détail sa composition, son organisation et le développement des tissus qui la composent, et enfin en listant les pathologies les plus connues qui affectent cet organe.

Dans un second chapitre introductif, volontairement plus court que le premier, car développé à de nombreuses reprises dans des mémoires récents du laboratoire, il est fait une brève mais complète revue des mécanismes cellulaires et moléculaires responsables des mécanismes de minéralisation physiologique et pathologique. Suivent deux chapitres consacrés respectivement aux résultats expérimentaux obtenus chez la souris au cours de ma thèse. Ainsi chaque chapitre inclut un article publié ou en préparation dont les résultats principaux sont complétés, discutés et placés en perspectives.

INTRODUCTION

PREFACE

La trachée fait partie du système respiratoire, un système qui a subi un nombre de modifications non-négligeables au fil de l'évolution. Ces changements sont notamment dépendants de deux facteurs majeurs que sont les besoins métaboliques et l'habitat naturel des organismes vivants. Ainsi, les organes respiratoires des Arthropode*s* sont différents de ceux des différentes classes de Vertébrés. Chez les Poissons, seul *phylum* au mode de respiration aquatique, les organes respiratoires sont en contact direct avec le milieu. Chez les autres classes, notamment les Mammifères, qui ont adopté un mode de respiration aérien, les organes respiratoires sont invaginés.

L'invagination de système respiratoire a été possible grâce à l'apparition de la trachée, un conduit élastique complexe formé de trois types de tissus différents: le cartilage hyalin le plus souvent en forme de fer de cheval dont les bords sont reliés par du tissu musculaire, les deux étant bordés d'un épithélium respiratoire de type pseudostratifié

L'élasticité et la rigidité de la trachée sont conférées respectivement par le tissu musculaire et le tissu cartilagineux. Ces propriétés permettent à la trachée de garder un courant d'air continu durant l'inspiration et l'expiration, indépendamment du changement de pression extérieure (atmosphérique) et intérieure (intra-thoracique). De surcroit, la muqueuse trachéenne permet, quant à elle, de filtrer l'air inhalé et de conférer un premier système de défense contre les agressions extérieures.

L'épithélium trachéal est de type pseudostratifié, il est formé de plusieurs types cellulaires reposant sur une membrane basale qui borde la totalité de la trachée. Le tissu musculaire, de type muscle lisse et formé de deux couches longitudinale et transversale, se trouve juste du côté dorsal. Le cartilage trachéal est de nature hyalin, possède des caractéristiques spéciales qui lui confèrent des propriétés uniques.

Deux théories s'affrontent pour expliquer la formation initiale de la trachée: 1/ la première suggère que la trachée se forme par septation de l'endoderme antérieur, qui donne naissance à la trachée du coté ventral et à l'œsophage de coté dorsal; 2/ la deuxième théorie propose que le système respiratoire et la trachée se forment par un processus de bourgeonnement. Quel que soit l'ordre chronologique des événements suivis par la trachée, le développement trachéal est fortement dépendant d'interactions réciproques entre mésenchyme et épithélium. Selon le stade de développement et le tissu concerné, les signaux et les facteurs responsables de la différenciation varient; Ainsi NKX2.1, SOX2, FGF10 et SHH sont des acteurs essentiels

non seulement pour le développement de la trachée mais aussi de l'œsophage. Pour l'épithélium respiratoire, les facteurs essentiels sont P63, Sox2, SPDEF, Foxj1, NKX2.1 et la voie de signalisation NOTCH. Pour le cartilage, les mécanismes responsables de sa formation et de sa différenciation sont complexes et régulés par un nombre important de facteurs, tels que FGF 10 et 18, Wnt5a, RSPO2, Hoxa5, Tbx4, Tbx5, SHH, Gli, BMP4, Sox9, TRAF4, CaV3.2, l'acide rétinoïque et ses différentes récepteurs. En ce qui concerne le tissu musculaire de la trachée, quelques facteurs ont été identifiés tel-que TMEM16a, FGF10 et SOX2.

Le dérèglement des signaux impliqués dans le développement de la trachée est responsable du développement de pathologies congénitales souvent sévères voire létales comme dans le cas de l'agénésie trachéale, des syndromes d'Apert, de Crouzon, de Pfeiffer et de la fistule trachéo-œsophagienne. D'autres maladies congénitales sont moins sévères comme dans le cas du kyste aérien d'origine trachéale. Les maladies acquises de la trachée sont, pour la plupart du temps, provoquées par des infections de la muqueuse respiratoire, et dans des cas plus minoritaires, l'origine de la maladie est un des tissus de la trachée comme dans le cas de l'asthme ou dans le cas des tumeurs de la trachée. Les pathologies affectant la trachée peuvent être aussi associées à d'autres maladies comme la tétralogie de Fallot, un défaut cardiovasculaire qui a comme conséquence la sténose de la trachée.

Le traitement de la trachée vise souvent à atténuer les symptômes de la sténose, souvent intrusive et pas très efficace comme dans le cas de trachéostomie. Des procédés chirurgicaux peuvent prendre lieu quand une petite partie de l'organe doit être éliminée et dans ce cas une section de la partie affectée suivit de l'anastomose des bords flanquant est appliquée. Lorsque la sténose de la trachée affecte une plus grande partie, l'implantation d'une endoprothèse ou la substitution de la trachée doit être réalisée.

CHAPTER I

TRACHEA A COMPLEX ENTITY

1. RESPIRATION

1.1. DEFINITION

Respiration is a vital process, whose importance for life is highlighted in the metaphoric sentence of Max Kleiber "the kiss of life". August Krogh defines respiration as "The call for oxygen", which leads us to its main role: the acquisition of oxygen from the respiratory medium, which can be water and air.

The importance of respiration comes from the fact that, in contrast to other metabolic substrates that can be stored in tissues within the body, contracted oxygen from the atmosphere cannot be stored, and that is what makes respiration a continuous necessity for living creatures.

Gas exchangers are the organs by which respiration happens. Their design is closely matched to the oxygen needs of an animal. Structures have evolved from the plain cell membrane of the primeval prokaryotic unicells to complex multi-functional one of the modern Metazoa.

Many factors are responsible for shaping our respiratory system, as the transition from anaerobic environment to aerobic one, the change from unicellular to multicellular organisms, the development of closed circulatory system, the formation of gas transporter, the development of invaginated gas exchangers, the transition from water- to land-breathing, the development of double circulatory systems, the shift from buccal-force-pumping to suctional breathing, the switch to homoeothermic life style and the exhibition of highly energetic life style as in bird case (Maina 2002).

1.2. THE NEED FOR OXYGEN

1.2.1. When and how

The switch from anaerobic to aerobic environment happened around 2 and 2.5 billion years ago (Kump 2008). The presence of oxygen producing bacteria before the arise of atmospheric oxygen (Brocks et al 1999) suggests that they produced oxygen at a prodigious rate. However, Tectonic-related factors seems to be involved in this atmospheric enrichment with oxygen (Brocks et al 1999).

1.2.2. Oxygen and respiratory media

On our blue planet, there are two respiratory media: water and air. Water was the first used respiratory media in the life history and is also the least efficient. This lack of efficiency can be attributed to the higher viscosity of water, its lower concentration in oxygen and to the fact that in water the diffusion of oxygen is 8.10^3 time lower than its diffusion in air (Maina 2002).

1.3. Gas exchangers

1.3.1. Main features

Gas exchangers are the organs where the exchange of breathing gas, i.e. oxygen and carbon dioxide, occurs. "Passive diffusion "is the first and ultimate way by which gas exchange happens, a stable mechanism shared among all species (See Fig.1.1.1.).

Gas exchanger main features are:

1. The position toward the body surface that can be both evaginated or invaginated.
2. The big surface of contact with air in a very limited space by stratification or compartmentation.
3. The presence of rich conducting tissues of circulatory system in the region where gas exchange happens.
4. The thin nature of the barrier between water/air and the circulatory system.
5. The geometric organization of the structure to determine the interaction between the respiratory media.

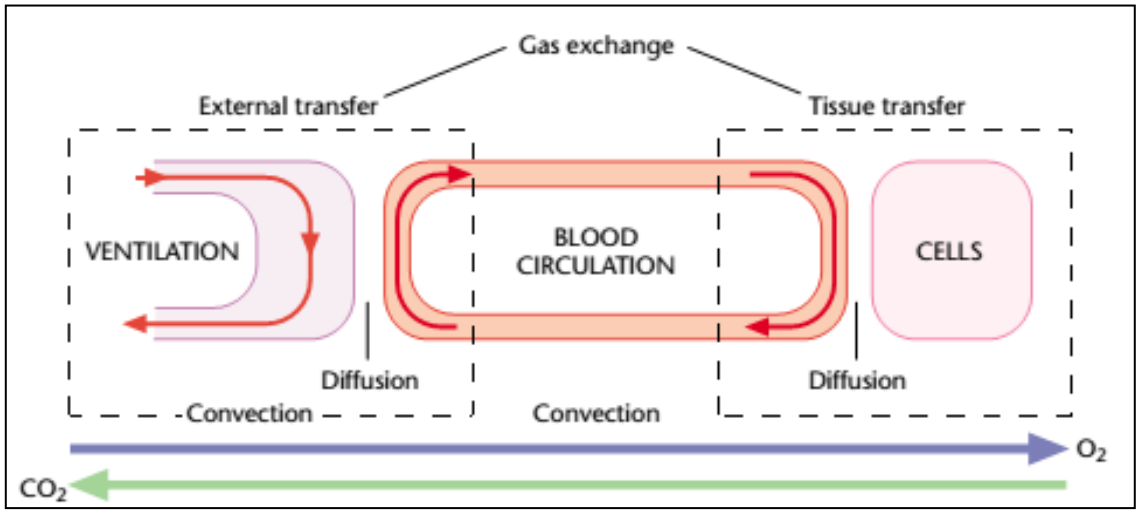

Fig.1.1.1. Air from outside to inside through gas exchangers.
The various components of the gas transfer system in vertebrates. The path of oxygen and carbon dioxide takes four serially arranged steps: convection of the ambient medium or ventilation, diffusion through external exchange surfaces in gills or lungs, convective transfer by blood circulation, and diffusion from tissue capillaries to the cells and mitochondria.(Truchot)

1.3.2. Brief look at different types of gas exchangers

The most drastic changes of gas exchangers in Arthropods, Fish, Amphibians, Reptiles, Birds and Mammals are briefly reviewed in the following paragraphs. (Fig .1.1.2)

1.3.2.1. Invertebrates

The best studied respiratory system in Invertebrates is that of Arthropods and especially that of Insects.

It is formed of different structures called spiracles, trachea, tracheoles and air sacs. The tracheal system is described as the simplest and most efficient respiratory system (Maina 2002). Spiracles are what conduct air from the outside to the internal trachea that can compress, relax and act in a lung-like manner (Fig. 2) (Westneat et al 2003). Tracheoles are very fine branches that can be less than a micrometer in diameter (Hetz & Bradley 2005). They are analogous to blood capillaries as they contain sort of a fluid that is osmotically discharged directly into cells in which exists a mitochondrial continuum underneath the cell membrane located next to the tracheoles.

1.3.2.2. Vertebrates

Amphibians

The respiratory system of Amphibians shows a big diversity, which seems to be related to the multiplicity of the habitat environment, the stage of metamorphoses, and the metabolic needs. During larval stage, gas exchanges happen through internal or external gills. Once adult stage is reached gas exchange occurs through lungs for terrestrial species and through the skin or at the bucco-pharyngeal cavity in aquatic species (Gatz et al 1974; Keith.A 1904).

Fish

The respiratory system of Fish is made of gills that are complex evaginated gas exchangers, which transport oxygen from ambient water to blood and excrete carbon dioxide in the reverse direction using a thin water blood barrier going from 1 to 5µm in most of cases. Besides their role as gas exchangers, gills perform different functions as osmoregulation, ammonia excretion and acid-base balance regulation (Hughes & Morgan 1973)

Gills display a large variety of structures: it can be simple and external or internal inside branchial chambers and multifunctional (Maina 2002).

Reptiles

Reptilians are the first class of Vertebrates to adopt a fully terrestrial respiratory system, with lungs that display a large diversity between species. Among reptilians, Crocodilians posses the most complex respiratory system with multiple tubular monopodial branching chambers that are connected by intrapulmonary bronchi, and lined with perforated septa (Hsia et al 2013) (F.Perry 1988)

Birds

Compared to other phyla, Birds have high metabolic needs. Indeed, the metabolic need of a bird is 4 to 15 times greater than the metabolic needs of a reptile at equivalent body temperature. These high metabolic needs require highly efficient gas exchangers. In fact, the avian respiratory system is described as the most efficient among all others (Lasiewski 1962). This efficiency is due to the presence of non vascularized air sacs and a rigid bronchial lung that guaranty a unidirectional airflow during inspiration and expiration (Duncker 1972), which means a constant air supply through bird lungs.

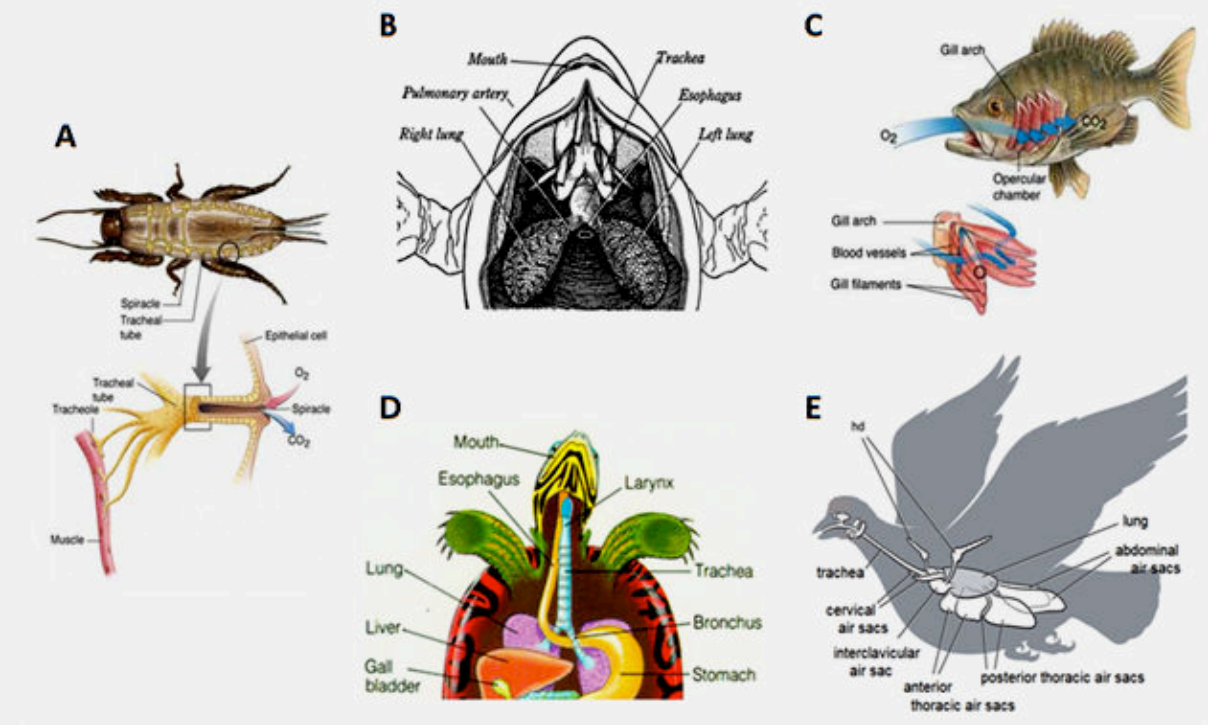

Fig.1.1.2. Schematic representation of the respiratory system in (A) *Arthropod*, (B) *Amphibian*, (C) *Fish*, (D) *Reptile*, (E) *Birds* From (Biology ; deftstudios ; Ornitology ; Standardnote ; StudyBlue) respectively.

Mammals

The respiratory system in Mammals covers the region extending from the trachea to the acini and alveolar ducts that give rise to alveolar sacs (10.000 alveoli exist per acinus) and follows a dichotomous branching pattern. This branching process starts from the trachea (to see in details in the following chapter) where it divides at its end into two bronches making the first branching generation, and will split successively 22 more times, with a reduction of cube root of 2 in diameter at each branching (Weibel 1984). (Fig.1.1.3)

From a functional standpoint, the mammalian respiratory tract can be divided into three zones. The first conducting zone contains the trachea, bronchi and bronchioles. The second transition zone is formed of the respiratory bronchioles. These two first regions cover the first 14 dichotomous branching generations. The third category is the gas exchange zone *per se* formed by the alveolar ducts, sacs and walls starting from the 15th generation till the 23rd. In the adult, human lung alveoli count vary from 290 to 480 million alveoli (Hsia et al 2013), which represent a 70 meter square gas diffusion surface (Unbekandt et al 2008).

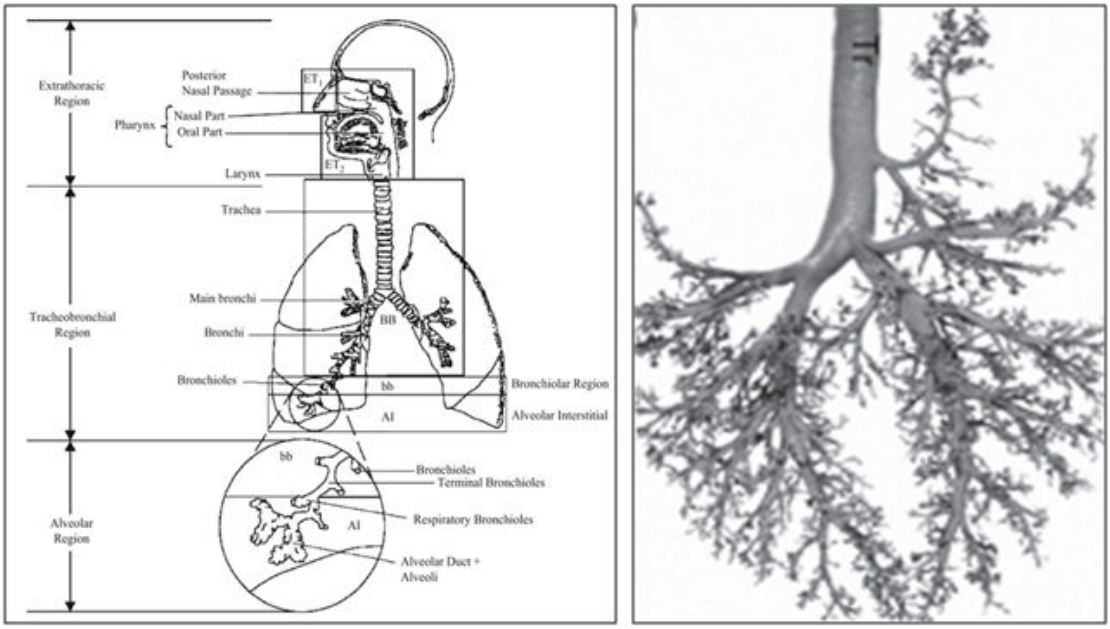

Fig.1.1.3. Mammal respiratory system (A) in human , schematic representation from (Hopke & Wang 2012) (B) in the pig, *Sus scrofa* showing dichotomous branching. Tr, trachea. from (Hsia et al 2013).

1.4. Where is the trachea in this long journey?

In the Vertebrates, the presence of the trachea in the respiratory system has emerged with the switch of the respiratory medium from water to air and the concurrent occurrence of the lungs. Thus trachea, also called windpipe, is present in all air-breathing animals of the Vertebrate phylum, with the sole exception of lungfish where pharynx is directly connected to the lungs. Throughout evolution, trachea function has diverged and its organization was found to be very heterogeneous among species.

However, on a structural point of view, the hallmark of the trachea is the presence of a cartilage component. Cartilage can be first seen in the short trachea of Amphibians as whole C-shaped rings in the apical part, whereas it is more sparse in the lower part of the trachea and in the bronchi (Kuehne 2000) (Fig.1.1.4. A and B). Cartilage can also be found in the trachea of Crocodile (Reese 1926). Interestingly, in avian, domestic fowl airway cartilage form complete rings (Carlyle 1962; Hogg 1982), which eventually mineralize in a later stage at 126

days post-hatching (Fig.1.1.4. C). In Mammals, tracheal cartilage is a perpetual part of the conducting airway that can also be found in marine Mammals (Moore et al 2014). Interestingly, physical anthropological studies revealed that the morphology and the distribution of all hominid trachea were similar to that found in modern humans (Gea 2008).

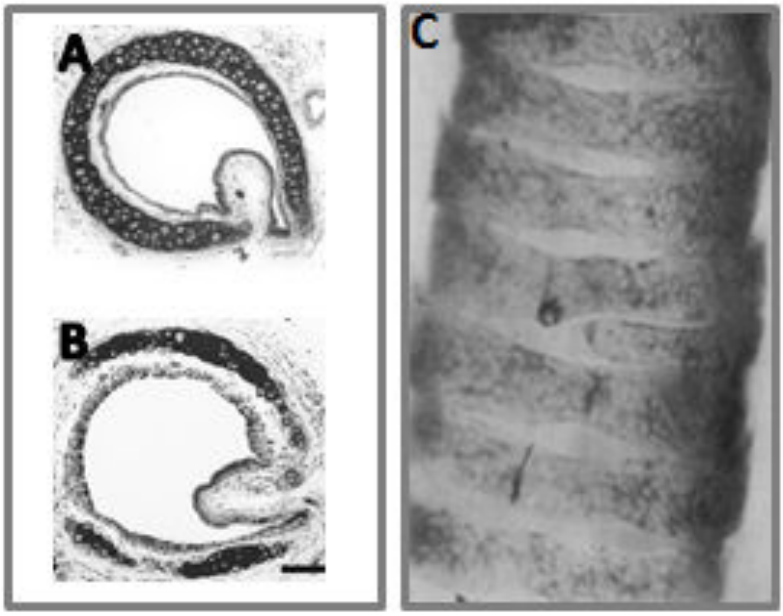

Fig.1.1.4. Tracheal cartilage in (A-B) amphibian from (Kuehne 2000) and (C) bird from (Hogg 1982).

From a functional point of view, trachea function as the main respiratory organ in Arthropods was lost in Vertebrates where its function switched to a central conducting zone (Westneat et al 2003), with no direct function in the contraction of atmospheric oxygen, a role dispensed by alveoli in the lungs. In addition, trachea development was essential to switch from evaginated gas exchangers to invaginated ones (McCutcheon 1964). Thus, the essential function of the windpipe is to maintain the air circuit from outside to inside and vice versa, regardless of the difference between intrathoracic pressure and extrathoracic the atmospheric pressure

In the air journey through the respiratory system, the trachea constitutes the greatest part of the conducting zone where no gas exchanges happens. For that reason, it is often called "the dead zone". However, this does not reflect the importance of this organ; it is well known nowadays that any disease affecting the integrity of one or more tracheal structures would affect respiration. Symptoms may vary from wheezing, stridor, coughing to the ultimate obstruction of respiratory airway and death (to see in 5.1) (Al-Qadi et al 2013).

The next parts of this chapter explore the trachea in details.

2. ANATOMY

2.1. Trachea proper

Air enters through pharynx and flows via the larynx into the trachea or windpipe. Thus, the trachea starts where the larynx end, at the lower border of cricoid cartilage, and end at the carina, or tracheobronchial bifurcation, where it splits into two bronchial tubes with a 60° angle from lateral view to makes an angle of 23° to 34° with body major axis, assuming an oblique course (Amorós & Lluberas 2013). Trachea enters the thoracic inlet opposite of the upper border of the manubrium of the sternum and ends at its lower border (Thorek 1985), approximately 1 or 2 cm below a horizontal plane passing through the Louis sterna angle (Amorós & Lluberas 2013).

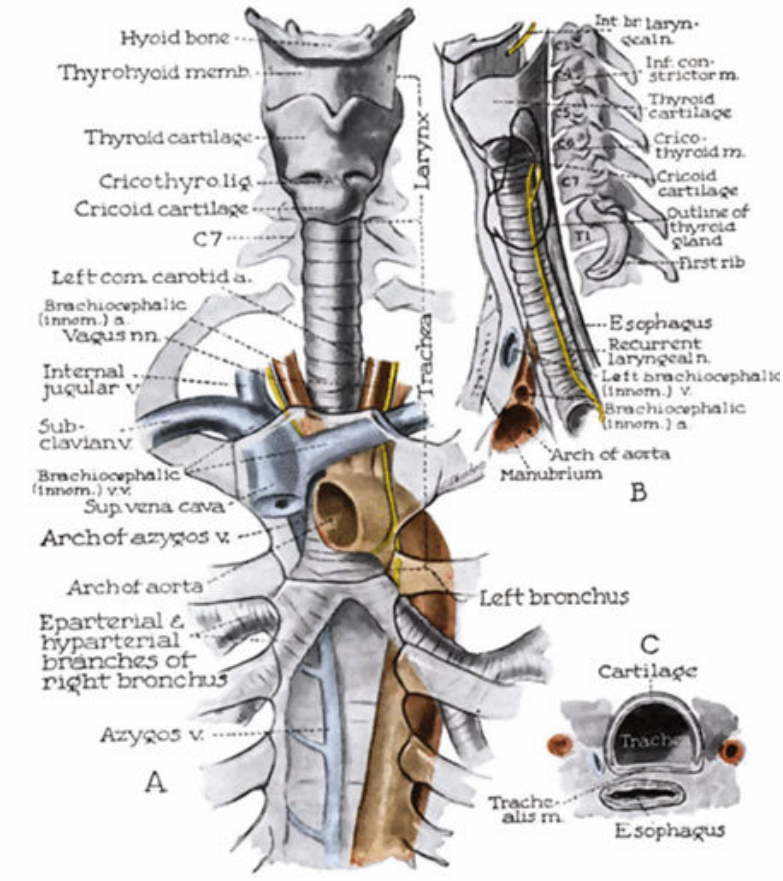

Fig.1.2.1. The trachea and extrapulmonary bronchi
Relations as seen from the front (A), viewed from the left side (B). (C) the trachealis muscle seen in cross section after (Thorek 1985).

Trachea extends around 11cm from the sixth or seventh cervical vertebra (C6-C7) to the fourth or fifth thoracic vertebra (T4-T5) (Zur 2014).

Attached to the larynx via the cricoid cartilage, sole complete ring of cartilage of the respiratory airways, the trachea is mainly composed of 15 to 20 incomplete C-shaped rings made of hyaline cartilage that are staggered and horizontally and segmentally distributed. Each posterior portion of the tracheal cartilaginous ring is closed by a band of smooth muscle, called the trachealis muscle. (See Fig.1.2.1. A, B and C)

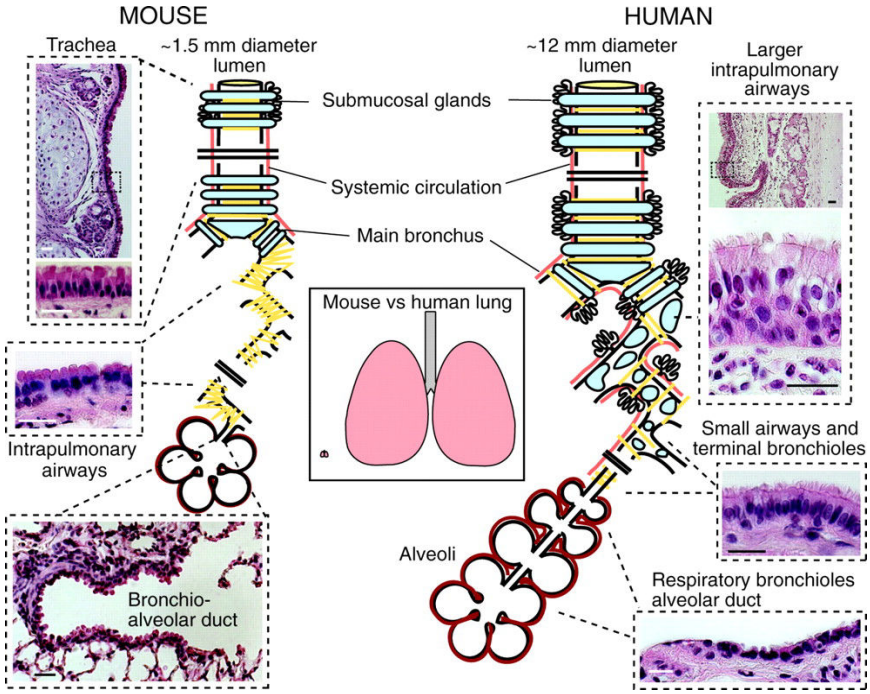

Fig.1.2.2. Schematic comparison of the structure and epithelial organization of rodent and human lungs.
Scale bars: 25 µm. Left panel: mouse lung. The trachea, ~1.5 mm internal diameter, is lined by a pseudostratified epithelium with about 55% ciliated cells, 30% BCs, secretory cells and sparse neuroendocrine cells. In the rat (but not apparently in the mouse), there are more ciliated cells in the epithelium overlying intercartilage segments versus cartilage (Toskala et al 2005). The submucosal glands are typically restricted to the four most proximal intercartilage regions. In the mouse, there are ~six to eight generations of intralobar branches (intrapulmonary airways), which have a stereotypical branching pattern (Metzger et al 2008). In these airways, the epithelium is simple and columnar, and is made up of ~48% ciliated cells and the remainder of secretory and neuroendocrine cells. Most of the secretory cells have electron-dense cytoplasmic granules and domed apical surfaces that project into the lumen. They are therefore defined as Clara cells (Mercer et al 1994). There are no BCs and, in laboratory mice, few goblet cells in these intrapulmonary airways. Smooth muscle (yellow lines) surrounds the airways, but there are no cartilage plates. The terminal bronchioles leading into the bronchio-alveolar duct have fewer ciliated cells (~26%) compared with more proximal airways. Right panel: human lung. The average human trachea has an internal diameter of ~12 mm. There are more generations of intrapulmonary branches than in the mouse, and cartilage plates and smooth muscle surround the intrapulmonary airways deep into the lung. A pseudostratified epithelium with ~30% BCs, 30% ciliated and 30% secretory cells lines these airways. The latter are predominantly goblet cells with a few Clara cells (Mercer et al 1994). The respiratory bronchioles are lined by a simple cuboidal epithelium. The precise identity and gene expression profiles of these cells are poorly understood. After (Rock et al 2010).

The special configuration of the windpipe characterized by the presence of C-shaped cartilage rings separated by fibrous tissue and connected dorsally by smooth muscle gives the trachea the ability to elongate up to third of its length and contribute to the flawless passage of the air throughout the trachea and its further progression into the bronchi (Amorós & Lluberas 2013). Griscom and Wohl reported that no changes in trachea size were observed between genders till early adolescence, a time when the trachea of female stops growing. As a result, male adult trachea are 7% longer than female adult trachea (Griscom & Wohl 1986). In addition, the same study reported that a difference of 18% in anterior-posterior diameter, 14% in transverse diameter, 28% for cross section and 44% in volume capacity were found between male and female trachea (Griscom & Wohl 1986) (See Fig.1.2.2.).

2.2. Trachea and neighborhood

Anteriorly, the cervical portion of the trachea is covered till the fourth tracheal ring with the right lobe of the thyroid gland. Posteriorly, trachea is accompanied by the esophagus with a slight left side deviation, the esophagus originated from the posterior margin of the cricoid cartilage keeps a distance lesser than 0.5mm to the posterior wall of the trachea for 7 to 8cm down to the tracheal bifurcation (Liebermann-Meffert et al 1993).

In front of the trachea are placed the roots of the innominate and the left common carotid arteries.

More anteriorly, the *mambrium sterni* is situated with the lower part of the sternohyoid and the sternohyoid muscles that arise from the back of it.

The lower part of the thoracic portion of the trachea is crossed by the arch of the aorta, with the deep cardiac plexus intervening (Thorek 1985). (See Fig.1.2.1.A and B).

The changes in the position and in the degree of angulations of trachea can orient the diagnose of some pathological conditions, when the affected organs are located distally to the bifurcation, such as left atrium dilatation in mitral stenosis or enlarged lymph node (Amorós & Lluberas 2013). In infants, the side of aortic arch is frequently inferred from the position of trachea (Stewart et al 1966), the aortic arch position is undetectable by itself, because it is covered by the thymus gland. In fact the recognition of a right aortic arch depends upon one of four signs, two of them are based on the trachea position (Mauer 1964). However, it is worthy to mention that trachea remains in the same position in 47% of cases of right aortic arch in infants (Strife et al 1989).

On the right side, the trachea is related to the right pleura and lung, the right vagus nerve and the arch of the azygos vein. On the left side, it is related to the left common carotid and the subclavian arteries, as well as the phrenic and the vagus nerves.

Finally, many tracheobronchial lymph glands are associated with the trachea at its bifurcation. Along the lateral posterior aspect of trachea passes the right recurrent laryngeal nerves on the right side and the left recurrent laryngeal nerves on it left side (Thorek 1985).

2.3. Innervation

The windpipe of Mammals is innervated by a group of ganglia situated at the dorsal side of the trachea in addition to nerves fibres from the vagus nerve and from the sympathetic chain from the middle cervical ganglion. The ganglion receives branches of the laryngeal nerves and is joined to one another into a plexus called "the ganglionated plexus of the trachea".

A study carried out by Chiang-Hsun *et al.* in mice shows that these plexus covered with a capsule (perineurium) change with age. In fact the number of neurons within the plexus remain unchanged but the size of these neurons increases from 251µm^2 to 341µm^2 in average (Chiang & Gabella 1986).

2.4. Blood and Lymph supply

The trachea gets its blood supply in two regions:

1. The lateral tracheal wall that gets it blood from the longitudinal vessels of the inferior thyroid artery, subclavian artery, supreme intercostal artery, internal thoracic artery, bronchio-cephalic trunk, and the bronchial arteries at the bifurcation of the trachea.

2. The lateral-anterior tracheal walls: transverse segmental vessels that run in the soft tissue between the cartilage rings. These vessels originate from the vessels mentioned above, and then arborize to supply the sub-mucosal capillaries.

The inferior thyroid vein originated from the thyroid isthmus is responsible of the tracheal venous drainage. Lymphatic drainage irrigates into the pretracheal, paratracheal and tracheobronchial nodal groups (Zur 2014).

In a recent study published in the American Journal of Pathology, the authors used the tracheal model to study angiogenesis, by whole-mount staining of the trachea by antibodies specific for lymphatic vessels and endothelial cells. The authors showed that the lymphatic vessels and larger blood vessels are located between cartilage regions, whereas blood capillaries cross the cartilage-covered regions in a ladder-like pattern (Bielenberg & D'Amore 2013) (Fig.1.2.3.).

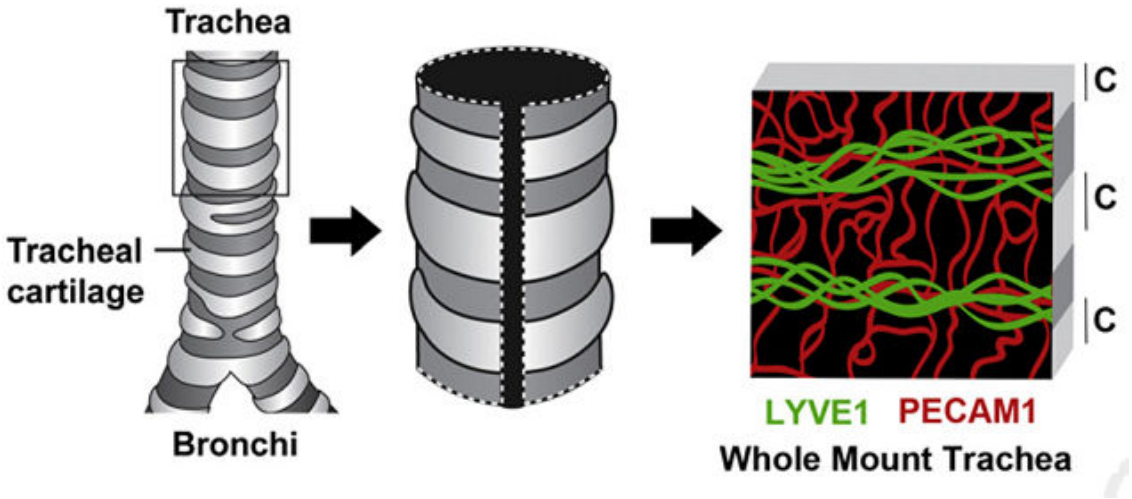

Fig.1.2.3. Blood and lymph vessels in the trachea.
The trachea is dissected, cut longitudinally, and stained by whole mount with antibodies to lymphatic vessel endothelial hyaluronan receptor 1 (LYVE1) and platelet endothelial cell adhesion molecule 1 (PECAM1). Lymphatic vessels and larger blood vessels are located between cartilage regions, whereas blood capillaries cross the cartilage-covered regions in a ladder-like pattern. Adapted from (Bielenberg & D'Amore 2013).

3. TISSULAR AND CELLULAR ORGANIZATION OF THE TRACHEA

As previously mentioned the trachea is a complex organ formed of three types of tissues (illustrated in Fig.1.3.1.), tracheal mucosa, trachealis or the smooth muscle layer and the tracheal cartilage.

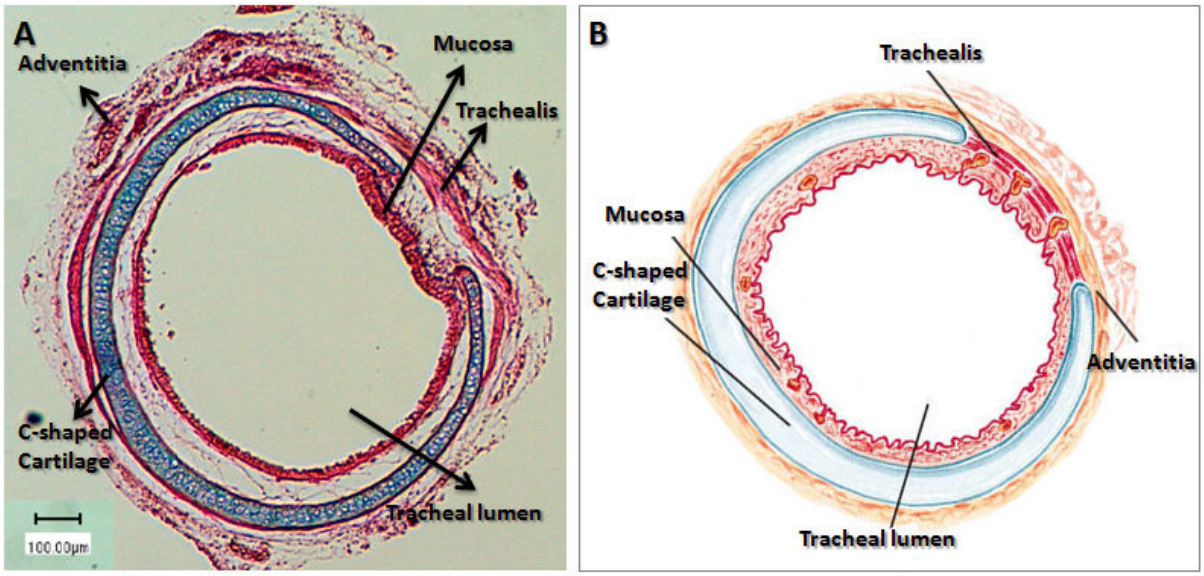

Fig.1.3.1. Trachea in transversal sections (A) after Alcian-Blue staining, the cartilage is presented in blue, eosine was used for counter-staining (B) in schematic view.

3.1. The respiratory mucosa

3.1.1. Epithelial cells

At the interface between the outside environment and the inner part of the body, the airway epithelium constitutes the first line of defense against inhaled pathogens (environmental pollutants, microbes, etc.).

The tracheal epithelium is composed of pseudostratified epithelium lined on a basement membrane. This epithelium is occupied by three major subsets of cells: ciliated columnar epithelial cells, basal cells and Goblet cells. Moreover, other populations of cells exist in a lesser extent as intermediate basal cells, Clara cells and neuroendocrine cells.

3.1.1.1. Ciliated cells

Ciliated columnar cells are the most abundant type of cells in the upper airway (Fig1.3.2 and Fig.1.3.3.). The different positioning of their nuclei gives the stratified look to the epithelium, while in reality all of these cells are indirectly linked to the basement membrane by desmosomes junctions with basal cells (Evans et al 1999; Shebani et al 2005). Every

columnar cells possess around 300 cilia (Rubin 2014) on the apical surface. The tracheal columnar cells possess the longest cilia measuring between 5 to 7µm in length (Serafini & Michaelson 1977).

Ciliated cells in upper airway are responsible of the mucociliary clearance, a process by which the respiratory airway gets rid of the mucus layer that entraps undesired exogens. Two factors are essential for mucociliary clearance process: the beating pattern of cilia (12-15 Hz) (Helleday et al 1995) and the airway surface liquid (Tarran et al 2001; Voynow & Rubin 2009), which is composed of two layers. The first, known as the periciliary liquid layer, is a liquid layer in contact with ciliary apparatus (Matsui et al 1998) and confers a low resistance environment in which cilia can bend easily. The second is an outer layer in direct contact with air, consisted of a mucus layer rich in mucin secreted by secretory cells as Goblet cells and Clara cells.

3.1.1.2. Basal cells

Unlike other subtypes of cells in the airway mucosa, basal cells are the only subset of cells in direct contact with the basement membrane through hemidesmosomes (Fig.1.3.2 and Fig.1.3.3). As such, they play a role in anchoring the pseudostratified respiratory epithelium to the basement membrane (Evans & Moller 1991).

In addition to their function as an anchor to stabilize the columnar cells, basal cells represent the progenitor cells in the tracheobronchial epithelium (Ayers & Jeffery 1982; Donnelly et al 1982) (Fig.1.3.3).

3.1.1.3. Goblet cells

Goblet cells are the principal secretory cells in the respiratory airway (Fig.1.3.2). Their apical portion extends into airway lumen and is rich with big mucus granules of almost 800 nm in diameter (Jeffery 1983). Goblet cells can be found in all the parts of respiratory epithelium with maximal density (around 6000 and 7000 cell per mm^2) in large conducting airway. This density decreases with the diameter of the different regions of the airway, even though Goblet cells can still be found in bronchioles (Ellefsen & Tos 1972) (Fig1.3.3).

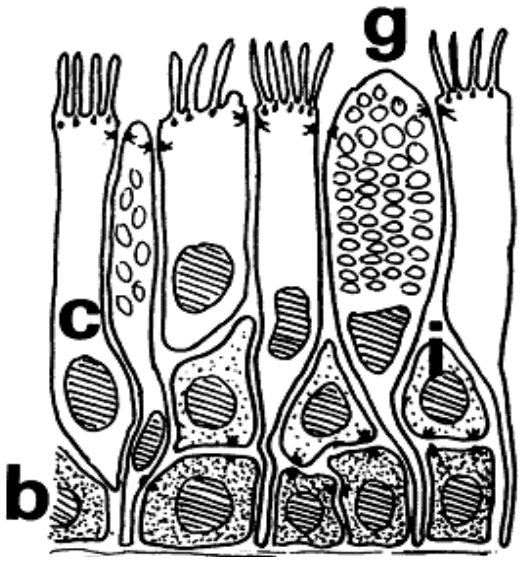

Fig.1.3.2. Diagrammatic representation of the normal tracheal epithelium.
(b) basal cells ,(i) intermediate cells ,(g) goblet cells, (c) ciliated cells. After (Emery & Haddadin 1971).

3.1.1.4. Parabasal cells or Intermediate cells

Parabasal cells are a sparse subset of cells located just above the basal cells (Breeze & Wheeldon 1977) (Fig.1.3.2). The absence of common morphological characteristics between parabasal cells and other epithelial cells in airway, led Donnelly to define these cells as nonbasal, noncolumnar cells (Donnelly et al 1982).

The origin and the function of Parabasal cells are controversial. They have been considered by some investigators as undifferentiated columnar cell, with secretory function, that do not derive from basal cells (Evans et al 1986). Others consider parabasal cells as differentiated cells that derive from basal cells with an involvement in cell renewal in rodent tracheo-bronchial epithelium (Breuer et al 1990; Donnelly et al 1982).

3.1.1.5. Clara cells

Clara cells are a subset of cells with secretory function in the distal airway (Fig.1.3.3), they generally rapidly synthesize and secrete mucins without storing them in vacuoles as in the case of Goblet cells (Verkman et al 2003). Beside their secretory function, Clara cells also contribute to cell renewal, and in fact appear to be the stem cells of the small airways, where basal cells are sparse or even absent (Boers et al 1998).

3.1.1.6. Neuroendocrine cells

Neuroendocrine cells are sparsely scattered in the respiratory mucosa, where they represent only 1/2,500 cells (Gosney et al 1988). They have a pyramidal shape and look like basal cells. They are in contact with the basal membrane. In light microscopy, these cells seem to have granules in their basal portion, and they possess cytoplasmic extensions that get in touch with the airway lumen (Weichselbaum et al 2005).

3.1.2. Airway submucus glands

Airway submucus glands are complex structures localized beneath the respiratory epithelium and more common in large airway (Verkman et al 2003) (Fig.1.3.3). They secrete antibacterial factors, fluid through their serous cells and mucus through their mucous tubules. The secreted products get to the airway lumen via the collecting ducts and ciliated ducts. Myoepithelial cells are another compound of submucus glands, their contractility help the expulsion of submucus gland secretion to the lumen (Jeffery 1983; Springer et al 2005).

In addition to their secretory function, it has been suggested that submucus gland may play a function as a progenitor cell niches of the proximal airways (Liu & Engelhardt 2008) (Fig.1.3.3).

3.1.3. Tracheal epithelium specificity

The tracheal respiratory epithelium differs from the bronchial airway epithelium (Fig.1.3.3). This difference can be detected on morphological scale through the length of cilia as the length of the cilia range from 5-7µm in the trachea and 2-3µm in the smaller airways (Serafini & Michaelson 1977).

In addition, while the mucus layer is secreted all over the respiratory epithelium, the mucus producing cells are not the same. In the upper airway, Goblet cells are responsible for mucus production together with submucus gland, while in the distal airway, Clara cell take over the former cells regarding mucus production (Verkman et al 2003).

In adult humans, many investigators showed that the number of submucus glands declines at $\approx 0{,}2 mm^{-2}$ per airway generation, considering that the tracheal epithelium has the bigger number of glands with a reparation of 1 gland opening per mm, it is worth noting that this decrease in number is accompanied with a decrease in gland volume (Tos 1966; Whimster 1985).

The percentage of basal cells decreases all along the respiratory epithelium, to represent only 6% in the distal airway epithelium. Parabasal cells are less common than basal cells in large airway as they represent 7% of the epithelial population in the upper airway but disappear in the distal airways, suggesting that the possible function of these cells as progenitor cells is also replaced by Clara cells (Boers et al 1998).

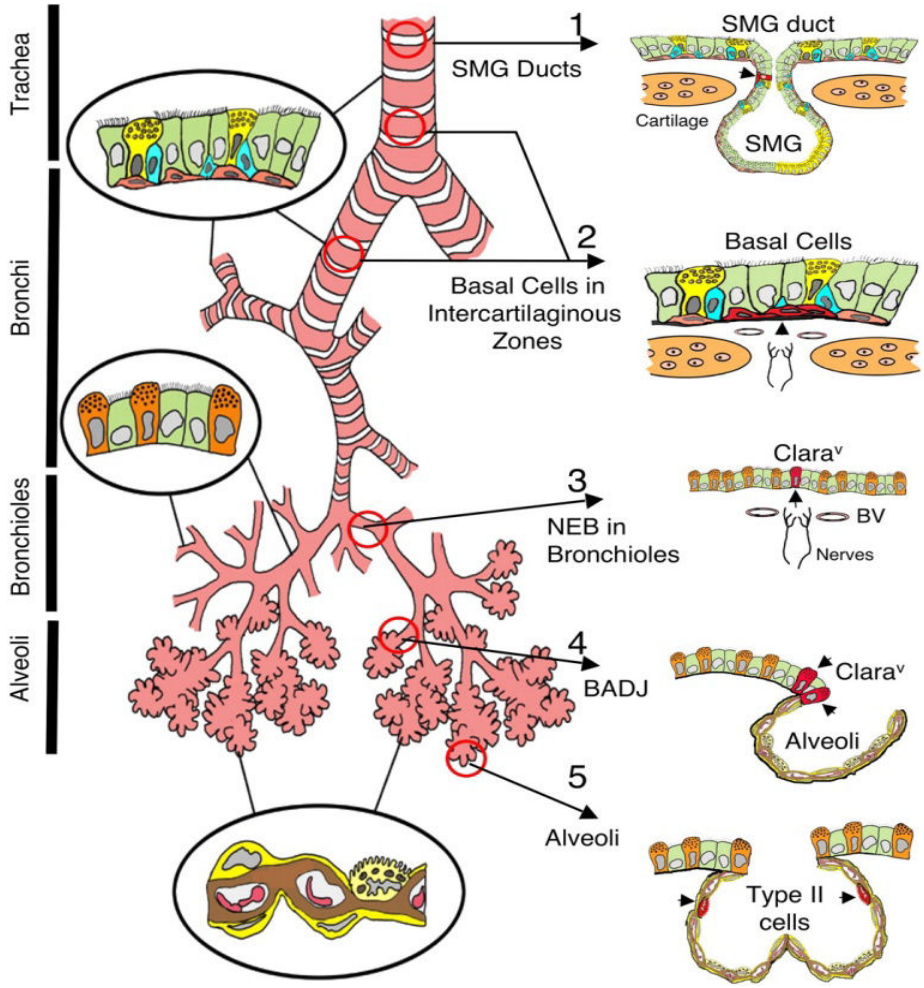

Fig.1.3.3. Illustration of putative stem cell niches in the adult mouse lung.
Epithelia of the adult mouse lung can be divided into four major, biologically distinct trophic units (trachea, bronchi, bronchioles, and alveoli), each of which encompasses unique types of airway epithelial cells (epithelia relevant to each unit are shown inside *circles*). Five potential stem cell niches for these various trophic units are shown on the *right*, with locations of candidate stem cells marked by *arrowheads* (cells are in *red*). Stem cells and niches include the following: (1) an unknown cell type in the submucosal gland (SMG) ducts of the proximal trachea, (2) basal cells in the intercartilaginous zones of the lower trachea and bronchi, (3) variant Clara cells (Clarav) associated with NEBs in bronchioles, (4) Clarav cells associated with bronchiolar alveolar duct junctions (BADJ), and (5) alveolar type II cells of the alveoli. From (Liu & Engelhardt 2008)

3.2. Airway muscle cells

3.2.1. Muscle, but smooth muscle

In the human body, two types of muscles can be found: i) the striated muscles found in the skeletal system and in the heart; and ii) the smooth muscles, that lacks the cross striation pattern found in the former ones.

In addition to the vasculature where they are highly abundant, smooth muscles are also found in inner organs, such as the intestine and the tracheobronchial tree. Besides structural organization, smooth muscles diverge from striated muscles by their function. Much slower than striated muscles, they are implicated in holding function because of their ability to

maintain force for prolonged period without a remarkable expenditure in energy. Also smooth muscle can be spontaneously active or stimulated by a varied number of neurotransmitters and hormones, and they can respond to these stimuli in two major ways, a brief and phasic contraction or a prolonged contraction.

3.2.2. Structure and function

3.2.2.1. Structure: two or three layers!?

Airway smooth muscle (ASM) firstly appears as a ring of cells that express smooth muscle-specific proteins. These cells are found around the base of lung buds and derive from mesenchyme (see section 4 of this chapter). They grow rapidly from bronchi to trachea to form interlocking bundles; progressively these bundles become more compact and wider and maintain a perpendicular orientation toward the long axis of the airway (Sparrow & Lamb 2003).

Once formed, the smooth muscle of the trachea, called trachealis muscle, completely encircles the trachea in the human, but once the cartilage get formed the space taken by the muscle cells narrows down to cover the tips of the crescent shaped cartilage on the dorsal side (Sparrow et al 1999).

The presence of three layers of muscle in the trachea is subject to controversy. The presence of transversal layer of muscle is certain, this layer being consistently uniformly arranged. In contrast, the presence of a longitudinal muscle layer is less evident. Tollet et al reported the presence of poorly developed longitudinal bundle of 3-4 cm in length, in the region near tracheal bifurcation but not all along the trachea (Tollet et al 2001), as in the case of bundles seen by Kamel et al (Kamel et al 2009) (see Fig. 1.3.4.) Still the majority of authors report that longitudinal muscle layer does exist, this layer is outer to the inner transverse layer. Fisher was the only one to report the presence of three muscle layers, transversal, longitudinal and oblique one (Fisher 1962). However, the longitudinal muscle bundles are more abundant in the lower part of the trachea, they are stiffer than the transversal one (Trabelsi et al 2010) and they seem to have a function in preventing tracheal collapse, they are at their lower rate in preterm infants, and at their highest in children of 1 year of age (Wailoo & Emery 1980).

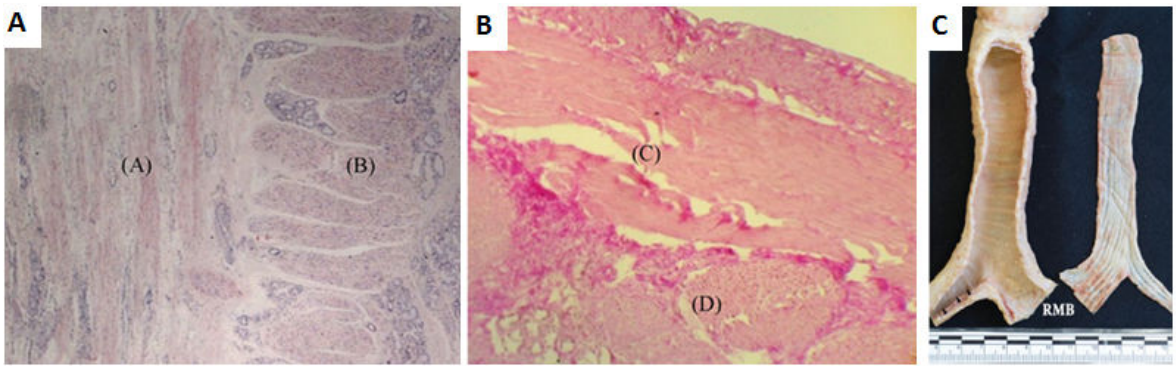

Fig.1.3.4. Trachealis Histological view (A)(B) and anatomical view (C).
The two directions of collagen bunches: one running longitudinally and other orthogonally are seen in both pictures.
-Panel (A) Longitudinal cut of the human smooth muscle, X10 Van Gieson's Trichrome stain: collagen fibers in red; the inside (A) parallel collagen fibers to the cutting direction; the inside (B) perpendicular collagen fibers to the cutting direction; Panel (B) transversal cut of the human smooth muscle, X10 Van Gieson's Trichrome: collagen fibers in red; (C) parallel collagen fibers to the cutting direction; (D) perpendicular collagen fibers to the cutting direction. After (Trabelsi et al 2010); Panel (C) The membranous wall of the trachea has been excised and reflected to reveal a luminal view of the longitudinal elastic fiber bundles (right). Note the fine elastic bundles in the nonmembranous part of the left main bronchus (arrowheads). RMB, right main bronchis. After (Kamel et al 2009).

3.2.2.2. Function

Before birth

Intraluminal pressure is a very important factor in respiratory system development, especially for lung development (Unbekandt et al 2008).

Once formed, ASM exhibits rhythmic contractility, the narrowing of airway caused by these contraction shifts the lung liquid distally and lead to the expansion of tubule walls (Sparrow & Lamb 2003), the ability of ASM to generate a positive pressure in the liquid-filled tubules made of them a prerequisite in lung growth (Tollet et al 2001).

After birth

In postnatal phase of life, airway smooth muscle contractility switches from a rhythmic (Schittny et al 2000) to a tonic mode (Solmyo 1994).

During normal breathing smooth muscle regulates the diameter of tracheal lumen by increasing the section during inhalation and decreasing it during expiration, these changes contribute to the pressure balance inside the lung (Malvè et al 2011).

3.2.3. Muscle, smooth and still...

Smooth muscle cells in the respiratory system are divided into two types, the vascular smooth muscle (VSM) and the airway smooth muscle (ASM) cells. These two types of smooth muscle have their share of similarities and differences.

Differentiation of both kinds is inducible by elongation and positive hydrostatic pressures. In addition, the differentiation of these two kinds is dependent on mesenchymal-epithelial

interactions with critical dependence on Sonic Hedgehog (SHH) signaling, that seems to be less implicated in other visceral smooth muscle differentiation (Pepicelli et al 1998; Ramalho-Santos et al 2000).

However, the differentiation of airway smooth muscle cells precedes the appearance of vascular musculature by several days (McHugh 1995; Miano et al 1994; Mitchell et al 1990). In addition, the implicated signaling molecules differ between ASM and VSM cells. For instance, different transcriptional regulatory programs seem to control Transgelin SM22α promoter activity in VSM and ASM (Hoggatt et al 2002; Li et al 1996; Moessler et al 1996). In fact, airway VSM differentiation has been found to be Nkx2 homeobox 1(Nkx2.1) and wingless-type MMTV integration site family member 7b (Wnt7b)-dependent (Shu et al 2002; Yuan et al 2000). In contrast, ASM differentiation is more likely to be dependent on SHH, Forkhead box F1 (Foxf1), Fibroblast Growth Factor 9 (FGF9) (Weaver et al 2003), Laminin (Yang et al 1998). As demonstrated in a recent study, ASM differentiation is under the influence of Wnt2 signaling, that in turn activates Wnt7b and through the Wnt-β-catenin canonical signaling leads to proper VSM and ASM development in the respiratory system (Goss et al 2011).

These differences in the differentiation process of the different smooth muscle cells that populate the airways also lead to functional differences as in ASM the velocity of contraction is particularly rapid when compared to other smooth muscles (Fernandes et al 2004).

3.3. Tracheal cartilage, Hyaline cartilage; not quite the same

3.3.1. Cartilage, but hyaline cartilage

The first documented recognition of cartilage has been attributed to Aristotle (384-322) in the fourth century BC: ‘‘Cartilage is found where it is an advantage that the solid framework should be pliable and glutinous for the benefit of the flesh that surrounds them. This applies to the ears and the nostrils. Such projecting parts quickly get broken if they are brittle. Cartilage and bone are the same in kind and differ only by ‘the more and less’ (Aristotle 1918)(Aristotle 1918)(Aristotle 1918). Cartilage is essentially avascular, alymphatic and aneural, although some hyaline cartilages such as epiphyseal, costal and laryngeal cartilages contain vascular canals. It is covered by a fibrous perichondrium except at osseous junctions and at synovial surfaces, composed predominantly of extracellular matrix within which are embedded chondrocytes, the cells that maintain cartilage matrix structure by continued remodeling activity throughout life.

In normal situations, in adulthood, cartilage is characteristically present in the skeleton (articular surfaces of synovial joints, intervertebral discs), ears, respiratory tract and nose.

There are three main types of cartilage, which differ in the number and morphology of the constituent chondrocytes and the biochemical composition of the matrix:

- Elastic cartilage, if elastic fibers are present in the extracellular matrix
- Fibrocartilage, when the extracellular matrix is enriched with collagenous fiber content, usually accompanied by deposition of type I collagen.
- Hyaline cartilage, when the matrix is composed predominantly of glycosaminoglycans and enriched with type II collagen.

Although it has been occasionally described as fibrocartilage by some investigators or as elastic cartilage by others (Hall 2005), tracheal cartilage is considered as a permanent hyaline cartilage throughout life (Gradus et al 2011; Kojima et al 2003; Young 2006).

As such, the tracheal cartilage contains an abundant amorphous matrix reinforced by collagen type II and small aggregation of chondrocytes in lacunae. The matrix of tracheal cartilage is formed of glycosaminoglycans, mostly chondroitin sulfate and keratan sulfate, hyaluronic acid and water (Young 2006).

The collagen fibers orientation in tracheal cartilage changes with the depth of cartilage. In the thin outer layer, close to the lumen collagen fibers are oriented in two directions, either circumferentially (tangentially to the lumen axis) or longitudinally (parallel to the lumen axis). In the deeper part, close to the center of the cartilage, the collagen fibers orientation is less regular with circumferential tendency.

The perichondrium of the tracheal cartilage is composed of collagen fibers and spindleshape cells that resemble fibroblasts (Roberts et al 1997).

3.3.2. Structure and function

As we mentioned in the anatomy section of this chapter, the trachea has from 15 to 20 cartilage rings. These rings share the same nature (cartilage), the same function of ”preventing airway from collapsing” (see below), but do not share the same shape.

In fact, differences in cartilaginous ring morphology can be depicted between individuals on the longitudinal plan, and even in the very same person when considering the transversal view.

Longitudinal plan

When looking at the ventral side of the human trachea, morphological differences between the tracheal rings are easily observed. Those differences are discussed in a study made on the lower part of the trachea, in which the authors noted 15 shapes of tracheal cartilage rings (Fig.1.3.5). These shapes are subdivided into two categories: free rings or compound rings (Vanpeperstraete 1973).

Free rings: in this group, rings are separated by parallel, regular bands of fibrous tissue, their course is horizontal in the majority of cases or slightly sloping, except the last ones which were curved downward in their middle, the majority of rings fall into this group. Single rings could be shorter than usual or incomplete fenestrated, boarder at one end or L-shaped curved twice or S-shaped or forked at one end or Y-shaped (Vanpeperstraete 1973).

Compound rings: Compound rings are the result of the fusion of many rings together, two or three adjacent rings can be fused, see (Fig.1.3.5). Although very rare the fusion of four adjacent rings can occur in the neighborhood of the bifurcation (Vanpeperstraete 1973).

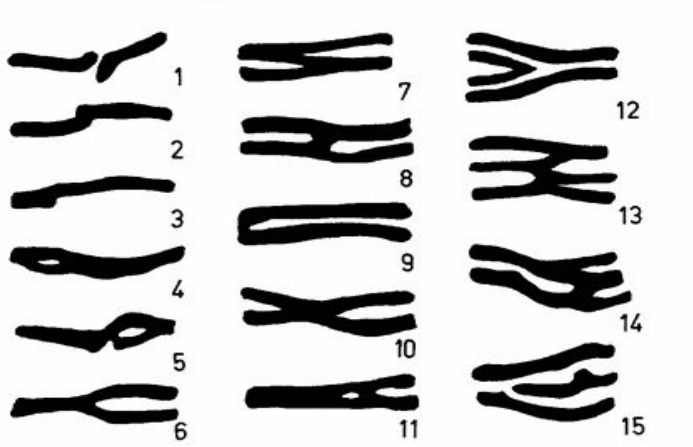

Fig.1.3.5. Single and compound rings found in the lower trachea
1 Interrupted, 2 S- shaped, 3 L-shaped, 4 and 5 fenestrated, 6 Y-shaped or forked, 7 N-shaped, 8 H-shaped, 9 U-shaped, 10 X-shaped, 11 A-shaped, 12 V-shaped, 13 and 14 M or W-shaped, 15 incomplete. After (Vanpeperstraete 1973)

Transversal plan

The shape of tracheal cartilage is considered to be circular, although a study made by Baer showed that circular shape is found in less than 10% of the studied population (Baer et al 1987).

Mackenzie et al reported that there exist six different shapes of cross sections of the human trachea (MacKenzie et al 1978) as presented in Fig.1.3.6.

Still not all the ring of the same trachea has the same shape. In fact it has been demonstrated that the shape of the seventh ring (at the sterno-clavicular joint, where the lower end of an intubation tube cuff should be (MacKenzie et al 1978)) was different from that of the twelfth in 46% of the male and 60% of the female cases (Baer et al 1987).

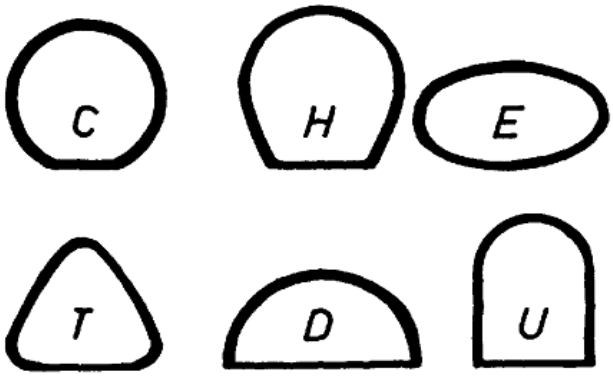

Fig.1.3.6. The 6 shapes of tracheal cartilage.
The C (circular) is almost a cylinder, H (horseshoe) is the classic shape; E (elliptic) has a larger transverse than a sagittal diameter; T (triangle) is almost a triangle with two straight-lined sides; the D is almost a half-circle, its largest transverse diameter being at the pars membranacea; the U is composed of a half-circle and (two straight sides, the diameter of the half-circle and the transverse diameter at the membrane being the same. From (Baer et al 1987)

3.3.2.2. Functions

Since the tracheal cartilage stiffness is much higher than the mucosal membrane, and as the ratio of cartilage/muscle cell in trachea is 4:1 (Mair & Parsons 1992; Wailoo & Emery 1979), it seems logical to consider that the tracheal cartilage stiffness is the principal factor that prevent airway from collapsing.

The stiffness of tracheal cartilage is the result of unique morphological characteristic of the trachea, and it does not seem to be equally divided on the trachea. It has been reported that the tracheal cartilage near the bifurcation is stiffer than the cartilage of other parts. Also tracheal cartilage does not have the same thickness all over the ring. The thickness at the middle of the rings is approximately 3 times the value of the position close to the tip. According to these findings, the authors estimate that the cartilage ring stretching is much less than 1%. The tips of the tracheal rings were not in a horizontal line so the tracheal cartilage is supposed to have an asymmetric shape approximated by a skew ellipse (Teng et al 2008). In another study, the same authors reported that the curvature on the left side of the tracheal ring is larger than the curvature on the right side, defining tracheal cartilage as anisotropic (possessing identical properties in all directions) material (Teng et al 2009). Still the isotropic properties of tracheal

cartilage is controversial, as for instance, Roberts et al. mentioned that tracheal cartilage should be an anisotropic material to maintain its function (Roberts et al 1997).

To resume, tracheal cartilage is a nonlinear material displaying higher strength in compression than in tension, in order to avoid collapsing, and with a very small variation in its length during deformation when small force is applied. (Teng et al 2008)

3.3.3. Cartilage, Hyaline, and still

Tracheal cartilage converges in its nature as hyaline cartilage with joints and other cartilages. Still besides structural shape (see above) and embryonic origin (see next section), meticulous reading of the literature shows that tracheal cartilage also differs from other hyaline cartilages at the molecular level

3.3.3.1. Snail1 and miRNA

Snail family zinc finger 1 (Snail1), is a zinc finger transcription factor found in pre-hypertrophic chondrocytes, it acts downstream of FGF, its overexpression represses hyaline cartilage markers expression as Collagen 2a1 and Aggrecan and inhibits proliferation via its interaction with histone desacetylases, i.e. HDAC1 and HDAC2 (de Frutos et al 2007; Hong et al 2009; Seki et al 2003).

It has been reported that Snail has a very low expression rate in tracheal cartilage. In fact the repression of Snail1 expression depends on two miRNAs: miR-125 and miR-30. The repression happens due to an exceptionally long paired-recognition sequence that binds to Snail mRNA. MiR-125 and miR-30 are highly expressed in tracheal cartilage comparing to other types of hyaline cartilage.

Taken together, the expression of miRNA in tracheal cartilage inhibits Snail, and permits to the tracheal cartilage a permanent expression of Aggrecan and Coll2 (Fig.1.3.7).

Gradus and colleagues in their study showed that this miRNA activity is essential for tracheal cartilage and its loss induces a flaccid tracheal cartilage similar to that found in tracheomalacia (see section 5 of this chapter), the same effects were not seen in articular cartilage (Gradus et al 2011).

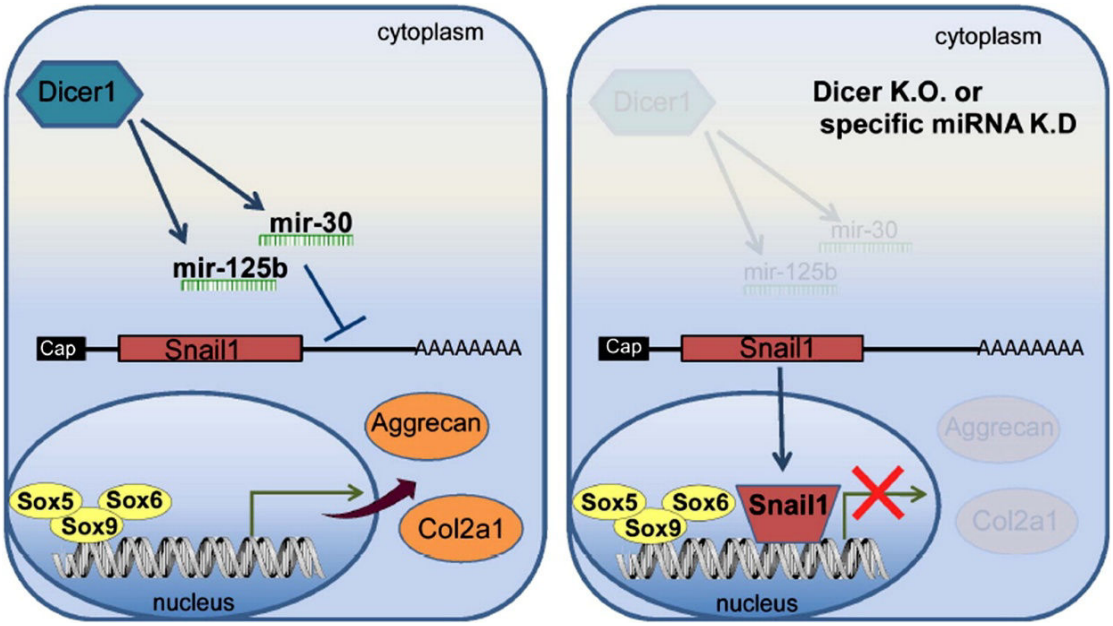

Fig.1.3.7. Snail regulation by miRNA in tracheal cartilage.
miR-125b and miR-30 control Col2a1 and Aggrecan synthesis through Snail1 expression. ATDC5 cells were transfected with 2′-O-methyl antisense inhibitor against miR-125b and miR-30. From (Gradus et al 2011)

3.3.3.2. Fibronectin (FN) isoforms

Fibronectin is a glycoprotein found in extracellular matrices and in body fluids, it belongs to the category of adhesives molecules, and possesses three types of modules: type I (twelve domains), type II (two domains) and type III (fifteen-seventeen domains). These three modules confer to fibronectin molecules its capacity to bind to many extracellular compounds as collagen, gelatin, integrin, heparin, fibronectin and others.

Alternative splicing produces many isoforms of fibronectin (12 in rodents and 20 in humans). It occurs by skipping of the IIIA/EDA or IIB/EDB exon or by exon subdivision at the region V/III CS. FN isoforms repartition is tissue- and developmental stage-dependent, however a difference in FN was observed in different kind of cartilage (Hynes 1981; Schwarzbauer 1991). Zhang demonstrates in his study that the FN mRNA in the cartilage has no ED-A region (A^-B^+) and that the Fibronectin within the cartilage of the trachea has neither ED-A nor ED-B (A^-B^-) (Zhang et al 1995).

This highlights the difference there exists between the tracheal cartilage and other types of hyaline cartilage.

4. DEVELOPMENT OF THE TRACHEA

4.1. At the origin of the trachea was the foregut

Although countless embryologic studies have established the anterior foregut as the precursor of the respiratory system (lungs and trachea), there has been strong controversy between scientists, especially with regard to the formation and separation of the tracheal anlage from the esophageal wall.

Very soon (8-10 hours) after the beginning of gastrulation, the endoderm, aka "the inner most germ layer of the embryo", emerges from the anterior segment of the primitive streak (Lawson et al 1991; Tam & Beddington 1992). At the end of gastrulation, the foregut develops from the anterior part of the definitive endoderm (Sox17 positive) as a crescent-shaped depression beneath the neural folds. At this stage the definitive endoderm is formed of squamous epithelium (Lewis & Tam 2006a) (see Fig.1.4.1).

Then, the foregut starts to invaginate. Tremblay and Zaret (Tremblay & Zaret 2005) reported that during this invagination, three major morphogenetic movements occurred:

- The first movement occurs in the anterior most definitive endoderm where the midline cells move ventrally then posteriorly to give rise to the floor of the foregut invagination.
- In the second movement, the lateral endoderm moves towards ventral midline.
- The third movement consists of the extension of the most posterior cells in the anterior definitive endoderm on a rostro-caudal axis to occupy the dorsal wall of the embryonic foregut.

The gut tube closure happens when the embryo changes its posture from a lordose to a fetal position (Lewis & Tam 2006a).

From the medial region of the foregut arises the respiratory diverticulum (Zur 2014), also known as the laryngo-tracheal groove, that sits between the fourth pair of pharyngeal or branchial-pouches (Gilbert et al 1996)

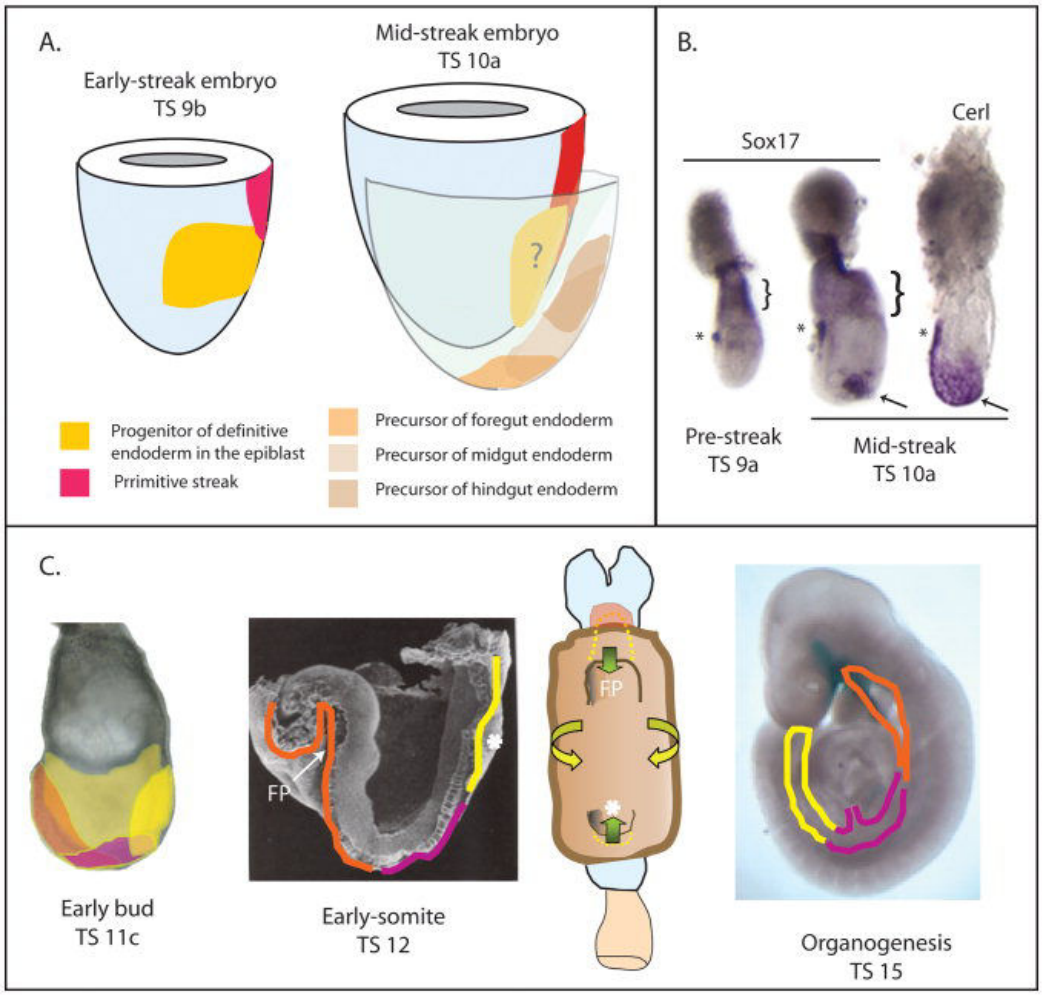

Fig.1.4.1. Foregut development in mouse embryo.
A: Fate maps showing the regionalization of the progenitors of the definitive endoderm in the epiblast of the early- and midstreak embryo (Lawson et al 1991) and the localization of the precursors of the endoderm of the embryonic fore-, mid-, and hindgut in the endoderm of the midstreak embryo (Lawson et al 1991), which is shown as an exploded view of the epiblast and the endoderm with the mesoderm omitted. Mouse embryos are staged according to Theiler staging criteria (Web site: http://genex.hgu.mrc.ac.uk/Atlas/intro.html). **B**: Formation of the definitive endoderm at the midstreak stage visualized by molecular markers. *Sox17* is expressed in the anterior visceral endoderm (asterisk) and extraembryonic visceral endoderm (bracket) of the embryonic day (E) 6.0 prestreak embryo and in the definitive endoderm (arrow) of the midstreak embryo. *Cerl* is also expressed in the definitive endoderm (arrow) and anterior visceral endoderm (AVE, asterisk). **C**: Formation of the gut tube showing the location of the endodermal precursors of the foregut (orange), midgut (pink), and hindgut (yellow) at the early-bud, early-somite, and forelimb-bud stages. At the early somite stage, the foregut pocket (FP) is extending deeply into the anterior region of the embryo and closing, but the hindgut pocket (asterisk) is just beginning to form. The embryonic gut is shown schematically in a ventral view to illustrate the morphogenetic movement (arrows) associated with the closure of the foregut and hindgut pockets and the ventral folding of the lateral body wall in the formation of the embryonic gut. At the organogenesis stage, the foregut pocket, hindgut pocket, and the lateral endodermal walls have met at the yolk stalk, thus closing the gut tube. After (Lewis & Tam 2006b)

4.1.1. Tracheal development theories

The first traditional theory, adopted by Grosser (Grosser 1912) and others, considers that, after the formation of the respiratory diverticulum, a septum gets formed and divides the foregut into a ventral portion or “respiratory part” and a dorsal portion or “digestive part”.

In this theory, the septum is the result of fusion of the lateral ridges, which appears in the lateral wall of the foregut. This fusion starts caudally and ends up cranially.

The second theory, adopted by O'Rahilly and Muller (O'Rahilly & Muller 1984) and others (Zaw-Tun 1982), claims that the bronchi can be seen branching and connecting with lung buds while the trachea and esophagus remain unseptated, but get divided in a later stage in a caudo-rostral direction. Only after this separation, a common wall between trachea and esophagus would be formed and the lungs start developing (Kluth & Fiegel 2003; Metzger et al 2011; Yamada et al 2010).

These two theories that I have outlined in a schematic form in Fig.1.4.2 seems to be redundant with the two theories concerning the true nature of the lung bud (Kluth & Fiegel 2003), one of these theories suggesting that the first lung anlagen is a "tracheal bud", while the other proposes that lungs develop from primarily primordia in a way that the bronchial buds get formed at first and trachea would follow (Hamburger & Hamilton 1992).

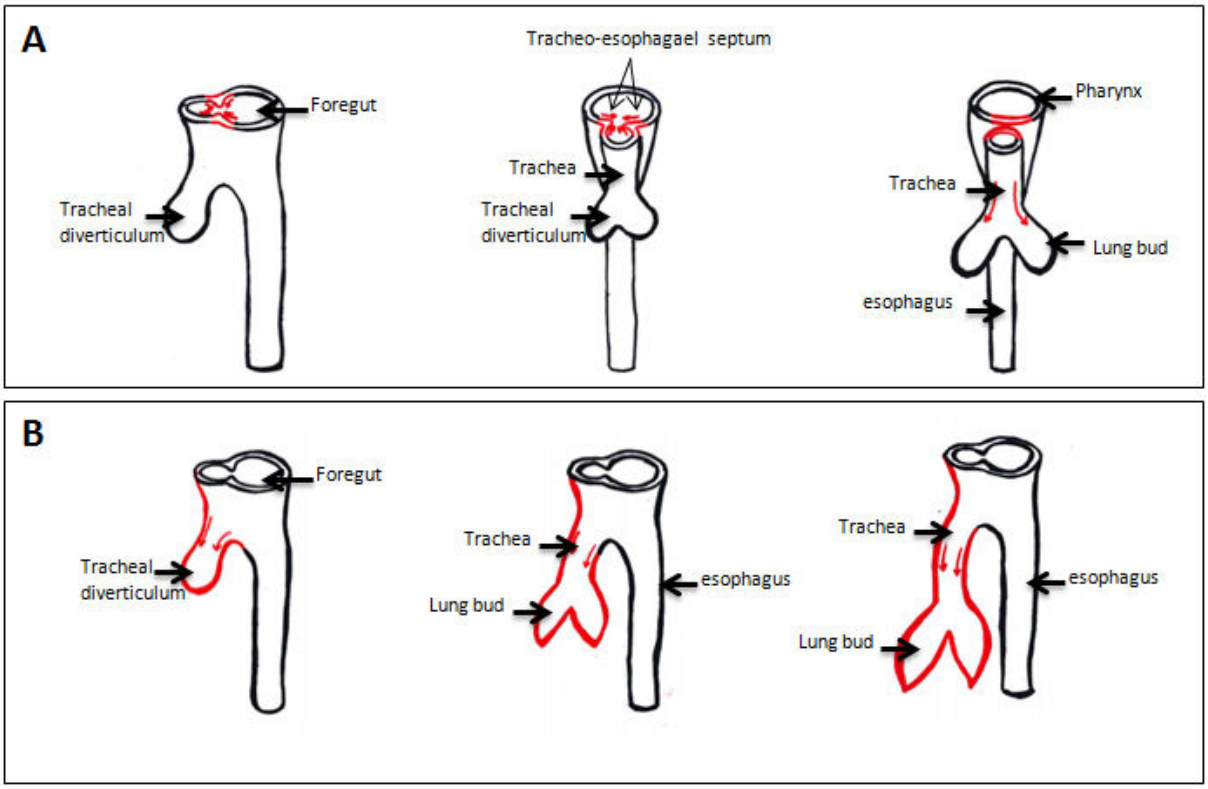

Fig.1.4.2. Schematic presentation of tracheal development according to (A) first theory (and B) second theory.

4.1.2. Example of the first theory: Study made on human Embryo by O'Rahilly and Boyden

The respiratory system development starts at Carnegie Stage (CS) 10 (2-3.5mm; 4-12 pairs of somites; ca 22 days), when the pulmonary diverticulum appears at the caudal end of the laryngotracheal sulcus.

At stage 12 (ca. 3-5mm; 21-29 pairs of somites; ca. 26 days), the tracheo-esophageal septum is formed by the fusion of endodermal ridges (Corner 1929; Streiter 1951).

At stage 13 (ca.4-6mm; 30 or more pairs of somites; ca. 28 days), there is evidence of necrosis in the central cells of the endodermal septum (Smith 1957). Bronchi are detected at this stage as lung buds with a little difference in the right bud, that takes a caudal position and get to be aligned with the trachea, while the left bud is situated transversally (Streeter 1945).

At stage 14 (ca.5-7mm; ca. 32 days), the epithelium of the trachea and lungs are active enzymatically (McKay et al 1956), trachea and esophagus are fully detached from each other (Streeter 1945).

At stage 15 (ca.7-9mm; ca. 33 days), Streeter reported that angiogenesis is visible around the primary bronchi (Streeter 1945).

At stage 17 (ca. 11-14mm; ca.41 days), the condensation in the cricoid starts to appear (O'Rahilly & Boyden 1973).

At stage 18 (ca.13-17mm; ca. 44 days), the process of chondrification starts at this stage, the tracheal wall became riche in dense connective tissue (O'Rahilly & Boyden 1973).

At stage 19 (ca.16-18 mm; ca.48 days), the trachea is fully developed and the first generation of sub-segmental bronchi is complete (Smith 1957).

4.1.3. Example of the second theory

The second theory is discussed in a study made by Metzger *et al.* in chicken embryos, the major steps in foregut division are listed in the table below (Metzger et al 2011). The same observation was made in a separate study also carried on chicken embryo (Kluth & Fiegel 2003). Yamada *et al* found that the respiratory system develops in the same manner in human embryo, with the bronchi formed and connected to the lung at CS13 and by CS 14 the trachea and esophagus are fully separated (Yamada et al 2010).

HH Stage	Embryonic day	Development
10	1,5	The head, the pericardial cavity and the heart are developed. The foregut can be subdivided in a cranial and caudal part. The caudal part is located behind the heart and the pericardial cavity and opens into the midgut via the anterior intestinal port. The cranial part of the foregut extends into the head region with the bucco-pharyngeal membrane as cranial border.
11	1,75	The epithelium of the early foregut anlage is seen. There are no clear signs of primitive foregut organs visible with the exception of a small fold which marks the first appearance of the pharyngeal pouch. Signs of a lung anlage are missing. Cranial to the pharynx pouch and distal, the liver diverticulum is seen.
12	2	The caudal end of the foregut widens to form the anterior intestinal port. At its caudal end the foregut becomes smaller in the region of the anterior intestinal port. The pharyngeal pouches are more pronounced. The anlage of the thyroids can be seen as a pouching in the midline of the ventral foregut between the 1st and 2nd pharyngeal pouch. The lung anlage is lacking.
15-17	2,5	Directly caudal to the pharyngeal pouches 2 folds appear, which grow into the foregut and form the anlage of the larynx. At the caudal end of the foregut, the liver anlage is seen. Halfway, between the liver anlage and the anlage of the larynx, the very early anlage of the respiratory tract is seen as an oblique shallow fold. Between the larynx folds cranially and the outlet of the esophagus caudally, the “undivided” foregut chamber can be seen.
18	2,75	The anlage of the esophagus and stomach appears. Cranial to that area, an “undivided” foregut chamber can be seen. The lung bud is more advanced and also the liver anlage shows differentiation into two ducts.
19/20	3	The definitive anlage of the lung buds can be seen as a bilateral swelling of the foregut. In addition, the esophagus anlage can be identified with its narrower lumen. The “undivided” foregut is clearly visible.
20/21	3,5	The tracheal anlage appears as a broadening of the ventral foregut. This anlage extends cranially from the larynx to the offspring of the bronchi and is still part of the “undivided” foregut chamber.
22/23	4	The trachea is seen for the first time as a partially isolated structure. Its cranial portion is still part of the foregut chamber. In this age group the trachea is still short and has a triangular shape. The “undivided” foregut chamber becomes smaller but never disappears.
24/25	4,5	The trachea is now a completely isolated structure. The esophagus is clearly separated from the pharynx by the dorsal foregut fold. The differentiation of the distal foregut into its structures larynx/ pharynx/ trachea/ esophagus is complete.
26	5	The “undivided” foregut chamber becomes smaller but never disappears. It will be incorporated into the larynx as the pharyngo-tracheal canal. The tip of the trachea-esophageal fold never reaches the laryngeal folds. The borderline between the pharynx and the esophagus is represented by the dorsal fold of the foregut.

Table 1.4.1. Tracheal development according to the second theory. After (Metzger et al 2011).

4.1.4. Tracheo-esophageal wall formation

The formation of trachea and esophageal wall was the subject of many studies in recent years, mostly because of the congenital diseases affecting this region as tracheo-esophageal fistula. The separation of trachea and esophagus in human embryo occurs between Carnegie stages 13 and 16 (28-37 days post fertilization) and between E11-E12 in mice (Ioannides et al 2010).

In accordance with the theories concerning tracheal development and the foregut division discussed above, there are two theories concerning the trachea-esophageal wall formation.

In the first theory or ”Septation model”, the foregut division is the result of the formation of a septum across the foregut tube. This septum is formed by the fusion of ridges resulting from the active growth of the endodermal epithelium. In a later stage, investigators reported the presence of an apoptotic activity in the fusion area accompanied by necrosis in the central cells of the endodermal septum (Rosenthal 1931; Smith 1957).

In the second theory, or model of “tracheal outgrowth”, the trachea is formed as a separate structure. The tracheo-esophageal is formed through the outgrowth of the respiratory primordium from the caudal end of the laryngeal sulcus of the foregut (Zaw-Tun 1982). In contrast to the first theory, no sign of apoptosis during tracheal-wall formation was observed (Metzger et al 2011).

4.1.5. Trachea from epithelial tube to a complex structure

Mammalian trachea is a complex structure composed of three compounds: pseudostratified epithelium, hyaline cartilage and smooth muscle cells. As detailed in the previous paragraphs, the epithelium of the trachea derives from the endoderm (Whitsett et al 2011). Tracheal cartilage and tracheal smooth muscle layer have a distinct origin than other cartilage and smooth muscle in the neighboring region. In fact, while the cartilage and muscles in tracheal surrounding tissues are derived from the fourth branchial arch (Menéndez et al 2011), the splanchnic mesoderm which differentiates close to the ventral surface of the foregut seems to be the origin of both tracheal cartilage and smooth muscles (Kaufman & Bard 1999).

The first mesenchymal condensations of the future cartilage rings are detectable at 22mm CS. With a differentiation more marked cranially than caudally. At 30mm CS, the rings become hyaline cartilage in the trachea as incomplete rings. At 38mm CS, the cartilaginous rings are finally well defined (Harjeet 2004).

Trachealis or tracheal muscle differentiation occurs after tracheal cartilage differentiation. Harjet *et al.* showed that the primordium of the circular muscle layer is not detectable before 30mm CS. At 42 and 50mm CS the circular muscle coat is well defined, and at 62 mm CS longitudinal bundles of muscle fibres are located posteriorly to circular muscle (Harjeet 2004).

Once the cartilage of the trachea get formed, the circular smooth muscle layer retracts to fill the gaps made by the incomplete tracheal cartilage rings (Sparrow & Lamb 2003). In fact the development of the trachea is a process that needs coordination between the different kinds of tissues. In fact, the loss of smooth muscle cells or cartilage results in an increase in cell number of the second lineage. However, only in bronchi this increase in proliferative rate was accompanied with circumferential expansion of over-proliferated tissues (Hines et al 2013).

4.1.6. Tracheal growth

After all tissues being established, the trachea starts its growth. Several studies performed by Szpinda *et al* showed that, during development, tracheal wall get thicker and tracheal lumen decreases (Szpinda et al 2012a; Szpinda et al 2012b; Szpinda et al 2012c). In one of the study investigating 73 human fetuses of both sexes (39 male and 34 female) and Caucasian origin, Szpinda concluded that:

- The value of tracheal wall thickness ranged from 0.36 ±1.11mm for the first 14 week group to 1.23±0.17mm for the 25 week group of gestation.
- The tracheal wall lumen (proximal internal to external cross sectional area ratio) decreased from 42.61 ±1.11% to 26.78±4.95%.
- The tracheal wall volume rose from 16,.28±4.18mm^3 in fetuses aged 14 weeks to 269, 22±29.26mm^3 in 25 week-old fetuses (Szpinda et al 2012b).

Sexual dimorphism was not seen regarding tracheal size (Szpinda et al 2012b), although sexual dimorphism was reported for thyroid cartilage and glottis opening (Fayoux et al 2008).

4.2. Cellular and molecular bases of trachea development

4.2.1. Interaction between epithelium and mesenchyme

4.2.1.1. Mesenchyme and epithelium

Interaction between mesenchyme and epithelium seems to be crucial for organs development. Trachea and respiratory system are no exception. One study in particular has shown the importance of foregut surrounding mesenchyme in the differentiation of the respiratory

epithelium (Shannon et al 1998). In this study, the authors highlighted the high plasticity of the respiratory epithelium, not only in the lung bud but also in the trachea during early stages of development. This plasticity is revealed when the tracheal surrounding mesenchyme is replaced by the distal lung mesenchyme, since the authors demonstrate that such replacement induces the differentiation of tracheal epithelium into lung epithelium. Thus, the distal lung mesenchyme is capable of reprogramming tracheal epithelium (Shannon et al 1998). Reverse experiments showed that the branching process in lung epithelium totally ceases when the lung mesenchyme is replaced by the tracheal mesenchyme. This demonstrates that tracheal mesenchyme is able to reprogram lung epithelium differentiation (Wessells 1970).

Altogether this data bring strong evidence that the epithelium has a very significant plasticity. However, this plasticity vanishes over time, as it was additionally showed that E16 tracheal epithelium does not respond to signals from E13 lung mesenchyme. Unfortunately, the authors did not investigate further to elucidate the mechanism by which the restriction of induction occurs (Shannon 1994).

4.2.1.2. From mesenchyme to tracheal tube

Even though mechanisms by which the mesenchyme induces epithelium differentiation still require further investigations, many implicated factors has started to be identified during the last few years. These factors have to cross the surrounding mesenchyme to get to the epithelial tube or primitive trachea. And usually their influence is not limited to one type of tissue in trachea.

Fibroblast Growth Factors (FGFs) represent a family of signaling molecules that plays a major role in the development of the respiratory system. FGF effect starts once the foregut gets formed. Early on, it is expressed by the cardiac mesenchyme and it is responsible of defining the respiratory lineage (Whitsett et al 2011). At a later stage, it gets expressed in the lung mesenchyme and impacts on tracheal formation. FGF10 and FGF18 are two FGFs that are particularly implicated in tracheal development, especially tracheal cartilage differentiation and FGF18 in the proper patterning of the trachea (Fig.1.4.3) (Elluru et al 2009).

Another kind of factors is R-spondin2 (Rspo2) (see §4.2.4.5). Rspo2 is expressed in the distal tip mesenchyme and has a function not only in the tracheal and bronchial cartilage, that seems to be the most affected by its absence, but also on tracheal surrounding cartilage as the cricoid ring and arytenoids within the larynx (Bell et al 2008).

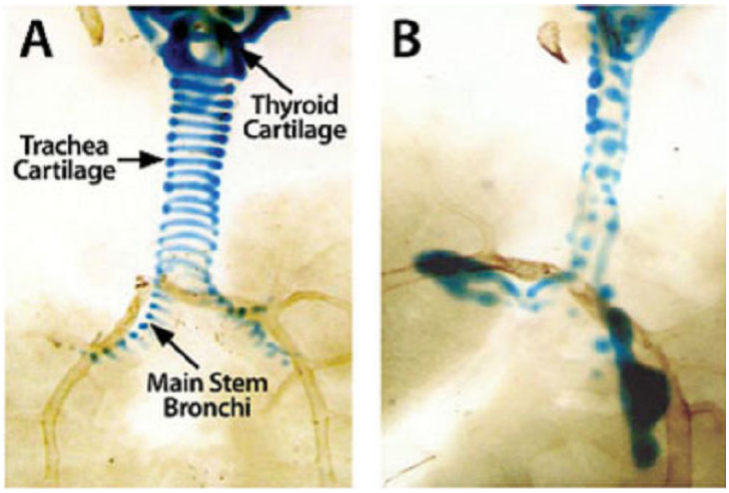

Fig.1.4.3. Alcian blue staining highlights the cartilaginous structures of the larynx and the trachea from E18 wild-type FVB/N (A) and FGF18 overexpressing (B) embryos. From (Elluru et al 2009).

4.2.1.3. Primitive epithelium function: SHH and splanchnic mesoderm

The plasticity of respiratory epithelium makes it susceptible to surrounding mesenchyme signals. And while these signals are known to regulate the development of all tracheal tissues, the contribution of respiratory epithelium in mesodermal differentiation is less studied.

Sonic Hedgehog (Shh) is a glycoprotein whose early secretion from the floor plate and the notochord promotes chondrogenesis of mesenchymal cells of presomitic mesoderm (Zeng et al 2002).

In the developing respiratory tract, it is expressed in the epithelium of the airways from E9.5 to E16.5 in mice (Miller et al 2001) and repressed by FGF10 (Sala et al 2011). Although it is expressed in the epithelium (mostly lung epithelium), its main effects are seen on splanchnic mesenchyme differentiation into tracheal cartilage rings in the developing trachea. Indeed, conditional deletion of Shh in the respiratory epithelium leads to abnormal formation of tracheo-bronchial rings or a complete lack of cartilaginous rings. The spatial expression of Shh seems to be important since its peripheral expression was unable to correct these cartilage defects (Miller et al 2004).

It is worth mentioning that Shh also regulates tracheal cartilage formation in a time dependent-manner. Whether Shh expression in the epithelial lung is crucial for the tracheo-bronchial development between E8.5 and E12.5 in mice (Miller et al 2004), its ablation from the epithelial lung after E13.5 induces no effect on the tracheo-bronchial development.

4.2.2. From epithelial tube to respiratory mucus; NKX2.1/SOX2:

Once the foregut gets formed, a difference between the ventral side or future respiratory system and the dorsal side or the future digestive system can be noticed. In fact, the

epithelium of the ventral side is pseudostratified and tightly packed while the epithelium of the dorsal side is flattened, elongated and loosely connected (Jacobs & Que 2013), which means that the fate of the ventral side and the dorsal side has already been determined.

Study has shown the implication of two main transcription factors in foregut cell fate determination, the first one is Nkx2.1 and the second one is Sox2.

Nkx2.1, also known as Thyroid transcription factor-1 (TTF-1) is a homeodomain transcriptional factor that marks specifically the respiratory epithelium. It is expressed all along the conducting airway, with the highest expression level in basal and secretory cells except goblet cells. It is essential for respiratory epithelial cell differentiation (Perl et al 2002). It is also expressed in all epithelial cells of the lung in early stage of morphogenesis, but with time it gets restricted to two type of cells, Clara cells and alveolar type II cells (Minoo et al 1999).

SOX2 is a transcription factors containing a Sry-related high mobility group (HMG) box, it is expressed in an early stages prior to foregut development. In this period, it plays a role in maintaining cell renewal and pluripotency. Later it is expressed in the endodermal epithelium of the trachea, lung, tongue and esophagus, where SOX2 plays a role in differentiation and morphogenesis. Once the foregut gets formed, *Sox2* expression is at its highest level in the dorsal side of the foregut (future esophagus). This high level of *Sox2* expression leads to the formation of stratified and keratinized epithelium via the regulation of two genes *p63* and *K14* (Que et al 2007). Moreover, *Sox2* expression can also be found at a lower degree in the ventral part of the foregut (future trachea and lung) as its expression shows a gradual antero-posterior decrease. *Sox2* gene is also expressed in the adult trachea and its function is to maintain the level of $P63^{+}$ cells (Que et al 2009).

A reduction in the expression of Sox2 in mice leads to a tracheal-like esophagus, while *Nkx2.1*$^{-/-}$ mice showed a keratinized $P63^{+}$ riche epithelium, with high level of *Sox2* expression. These findings led Que *et al.* to suggest a reciprocal regulation between Nkx2.1 and Sox2 (Que et al 2007)

Que *et al* also found that Fgf10 down-regulates *Sox2* in the ventral foregut and lung and promotes Nkx2.1 expression (Que et al 2009), in agreement with the fact that an E11.5 esophagus in culture respond to FGF10 high level by increasing *Nkx2.1* expression and a decrease in *Sox2* and *p63* expression (Que et al 2007).

4.2.3. Different signals; different type of cells: Tracheal epithelium

4.2.3.1. SPDEF

SPDEF (or SAM pointed domain-containing ETS transcription factor) is widely expressed in the body, mostly in prostate and ovaries and in the epithelium of many other organs.

The pattern of expression of SPDEF and its overlap with Nkx2.1 expression in conductive airway epithelium led investigators to study its role in epithelial airway development and differentiation.

It has been reported that SPDEF is necessary and sufficient for the differentiation of goblet cells from basal and nonciliated columnar epithelial cells (Chen et al 2009), while Park *et al.* have suggested the implication of other factors with SPDEF in goblet cells differentiation (Park et al 2007).

It has been demonstrated that SPDEF binds to the C-terminal domain of Nkx2.1 to coactivate the expression of genes expressed selectively in airway epithelium as Foxj-1, Sox17, Sftpa, Scgb1a1 (Park et al 2007) and to regulate the expression of a group of genes involved in the synthesis, glycosylation and packaging of mucus in submucosal gland and in goblet cells where it is selectively expressed (Whitsett et al 2011).

4.2.3.2. Notch signaling

Notch in mammals has four types of receptors and five types of ligands, it exerts its effect via two Notch downstream target genes Hes and Hey (Radtke & Raj 2003). It has been reported that Notch controls the fate of many cell types within the body and in many species (Liu et al 2007).

In respiratory airway, it has been demonstrated that Notch1 signaling is implicated in goblet cells and in the secretory lineage differentiation in airways (see Fig.1.4.3). While Notch seems to share this function with SPDEF, it is still not known if Notch is expressed before or after the expression of SPDEF (Rock et al 2010). The loss of Notch activity is marked by an increase in ciliated cell population in upper airway with a total ablation of Clara cell secretory lineage. However, no changes in proliferation or cell death were observed in Clara cell population. In addition, Notch signaling affect goblet cells, where these last one showed to be metaplasic, when there is excess of Notch signaling (Guseh et al 2009; Tsao et al 2009).

4.2.3.3. Foxj1

Foxj1 is a member of the forkhead transcription factor family. Its expression is essential for the differentiation of ciliated cells in airway epithelium because of its function in the assembly of the ciliated apparatus in epithelial cells (Roy 2009).

In the epithelium, Foxj1 expressing cells are responsible of the induction of Notch1 signaling, which suggest that Clara cells in the lateral part of trachea is the result of Notch1 inhibition, in the absence of foxj1 signaling (Morimoto et al 2010).

4.2.3.4. P63

The most important role of P63 as a transcription factor is seen in the epithelium of digestive system, where it is responsible of the development of keratinized stratified epithelium (Seery & Watt 2000), and where it regulates the expression of many genes implicated in shape, survival, proliferation and adhesion of epithelial cells (Carroll et al 2006).

Moreover, p63 transcription is also required for tracheal basal cells, which are the main progenitor cells in large conducting airway, seen as a discontinuous population of $P63^{+}$ cells. (Daniely et al 2004). The loss of p63 leads to the formation of tracheal epithelium mainly composed of ciliated cells with no basal cells (Daniely et al 2004). Nevertheless, even though *p63* expression is down regulated by FGF10 in the ventral part of the foregut, *p63* expression is sufficient to maintain the presence of basal cells in the region of the trachea that also expresses selectively SOX2 and NKX2.1 (Rock et al 2010).

4.2.3.5. Sox9

Although it has been reported that SOX9 has no direct influence on the differentiation or formation of epithelial cells of the trachea, and that its function seems to be restricted to the cartilaginous part (see paragraph 4.2.4.4), it seems important to note that in *Sox9* mutant mice tracheal epithelium was also altered. This alteration is marked by a reduction of the number of basal and goblet cells and an increase in Clara cells (Turcatel et al 2013).

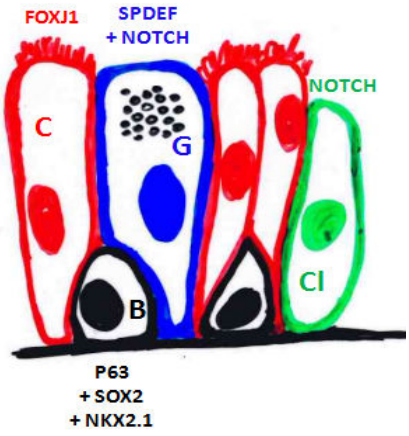

Fig.1.4.4. Transcription factors implicated in tracheal mucous differentiation. (C) for Ciliated cells presented in red, (G) for Goblet cells presented in blue, (B) for basal cells presented in black, (Cl) for Clara cells presented in green.

4.2.4. Cartilage to be

4.2.4.1. Shh

As already briefly mentioned (see 4.2.1.3. section), Shh has a well known function in promoting chondrogenesis in presomitic mesoderm (Zeng et al 2002). Another well known function of Shh is regulating chondrogenesis in tracheal cartilage via Sox9 (see below).

At first SHH becomes biologically active when it is autoproteolytically cleaved, the active N-terminal fragment of SHH (SHH-N) binds to its receptors Patched-1(Ptch-1) or Patched-2 (Ptch-2). The receptor-ligand binding relieves constitutively PTCH1-mediated inhibition and activates Smoothened (SMO) protein complex (Lewis et al 2001), which in turn leads to the activation of Gli genes (Gli1, Gli2, and Gli3) (Villavicencio et al 2000). The GLI proteins translocate to nucleus and bind to SHH-responsive element (Hammerschmidt et al 1997).

A study where Shh is conditionally deleted in the respiratory epithelium showed that the spatial and the severity of associated defects is time dependent, as the deletion of Shh before E12.5 affect the morphogenesis of peripheral lung mostly, while Shh epithelial signaling to the surrounding mesenchyme seems to be most crucial for tracheal patterning in the gap between E8.5 to E12.5. In these mice, the cartilage of trachea and bronchi was malformed, these malformations were also accompanied with tracheo-esophageal fistulas (Fig.1.4.5) (Miller et al 2004).

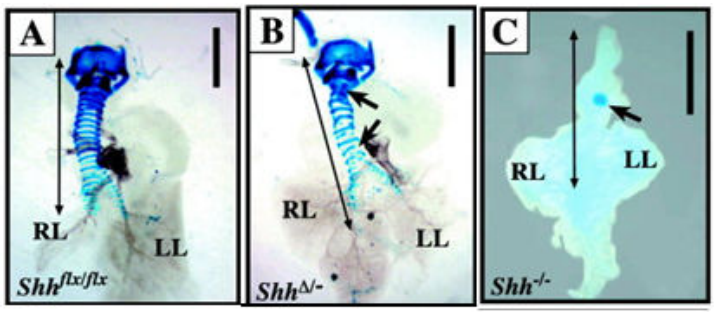

Fig.1.4.5. Alcian blue staining revealed abnormal tracheal–bronchial cartilage patterning in *Shh*$^{\Delta/-}$ mice. From (Miller et al 2004).

A: Tracheal rings in control littermates *Shh*$^{flx/flx}$ form an almost complete circle and are attached dorsally to a fibrous membrane. **B:** Alcian blue staining revealed abnormal tracheal–bronchial cartilage patterning in *Shh*$^{\Delta/-}$ mice wherein tracheal rings 1–4 fail to connect ventrally (arrows). Various rings along the length of the trachea were incomplete or misaligned. **C,D:** The tracheoesophageal fistula observed in *Shh*$^{-/-}$ (C)

Another evidence of the importance of SHH expression to normal foregut formation is VACTERL syndrome where SHH expression is disrupted, in addition to many deformities patients suffering from VACTERL syndrome are diagnosed with tracheo-esophageal deformities (Kim et al 2001; Oldak et al 2001). These deformities are reproduced in animal

model were pregnant rats are treated with Adriamycin, which leads to a reduction in Shh expression level (Arsic et al 2003).

Cartilage lesions can also be detected when Gli gene was mutated, in fact the $Gli2^{-/-}$ and $Gli2^{-/-}$,$Gli3^{+/-}$ showed an hypoplastic tracheal cartilage (Motoyama et al 1998). The theoretical effect of Gli absence was thought to be more drastic than the practical effect seen in experience. Park explained this finding in his study, by suggesting that Shh can regulate Sox9 expression directly via Gli and indirectly via Bmp4 and Noggin regulation (Fig.1.4.8), or the presence of a compensatory pathway (Park et al 2010b).

4.2.4.2. Fgf10, Tbx4 and Tbx5

FGF10 is another member of the family of FGF that is crucial for the embryonic development of many organs including the lung; FGF10 seems to be more implicated in lung formation and branching process than in trachea formation. In fact, $Fgf10^{-/-}$ mice die at birth, due to lung deformities although, trachea formation occurs (Sekine et al 1999). However, trachea does not seem to be normally developed in Fgf10 deficient mice, where the Fgf mutation has its bigger impact on the cartilaginous compound of the trachea. Sala (Sala et al 2011) demonstrated in his study that Fgf10 controls the proper patterning of tracheal mesenchymal differentiation and has no effect on the induction of cartilage differentiation, and that its effects is exerted through the induction of periodic pattern of Shh expression in the ventral epithelium between E11.5 and E13.5. The critical function of FGF10 in tracheal cartilage patterning are confirmed by Tiozzo (Tiozzo et al 2009) in Fgf10 deficient mice affected by what looks like Apert syndrome. Although, Apert syndrome is the result of gain of function mutation in the Fgfr2 gene coding for Fgf10 receptor and expressed in mesenchymal cells rather than Fgf10 mutation (Fig.1.4.6). However, the ectopic expression of Fgfr2b leads to the same features found when Fgf10 is over-expressed (Bochukova et al 2009; Cohen & Kreiborg 1993; Lumaka et al 2014). Interestingly, the reduction of Fgf10 expression level corrects the phenotype found in Apert syndrome and associated to Fgfr2b gain of function mutation (Hajihosseini et al 2009).

While tracing the effect of Fgf10 on its main receptor in embryogenesis which is the Fgfr2b, one study demonstrated that FGF10 signaling acts up stream β-catenin signaling (see Wnt signaling) to control the expression of its receptor in addition to Tbx4 (Tiozzo et al 2009).

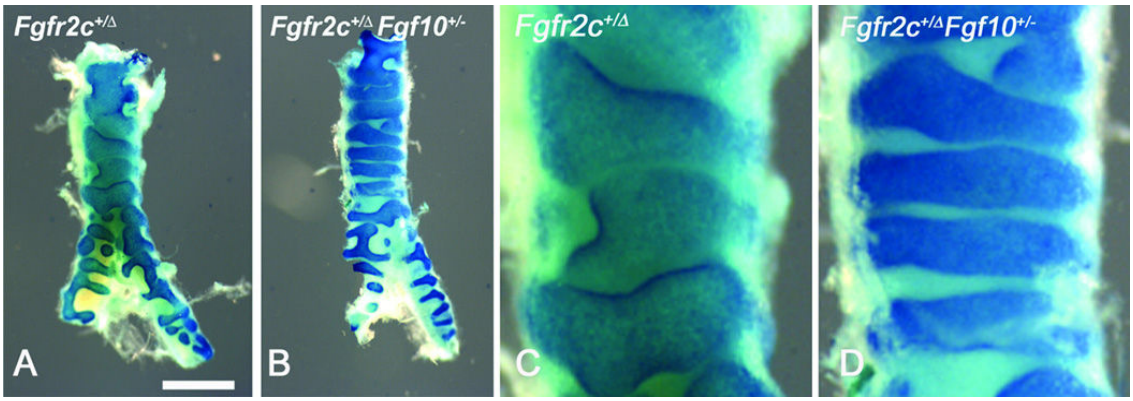

Fig.1.4.6. Heterozygous knockdown of *Fgf10* levels partially rescues the tracheal cartilage phenotype of *Fgfr2*$^{+/\Delta}$ lungs. From (Tiozzo et al 2009)

(A) *Fgfr2c*$^{+/\Delta}$ trachea at PO showing excessive expansion of the cartilage with absence of non-cartilaginous mesenchyme. (B) [*Fgfr2c*$^{+/\Delta}$; *Fgf10*$^{+/-}$] neonates tracheas show a rescue of the tracheal defects. (C and D) High magnification of a and B respectively.

Tbx4 is a member of T-box transcription factor genes characterized by a conserved DNA-binding T-box domain that binds to the T-box binding element (Naiche et al 2005), Tbx4 expression can be detected in the lung and trachea mesenchyme at E12.5 and later in mice embryo. However, to exert its function Tbx4 interacts with another member of T-box transcription factor, Tbx5, that is also expressed in the tracheal and lung mesenchyme at the same embryonic stages (Chapman et al 1996). Indeed, Tbx4 and Tbx5 interact to regulate lung branching. This function is FGF10-dependent. Also, Tbx4 and Tbx5 interact in the formation of mesenchymal condensation in the trachea and bronchi (Fig.1.4.7). This function is independent of FGF10 signaling (Arora et al 2012).

It is worth mentioning that Tbx5 has a function in the specification of trachea and lung at early developmental stage, independently of Tbx4 (Arora et al 2012).

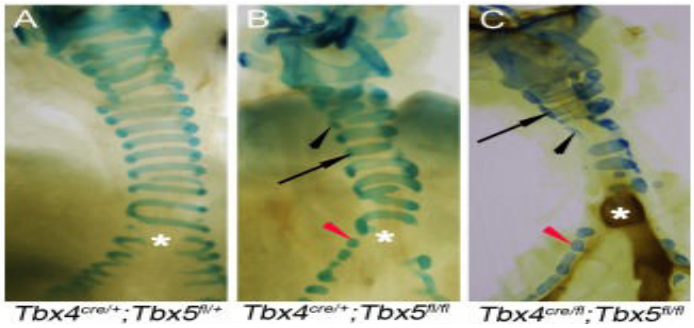

Fig.1.4.7. Alcian blue staining used to visualize tracheal/bronchial cartilage. From (Arora et al 2012).

(A–G) Alcian blue staining was used to visualize tracheal/bronchial cartilage. Ten-eleven cartilage rings were seen in control tracheas (E18.5, A); normal (arrow) and incomplete rings were seen in tracheas and bronchi (black and red arrowheads respectively) of lung-specific *Tbx5* null (E18.5, B) and lung-specific *Tbx4* heterozygous;*Tbx5* nulls (postnatal day (P) 0, C). Asterisks in (A–C) indicate the point of bronchial separation from the trachea.

4.2.4.3. BMP4, BMP2 and Noggin

Bone Morphogenetic Protein 4 and 2 (BMP4, BMP2) are members of the Bone Morphogenetic Protein family, which is part of the Transforming Growth Factor-Beta superfamily; BMP signaling is essential for a normal trachea development, with esophageal atresia and tracheo-esophageal fistula as main consequence of impaired BMP signaling (Que et al 2006).

BMP4 and BMP2 have been reported as pro-chondrogenic molecules. The expression of BMP4 is detected in the ventral foregut mesenchyme that surrounds the lung buds and future trachea (Weaver et al 1999). While BMP2 expression was fairly expressed all over the mesenchyme (Que et al 2006).

The regionalized expression pattern of BMP4 suggests that it might be of great importance for the proper development of anterior foregut. In fact, the absence of Bmp4 leads to type II of Floyd disease characterized by complete tracheal agenesis, with normal bifurcation (Li et al 2008). BMP4 exerts its functions all over the body through many signaling pathway, as P38 MAPK (Kendall et al 2005), Ras, Erk (Haynes et al 2007) and Smad1/5/8 (Aubin et al 2004).

The early respiratory system marker Nkx2.1 was normally expressed in *Bmp4*-deficient mice which led the investigators to assume that the effect of BMP4 is mostly implicated in the outgrowth of the trachea. The overlapping expression fields at E11.5 of Bmp4 and Sox9 in wild type trachea suggest an interaction between these two genes (Park et al 2010b).

The importance of BMP4 in trachea development was deduced after a serious of studies where BMP4 expression was disrupted. On the other hand, BMP4 importance in tracheal development can also be deduced when Noggin is ablated. Noggin is BMP antagonist. In the anterior foregut, Noggin is expressed in the dorsal side in the single cell layer epithelium at E9.5 (Que et al 2006), where it is secreted and diffused into the extracellular-matrix to bind and inactivate BMP, this function is essential for proper foregut development as 70% of homozygous null for Noggin in mice are presented with esophageal atresia/tracheo-esophageal fistula (EA/TEF) (Fig.1.4.8), and cartilage nodule in the stomach and esophagus. These defects thought to be related to defect in SHH originated from the notochord, as SHH expression is not altered in the epithelium of the ventral foregut (Que et al 2006).

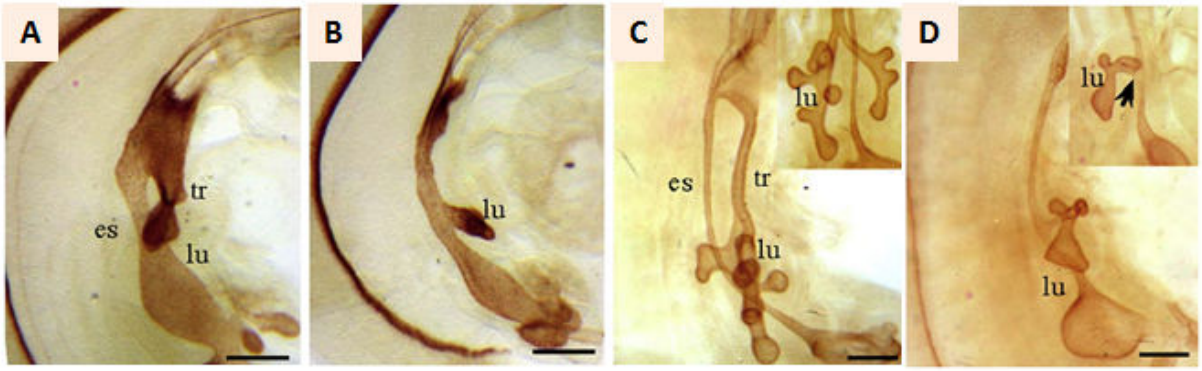

Fig.1.4.8. BMP4-deficient foregut displays loss of trachea. From (Li et al 2008).

$Bmp4^{cKO}$ embryos display a single tube and hypoplastic lungs, at E10,5 (B) and E11,5(D) While wildtype embryos display two distinct gut derivatives. The esophagus and trachea (A,C).

Foxf1, a member of the forkhead transcription factor family, might be another way by which BMP governs tracheal development. BMP4 can regulate Foxf1 expression positively as demonstrated by Tseng (Tseng et al 2004) in Xenopus embryo. Also, Foxf1 haploinsufficiency in CD1 outbred mouse genetic background shows a thinner and narrower esophagus and tracheal cartilage deformities (Fig.1.4.9) (Mahlapuu et al 2001).

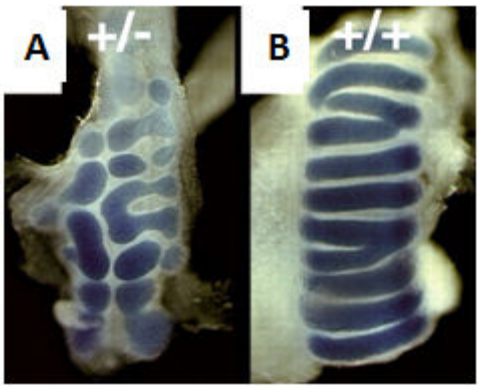

Fig.1.4.9. Ventral view of Alcian Blue-stained tracheas from E18.5 Foxf1+/− (A) and wild-type (B) fetuses. From (Mahlapuu et al 2001).

The C-shaped cartilaginous rings, which are segmentally arranged along the trachea, are replaced by irregular, hypoplastic patches of cartilage in Foxf1+/− embryos

Li et al in their study shows that this outgrowth is not dependent on Wnt canonical signaling, and happens through Erk signaling activation (Li et al 2008). Despite the divergence in BMP4 and WNT signaling this last one is crucial for tracheal development.

4.2.4.4. SOX9

Sox9 is a transcription factor containing the high-mobility-group (HMG) DNA-binding domain. It is essential for chondrogenesis, from the early step of mesenchymal condensation

till the terminal differentiation. In fact, the inhibition of Sox9 in early stage prior to the mesenchymal condensation inhibits cartilage formation, while the inhibition of Sox9 after the occurrence of condensation leads to the arrest of differentiation (Akiyama et al 2004). The dosage of SOX9 has also been shown to be important for cartilage formation. In fact $Sox9^{+/-}$ mice show abnormal cartilage formation, including tracheal cartilage (Bi et al 2001). In addition, the overexpression of Sox9 leads to chondrodysplasia due to the inhibition of chondrocytes proliferation (Akiyama et al 2004).

In accordance with its general function, Sox9 has been suggested as an important factor in specifying spatiotemporal patterning of tracheal cartilage primordia in early tracheal development (Fig.1.4.10) (Elluru & Whitsett 2004).

Sox9 is regulated by SHH via the bias of BMP4 and NOGGIN, the regulation of Sox9 expression is done both directly through Gli1 and indirectly through interaction with the pro-chondrogenic BMP4 (Park et al 2010b).

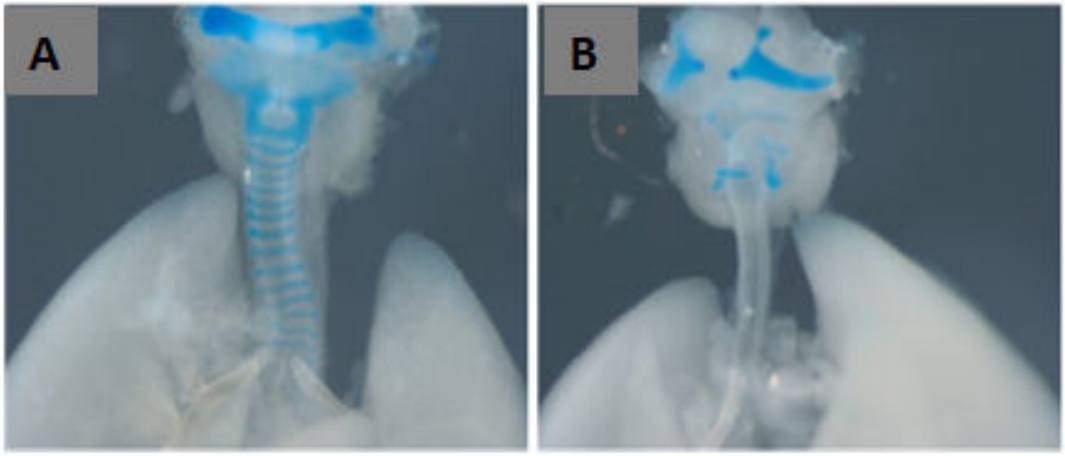

Fig.1.4.10. Lung phenotype after mesenchymal *Sox9* knockout. From (Turcatel et al 2013).

(A) Pups were collected at birth. Mutant pups died less than an hour after birth, and showed gasping, retractions, and cyanosis. **(B)** Mutant pups did not survive postnatally.

4.2.4.5. Wnt canonical signaling or non canonical signaling; this is the question?!

WNT is a large family of cysteine-rich secreted glycoprotein; members of this family are expressed in adulthood stage as well as in early developmental stage in a different pattern. WNTs are critical for proliferation, differentiation and thereby organogenesis, the majority of Wnt signaling occurs through what is referred to as Wnt canonical pathway. The Wnt receptor formed of frizzled a 7- transmembrane domain receptor, and a low density lipoprotein receptor related protein (LRP), once this complex is activated by Wnt the intracellular protein Disheveled promotes the inhibition of a destruction complex conposed of three proteins: Axin, APC (adenomatous polyposis coli) and GSK3 (glycogen synthase kinase 3). Once this

destruction complex is inhibited, β-catenin accumulate in the cytoplasm to be translocated in further time to the nucleus where it interacts with the T cell factor/ Lymphoid enhancer factor (TCF/LEF) to regulate the transcription of Wnt target genes (Nusse et al 2008).

Two members of this family seem to be actively involved in respiratory tract development: Wnt5 and Wnt7, with Wnt7b being the only autocrine-paracrine member of Wnt family with restricted expression to the epithelium in developing lung (Weidenfeld et al 2002). The activity of this Wnt is associated in defining ventro-dorsal and antero-posterior polarity axis in developing limb as found in Wnt7 KO mice (Parr & McMahon 1995). Wnt7 promoter can be activated by Foxa2, TTF-1 and GATA6 (Weidenfeld et al 2002). While Wnt7b expression is restricted to the epithelium the Wnt5 expression pattern shows a switch in the time from the mesenchyme where it is expressed in early time at E12 to the epithelium, the expression pattern of Wnt5a is presented in the Fig.1.4.11.

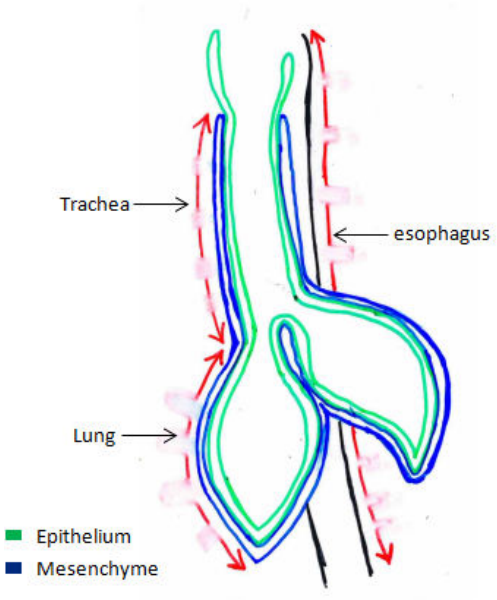

	E 12	E 16	E 18
Lung	+ +	++ ++	+++ +
Trachea	+ ++	+++ +	+++ +
esophagus	+ ++	+++ +	

Fig.1.4.11. WNT5a repartition in the tracheal and lung Epithelium (green) and mesenchyme (blue) at E12, 16 and 18.

B-catenin expression in trachea was detected between E14.5 and E18.5 where its expression in trachea is mostly detected in the epithelial layer. Nevertheless, the most remarkable feature of the respiratory tract in β-catenin KO mice is a transformation of the lung into trachea-like structure. In addition, the absence of β-catenin did not affect the expression of Shh nor Nkx2.1 in the lung (Mucenski et al 2003).

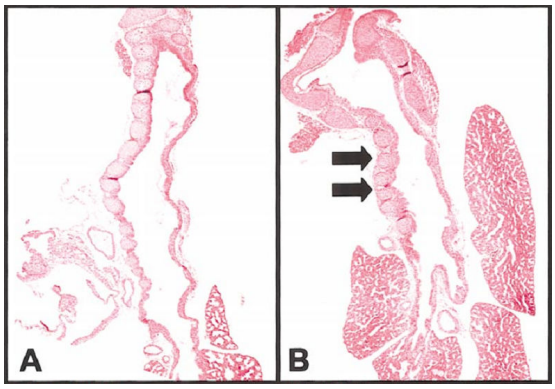

Fig.1.4.12. Histology of the Wnt5a-/- and control lungs. From (Li et al 2002)
(A, B) Sagittal sections of the E18 control trachea and Wnt5a (-/-) trachea, respectively, are shown with H&E staining. The number of cartilage rings was 16 for the control and 8 for the Wnt5a-/- trachea.

The expression pattern of β-catenin suggests that the effect of Wnt canonical signaling in the trachea must be the most drastic in the epithelial layer. However, this suggestion does not fit with the defective features of respiratory tract found in Wnt5a KO. In fact, *Wnt5a*$^{-/-}$ respiratory tract is characterized by a foreshortened trachea and a remarkable reduction in cartilage ring number (Fig.1.4.12), without affecting the mucous layer, which has a normal aspect. In addition, the absence of Wnt5a is accompanied with BMP4 and SHH overexpression, as previously mentioned, but Shh expression was not affected in β-catenin mouse KO (Li et al 2002). This unexpected divergence can be the outcome of another signaling pathway followed by Wnt5, as Wnt5a is known to follow the phosphatidylinositol non-canonical pathway (Gavin et al 1990). In addition, WNT canonical pathway can be activated independently of Wnt through R-spondins.

R-spondins is a new family of ligands that can activate the Lrp6 mediated pathway, Rspo2 is expressed in the distal tip mesenchyme. Fetuses who do not express Rspo2 showed laryngeal and trachea-bronchial abnormalities. The tracheal cartilage rings in these fetuses are malformed or absent (Fig.1.4.13) (Bell et al 2008).

Rspo2 exhibits its function on tracheal cartilage via the canonical WNT pathway, and via potentiating the WNT1 and WNT3a signaling, to activate the canonical WNT signaling. Rspo2 interacts with many factors as Lrp6 (Fig.1.4.13) and Fzd1, Fzd2, Fzd4, Fzd5 and Fzd8 (Kazanskaya et al 2004; Nam et al 2006; Weidenfeld et al 2002).

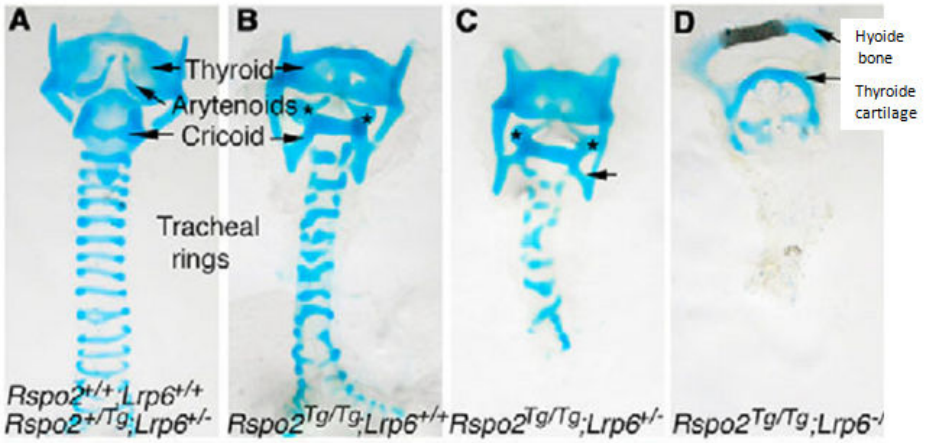

Fig.1.4.13. Laryngeal-tracheal-bronchial and lung malformations in Rspo2/Lrp6 mutant mice. From (Bell et al 2008)

(A-D) Alcian Blue stained cartilages in the larynx, trachea and bronchi from E18.5 fetuses of indicated genotypes. Asterisks in B and C indicates the fusion of the arytenoids to the cricoid cartilage. (C) Arrow indicates the cricoid; cartilage is absent on the dorsal aspect of the ring. Also observed in B and D.

4.2.4.5. HOXa5

Hoxa5 gene belongs to the large family of the HOX genes which contains 39 members of transcription factors that regulate, the transcription of others genes through the DNA-binding homeodomain, the down-stream genes are morphogenetic genes that regulate antero-posterior body axis (Krumlauf 1994; van der Hoeven et al 1996).

Many members of HOX genes are essential for life as Hoxa-1, Hoxb-1, Hoxa-2, Hoxb-2 Hoxa-3, Hoxd-3, Hoxb-4, Hoxc-4 and Hoxa-5 (Stein et al 1996).

Among HOX genes, Hoxa-5 and its paralog the Hoxb-5 are the most related to the respiratory tract development and proper patterning. While Hoxb-5 is mostly related to lung development where it is expressed in the mesenchymal layer, Hoxa-5 expression is more extended in the developing airway, where in addition to its expression in the lung mesenchyme it is also expressed in the tracheal mesenchyme and have an essential function in tracheal cartilage patterning in addition to the partially redundant function of Hoxb-5 in the lung (Boucherat et al 2013).

In fact, Hoxa-5 expression can be detected in various tissues including spinal cord and the mesenchymal compound not only of the lung and trachea but also intestine, stomach and kidneys (Dony & Gruss 1987; Gaunt et al 1988).

Hoxa-5 KO mice show a high rate of perinatal lethality and show vertebral defects (Jeannotte et al 1993) and respiratory distress at birth accompanied with laryngotracheal airways obstruction and abnormal pulmonary histology. The reason of death in Hoxa-5 KO mice is likely related to tracheal occlusion. In fact KO trachea is narrower and less extended dorsally

than the trachea of WT mice. In addition KO trachea shows an abnormal banding pattern, a reduction in the number of formed cartilage rings and a fusion between the cricoid and the first cartilage ring (Fig.1.4.14) (Aubin et al 1997b).

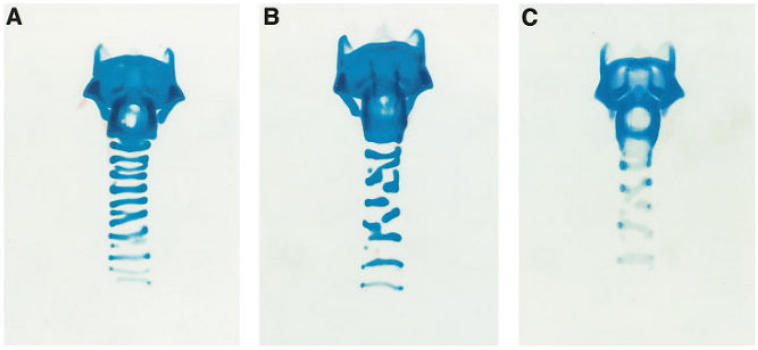

Fig.1.4.14. Laryngotracheal malformations in Hoxa-5 mutant newborn mice. From (Aubin et al 1997b).
Frontal views of a control wild-type (A) and two homozygous mutant newborns (B and C). Alcian blue staining revealed cricoid malformation, disorganized bandling pattern and narrowing of the trachea in all mutant specimens. The number of tracheal rings formed was reduced and the cartilage did not extend dorsally in the mutants when compared to control.

On the molecular level Nkx2.1 expression was reduced in KO mice, which suggest that Hoxa-5 exerts its function on epithelial Nkx2.1 via epithelial-mesenchymal interaction (Aubin et al 1997b).

4.2.4.6. Retinoic Acid

All-trans retinoic acid (RA, ATRA) is a pleiotropic activation factor that derives from Vitamin A (all-trans-retinol) and its esters. RA regulates a large panel of genes associated with normal vertebrate cellular process such as cell differentiation, cell proliferation, apoptosis and embryonic development (Evans & Kaye 1999).

Considering the highly diverse effects of RA, it is predictable that its absence would generate serious defects. This effect was studied by targeting retinoic acid receptor (RAR) genes. In fact all null mutations of RAR lead to lethality *in utero* or shortly after birth (Lohnes et al 1994).

Regarding the trachea, no matter what was the type of RAR targeted mutation, every compound mutant showed tracheal cartilage malformation (Fig.1.4.15) (Mendelsohn et al 1994).

The effect on RA on the respiratory tract development may occur by regulating Hox genes, as seen by a study conducted on lung explants. The author demonstrated that RA increases the proliferation rate in both mesenchymal and epithelial layers, and while the RA effect on

mesenchyme was direct, its effect on epithelial layer occurs indirectly through mesenchymal-epithelial interactions.

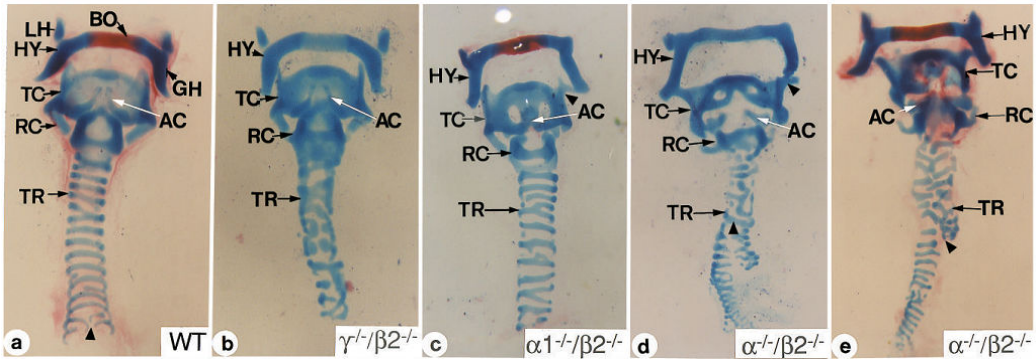

Fig.1.4. 15. Whole mounts of tracheas and hyoid bones derived from E18.5 mutant and wild-type fetuses stained with alcian blue and alizarin red. From (Mendelsohn et al 1994)

(a). A wild type trachea with hyoid bone attached. (b). The trachea and hyoid bone from a β2/γ mutant fetus. (c). The trachea and hyoid bone from α1β2 fetus. The fusion between the thyroid cartilage and the lesser horn of the hyoid bone is denoted by a black wedge. (d). The trachea and hyoid bone from αβ2 fetus. The premature bifurcation of the tracheal cartilage and the fusion between the lesser horn of the hyoid bone and the thyrovd cartilage are indicated by black wedges. (e). The trachea and hyoid bone from αβ2 fetus. The black wedge indicates the premature bifurcation of the right stem bronchus and the premature termination of the left stem bronchus.

Whether on mesenchyme or epithelium, the effect of RA can be related to Hoxa5 (see 4.2.4.5). RA was demonstrated to activate Hoxa5 expression by activation of Hoxa4 expression, in the same study, also RA was able to extend the expression zone of these two genes (Packer et al 2000).

4.2.4.7. CaV3.2

$Ca_v3.2$ is a T-type voltage-gated Ca^{2+} channel expressed in both cartilage and bone during endochondral development (Shao et al 2005). Recently, it has been demonstrated that these channels are of main interest in tracheal cartilage development as $Ca_v3.2^{-/-}$ mice are born with incomplete cartilage ring. This defect can be detected at E14.5 only the tracheal cartilage was defective in these mice, while all other cartilage type remains healthy (Fig.1.4.16).

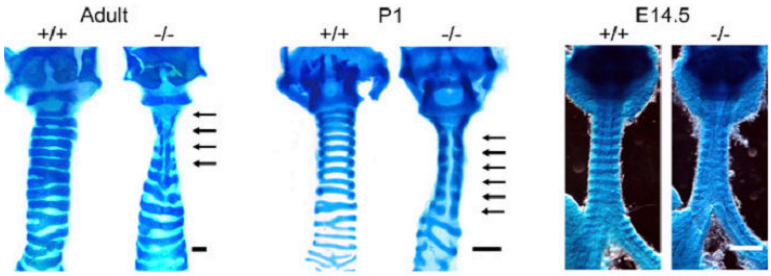

Fig.1.4.16. $Ca_v3.2^{-/-}$ mice show abnormal tracheal development. From (Lin et al 2014).

Alcian blue staining of Wt and $Ca_v3.2^{-/-}$ cartilaginous rings in tracheas of 12-wk-old mice (adult), postnatal day 1 mice (P1), and E14.5 embryos. Arrows indicate incomplete cartilage.

$Ca_v3.2$ regulates the tracheal cartilage development through activation of *Sox9*. In fact, the Ca^{2+} flux through these channels activates the calcineurin/nuclear factor of the activated T-cell (NFAT) signaling pathway, NFAT binds to *Sox9* promoter and induces its expression.
And while *Sox9* has a wide array of functions (see 4.2.4.4), $Ca_v3.2$ affects the differentiation process utmost with no alteration of neither the proliferation nor the apoptosis of mesenchymal cells responsible of cartilage formation (Lin et al 2014).

4.2.4.8. TRAF4

Tumor necrosis factor Receptor Associated Factor 4 (TRAF4) belongs to the TRAF family of proteins, formed of 6 members (Wajant et al 1999).
The absence of TRAF4 leads to impaired neural tube closure, malformation of axial skeleton and tracheal cartilage ring disruption. This disruption is mainly localized in the first six tracheal cartilage rings (upper part of the trachea). It is worthy to mention that there was no defect neither in cricoid cartilage or thyroid cartilage (Fig.1.4.17) (Régnier et al 2002).

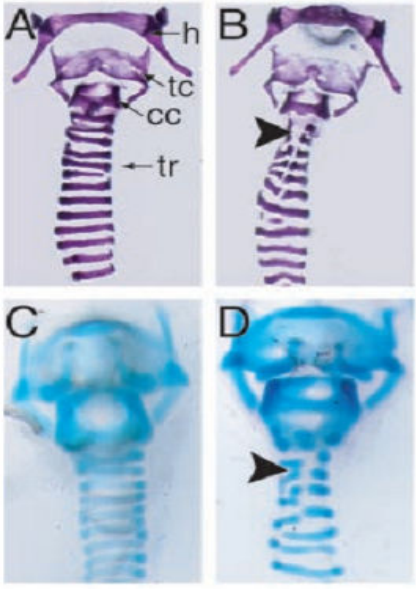

Fig.1.4.17. Cartilage defects in traf4$^{-/-}$ embryo and adult mice. From (Régnier et al 2002).
(A-D) Frontal views of traf4$^{+/+}$ (A and C) tracheas and attached hyoid bones from adult (A and B) an newborn (C and D) mice. Cartilage staining revealed a focal narrowing of the rostral trachea with disorganization of the C-shaped cartilaginous tracheal rings (tr) (B and D, arrowheads), resulting in stenosis in all mutant specimens.

In fact homozygous mutation of TRAF4 in mice is lethal in third of the cases, while the remaining two third reach adult age but with developmental abnormalities as respiratory disorder and axial skeleton deformities (Régnier et al 2002).

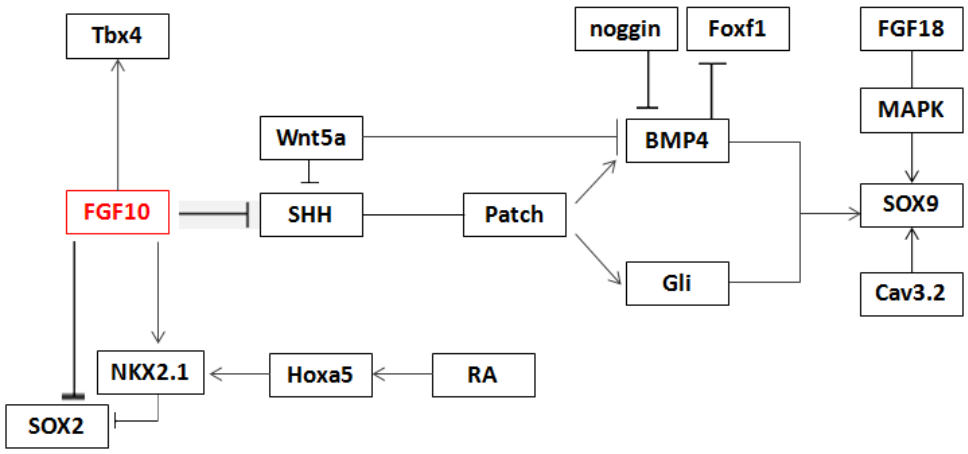

Fig.1.4.18. Schematic summarizing the network of the molecules involved in tracheal cartilage formation.

4.2.5. Smooth muscle to be:

4.2.5.1 SOX2

Sox2 mutant mice shows big anomalies concerning the tracheal cartilage, seen as a reduced number and deformed tracheal, and an expansion of smooth muscle cells area to cover a big part of the ventral side of the trachea at E15.5 (Que et al 2009) (see Fig.1.4.19).

4.2.5.2. TMEM16

Anoctamin1, known also as Tmem16a, is a calcium activated chloride channel, formed of eight predicted transmembrane domains and C-terminal domain of unknown function.

While in pathology, Tmem16a seems to be involved in squamous cells carcinoma and gastrointestinal stromal tumors (Huang et al 2006; West et al 2004), under physiological circumstances Tmem16a expression was detected in epithelial cells of many organs as liver, kidney, salivary gland, pancreas and lung, in surface epithelium, as in submucosal gland with a higher level in mucous cells than from serous cells (Sondo et al 2014). In respiratory tract, murine Tmem16a is expressed in the developing tracheal smooth muscle layer.

In vivo studies showed that TMEM16a can be found in a variety of muscular tissues as cardiac and skeletal muscle. In contrast, the expression of Tmem16a has not been identified in the chondrogenic lineage of the trachea (Rock et al 2008).

Tmem16a KO mice showed an overexpansion of the trachea with abnormal trachealis, unproperly stratified epithelium with the nuclei at the proximal side of the basement membrane, and lack in differentiation or displaced chondrocytes. The expression pattern of Sox9 was not disturbed in these mice which suggest that trachealis SMC or epithelial cells are responsible for the disruption in cartilage formation (Rock et al 2008) (see Fig.1.4.19, A, B and C)

4.2.5.3. Notch signaling versus Fgf10

It has been suggested by Morimoto *et al* that the difference between the expression of Fgf10 and Notch1 separate the fate of vascular smooth muscle cells from para-bronchial smooth muscle cells. Morimoto highlighted in his work the importance of Notch1 in the formation of vascular smooth cells around the lung (Morimoto et al 2010). Also it has been reported by Mailleux in 2005 that smooth muscle in bronchi formation are dependent of Fgf10 (Mailleux et al 2005). Both authors did not discuss the formation of smooth muscle in trachea.

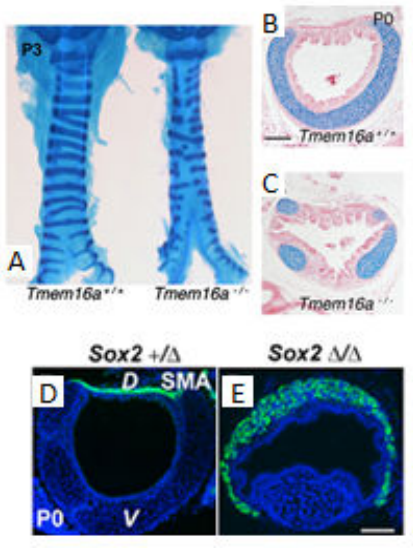

Fig.1.4.19. Trachealis deffects in Tmem16a -/- (A, B,C) and Sox2-/-(D, E).

(A) Ventral view of whole mount tracheae from 3 day-old (P3) wild type and Tmem16a−/− pups stained with alcian blue to reveal tracheal cartilage rings. Gaps are observed along the ventral aspect of mutant tracheae. (B, C) Transverse sections of a newborn wild type and Tmem16a$^{-/-}$tracheae stained with alcian blue and eosin demonstrated multiple lateral cartilage elements with intervening epithelial evaginations in mutants instead of a single ventrolateral cartilage ring. After(Rock et al 2008) (D,E) Immunostaining with anti-SMA antibody to show ectopic expression of smooth muscle actin in the ventral side of the trachea in mutants. After (Que et al 2007).

Gene symbol	Gene name	Expression pattern	Phenotype	Refrence
Fgf9	Fibroblast growth factor 9	Epithelium and pleura	Impaired branching, reduced mesenchyme	(Colvin et al 2001)
Shh	Sonic hedgehog	Epithelium	Impaired branching, tracheoesophageal fistula	(Litingtung et al 1998)
Wnt7b	Wingless-related MMTV integration Site 7B	Epithelium	Vascular defect, reduced mesenchyme	(Shu et al 2002)
Catnnb1	β-Catenin	Epithelium	Impaired branching, proximal/distal specification	(Mucenski et al 2003)
Wnt5a	Wingless-related MMTV integration Site 5A	Mesenchyme and epithelium	Increased branching, tracheal defect	(Li et al 2002)
Traf4	Tnf receptor associated factor 4	Not reported	Tracheal defect affecting the first 6 cartilage rings	(Régnier et al 2002; Shiels et al 2000)
Foxa1/Foxa2	Forkhead box A1/A2	Epithelium	impaired branching, reduced smooth muscle	(Wan et al 2005)
Hoxa5	Homeobox A5	Mesenchyme	impaired branching, narrowing of trachea reduction in cartilage rings	(Aubin et al 1997a)
p63	Transformation-related protein 63	Epithelium	Tracheobronchial defect	(Daniely et al 2004)
Titf-1	Thyroid transcription factor 1	Epithelium	Loss of distal lung fate, imparied branching, tracheoesophageal fistula	(Kimura, Hara et al. 1996)
Crh	Corticotropin releasing hormone	Epithelium	Defective epithelial and mesenchymal maturation	(Muglia et al 1999)
Gli2/Gli3	GLI-Kruppel family member GLI2/GLI3	Mesenchyme	Lung agenesis	(Motoyama et al 1998)
Gli2$^{-/-}$,Gli3$^{+/-}$	GLI-Kruppel family member GLI2/GLI3	Mesenchyme	Esophageal atresia, tracheosophageal fistula, severe lung phenotype	(Felix et al 2004)
Gli2$^{-/-}$,Gli3$^{-/-}$	GLI-Kruppel family member GLI2/GLI3	Mesenchyme	No formation of esophagus, trachea, Lung	(Felix et al 2004)
Sox2	SRY (sex determining region Y)-box 2	Epithelium	Tracheal defects	(Que et al 2009)
Sox9	SRY (sex determining region Y)-box 9	Mesenchyme	ablation of tracheal cartilage	(Turcatel et al 2013)
Fgf10	Fibroblast growth factor 10	Mesenchyme	Lung agenesis, defects in the patterning of tracheal cartilage	(Sala et al 2011)
Notch	notch	Not reported	Increase in ciliated cells population, ablation of clara cells	(Guseh et al 2009; Tsao et al 2009)
Tbx4	T-box transcription factor genes	Mesenchyme	impaired branching, anomalies in mesenchymal condensation	(Arora et al 2012)
Bmp4	Bone morphogenetic protein 4	Mesenchyme	Tracheal agenesis	(Li et al 2008)
Rspo2	R-spondins	Mesenchyme	Laryngeal and tracheo-bronchial abnormalities	(Bell et al 2008)
Cav3.2	calcium channel, voltage-dependent, T type, alpha 1H subunit	Mesenchyme	tracheal cartilage differentiation	(Lin et al 2014)
Tmem16a	anoctamin 1, calcium activated chloride channel	Trachea except cartilage	Tracheal defect, ubnormal trachealis, disruptetd epithelium and cartilage	(Rock et al 2008)

Table.1.4.2. Main genes implicated in tracheal development and the tracheal phenotype of their KO.

5. PATHOLOGIES AND TREATMENTS

5. 1. Major diseases

The direct contact between tracheal mucosa and the environment makes the trachea a nest for many infectious diseases. Besides the undesirable environmental assaults on the airway, the trachea itself may be the subject of many types of congenital disease, rare cancers and other pathological conditions. This chapter presents a glimpse of the major diseases affecting the trachea.

5.1.1. Congenital diseases

5. 1.1.1. Tracheal Agenesis

Tracheal agenesis (TA), first reported by Payne in 1900 (Payne 1900), is a rare and fatal congenital malformation with an incidence rate of 1/50,000 (Felix et al 2006) and a male/female ratio of 2:1 (Geisler & Smevik 2009).

It is diagnosed in neonates with cyanosis and severe respiratory distress. In 90% of the cases, tracheal agenesis is associated with a wide diversity of congenital diseases (cardiovascular, gastrointestinal, pulmonary and central nervous system) (Evans et al 1999; Faro et al 1979).

The Floyd anatomical classification describes three types of TA (Floyd et al 1962) (Fig.1.5.1). The occurrence of Type II is the highest with 60%. No efficient treatment has been described until now, although a surgical Ex-Utero Intrapartum Therapy procedure (EXIT) (see section 5.2) can be used in tracheal agenesis of type I (Bouchard et al 2002; Hedrick 2003).

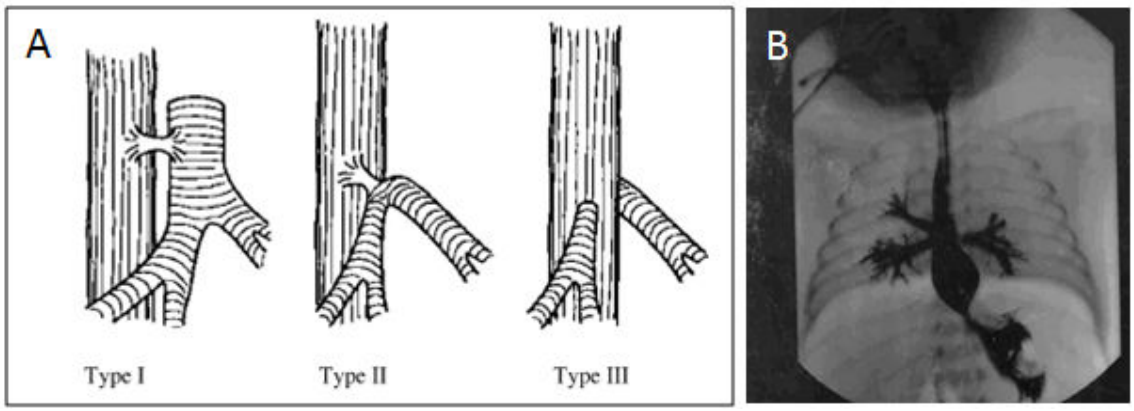

Fig.1.5.1. Tracheal agenesis.
(A) Types of tracheal agenesis according to Floyd, (B) Postmortem contrast study of tracheal agenesis. Contrast was administered postmortem through the esophagus. The esophagus and the stomach are clearly visible, as well as three bronchi. After (Felix et al 2006)

5.1.1.2. Apert syndrome, Crouzon syndrome, Pfeiffer syndrome

Apert, Crouzon and Pfeiffer syndromes are three congenital diseases, characterized by craniosynostosis and by recurrent cases of tracheal cartilaginous sleeve in the place of a normally ribbed cartilaginous trachea (Fig.1.5.2) (Cohen & Kreiborg 1993; Sagehashi 1992; Stone et al 1990).

Mutations in the Fibroblast Growth Factor receptor 2 (FGFR2) have been found in these three autosomal dominant diseases (Freiman et al 2006; Glaser et al 2000; Zackai et al). Although the type of mutations can deviate among patients, all occur in the same extracellular region and lead to a FGFR2 gain-of-function, inducing ligand-independent receptor activation or altered ligand binding (van Ravenswaaij-Arts et al 2002).

The tracheal cartilaginous sleeve, whose length may vary from 5 cartilaginous rings to the entire trachea and even the main bronchi, is suspected to interfere with clearance of secretions and passive airway immunity (Hockstein et al 2004). This deformity in the cartilage compound of the trachea is reflected by tracheal stenosis, sleeping apnea and airway obstruction leading to death for most patients with Apert syndrome (Chen & Holinger 1994; Cohen & Kreiborg 1992; Hutson Jr et al 2007).

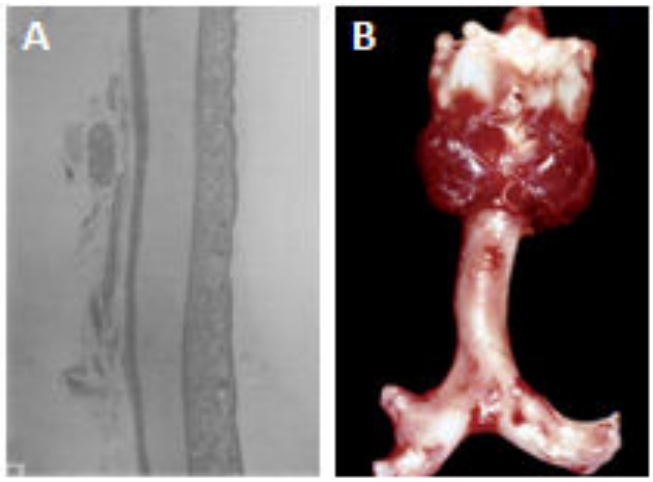

Fig.1.5.2. Cartilage sleeve in (A) Crouzon and (B) Pfeifer syndroms.

(A) Longitudinal section of the trachea, absence of ring formation. After (Sagehashi 1992) (B) Gross postmortem photograph of the trachea and main bronchi in patient with Pfeiffer Syndrome demonstrating severe deformity of the trachea and primary bronchi and replacement of the usual tracheal and bronchial cartilaginous rings by a continuous cylinder of cartilage . The trachea is abnormally curved, with convexity to the right. The right entrolateral wall of the distal trachea and proximal right main bronchus are indented. The branches of the right bronchus are hypoplastic.After (Hockstein, McDonald-McGinn et al. 2004).

5.1.1.3. Tracheo-oesophageal fistula

Congenital tracheo-oesophageal fistula (TOF) is a medical condition characterized by the presence of fistula between the trachea and eosophagus. The fistula is usually localized above the level of the second thoracic vertebra (Beasley & Myers 1988). Congenital TOF can be due to an aberrant fusion between the tracheal and esophageal ridges during the third week of embryological development (Fig.1.5.3). Clinical features vary from recurrent respiratory symptoms, aspiration during feeding with cyanosis, and abdominal distension (Riazulhaq & Elhassan 2012). The localization of fistula at the level of the neck root allows the repair of this defect by cervical approach with no need for thoracotomy (Kent et al 1991).

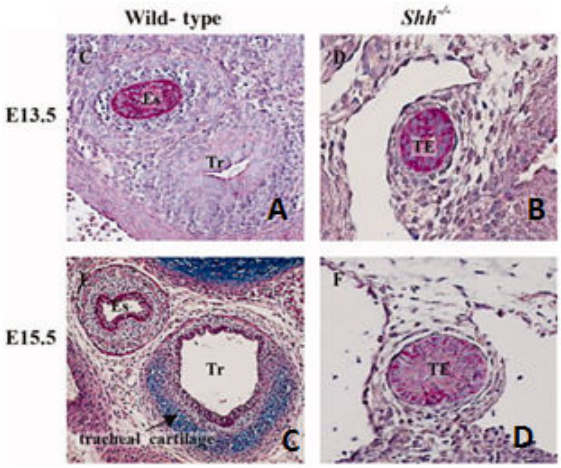

Fig.1.5.3. Example of tracheo-esophageal Fistula in Shh-/- mice.
A–D: AB-PAS staining of wild-type (A,C) and *Shh*$^{-/-}$ (B,D) transverse tracheal sections (200×) demonstrate:
1-Failure of tracheo-esophageal separation in the absence of *Shh* signaling (B,D).
2-Formation and differentiation of tracheal cartilage by E15.5 (C) and its absence in *Shh*$^{-/-}$ embryo (D). After (Park et al 2010b)

5.1.1.4. Cystic fibrosis (CF)

Cystic fibrosis is an autosomal recessive disorder caused by mutations in the cystic fibrosis transmembrane regulator (CFTR) gene. Symptoms of CF can be attributed to abnormalities of epithelial surfaces in the respiratory, digestive, and reproductive tracts, although lung complications account for most case of morbidity and mortality in CF patients (Ratjen 2009; Snouwaert et al 1992). Defect in mucociliary clearance is suspected to be the reason behind lung disease. However, recent studies suggest that airway smooth muscle can also be affected in this disease as CFTR expression has been detected in smooth muscles and may have a function in regulating contractility of those cells in both airways and vasculature. Also a difference in lower airway ASM has been described, as ASM content seems to be increased in children and adults suffering from CF (Regamey et al 2008).

5.1.1.5. Tracheomalacia

Both congenital and acquired (see also 5.1.2.3) tracheomalacia refer to the same conditions characterized by a loss of tracheal cartilage integrity, which leads to tracheal collapse predisposition during inspiration and expiration depending on the segment of the trachea affected. In fact, the collapsing during expiration occurs when the intrathoracic segment is affected, while the extrathoracic tracheomalacia is accompanied by collapsing during inspiration. Most cases of tracheomalacia are intrathoracic (Austin & Ali 2003; Choo et al 2013).

Tracheomalacia can be idiopathic (isolated) or associated with other disease (syndromic). One example of tracheomalacia is the one seen in Mounier-Kuhn syndrome, leading to a congenital tracheobronchomegaly or a dilation of both trachea and bronchi. The etiology of this disease is unknown, but atrophy of smooth muscles and elastic tissue in the trachea has been observed. Tracheobronchomegaly can be associated with tracheal and bronchial diverticulum (Katz et al 1962; Simon et al 2014).

5.1.1.6. Tracheal diverticulum

Tracheal diverticulum is a rare entity observed in less than 1% of the population characterized by the occlusion of a supernumerary branch of trachea (Goo et al 1999). Two types of tracheal diverticulum can be found, the acquired one formed of a usual respiratory mucous layer and the congenital type of cyst that contains all normal tracheal compounds (Fig.1.5.4) (Caversaccio et al 1998).

The acquired type thought to be the result of sustained elevated air-pressure in the trachea while the congenital form seems to be the result of cartilage deformities. In most of the cases, trachea diverticulum is an asymptomatic condition. Nevertheless, when symptoms do occur, patient usually suffers from cough, dyspnea and stridor, all along with recurrent respiratory infection (Early & Bothwell 2002). In one case, hiccup and burking were reported and were the results of the compression of the esophagus and the subsequent deviation of the trachea (Srivastava et al 2014).

Fig.1.5.4. Tracheal diverticulum with its connection to the trachea in a 3-dimensional reconstruction After (Srivastava et al 2014).

5.1.2. Acquired Disease

5.1.2.1. Tumors

Primary tumors in trachea are a very rare condition accounting for less than 0.01% of all tumors. In most cases, they are malignant with intrathoracic localization. 90% of tracheal tumors are adenoid cystic carcinomas or squamous cell carcinomas (Shadmehr et al 2011). Symptoms associated to tracheal tumors are only detectable when the trachea is seriously obstructed (Fig.1.5.5) (Li et al 2014b).

Fig.1.5.5. Tracheal tumor.
Tracheal tumor at the thoracic inlet, orientating from the right lateral wall. It obstructs nearly 80% of the lumen and extends beyond the wall, in this bronchoscopic view the tumor is covered with a smooth mucous membrane. After (Umezu et al 2008)

5.1.2.2. Asthma

Asthma is a chronic inflammatory condition of the conducting airways and lung parenchyma. The walls of trachea in asthma are thickened, with excessive mucus secretion leading to luminal narrowing (Jeffery 2001). In addition to the alteration of epithelial cells and in the distribution of percentage in Goblet cells, it has been also reported that airway smooth muscle

cell phenotype is affected as these cells are subjected to abnormal hyperplasia and hypertrophy (Regamey et al 2008).

5.1.2.3. Acquired Tracheomalacia

Saber-Sheath deformities, occurring in men with chronic obstructive pulmonary disease (Tsao & Shieh 1994), mostly this deformities affect the intrathoracic part of the trachea, with a marked coronal narrow in association with sagittal widening (Fig.1.5.6). It can be detected by chest radiography (Ciccarese et al 2014) Saber sheath deformities are asymptomatic, though it can be recognized when the ratio of coronal on sagittal diameter of the intrathoracic trachea (1cm above the aortic arch) is equal or less than 0.5 (Greene 1978).

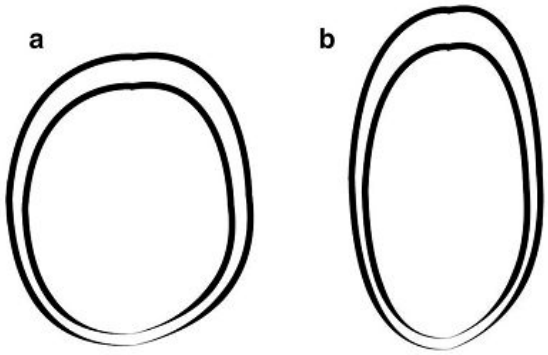

Fig.1.5 6. Schematic representation of normal trachea (a) versus Saber-Sheath trachea deformity (b). After (Ciccarese et al 2014)

5.2. Treatments

5.2.1. The Ex utero intrapartum treatment Procedure

Ex-utero intrapartum treatment (EXIT) is a surgical procedure, made during caesarean section. It was firstly described to correct lung or airway defection in fetuses with severe congenital diaphragmatic hernia (Mychaliska et al 1997). Exit procedure is indicated for many congenital deformities including tracheal atresia and tracheoesophageal fistula (CHAOS: congenital high airway obstruction syndrome), which lead to airway obstruction, a life threatening condition associated with high mortality at birth. EXIT procedure is done during Caesarean section because this provides the needed time to the medical intervention as bronchoscopy and mass resection before delivery in order to secure the newborn airway (Liechty 2010).

5.2.2. Long term ventilation

Ventilatory support is described for patients who are unable to breathe on their own, for part or all of the day on an on-going basis. Ventilatory support can be provided non-invasively through a mask or invasively through a tracheostomy.

5.2.3. Resection of tracheal affected segment

Sleeve resection is the basic radical operation for tumors and cicatricial stenosis. Sternotomy and thoracotomy both can be used depending on the place of operation. For anastomosis, a suture should link the fibro-cartilaginous part to the mucous membrane of both edges should be in contact for normal epithelialization to occur. If resection operation were done to correct stenosis cases, strengthening of membranous section of the tracheal wall should be done (Perelman & Koroleva 1980).

5.2.4. External stenting

External stents are palliative or supportive therapy of obstructive disease. The most commonly used stents are made of silicone or metal, but hybrid stents can be formed by combination between the silicone and synthetic coating. The characteristics of each stent vary as metal stent is more extensible while silicone stent are more easily replaced or removed. Stent displacement, mucus impaction, tissue granulation and pressure changes after removing obstruction are potential complications that follow external stenting (Al-Qadi et al 2013; Kim 1998). The newest type of stent under studies is the 3D stent designed based on tracheal CT images and made using the resorbable polymer polycaprolactone (Hollister & Green 2013; Zopf et al 2014) (Fig.1.5.7).

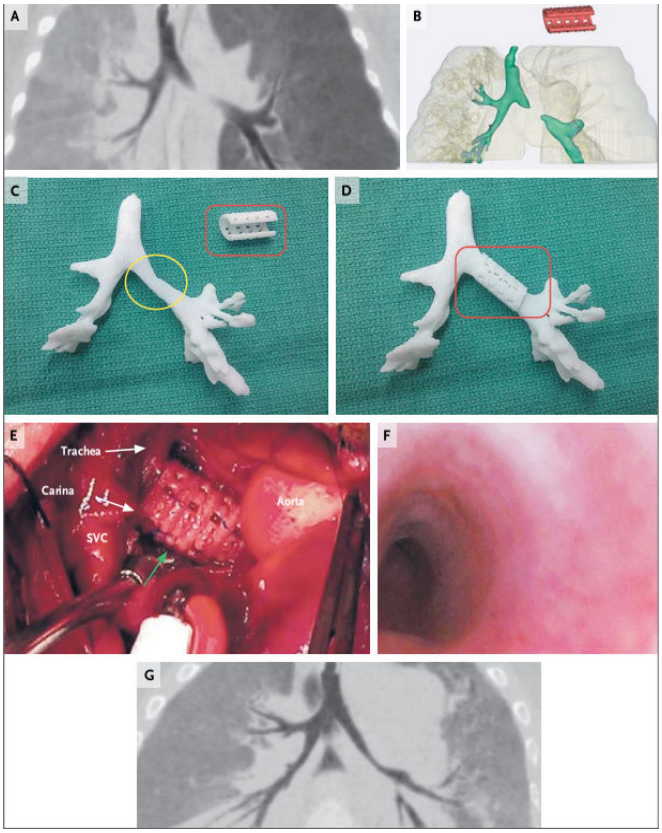

Fig.1.5.7. Placement of the printed airway splint in the patient.
Panel A shows the airway in expiration before placement of the splint; the image was reformatted with minimum-intensity projection. Panel B shows the patient-specific computed tomography-based design of the splint (red). Panel C shows an image-based three-dimensional printed cast of the patient's airway without the splint in place, and Panel D shows the cast with the splint in place. Panel E shows intraoperative placement of the splint in place. Panel E shows intraoperative placement of the splint (green arrow) overlying the malacic left mainstem bronchial segment. SVC denotes superior vena cava. Panel F shows the bronchoscopic view, from the carina, of the left mainstem bronchus after placement of the splint. Panel G shows the airway in expiration 1 year after placement of the splint; the image was reformatted with minimum-intensity projection. After (Zopf et al 2014).

5.2.5. Searching for trachea twins

Airway defect correction in normal basis should guaranty not only a normal airway function, better quality of life, but also an appropriate growth in addition to the prevention of relapse and thus prevent repeated surgical interventions.

The failure of all the previously mentioned treatment, whether invasive or not, in covering all the characteristic of a definitive treatment for airway defect, and the large number of patients affected with airway obstructional diseases makes the development of new treatment strategies of first importance in this particular medical field.

Indeed looking throughout scientific literature, the presence of tracheal homologue was always thoroughly looked for. In the past decades, the trachea was replaced with different

kinds of tube construction formed of different materials. The four conventional type of tracheal replacement were formed of synthetic materials (alloplastic transplantation), xenotransplantation, allotransplantation and finally the replacement of the trachea with autologous tissue (Fishman et al 2011).

Depending on the used material, side effects vary. For example, the side effects when prosthetic materials were used are: infections, stenosis followed by obstruction, migration of the implanted structure, dislodgement... Nevertheless, some progress was made regarding the porosity of the material. In fact, the use of porous materials has been shown to encourage the epithelialization of the implant and even capillary growth (Farwell et al 2013). The secondary effects of cross-species transplantation in the case of xenotransplantation vary from ethical with the fear of the transmission of infectious particles across species-barriers to rejection or coagulation dysfunction (Badylak & Gilbert 2008; Ekser et al 2012).

Recurrent side effects faced in allotransplantation are: shortage in organs from donors, risk of rejection with consequent need of immunosuppressive medication and reduction in life-span (Reynolds et al 2006). However, many types of allografts have been tried, with no big success for esophagus homograft (cadaveric origin), that showed a high level of morbidity and mortality (Gallo et al 2012). Even tracheal homograft was not also a big success with pre-transplant preparation complication, risk of Prion infection in addition to the shortage in organ donors (Jacobs et al 1999). Another type of homograft consists of replacement of the trachea with vascular tissue as aortic homograft. This allotransplantation is limited also by the number of donors. However, it seems to have a better outcome. For example, the replacement of trachea with fresh aortic allograft, in a study made in 2006 on two cases, showed no graft ischemia, problematic suture dehiscence, infection, or graft rejection even in the absence of immunosuppressive therapy after 18 months of follow-up (Wurtz et al 2006).

The side effects of autologous replacement are the limited availability of tissues for reconstruction, significant morbidity and pain in addition to complication and at the end the autologous tissues do not fully restore tracheal functions (Fanous et al 2010).

Altogether although promising therapies, secondary effects of each intervention keep them far away from being a definitive treatment.

5.2.6. A brand new trachea

The need for an adequate treatment initiates the call of a bioengineered trachea with a complexity similar to the authentic one. Three main compounds are used to synthesize bioengineered transplants: appropriate scaffold, cells and pharmaceutical agents or

endogenous chemicals and cytokines. These signals are mainly used for peripheral mobilization of cells, differentiation of cells and the promotion of vascularization (Fishman et al 2014).

The type of scaffold can be classified on different criteria as the composition that can be natural and synthetic (see Table.1.5.1), the biodegradability, and the source of tissue (autologous, allogenic or autogenic) (Fishman et al 2014).

The origin of cells may vary too, usually cells with self-renewal capacity are the center of interest. They can be of different types: embryonic, derived from amniotic fluid, induced pluripotent cells or adult mesenchymal stem cells (Atala et al 2012; Fishman et al 2011; Fishman et al 2013).

The use of autologous differentiated cells extracted from the same type of tissue but from different organ was also subject to study. As in the case of chondrocytes, where it has been demonstrated that autologous auricular chondrocytes are the most convenient to replace the tracheal chondrocytes when compared to articular or costal chondrocytes (Henderson et al 2007), although when transplanted the auricular chondrocytes were subjected to ossification or mineralization and they did not retain their original state of differentiation (Weidenbecher et al 2008).

The 6 essentials steps to create a bioengineered organ (trachea included) are presented in the Fig 1.5.8.

Natural	Synthetic
Biological scaffolds—composed of ECM, mimics native tissue and can accommodate growth	Artificial materials (e.g., polycaprolactone)
Contain donor antigens: decellularization makes them non-immunogenic	More likely to cause a foreign body reaction when implanted into the host
Better biocompatibility	Biocompatibility depends on material
Excellent tissue microarchitecture	Microarchitecture does not resemble tissue it is being used to replace
Excellent bioactivity if ECM components and growth factors preserved	Bioactivity depends on material
Preserved microvasculature	Absent vasculature
Less control over biodegradation properties	Biodegradation and porosity can be controlled to some extent
Biomechanical properties depend on material	Biomechanical properties can be controlled
Possibility of microbial contamination during preparation and storage	Contamination less likely
Requires times for harvesting and preparation (weeks). Supply depends on donor tissue availability	Off-the-shelf availability (h)
Cheaper to manufacture	More expensive to manufacture

Table.1.5.1. Main differences between natural and synthetic scaffolds for airway tissue engineering (Fishman et al 2014).

It is worthy to mention that a fully functional bioengineered trachea has been made and already used. This trachea was made on decellularized scaffold taken from a human donor and seeded with *in vitro* expanded and differentiated autologous epithelial cells and chondrocytes of mesenchymal-stem cell origin, maturation of implants was done in vitro in a special bioreactor and then bioengineered trachea was implanted, no immunosuppressive treatment was used. In a 4-month follow-up study, no complications or signs of antigenicity were found and the patient had a normal quality of life (Macchiarini et al 2008). Five years after surgery, there were no signs of rejection even with the absence of immunosuppressive treatment with no evidence of tumor. In addition, implanted airway matrix was repopulated with patient cells and there was no significant loss of airway nerve function as suggested by the improved cough sensitivity and expulsive force (Gonfiotti et al 2014).

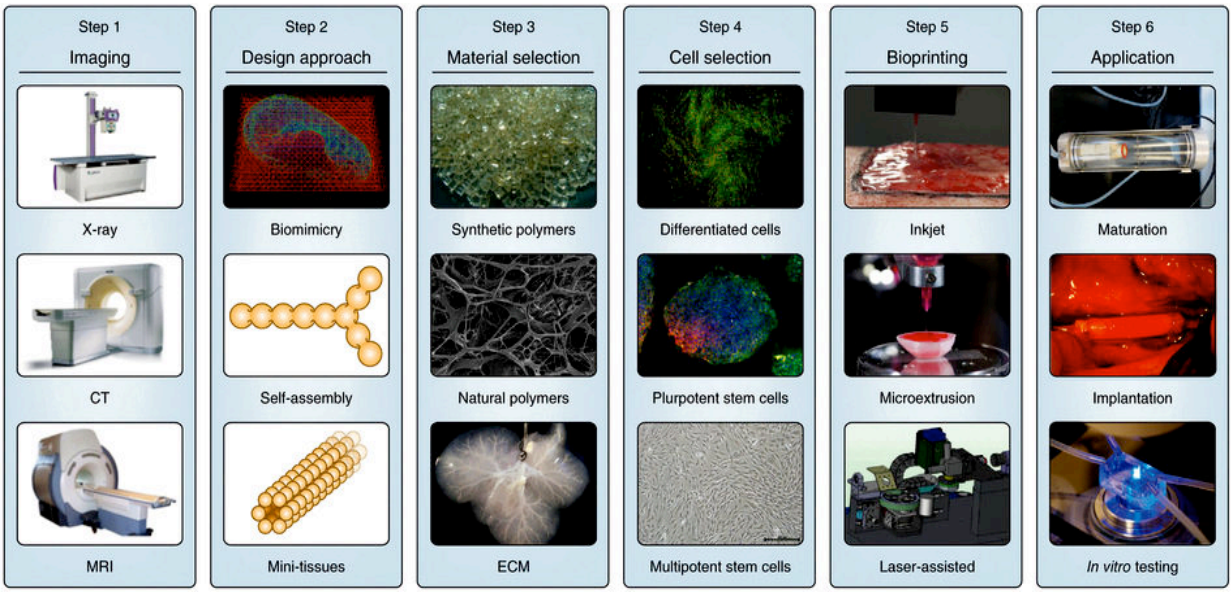

Fig.1.5.!. Required steps for making bioengineered organs.

Imaging of the damaged tissue and its environment can be used to guide the design of bioprinted tissues. Biomimicry, tissue self-assembly and mini-tissue building blocks are design approaches used singly and in combination. The choice of materials and cell source is essential and specific to the tissue form and function. Common materials include synthetic or natural polymers and decellularized ECM. Cell sources may be allogeneic or autologous. These components have to integrate with bioprinting systems such as inkjet, microextrusion or laser-assisted printers. Some tissues may require a period of maturation in a bioreactor before transplantation. Alternatively the 3D tissue may be used for *in vitro* applications. After (Murphy & Atala 2014)

CHAPTER II

PREFACE: LA MINERALISATION

Minéralisation :

La minéralisation est un phénomène naturel caractérisé par la formation des cristaux de différentes natures dans un milieu riche en sels, alors que la biominéralisation est une minéralisation qui se déroule via le support d'un organisme vivant uni- ou pluricellulaire dans un milieu adéquat. Cette dernière peut avoir lieu même sans la présence de sels à concentration élevée dans le milieu extracellulaire.

Les cellules vivantes peuvent induire et maintenir le processus de minéralisation *via* différents acteurs comme les vésicules matricielles, les enzymes membranaires qui inhibent ou activent la minéralisation comme TNAP, les phospholipides ou bien encore les mitochondries.

Les cellules sont aussi responsables de la synthèse d'une matrice extracellulaire compatible avec la minéralisation. La matrice elle-même stabilise et induit la minéralisation en créant un réseau approprié pour retenir et favoriser la croissance des cristaux. Dans le corps humain, cette matrice contient le plus souvent des réseaux de fibres de collagènes et des protéoglycanes.

Dans les conditions physiologiques, la biominéralisation se produit uniquement dans le squelette et les dents. Le phosphate inorganique (Pi), l'un des ions les plus abondants dans l'organisme, est un élément majeur favorisant la minéralisation. En effet, le Pi peut participer à ce processus non seulement comme constituant principal des cristaux d'hydroxyapatite, mais aussi comme molécule de signalisation avec des effets majeurs sur les cellules formant le squelette, comme les os et les chondrocytes. Afin de contrôler les effets pro-minéralisant de ce Pi, sa concentration est hautement régulée au niveau de la circulation sanguine par plusieurs facteurs et notamment le FGF23. Un autre levier pour contrôler les effets du Pi est la répression de son action au niveau de la matrice extracellulaire par différents inhibiteurs de la minéralisation comme le pyrophosphate inorganique (PPi) qui, dans le milieu extracellulaire, peut inhiber la minéralisation de trois façons différentes : 1/ en se liant aux cristaux d'hydroxyapatite en cours de formation et en inhibant leur croissance, 2/ en inhibant la TNAP, l'enzyme responsable de la dégradation du PPi en Pi dans le milieu extracellulaire et 3/ en activant la production d'ostéopontine, un inhibiteur de minéralisation.

La formation et la croissance des cristaux d'hydroxyapatite est le plus favorisé dans une matrice extracellulaire ou le rapport Pi/PPi est égal ou supérieur à 140. Cette formation est

complètement inhibée lorsque ce rapport est égal à 70. Inversement, si le rapport Pi/PPi devient inférieur à 6 la minéralisation est de nouveau favorisée mais ce sont des cristaux de pyrophosphate de Ca^{2+} dihydraté qui se forment. D'où l'importance d'une perpétuelle régulation du rapport Pi/PPi dans la matrice extracellulaire. Cette régulation est faite grâce aux transporteurs et enzymes producteurs de Pi et de PPi.

TNAP et PHOSPHO1 sont les producteurs essentiels de Pi au niveau de la matrice extracellulaire, alors que le transport de Pi du milieu extracellulaire vers le milieu intracellulaire se fait grâce à des co-transporteurs sodium-dépendants comme PIT1 et PIT2. La production de PPi dans le milieu extracellulaire est effectuée par ENPP1 et ce dernier peut être produit dans le milieu intracellulaire grâce à ENNP3. Le transport de PPi du milieu intracellulaire vers le milieu extracellulaire est effectué *via* ANK.

En dehors du PPi plusieurs inhibiteurs de minéralisation existent, telle-que l'ostéopontine et la matrice GLA protéine (MGP) qui agissent au niveau local. L'ostéopontine agit en inhibant la formation et la croissance des cristaux alors que l'effet de MGP est plus vaste. En effet, en plus de son effet inhibiteur sur la formation et la croissance des cristaux, MGP peut aussi inhiber l'effet des facteurs prominéralisants telle que BMP2.

La dérégulation d'un ou plusieurs facteurs impliqués dans la balance Pi/PPi ou des inhibiteurs de minéralisation est souvent traduite par des cas de minéralisation pathologique non seulement au niveau des lieux physiologiques de minéralisation, comme dans le cas du rachitisme où la déficience en phosphate est une des causes de la maladie, mais aussi dans des cas de minéralisation ectopique, impliquant des tissus mous, observés notamment au niveau de l'aorte dans les cas de patients diabétiques ou atteints d'insuffisance rénale. Des minéralisations ectopiques se retrouvent également au niveau des articulations (arthroses et chondrocalcinoses). Dans les cas des minéralisations rencontrées au niveau vasculaire et articulaire, une forte implication de la balance Pi/PPi est trouvée. Cette dernière est aussi impliquée dans des cas de minéralisations ectopiques non-pathologiques observées au niveau des glandes mammaires, des poumons et des testicules. La détection de ces minéralisations peut aider le pronostic dans certains types de cancer mais aucun effet clinique n'est directement lié à leur présence.

CHAPTER II

MINERALIZATION

1. MINERALIZATION

1.1. Introduction

Biomineralization as defined by Veis is the deposition of a mineral phase that requires or is occasioned by the intervention of living organism (Veis 2003).

The deposition of mineral phase can occur in mineral concentrated extracellular environment, in this case the function of the cells would be the nucleating and localization of mineral deposition, this process was called "biologically induced" mineralization mostly found in primitive species as single-cell organism or protoctists, the mineral deposit can occur intra- or extra cellularly in this type of mineralization.

In addition to the localization of mineral phase attributed to the living organism, the living organism can be directly responsible of the crystallization process that gives rise to a unique crystal that does not normally develop in a saturated solution, this mineralization was called "(organic) matrix-mediated". This type of mineralization is mostly found in eukaryotic species where the mineral deposits are extracellular (Lowenstam & Weiner).

The biomineralization is a process that depends on different biological compounds: mineral compound, extracellular matrix and cells.

1.2. Mineral compound

The three principal types (although there exist more than 70 different types of biominerals in organisms) of biominerals that can be found in the skeleton of eukaryotes are:

- Silica: siliceous skeleton is found in Sponge spicules;
- Calcium carbonates: prominent in Metazoans skeleton as in Mollusk shells;
- Calcium phosphate: found primarily in the skeleton of Branchiopods and Vertebrates (Lowenstam & Weiner 1989)

The earliest mineralized skeleton which was found in early Cambrian fossils of Metazoan is a calcium carbonate skeleton (Wilt et al 2003). Conodonts, that lived between the early-mid Cambrian till the end of the Triassic period (Donoghue et al 2000), were the first Vertebrates with mineralized skeleton, as their oropharynx was made of calcium phosphate.

A common point shared between all eukaryotic mineralized tissues is the presence of structural plan for mineral deposition in the extracellular matrix, presented as a restricted compartment where the mineralization will take place. For example, in urchin teeth, the mineralization occurs in channel spaces, or in various cases of invertebrate shells where the mineral deposition is limited into compartment with channels in some cases, and pores in

another, or in the case of avian egg shells where the matrix-mediated mineralization is not only restricted in space but also in chronological way. According to Veis, the physical size and shape of cell formed compartment can be the limiting factor in defining the mineral crystal volume and shape (Veis 2003).

Despite the presence of a big variety in composition, shape and characteristics of calcium phosphate crystals, the most prominent one is hydroxyapatite.

Apatite crystal in their geological forms differs from bone apatite or biologically synthesized apatite. Geological apatite has the $Ca_{10}(PO4)_6(OH)_2$ composition with a right rhombic prism conformation and a bigger size from those synthesized through a biological process. Bone apatite is found as small and plate needle-like crystals, oriented in a way to fill the gaps between extracellular matrix fibrils, they are non-stoichiometric with calcium-, hydroxyl- or phosphate- deficiency and with $Ca_{10-x}H_x(PO_4,CO_3)(OH)_{2-x}$ composition (Veis 2003).

To summarize, vertebrate skeleton mineralizes in matrix-mediated pattern to form a calcium phosphate skeleton.

1.3. Extracellular matrix (ECM) and mineralization

It is an outstanding fact that extracellular matrix is responsible for mineral deposit localization, through its collagenic compound, making a spider web to gather and control mineral localization. Still, ECM is not an inert structure and, as such, maybe an appealing or repelling area for cell-released crystals (Fig.2.1.1).

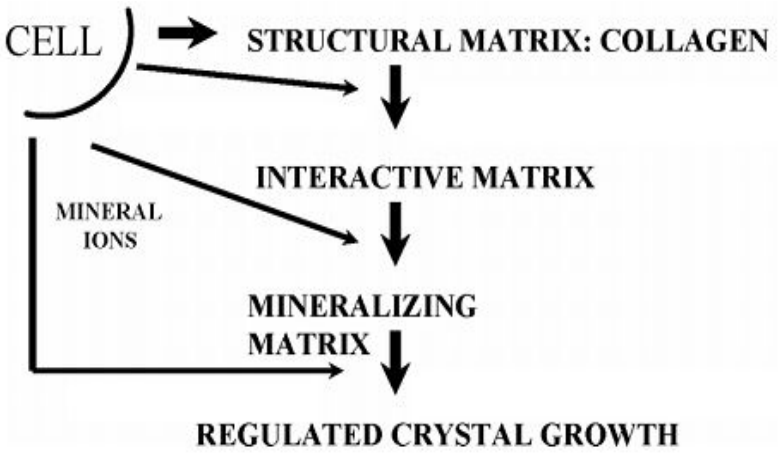

Fig.2.1.1. Biomineralization complex process from (Veis 2003).

1.3.1. Collagen fibers

The extracellular matrix of bone, mineralized, and connective tissues is mainly formed of fibrillar collagens (Coll), which confer a structural scaffolding and strength to the ECM. More

than 40 genes in Vertebrates belong to the family of Collagen (Pace et al 2003), macro-molecules which all adapt triple helical conformation (van der Rest & Garrone 1991).

Coll I is the main collagen in mineralized tissues and Coll II is the main type of collagen in cartilage and other connective tissues. In bone or in cartilage collagen represents 10% of the wet weight, and 40 to 50 % of dry weight of extracellular matrices (Mayne & von der Mark 1983).

The function of Coll I in mineralization has been long discussed by researcher in the field, relying on the periodicity of crystals and the periodicity of collagen fibrils. Glimsher *et al* in 1968 suggested that Coll I might be a nucleation centre (where mineralization get started and from it it expands) for the mineral crystals (Glimcher & Krane 1968).

The most recent researches indicate the presence of two types of inorganic structures. The first one is of granular type in bands within the holes of collagen gaps, the other kind is filament-like, which can be found in interfibrillary spaces and on the collagen fibrils surface (Ascenzi et al 1965; Lees et al 1994). In this case the nucleation center is supposed to be an organic component of ECM linked to the collagen fibrils. This suggests a plan of ECM within the collagen network built as an anchor of organic primary nucleation centers (Linde & Goldberg 1993) that gives rise to the mineralized deposit between collagen fibrils gap and makes a secondary nucleation center for the filamentous crystal on the top of the collagen fibrils network (Glimcher & Krane 1968).

However, it seems important to mention that the extent of the collagen network may differ from tissues to tissues. Actually, Brick and Linsenmeyer studying fibroblasts in tendon demonstrate that the exocytose of procollagen fibers occurs in confined spaces, while in bone and teeth, the procollagen is directly released into the pericellular space (Birk & Linsenmayer 1994).

1.3.2. Proteoglycans

Proteoglycans (PGs) are biological molecules with big varieties, and with ubiquitous repartition. Proteoglycans are composed of a specific core protein substituted with covalently linked glycosaminoglycan (GAG) chains. GAGs, made of disaccharide repeating regions, are linear, and negatively charged polysaccharides. They can be divided into two classes: the sulfated GAGs and the non-sulfated GAGs (Schaefer & Schaefer 2010).

Many functions can be attributed to proteoglycans depending on their location (ECM, membrane, intracellular compartment) and the type of tissues they are in. One of the tissues displaying highly abundant proteoglycans-ECM is cartilage, where they are produced by

chondrocytes and confer the elasticity to ECM. The loss of these cartilage proteoglycans is related to pathological condition as in the case of arthritis (Kempson et al 1970; Yin & Xia 2014). Proteoglycans can also be found in mineralized and connective tissues. Their contribution to the mineralization is mostly studied in the growth plate. *in-vitro* studies showed that proteoglycans inhibit mineral deposition (Howell et al 1969). However, the role of proteoglycans *in-vivo* is more controversial. On the one hand, some reports show decreasing concentration in the lower zone of growth plate, where the mineralization occurs in accordance with the role of PG in maintaining the rate of chondrocyte proliferation through Indian hedgehog signaling (Gualeni et al 2010), which suggests inhibitory role in accordance with *in vitro* data. The function of PG as mineralization inhibitor was also recognized in the predentin, as suggested for the large chondroitin sulfate proteoglycans the porcine Versican (Okahata et al 2011). On the other hand, it has been reported, in other studies, that the concentration of proteoglycans in the lower part of the growth plate is more elevated (Poole et al 1982) in a way to withstand its implication as a pro-mineralization factor. As PGs were detected to be colocalized with the collagen X in growth plate(Gibson et al 1996), Also some PGs as Aggrecan have been demonstrated to have an important function in maintaining a proper cytoarchitecture and differentiation of the growth plate (Lauing et al).

Moreover, perpetual changes and remodeling of proteoglycans occur during the mineralization process (Prince et al 1983). Recent studies suggest that the proteoglycans within the growth plate remain in the mineralized part but with a change in size and composition. With the increased mineral content of the tissues the ratios of proteins to polysaccharides, of chondroitin sulfate to keratan sulfate, and of 4-sulfated to 6-sulfated chondroitin sulfate increased in the proteoglycan fraction. Furthermore, a decrease in the very high molecular weight proteoglycans has been noted in calcified cartilage (Howell & Carlson 1968; Lohmander & Hjerpe 1975) these changes in PG was also demonstrated by Waddington *et al* in teeth (Waddington et al 2003).

1.3.3. SIBLING

The Small Integrin Binding Ligand N-Linked Glycoproteins or SIBLINGs by are represented by various members first introduced as a family by Fisher in 2001 (Fisher et al 2001). All are encoded in the 4q21 chromosomal region by genes with exon-intron organization similarities. These genes encode for proteins that contain one or more consensus sequences for phosphorylation by casein kinase II, such as osteocalcin, osteopontin, bone sialoprotein (BSP) and phosphophoryn.

For instance, phosphophoryn, the first SIBLING discovered in dentin by Veis and Perry in 1967 (Veis & Perry 1967), is a molecule rich in phosphorylated serine that can bind strongly to fibrillar collagen and induce crystal formation (Linde et al 1989). According to these findings it has been suggested that phosphophoryn might play a nucleating function (Hunter et al 1996). Alternatively, phosphophoryn in solution has a high capacity to bind multivalent cations such as Ca^{2+} through its negatively charged phosphorylated serine and inhibits the precipitation of calcium ions (Veis 2003; Villarreal-Ramirez et al 2014).

In addition, recent study demonstrate that the function of phosphophoryn can also be related to the differentiation of odontoblast, where the ablation of sialophosphoprotein the precursor of both phosphophoryn and dentin sialoprotein induce circular dentin formation within dental pulp cells and altered odontoblast differentiation (Guo et al 2014).

1.3.4. Lipids

Lipids can be found in the growth plate as phospholipids, where they are differentially distributed throughout the growth plate with the higher concentration in the hypertrophic zone (Boskey et al 1980). Phospholipids have the ability to bind to calcium and phosphate to form calcium-phospholipid-phosphate complex (Boyan et al 1989) that has a function in initiating the mineralization as shown in experiment carried out both *in vitro* (Boskey et al 1982) and *in vivo* (Raggio et al 1986). Lipid within mineralized tissue can also be found in matrix vesicles (Wuthier 1976). More recently, it has been shown that he disruption of the metabolic pathways responsible for phospholipids production can lead to an impaired mineralization (Li et al 2014c; Li et al 2014d).

1.4. Cells in mineralization

Cells are the manufacturing plant of crystals. They contribute to the mineralization process by synthesizing an extracellular matrix compatible with mineralization, that feeds back to the cells to control mineralization, and by regulating the phosphate/pyrophosphate (Pi/PPi) balance (see 3) through many membranous transporters and enzymes and via the matrix vesicles.

1.4.1. Matrix vesicles

Matrix vesicle (MV) is a feature detected in several numbers of physiological mineralization process. Also, it can be detected in some pathological mineralization. These small vesicles of 20-200nm (Golub 2011) were discovered in the cartilage by Bonucci (Bonucci 1967). In the growth plate, MVs seem to bud from the cytoplasmic membrane of hypertrophic

chondrocytes (Rabinovitch & Anderson 1976; Wuthier et al 1977). Although MVs originate from the cell membrane, their membrane does not share the same features than the cell membrane. Indeed the MV membrane shows a higher concentration in lipids especially cholesterol, sphingomyeline and phosphatidylserine (Glaser & Conrad 1981).

The observation that the first extracellular crystals in mineralized tissues are located inside or around MV (Anderson 1967; Bonucci 1967) led investigators to suggest that the MV contribute to the mineralization process by creating a primary nucleation center within their vicinity (Anderson 1983; Boskey 1992; Wuthier 1989). This suggestion is supported by the presence of Phosphate transporter as Pit1-2 (Anderson et al 2005; Houston et al 2004) and calcium transporter as annexins on the MV surface (Kirsch et al 2000) thus permitting the retention from the extracellular matrix of Ca^{2+} and PO_4^{3-} ions making a complex with the phospholipid inside the MV and then getting released in the extracellular region. Other investigators assume that MV function in mineralization refers to its capacity to regulate phosphate ions Po_4^{3-} concentration through the cluster of enzymes as TNAP (Ali 1976), PHOSPHO (Stewart et al 2006), PC-1 and others (to see further in the paragraph regarding Pi/PPi balance) integrated to the MV membrane (Golub 2011).

1.4.2. Mitochondria

The established function of mitochondria in calcium metabolism led Shapiro and Greenspan (Shapiro & Greenspan 1969) to suggest its involvement in mineralization through local increase of mineral ions concentration. Moreover, the presence of inorganic granules in mitochondria within calcified tissues (Burger & Matthews 1978) and the difference between the mitochondria in different regions of the growth plate with light mitochondria in the resting non-calcifying chondrocytes (Arsenis 1972) suggest the involvement of mitochondria in the mineralization process. Although there is no strong experimental findings to confirm this hypothesis, this may be attributed to the metabolic role of mitochondria in producing ATP, a major source of Pi and PPi molecules that are essential for mineralization and presented in the following paragraph.

2. Pi/PPi BALANCE IN MINERALIZATION

Extracellular Pi is the most potent pro-mineralization element. Its effect is usually opposed by the most potent inhibitory molecule extracellular PPi. Thus, the balance between these two molecules is the main determinant of ECM mineralization. In the next part, the main function of Pi and PPi is discussed separately in addition to the cell enzymatic machinery used to produce these molecules and the main transporters responsible for the traffic from the intracellular compartment to the ECM and *vice-versa*.

2.1. Pi, hydroxyapatite component and signaling molecule

Known among the most abundant mineral within the body, phosphorus is widespread in the body and displays many functions (Walker et al 1990). The highest level of phosphorus molecule can be found in bone (85%), where it makes a complex with calcium to form hydroxyapatite crystal deposits, the rest of phosphorus can be found in organic substances (14%) as nucleic acids, phosphoproteins and phospholipids (Op den Kamp 1979), and in body fluids (1%) as inorganic phosphate (Pi) (Walker et al 1990).

Phosphorus is highly implicated in the mineralization process either in its organic form (phospholipids as described above, nucleic acids as source for Pi) or in its inorganic form. Nevertheless, the major role of phosphorus in the mineralization seems to happen through the inorganic phosphate form whether it comes from being a substrate in hydroxyapatite crystals or from the direct effect of Pi molecule on skeletal cells.

As mentioned, the mineralization is the result of two interrelated components: cells able to induce mineralization and extracellular matrix compatible with mineralization (Veis 2003).

A compatible ECM requires an environment that promotes the formation of nucleation centers and the growth of hydroxyapatite crystals.

The presence of Pi is of high importance in the ECM since it is a prerequisite for hydroxyapatite crystal formation. Extracellular (and intracellular) phosphate production is regulated by a complex cellular machinery. Under physiological circumstances, many types of cells can possess this machinery, including the hypertrophic chondrocytes in the growth plate, the osteoblastic cells and the odontoblats.

Interestingly, many studies showed that Pi in addition to its direct involvement in mineralization (hydroxyapatite crystal formation) can be involved in an earlier phase by affecting the proliferation and differentiation of cells required for proper mineralization.

Study made by Naviglio et al showed that Pi can induce osteoblast proliferation (Naviglio et al 2006). Indeed, when treated with high level of Pi, osteoblasts showed an increased proliferation rate (Beck Jr et al 2003; Conrads et al 2005; Conrads et al 2004). Additional studies demonstrated that the Pi-induced osteoblastic proliferation occurs through a reduction in the intracellular cAMP accompanied with a reduction in adenylate cyclase activity and cell growth inhibition (Naviglio et al 2006). These effects seem to be related to insulin growth factor effect (Kanatani et al 2002).

Pi can also show effect on osteoblast differentiation as it was suggested and demonstrated by Beck's group (Beck et al 1998; Beck et al 2000). They showed that high level of phosphate is able to induce expression of mineralization inhibitors, such as osteopontin and MGP, in osteoblast through Erk pathway activation (see paragraph on mineralization inhibitor). High concentration of Pi can also stimulate the expression of stanniocalcin, a factor that activates the accumulation of Pit (Na^+/Pi cotransporters- to see further), which enhances crystals formation through Erk1/2 pathways (Wittrant et al 2009) and leads to high level of intracellular Pi which in turn induces osteoblast apoptosis (Yoshiko et al 2007). Also, a high level of Pi leads to state of arrest in osteoclast differentiation (Yates et al 1991) and can lead to apoptosis and thus contributes negatively to the bone resorption process (Baylink et al 1971; Thompson et al 1975).

Pi can also affect chondrocytes maturation. It has been demonstrated that a high extracellular Pi level can lead to the suppression of type II collagen from ECM and an acceleration in Coll X expression and an abolishment of PTH receptor expression (regulator of chondrocyte proliferation) (Fujita et al 2001; Magne et al 2003). These results were confirmed in another study using a different clone of cells and in which the investigators showed that Pi plays a role in the commitment of chondrogenic cell to differentiation (Wang et al 2001). Many other studies are coherent with these two studies, and showed that extracellular Pi can induce both the maturation of chondrocytes and mineralization (Alini et al 1994; Cecil et al 2005; Magne et al 2003; Mansfield et al 1999; Mansfield et al 2001; Teixeira et al 2001). Nevertheless, a high extracellular Pi level can induce the apoptosis of hypertrophic chondrocyte (Mansfield et al 2001) through the activation of Pit1 expression (Wang et al 2001) and thus by increasing

the intracellular level of Pi in chondrocytes that seem to be more sensitive to high level of intracellular Pi than osteoblasts (Adams et al 2001; Meleti et al 2000).

2.2. Pi/PPi balance

As mentioned above, Pi is a very potent promoter of mineralization, whose systemic homeostasis is highly regulated by many factors such as parathyroid hormone (PTH), fibroblast growth factor 23 (FGF-23), Klotho, etc. In addition, Pi level is also regulated locally in the ECM of tissues

PPi is endogenously produced as it cannot be absorbed in the gut; it is the result of many intracellular metabolic reactions, and it can be released during the synthesis of the proteins, lipids, phospholipids and other components. However, the biggest portion of PPi is the result of NTP hydrolysis. The production of PPi is estimated to reach the order of kilograms on a daily rate (Rachow & Ryan 1988; Russell 1976).

The function of PPi in inhibiting the mineralization is studied in the bone where it appears to inhibit mineralization in three different ways: by binding directly to the mineral and thus arresting crystals further growth (Fleisch et al 1966; Meyer & Nancollas 1973; Moreno & Aoba 1987), by the upregulation of osteopontin (another key inhibitor of mineralization), through Erk1/2 and P38-MAPK signaling pathway, and by altering TNAP-mediated Pi release as demonstrated in a study where β-glycerophosphate was used to test the effect of PPi on TNAP activity (Addison et al 2007).

The mineralization of the bony extracellular matrix is tightly linked to the Pi/PPi ratio (Terkeltaub 2001). The level of extracellular PPi controls the type of crystal in the mineralized tissue; a PPi deficiency leads to excess in hydroxyapatite formation, the optimal formation of hydroxyapatite occurs when the Pi/PPi ratio is higher than 140, when this ratio decreases to 70 the formation of hydroxyapatite ceases completely (Johnson et al 2001). Whereas PPi elevation results in decreased skeletal mineralization (Fedde et al 1999; Narisawa et al 1997a; Russell et al 1971; Whyte 1994), when the PPi level exceeds certain level, it induces the formation of pyrophosphate dihydrate crystals (CPP) (Chuck et al 1989; Zaka & Williams 2005), a CPP crystal formation occurs only when the ratio of Pi/PPi is below 6 and it ceases when Pi/PPi ratio exceed 140 (experience made on chicken growth plate) (Abhishek & Doherty 2010).

2.3. Pi and PPi production

Pi and PPi production happens through ectonucleotidase activity. Four major families of ectonucleotidase exist: ectonucleoside triphosphate diphosphohydrolases (E-NTPDases), 5'-nucleotidase (eN), Alkaline Phosphatase (APs) and the NPP-type ectophosphodiesterases (E-NPPs) (Fig.2.2.1).

On the first hand the E-NTDases and E-NPPs are the ectonucleotidases that produce primarily the PPi. However, they can also produce Pi in a secondary reaction. On the other hand, the APs are mostly responsible of Pi production, while the 5'-nucleotidase produce Pi accompanied with Adenosine from Adenosine 5' monophosphate or AMP molecule (Stefan et al 2006).

In the next part, the 4 families of ectonucleotidases are briefly described in addition to PHOSPHO1 which also has the phosphatase activity and plays a major role in Pi production.

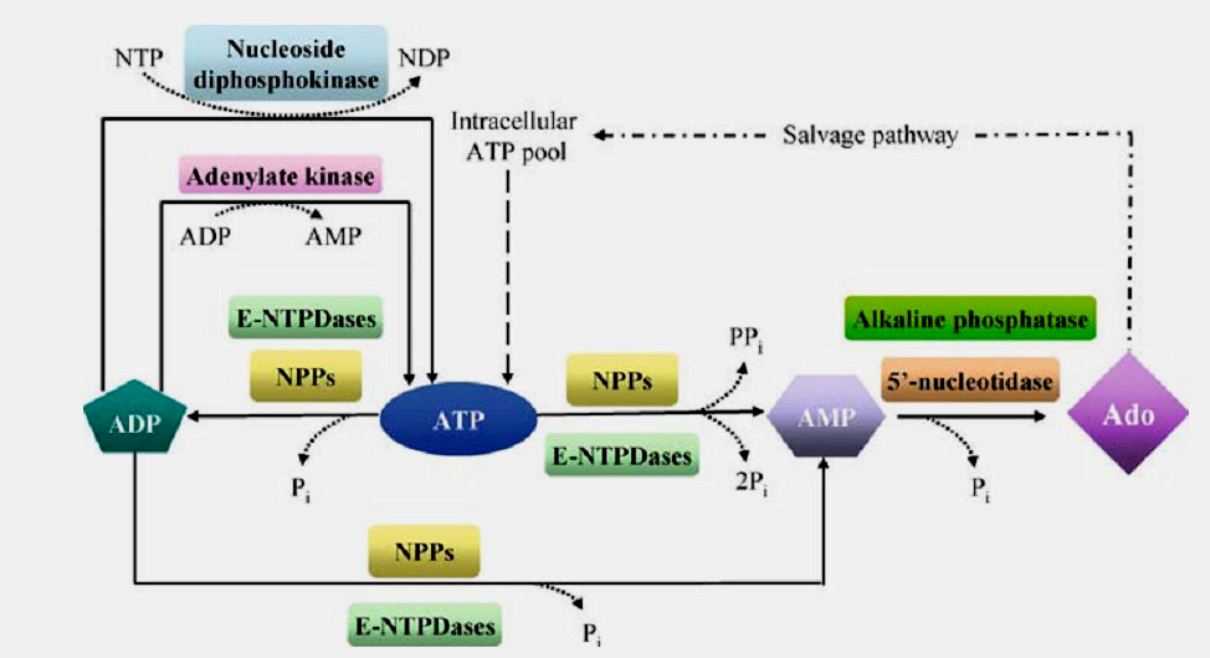

Fig.2.2.1. The 4 families of ectonucleotidases.

NPPs are part of the extracellular nucleotide-metabolizing network. The concentration of nucleotides in the extracellular milieu is the net result of the release of nucleotides from cells, their synthesis by nucleoside diphosphokinases and adenylate kinases, and their hydrolysis by ectonucleotidases. The examples shown here apply to ATP, the prototype extracellular nucleotide. Members of the E-NTDPase family, also known as apyrases, generally act as ATP diphosphohydrolases and hydrolyze ATP to ADP + P_i, and ADP to AMP + P_i, or ATP directly to AMP + $2P_i$. Individual members however display substrate preference. For instance, E-NTPDase-1 metabolizes equally well ATP and ADP, while E-NTPDase-2 prefers ATP as a substrate. ATP can be regenerated from ADP by nucleoside diphosphokinase or adenylate kinase. NPPs, at least NPP1-3, have a nucleotide pyrophosphatase activity and metabolize ATP directly to ADP + P_i or to AMP + PP_i. The hydrolysis of AMP to adenosine by 5'-nucleotidase/CD73 completes the dephosphorylation pathway of ATP. Adenosine can be taken up by cells such as lymphocytes and be re-used for intracellular nucleotide synthesis (nucleotide salvage). Several ectonucleotide species can be expressed by a given cell type, but the relative abundance, sorting to specific membrane domains and substrate availability are ultimately responsible for the net outcome of the nucleotide metabolism at the cell surface. From (Stefan et al 2006).

2.3.1. Ectonucleotide pyrophosphatase/ phosphodiesterase (ENPP)

As mentioned above, PPi can be the product of many metabolic reactions, although a big portion of PPi is produced through the nucleoside triphosphate pyrophosphohydrolase (NTPPH) activity (Belli et al 1995; Goding et al 1998). The ectoenzymes responsible of this activity are the ectonucleotide pyrophosphatase/phosphodiesterase (ENPP).

In our genome, 5 ENPP genes were discovered, with only three enzymes. The ENPP1 is also known as plasma-cell membrane glycoprotein-1 (PC-1) or phosphodiesterase nucleotide pyrophosphatase (PDNP). The second one is ENPP2 or PDNP2 also known as autotoxin/PD1α, the third one is ENPP3 also known as B10 and PDNP3 (Bollen et al 2000; Johnson et al 2001).

All the NTPPH activities are induced by TGF-β and inhibited by interleukin-1 in articular chondrocyte (Lotz et al 1995) and their matrix vesicles (Hashimoto et al 1998; Johnson et al 1999a). PC-1 is the most widely distributed NTPPH enzyme (Goding et al 1998; Harahap & Goding 1988), the monomeric form of PC-1 is soluble and can be found in the synovial fluid (Belli et al 1993), while PC-1, a transmembrane enzyme has a homodimerized structure through disulfide bond (Goding et al 1998).see Fig.2.2.2.

ENPP1 is thought to be responsible for the production of extracellular PPi (Johnson et al 1999b). The expressions of ENPP2 and ENPP3 are more restricted than ENPP1 expression, with ENPP2 mostly found in the brain, intestine and melanocyte (Goding et al 1998; Stracke et al 1997) and ENPP3 mostly expressed in neurons, intestine and within the genitourinary tracts (Goding et al 1998; Jin-Hua et al 1997), ENPP3 is thought to be responsible of generating intracellular PPi (Johnson et al 1999b).

2.3.2. Ectonucleoside triphosphate diphosphohydrolases (E-NTPDases)

In Mammals, 8 different E-NTPDases exist. They form a highly glycosylated protein with molecular weights that range between 70 and 80 KDa. These enzymes can be found within cellular membrane as in the case of NTPDase1, 2, 3 and 8, and also can be secreted or found in the intracellular compartment as in the case of NTPDases 4-7 (Iablons'ka & Rybal'chenko 2010) (see Fig.2.2.1).

The two main substrates for the E-NTPDases are the ATP and the ADP. In the presence of Mg^{2+} and Ca^{2+}, these enzymes hydrolyze the ATP and ADP into AMP. Despite their central role in purinergic signaling, these enzymes are able to hydrolyze neither the nicotinamide

adenine dinucleotide or AMP nor diadenosine polyphosphate (Iablons'ka & Rybal'chenko 2010).

2.3.3. 5'-ectonucleotidases (eNs)

The 5'-ectonucleotidase enzymes are phosphatases that hydrolyze nucleotide monophosphate, mostly AMP, into Pi and Adenosine. They are expressed in wide range of tissues, subtypes of Lymphocyte B and T. In addition eNs expression was detected in some tumor cells (Zimmermann 1992).

eNs are involved in many types of functions within the body. However, in mineralization eNs main function does not come from producing Pi but from producing Adenosine that inhibits the mineralization process by inhibiting TNAP.

CD73 is a member of eNs family, with high importance in mineralization, as can be deduced from cases with CD73 deficiency due to NT5E mutation. Patient with this condition suffer from arterial calcification, primarily in arteries of the lower extremities (Markello et al 2011).

Ectopic mineralization was also found in $Nt5e^{-/-}$ mice. In fact, these mice showed stiffened joints with mineralization of juxta-articular spaces of the lower extremities as well as of ligaments and capsules adjacent to the bony structures. However, vascular mineralization was not detected in these mice (Li et al 2014a).

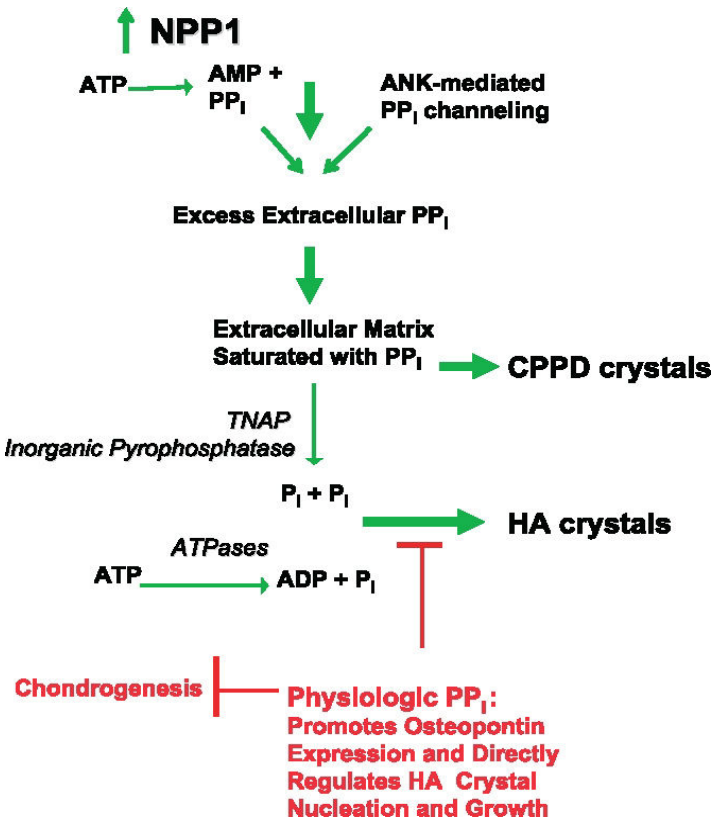

Fig.2.2.2. Proposed NPP1-mediated and PP_i-dependent mechanisms stimulating CPPD and HA crystal deposition in aging and osteoarthritis (OA).

Roles of ATP and PP_i Metabolism and inorganic phosphate (P_i) generation in pathologic cartilage calcification. This model presents mechanisms underlying the common association of extracellular PP_i excess with both CPPD and HA crystal deposition in OA and chondrocalcinosis cartilages, as well as the paradoxical association of extracellular PP_i deficiency (from defective ANK or PC-1/NPP1 expression) with pathologic calcification of articular cartilage with HA crystals *in vivo*. Factors driving pathologic calcification are indicated in green and physiologic factors suppressing calcification in *red*. Excess PP_i generation in aging cartilages in idiopathic CPPD deposition disease of aging, and in OA cartilages, is mediated in part by marked increases in NTPPPH activity, mediated in large part by the PC-1/NPP1 isoenzyme. In idiopathic chondrocalcinosis of aging and in OA, there are substantial increases in joint fluid PP_i derived largely from cartilage. NPP1 not only directly induces elevated PP_i but also matrix calcification by chondrocytes *in vitro*. Depending on extracellular availability of substrate PP_i and the activity of pyrophosphatases, the availability of substrate ATP and the activity of ATPases, and other factors such as substantial local Mg^{++} concentrations, HA crystal deposition, as opposed to CPPD deposition, may be stimulated. In this model, excess extracellular PP_i also may result heightened release of intracellular PP_i via increased ANK expression in OA and abnormal ANK function in familial chondrocalcinosis, as well as from deficient activity of pyrophosphatases (such as TNAP and possibly inorganic pyrophosphatase) in certain primary metabolic disorders. Also illustrated at the top of this schematic is the role in cartilage calcification in OA and aging of altered TGFβ expression and responsiveness, which drives PP_i generation and release mediated via NPP1 and ANK, and diminished responsiveness to IGF-I, which normally suppresses elevation of chondrocyte extracellular PP_i. From (Terkeltaub 2006).

2.3.4. TNAP or Tissue Non Specific Alkaline Phosphatase

In human four types of alkaline phosphatase exist: the intestinal, the placental, and the placental like, that are coded by genes located on chromosome 2, and the bony/kidney/liver alkaline phosphatase with no specific tissue of expression and thus named tissue non-specific alkaline phosphatase (TNAP) and coded by a gene on chromosome 1.

TNAP is a marker of osteoblastic cells (Hui & Tenenbaum 1998) (de Bernard et al 1986). TNAP can be detected on the cell membrane, MV and within the ECM of mineralizing cartilage and bone (Bonucci et al 1992). It can generate Pi through its Phosphatase activity using many type of substrate as nucleotide tri-, di- and even monophosphate, phosphate ester as β-glycerophosphonate (Bellows et al 1992), and pyrophosphate PPi (Moss et al 1967).

TNAP is essential for a proper mineralization, which is reflected by Hypophosphatasia and severe defect in matrix mineralization in case of loss-of-function mutations in the gene encoding for TNAP (Fedde et al 1999; McCance et al 1956; Narisawa et al 1997b; Whyte 1994) (Fig.2.2.3).

2.3.5. PHOSPHO1

PHOSPHO1 is a soluble cytosolic enzyme and a member of haloacid dehalogenase superfamily of hydrolases. PHOSPHO1 generates Pi through its phosphohydrolase activity (Houston et al 2004) that is highly specific to the two most abundant phosphomonoesters in cartilage (phosphocholine and phosphoethanolamine) (Kvam et al 1992; Roberts et al 2004). PHOSPHO1 share 30% homology at the amino acid level with the LePS2 family of acid phosphatase (Baldwin et al 2001) (Fig.2.2.3).

The expression of PHOSPHO1 is restricted to the site of mineralization in cartilage and bone in adult including MV (Roberts et al 2007; Stewart et al 2006). Its expression has been detected in the diaphysis of long bones in developing embryos and in the limb bud during the early stage of development. PHOSPHO1 expression mirrors the expression of TNAP (MacRae et al 2010); which suggest that PHOSPHO1 plays a complementary role for TNAP, which can be explained by the partial abolition of mineralization when TNAP loss-of-function mutation occurs (Whyte 2000). Indeed, double KO for Tnap and Phospho1 displays no mineralization (Yadav et al 2011).

2.4. Pi/ PPi transporters

2.4.1. Pit and other Pi transporter

The negative charge of Pi molecules makes it impossible to get to the electro-negatively charged cells by simple diffusion. Thus, the transport of Pi from the extracellular environment to the intracellular lumen occurs through Na^+ coupled Pi cotransporters (Murer et al 2000; Tanaka & DeLuca 1973). These cotransporters or solute carrier can be distributed into three series: the SLC17, SLC34, and SLC20. The first one SLC17, also called NPT1 and identified as type I, can transport Pi and other anions and thus has no specific activity toward Pi. The type II of cotransporters is the SLC34. This renal-specific NaPi is responsible for the renal reabsorption of Pi and thus implicated in the regulation of Pi concentration in the blood. The type III of cotransporters or SLC20 family includes 2 members: the PiT1 (SLC20A1) and PiT2 (SLC20A2) with 60% of homology, and high affinity to Pi (Collins et al 2004).

2.4.2. Progressive ankylosis (ANK)

Intracellular PPi can be degraded by many enzymes as the acid phosphatase. Another alternative of intracellular PPi is to be transported through ANK to the ECM to fulfill its function as mineralization inhibitors or get degraded by TNAP (Terkeltaub 2001).

ANK is a transmembrane protein with at least 8 predicted transmembrane domains. The expression of ANK can be detected in many tissues as in the liver, heart, lungs, kidney, spleen, brain and others. Its main function is to transport the intracellular produced PPi to the ECM (Ho et al 2000; Johnson et al 2003).

ANK can play some functions on the osteoblastic lineage, as it can be a positive regulator of osteoblastic and osteoclastic differentiation (Kim et al 2010). Also, ANK can be a modulator of mineralization in many tissues as the joints and the kidney (Carr et al 2009) (Fig.2.2.3).

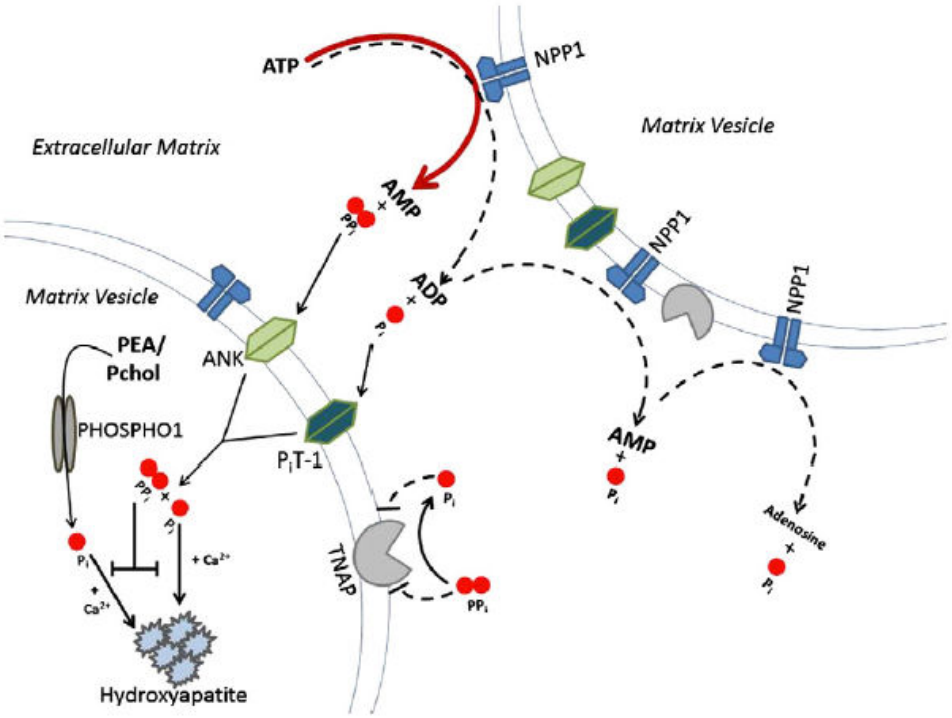

Fig.2.2.3. The main implicated actors in Pi/PPi balance from (Mackenzie et al 2012).

NPP1 main function is to hydrolyze ATP into AMP and PPi, in secondary reaction (in dotted line) NPP1 hydrolyze ATP into ADP and thus liberating Pi. The released PPI can be digested into Pi *via* TNAP; released Pi can be transported by PiT while PPi transport occurs through ANK. In the vicinity of the cells or vesicles PHOSPHO exert its function by releasing Pi through hydrolyzing PEA and Pchol. All these factors regulate the Pi/PPi balance and thus the process of mineralization.

3. MINERALIZATION INHIBITORS

In addition to PPi, many other molecules within the body can inhibit the mineralization whether to prevent its occurrence in soft tissues or to regulate the physiological mechanism. Depending on the type of the inhibitor, the mechanism of inhibition differs. For example, FGF23 and Klotho act on inhibiting mineralization by reducing the level of Pi in the blood while, some SIBLING as Phosphophoryn (see 1.3.3), Osteoprotegerin and even PPi act locally. Other inhibitors and their effects are listed in the (table 2.2.1)

3.1. Fetuin-A (FA)

Fetuin A (2 α-Heremans-Schmid glycoprotein) is a subset of glycoprotein firstly described by Pedersen in 1944 (Pedersen 1944). This 59 kDa glycoprotein is synthesized in the liver and can be ubiquitously found in ECM. A circulating calcification inhibitor function was attributed to Fetuin A (Schäfer et al 2003a). It has been demonstrated that circulating Fetuin A is an important inhibitor of ectopic calcification, as low level of Fetuin A is associated with cardiac valvular calcification (Wang et al 2005); the presence of reduced level of Fetuin A in the serum in patient with CKD and under haemodialysis is related to higher risk of cardiovascular mortality (Ketteler et al 2003). In addition, the function of Fetuin A as a mineralization inhibitor can be deduced from animal models, where the knockout mice for Fetuin A showed ectopic mineralization in variant number of tissues as kidney, lung, muscle, skin and vessels (Schäfer et al 2003b), mineralization defect was also noticed in long bone (Szweras et al 2002). Fetuin A also displays anti-inflammatory property (Wang et al 1997).

3.2. Osteopontin (OPN)

Osteopontin is a member of the SIBLING family, an acid phosphorylated glycoprotein, first discovered in bone where it is mainly found at the bone surfaces facing single cells, especially osteoclasts (Boskey et al 1993; Denhardt & Guo 1993). Osteopontin can regulate osteoclast formation as found in *in vitro* study (Rittling et al 1998). However, osteoclasts are not the only way OPN can regulate mineralization: OPN can bind to hydroxyapatite crystals and cells using the Arg-Gly-Asp motif and the polyacidic amino acid sequence and thus repress mineralization (Mckee & Nanci 1996) by inhibiting nucleation and crystal formation (Boskey et al 2002; Boskey 1995; Hunter et al 1996).

The absence of OPN in most of soft tissues and its abundance in sites of ectopic calcification suggest that it has a function in the ectopic mineralization as in the case of atherosclerotic

lesions (Giachelli et al 1993); whereas OPN is not expressed in the normal blood vessels (Fitzpatrick et al 1994).The activity of OPN as a vascular mineralization inhibitor is due to posttranslational modification and phosphorylation of the protein (Jono et al 2000b).

It is worth noting that OPN had other functions, as it can be involved in tissue inflammation, wound healing, angiogenesis and others (Cho et al 2009; Gerstenfeld 1999; Sodek et al 2000).

3.3. Matrix Gla protein (MGP)

MGP belongs to the family of Gla proteins. These proteins can be synthesized in the liver and in the skeleton (Furie & Furie 1988; Hale et al 1988; Hauschka et al 1989). Their mineral binding propriety is due to the presence of several γ-carboxylated glutamic acid residues. The γ-carboxylation happens through a specific γ-carboxylase whose action is post-transcriptionally controlled by vitamin K (Hauschka et al 1989). The liver synthesized Gla proteins include major coagulation factors while the skeleton Gla proteins are Bone Gla protein (BGP), MGP and a newly discovered protein called Gla-rich protein (GRP) (Viegas et al 2008).

MGP was firstly discovered by Price in 1983 (Price et al 1983). It is formed of 84-residues and contains one disulfide bond and 5 γ-carboxyglutamate (Gla) residues at the following positions: 2, 37, 41, 48 and 52. *Mgp* gene shows a big homology to the *Bone Gla protein (Ggp)* gene, although, the characteristics of the MGP and BGP proteins seem to be chemically and physically different (Price & Williamson 1985).

Mgp gene in *Homo sapiens* is mapped to the chromosome 12 and is formed of 4 exons. Luo *et al* showed in their study on mice embryos that the expression of *Mgp* can be detected at E10.5 in the lung buds and limb buds but only at the mesenchymal-epithelial interface. As the development proceeds, MGP expression becomes more restricted to the chondrocytic lineage and in the growth plate where MGP can be found in all the zones, the pre-hypertrophic zone excluded. In fact, during prenatal life, MGP is expressed mainly in the respiratory system, where its expression became restricted with time to the trachea, bronchiolar-ducts and to the cartilaginous component of the intrapulmonary bronchi at E17.5. MGP can also be found in all cells of chondrocytic lineage and in the uterus, muscle and kidney medulla. In adult mice, MGP expression is detected in the respiratory system, skeleton and growth plate and different organs and as the uterus, kidney, brain, heart, and spleen. The expression of *Mgp* was not detected in the bone cells (Luo et al 1995), although the level of MGP in bone and dentin can get to 0.4 mg/g (Price et al 1985).

After its transcription and translation, MGP can undergo two post-translational modifications: a vitamin K-dependent γ-glutamate carboxylation, crucial for the normal function of MGP, and a serine phosphorylation, which seems to be important for the regulation of MGP secretion as proposed by Wajih (Wajih et al 2004), and may partially inhibit the mineralization as demonstrated by Schrungers (Schurgers et al 2007).

The first function attributed to MGP was related to its calcium binding features allowing it to bind to hydroxyapatite through the side chains of arginine and γ-carboxyglutamate (Riordan 1979). Through this linkage, MGP is thought to inhibit hydroxyapatite crystal nucleation and growth. Nevertheless, as the first MGP purification took place in the beginning of eighties,the purified MGP was in a complex with BMP, which suggests that the MGP and BMP are associated *in vivo* (Price et al 1983; Urist et al 1984). Later, it has been demonstrated that MGP is an inhibitor of BMP-2 and 4 (Sweatt et al 2003; Yao et al 2006; Zebboudj et al 2002), both potent inducers of bone and cartilage (Ducy & Karsenty 2000). Also BMP2 can control bone mineralization and alkaline phosphatase expression through a Wnt autocrine loop (Rawadi et al 2003). Indeed, the presence of γ-carboxyglutamate Gla seems to be essential for MGP binding to the hydroxyapatite crystals and to inhibit BMP; However, Bostrom's team has shown that the most critical features for MGP in inhibiting BMP is not limited to the γ-carboxylated motif but rather entailed to well conserved proline motif (Pro 64), although the presence of two γ-carboxylated glutamate (Gla) residues on each side of Pro64 where indispensable (Yao et al 2008).

These observations made the function of MGP in inhibiting mineralization clearly evident, and were in agreement with other experimental and clinical findings to Warfarin treatment and MGP mutation in human and in mice model.

Warfarin is an inhibitor of the vitamin K-dependent γ-carboxylase. The treatment of pregnant rats with Warfarin alters the growth of newborn rats with absence of ossification center within the bones, and lead to a disorganized hypertrophic zone within the physis (Feteih et al 1990; Price et al 1982). Considering clinical cases, pregnant women treated with Warfarin is followed by in some cases by the death of newborn or a stillbirth (Cotrufo et al 2002), with tracheal collapse being the cause of the death as reported in one clinical case (Abbott et al 1977). In addition, infant treated with Warfarin after valve replacement surgery suffers from an extensive ectopic mineralization in the tracheo-bronchial airways. Also Warfarin and

vitamin K inhibitor can be associated to the calcification of coronary arteries n some cases (Schurgers et al 2012).

Warfarin is a vitamin K inhibitor, thus the phenotype seen can be the outcome of not only MGP alteration but maybe the effect of one or many if not all Gla protein family. However, to recognize the exact function of MGP, MGP gene should be the only one altered as in $MGP^{-/-}$ mice model. The absence of MGP in these mice is reflected by short stature explained by the mineralization of the proliferative zone, fast heartbeat, and a reduced longevity. Extensive arterial calcification leading to vessels rupture has been shown to be the cause of death (Luo et al 1997) with the appearance of cartilage nodules in the calcified aorta (El-Maadawy et al 2003; Leroux-Berger et al 2011). Ectopic mineralization of the lower end of the trachea and bronchi was also noted (Luo et al 1997). Keutel syndrome (see tracheal mineralization) hallmark is an abnormal cartilage calcification with brachytelephalangism, mid-face hypoplasia, depressed nasal bridge, hearing loss and peripheral pulmonary stenosis (Hur et al 2005). However, in humans, MGP absence is not sufficient for inducing the vascular calcification; the absence of another mineralization inhibitor or the expression of mineralization promoting factor should be added, as suggested by Cranenburg (Cranenburg et al 2011).

Interestingly, Bostrom's team made the observation that the absence of MGP leads to endothelial cells with stem cell like potency and, depending on the signaling factors synthesized locally, a differentiation of endothelial cells toward a specific lineage can be seen.

Whether the function of MGP is nucleation inhibitor or a gradient for the endothelial cells identity or others, it has been demonstrated by Murshed *et al* that it can exhibit its function only on a local level since overexpressing *Mgp* into the blood vessels did not correct defects in *Mgp* knock-out mice (Murshed et al 2004). Also, using vitamin K supplementation in human with uncarboxylated-MGP in Keutel syndrome fails to correct syndrome emerging defects (Cranenburg et al 2011).

Gene/Protein	Mouse mutant phenotype	Human syndrome/Pathology
Matrix Gla Protein (MGP)	Spontaneous arterial and cartilage calcification (El-Maadawy et al 2003; Luo et al 1997)	Keutel syndrome: cartilage and soft tissue calcification (Munroe et al 1999)
Endonucleotide Pyrophosphatase-1 (ENNP-1)	Vascular and cartilage calcification (Johnson et al 2005)	Idiopathiic infantile arterial calcification (Rutsch et al 2003)
PPi channel progressive ankylosis protein (ANK)	Vascular and cartilage calcification (Johnson et al 2005)	Idiopathic infantile arterial calcification (Zaka et al 2006)
Ecto 5' nucleotidase (CD73)	Vascular proinflammatory phenotype, autoimmune inflammatory phenotype (Blume et al 2012)	Arterial calcification with medial lesions that involves the entire circumference of the elastic lamina (Markello et al 2011). Joint calcification (St. Hilaire et al 2011)
Osteopontin (OPN)	Up-regulation associated to vascular calcification in LDLR-/- atherosclerotic mice (Towler et al 1998)(	Up-regulation associated to vascular calcification in atherosclerosis (Bostrom 1993, Shanahan 1994) and CKD patients (El-Abbadi et al 2009; Moe et al 2002)
Fetuin A	TGF-b up-regulation, myocardial calcification (Merx et al 2005)	Reduced serum level in dialysis patients (Ketteler 2003) Prevent atherosclerotic calcification in type II diabetic patients (Emoto et al 2010)
Fibroblast growth factor-23 (FGF-23)	Hyperphosphatemia, hypervtaminosis D, vascular calcification (Shimada et al 2004b)	Familial tumoral calcinosis, hyperphosphatemia, hypervitaminosis D, vascular calcification (Benet-Pagès et al 2005)

Table.2.2.1. Main mineralization inhibitors and their mutations effects in mouse and human.

4. WHEN MINERALIZATION GOES AWRY

4.1. Aberrant mineralization:

A pathological aberrant mineralization can be the result of defective or overactive mineralization in the right physiological place. There are numerous examples of aberrant mineralization-related diseases. They can be due to the disturbance in one of the ossification modulators as in the case of mutation in PTH/PTHrP receptor leading to Jansen's metaphyseal chondrodysplasia (Minagawa et al 2002; Schipani et al 1995) or in the case of lack of ascorbic acid reflected by abnormal development of collagen fibrils and leading to scurvy disease (Gould 1963).

Rickets, also called osteomalacia when it occurs in the adult life, is a skeleton disease, characterized by increased amount of uncalcified matrix in bone and abnormal development of hypertrophic and maturing zone in growth plate with decrease in matrix calcification. In rachitic chicken, it has been shown that the crystals can be formed but do not spread and the mineralization is arrested at an intra-vesicular stage (Takechi & Itakura 1995). Nevertheless, a defect in proteoglycans can also be detected in rachitic growth plate as a reduction in proteoglycans size was signaled (Roughley & Dickson 1980).

Rickets can be the results of vitamin D deficiency or phosphate metabolism defect, the first one is called vitamin D-dependent rickets and the second is called vitamin D-resistant rickets (Drezner & Harrelson 1979; Haussler & McCain 1977).

The autosomal-dominant hypophosphatemic rickets (ADHR) is a phosphate wasting disease characterized by bone pain, fracture and short stature. The mutation responsible of ADHR is mapped to chromosome 12p13 (Bianchine et al 1971; Econs & McEnery 1997) and affects the FGF-23 gene (White et al 2001b) leading to the synthesis of a polypeptide less sensitive to protease cleavage by abolishing the consensus cleavage site (RXXR) (Bai et al 2003; White et al 2001a). FGF23 is a member of FGF family, it has a main function in regulating intestinal (Haussler et al 1998) and renal phosphorus absorption (Baum et al 2005; Shimada et al 2004a).

4.2. Ectopic Mineralization:

Ectopic mineralization can be pathological, as in the case of vascular calcification or joints calcification, or can occur with absence of pathological aspect, as in the case of mammary microcalcification, pulmonary alveolar microlithiasis and testicular microlithiasis. The ectopic mineralization is the result of an imbalance in promoter/inhibitor of mineralization, as in the case of the loss of Mgp leading to ectopic mineralization in Keutel syndrome (Parmar et al 2006) or a high blood level of phosphate leading to vascular calcification in chronic kidney disease patient (Koleganova et al 2009). A brief look into some of mineralization defects and the involvement of phosphate implication is discussed in the following part.

4.2.1. Pathological ectopic mineralization

4.2.1.1. Vascular Calcification

The arteries are muscular blood vessels, in the wall of the arteries three different layers can be identified, the inner layer lining the lumen is the intima composed of one layer of endothelial cells, the middle layer is the media formed of many layers of vascular smooth muscle cells (VSMC) and are the thickest in the aorta, the outer layer of the aorta is the adventitia formed of connective tissues and dense ECM, rich with collagen fibers. In addition to its circulatory function the artery has the ability to regulate blood pressure by means of its muscular layer or the media.

The deposition of hydroxyapatite crystals in arteries can occur in the intima or in the media. Intimal calcification is found in the case of atherosclerotic plaque formation and can be found in arteries of big caliber and in the coronary arteries (Stary 2000). Medial calcification or Monckeberg's arteriosclerosis, is mostly found in diabetic and chronic kidney disease (CKD) patients (Shanahan et al 1999). Patients with CKD can also develop intimal calcification once at the stage 4/5 of the disease (Gross et al 2007; Nakamura et al 2009).

The vascular calcification is a risk factor for cardiovascular disease and mortality (Chiu et al 2010; London et al 2003), and cardiovascular diseases are the main reason for lethality in patients with CKD (Foley et al 1998).

The decreased level of circulating mineralization inhibitor as PPi and Fetuin A (Moe et al 2005; O'Neill et al 2010) or the increased level of the inactive uncarboxylated form of MGP (Schurgers et al 2010) can promote the mineralization of arteries. However, the presence of a high level of circulating calcium and phosphate in CKD patients can be a key feature in the

link between vascular calcification and CKD, as it has been demonstrated that a high level of circulating phosphate and calcium can induce mineral deposition in arteries (Adeney et al 2009; Goodman et al 2000; Oh et al 2002; Raggi et al 2002). In fact, it has been shown in a clinical study that even when there is no sign of CKD the high level of phosphorus in the serum is associated with an increased cardiovascular disease. Dhingra *et al* explain that the mechanism by which these mineralization occurs can be related to the increase in the propensity of mineral deposition in the arteries (Dhingra et al 2010), relying on *in-vitro* studies (Chen et al 2002; Giachelli et al 2005).

From another point of view, Murshed *et al* have suggested that any mineralization prerequisite is the concomitant presence of fibrillar collagen and TNAP in the ECM (Murshed et al 2005). The collagen rich matrix in the media fulfill one of the mineralization essential, while the expression of TNAP is not a common observation in VSMC of the media. However, alkaline phosphatase activity has been reported in vascular smooth cells under calcifying uremic conditions (Chen et al 2002; Tyson et al 2003). The detection of TNAP activity in VSMC of calcifying arteries is not a quite shocking fact as the presence of osteo/chondrogenic lineage cells has been reported (Abedin et al 2004), this lineage can be the results of a transdifferentiation of VSMC into chondrogenic or osteogenic lineage (Bobryshev 2005; Speer et al 2009). In fact the VSMC of normal human aorta express both Cbfa1 and Sox9 under normal conditions, which reveals their ability to undergo chondrogenic differentiation (Tyson et al 2003) (Fig.2.4.1).

The presence of high level of circulating Pi can be responsible for this differentiation. The presence of Pi above the physiological concentration are transported by Pit transporters into the cells where it induces osteogenic differentiation and upregulation of the transcription of Cbfa-1 (Jono et al 2000a) (Fig.2.4.1).

The implication of Pi in the process of vascular mineralization can be further seen in the cases where one of genes involved in Pi/PPi balance is mutated as in the case of Idiopathic infantile arterial calcification due to ANK mutation (Zaka et al 2006) or when ENPP-1 is mutated (Rutsch et al 2003) (Fig.2.4.1).

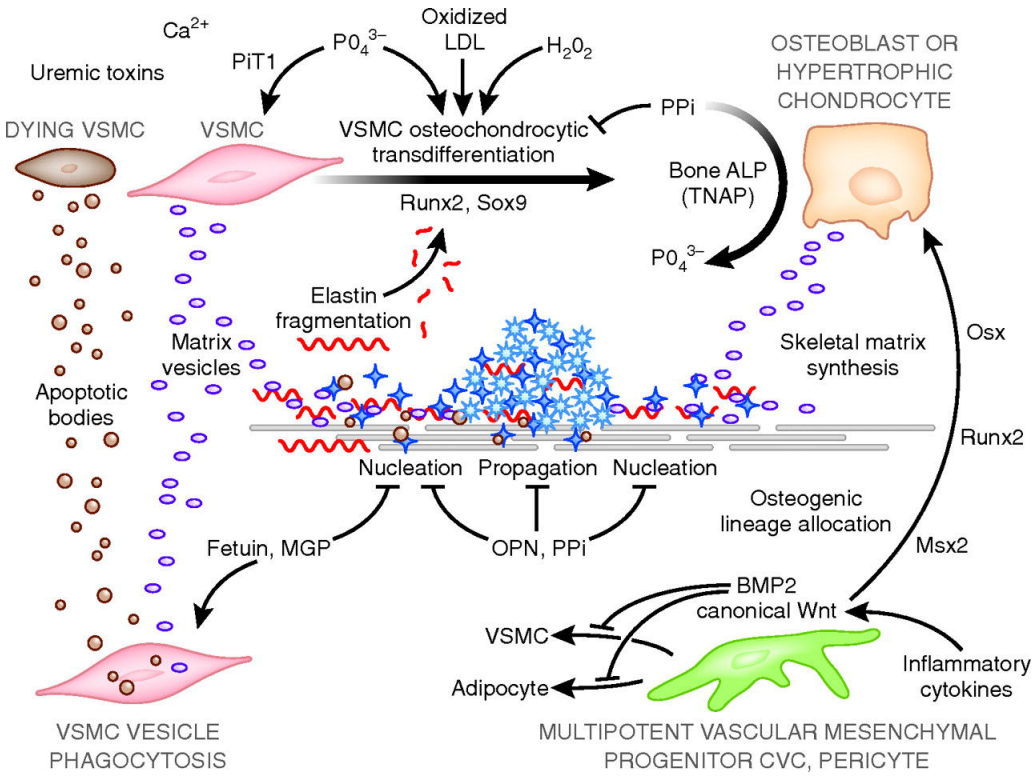

Fig.2.4.1. Cell fate, function, and phenotype in vascular calcification.
In response to uremic toxins or elevated calcium and phosphate levels, VSMCs elaborate lipidaceous vesicle from apoptotic cells or produce matrix vesicle. The latter, approximately one third the diameter of apoptotic bodies, are much more efficient in nucleating mineral deposition. These vesicles nucleate calcium deposition in the form of a poorly crystalline hydroxyapatite, associated with the elastin-rich extracellular matrix of arteries. The process of elastinolysis not only creates sites for vesicle, mediated nucleation, but also released EDPs that promote osteochondrogenic "transdifferentiation" of VSMCs. This latter process is stimulated by oxidized LDL and ROS, viz., hydrogen peroxide. With osteochondrogenic differentiation, gene expression profiles change dramatically, with induction of bone ALP, production of a highly collagenous extracellular matrix, and elaboration of matrix vesicle. Bone ALP locally degrades inorganic pyrophosphate, an important inhibitor of mineralization and transdifferentiation. In addition, multipotent vascular mesenchymal progenitors called calcifying vascular cells (CVC) or pericytes can yield cells of the osteoblast and chondrocyte lineage. This occurs through paracrine BMP and canonical Wnt signals that "shunt" these proliferating progenitors away from other fates, such as the mature VSMC, and toward osteogenic lineages. Inflammatory cytokines such and TNF play critical roles. Of note, as shown by Shanahan's group,19,20 the phagocytic clearance of matrix vesicles by VSMCs is critical in limiting the number of sites that nucleate mineral deposition. In severely advanced atherosclerotic lesions, cholesterol crystals have also been shown to nucleate calcium phosphate deposition as well. From (Mizobuchi et al 2009).

4.2.1.2. Articular cartilage and mineralization:

The articular cartilage is a hyaline permanent cartilage of few millimeters of thickness and with extraordinary mechanical properties and low metabolic activity. The only cellular component of the articular cartilage is chondrocyte. These cells synthesize the ECM of the articular cartilage, which consists mostly of water, proteoglycans, collagen primarily type II, glycoproteins and other proteins. The articular cartilage subdivides into four distinct zones,

within each zone not only the structure and composition of ECM vary but also the morphology and the distribution of chondrocytes (Flik et al 2007).

The articular cartilage can be the subject of great modifications with age as the changes in the size and molecular nature of proteoglycans: the size of proteoglycans aggregates decreases in old cartilage, with a decrease in chondroitin sulfate 4 concentration and an increase in chondroitin sulfate 6, also in old cartilage the proteins concentration increases while the water content decreases. All these changes lead to a more stiff cartilage (Flik et al 2007). However, pathological conditions can be related to aging cartilage. In fact, joint diseases are more prominent in the elderly population with osteoarthritis (OA) (Felson et al 1987) and calcium pyrophosphate crystal deposition disease (CPPD) (Felson et al 1989).

Millions of people are affected with OA, the most common form of rheumatic disease, with an expected increase in its prevalence with the increase in life expectancy (Arden & Nevitt 2006). In OA, the cartilage can get fully destructed but almost all the part of joint can be affected (Hunter & Felson 2006). CPPD is common in the population and can be associated in some cases to OA (Abhishek & Doherty 2010).

The presence of calcification within the articular cartilage was found in 100% of the cases of primary OA as basic calcium phosphate aggregates (BCP). Nevertheless, in 20% of the cases the presence of calcium pyrophosphate dihydrate crystals (CPP) was reported (Fuerst et al 2009a; Fuerst et al 2009b). Interestingly, the additional presence of both crystals in the joints of patients has been linked to aggravated OA (Ryu et al 2014). The CPP and BCP crystals make two different kind of deposits, while the BCP crystals produce a periarticular calcification the CPP crystals produce an intra-articular and linear calcification (Abhishek & Doherty 2010). Regarding CPPD, it has been established an implication of ANK in cases of familial polyarticular chondrocalcinosis (Andrew et al 1999; Doherty et al 1991; Hughes et al 1995; Netter et al 2004; Pendleton et al 2002; Williams et al 2003). The mutations in human *Ank* induce a gain-of-function of the protein, which leads to an increase in the extracellular PPi (Andrew et al 1999; Doherty et al 1991; Hughes et al 1995; Pendleton et al 2002; Williams et al 2003; Zaka et al 2006). The high extracellular PPi concentrations are responsible for CPP crystal formation (Pendleton et al 2002).

Although BCP and CPP crystals are considered as innocent bystanders by some investigators (Pritzker 2009), there is a growing evidence that they may be in the heart of both OA and CPPD diseases. In fact, when embedded within the ECM of cartilage the crystals are

protected from interaction with the surrounding environment and thus unable to promote inflammation (Lioté & Ea 2007) but once released they may induce inflammation. For instance, CPP crystals can activate synovial cells and promote prolonged neutrophilic inflammation by inhibiting the apoptosis of neutrophils (Higo et al 2010; Lioté & Ea 2007; Tudan et al 2000). In animal models of OA, the injection of CPPD crystals into the knee on a weekly basis worsened the cartilage destruction in rabbit (Fam et al 1995), while treatment with mineralization inhibitors can reduce the severity of OA lesions in pig (Cheung et al 2006). On the other hand, BCP crystals showed the ability to induce inflammation through promoting NO production by articular chondrocytes (Ea et al 2005), activation of fibroblast proliferation and the production of inflammatory cytokines in *in vitro* studies (Ea & Liote 2009; McCarthy & Cheung 2009).

BCP origin in OA is still unclear many factors can be implicated, however it is worthy to note that chondrocytes undergoing hypertrophy is a constant finding in OA articular cartilage (Tchetina et al 2005).

4.2.2. Non-pathological ectopic mineralization

4.2.2.1. Mammary microcalcification:

Described first in 1951, mammary microcalcifications are known as cases with calcium deposits within the breast tissue (Leborgne 1951). This deposition can take many shapes and can be formed with two types of crystals: calcium oxalate or hydroxyapatite (Frappart et al 1984).

The calcification by itself has no clinical impact but when associated with breast cancer it can be linked to a poor prognosis. It has been reported that the presence of casting type calcifications is related to poor survival rate (Peacock et al 2004; Tabar et al 2004). Also a connection between the type of crystal and the prognosis was established. Oxalate calcium has been linked to benign cancer and hydroxyapatite crystals to both benign and malignant cancers (Frappart et al 1984; Haka et al 2002).

An imbalance in the regulators of physiological mineralization is suggested to rely behind the ectopic mineralization within the breast tissues. It has been reported that TNAP and the type II family of Na-Pi cotransporters are implicated in the process of microcrystal formation. The formation of extracellular crystals is enhanced by the collagens fibrils (Kirsch 2006) despite the upregulation of osteopontin within the ECM in a attempt to inhibit the microcrystal formation (Cox et al 2012).

4.2.2.2. Pulmonary alveolar microlithiasis

Pulmonary alveolar microlithiasis (PAM) is a rare (only 242 cases reported worldwide) idiopathic disease introduced first by Malphighi in 1686. The etiology of the disease is unknown but an inherited trait thought to be involved. It is characterized by the presence of innumerable microliths or calcific concretion (Castellana & Lamorgese 2003; Mariotta et al 1997). The distribution of microliths can be clinically valuable as it gives a clue on the type of the disease. When microliths are secondary to adenocarcinoma or tubercular remnants or pleural mesothelioma the microliths would be concentrated in one region of the lung (Aliperta et al 1977).

Patients suffering from PAM can be asymptomatic or they can present with cough, fever, cyanosis and increasing dyspnea or respiratory failure. The microliths can be difficult to remove with a diameter larger than that of bronchioli (Palombini et al 1981). The deposition of the microliths in the alveoli is related to a calcium salt sedimentation within the alveoli with evidence of carbonic anhydrase enzyme involvement (Lopez-Areal et al 1965). It also can be in relation with increased endoalveolar pH or can occur after alveolar cell damage (Mariotta et al 1997).

4.2.2.3. Testicular microlithiasis

Testicular microlithiasis (TM) is an entity of unknown etiology (Rashid et al 2004). It is described as intratesticular microcalcifications with two histological varieties. The first one is hematoxylin body consisting of amorphous calcific debris and the second is laminated calcifications (Bach et al 2001).

Many hypothesis where created to explain the TM genesis. The most popular one, postulated by Vegni-Talluri *et al* , explains that the microcalcification formation is the result of cellular debris accumulation in the seminiferous tubules (Vegni-Talluri et al 1980). An additional role can be played by the deposition of concentric rings of glycoproteins (Bieger et al 1965).

TM is widely associated with different pathologies. Many of them are benign as in the case of hydrocele (Thomas et al 2008), variocele (Thomas et al 2008) or undescended testis (Nistal et al 1995). It can also be associated to malignant pathology with primary testicular malignancy being the most important one, although there has been no explanation for the association between testicular tumor and TM (Höbarth et al 1992; Ikinger et al 1982).

TRACHEA AND MINERALIZATION

WHAT DO WE KNOW?

A. Trachea getting old

Trachea goes through major changes during aging. The tracheal cartilage is the most affected by these changes, which can be translated by decreased compliance of the trachea with age (Croteau & Cook 1961). Tracheal mineralization is a common finding in adults, especially in the elderly human population. Accepted as a normal physiological process of aging, it is generally asymptomatic even though it can be in some severe cases accompanied by clinical significance as patients may complain from dyspnea associated with stridor or wheezing. If in humans, those calcifications are observed in patients over 40 years old, a few reports have described early mineralization of the respiratory tract in young birds and rodents (Hogg 1982; Sasano et al 1993).

E. Bonucci was the first to describe tracheal changes with age. In a study published in 1974 (Bonucci et al 1974). the authors showed morphological and biochemical modification of the tracheal rings. Bonucci *et al* found that old cartilage is marked by a reduced number of chondrocytes, an increase in glycogen deposit and an accumulation of lipidic material within large cytoplasmic vacuoles. And to our knowledge, he was the first to reveal that the tracheal cartilage, a hyaline cartilage supposed to be a permanent cartilage, mineralize in relatively young rats.

All along with this mineralization, Bonucci *et al* noticed changes in intercellular matrix composition in the tracheal cartilage of 30 day-old rats, similar to changes that occur in 20 day-old costal cartilage. They also found chondroitin sulfate decrease and heparan sulfate increase, with slight changes in glycoproteins in subperichondrial area in old rat.

Bonucci *et al* also noted some changes in collagen fibrils. Whereas there seem to be thin fibrils, non-periodic and associated with roundish electron dense granules in newborn rats, those became thicker, periodic and associated with few (less abundant) granules in old cartilage.

The authors also suggested the presence an abnormal synthetic activity of chondrocytes in old cartilage. These results were not confirmed or built on by further studies (Bonucci et al 1974).

B. Tracheal mineralization associated to pathology

If tracheobronchial calcifications are not uncommon in patients aged 40 years and older, there are considered very rare radiologic findings in children (Fig.A.A), even though probably overlooked because typical symptoms are absent except in severe cases. Although the cause

remains largely unknown, these early tracheobronchial calcifications have been reported in patients following extended warfarin treatment, with Keutel syndrome or with tracheobronchopathia osteochondroplatica.

B.1. Warfarin therapy

Warfarin-sodium is used as an anticoagulation therapy in adults or children who underent prosthetic valve replacement. In a vast majority of these patients, mineralization of the tracheobronchial tree is frequently observed (Fig.A.B), establishing a link between anti-vitamin K treatment and cartilage mineralization. In fact the percentage of tracheobronchial calcification is estimated to be 47% in adults receiving warfarin sodium and 19% in age-matched control subjects (Moncada et al 1992). In addition, tracheal mineralization is also associated to warfarin embryopathy (Abbott et al 1977). While the cause of tracheobronchial calcifications in patients treated with Warfarin remains unknown, it is worth mentioning that warfarin inhibits normal formation of the vitamin-K-dependent γ-carboxylation process essential for the function of Gla proteins. The absence of carboxylated-MGP is so likely to be responsible for the calcifications observed after Warfarin treatment (Joshi et al 2000).

B.2. Keutel syndrome

First descibed in 1972 by Keutel, this syndrome is a rare recessive hereditary disease, characterized by brachytelephalangia (short, broad distal phalanges), midfacial hypoplasia, abnormal cartilage calcifications, peripheral pulmonary stenosis and hearing loss (Acar et al 2010; Demirel et al 2012). One of the clinical features of this disease is an unsuspected and extensive calcification of the cartilage in the external ears, nose, larynx, trachea (Fig.A.C), and ribs (Meier et al 2001). This ectopic mineralization is caused by homozygous mutation in the gene encoding the human potent mineralization inhibitor Matrix Gla Protein (see Chapter II part 3.3.) leading to its complete absence or its presence as a defective form.

B.3. Tracheobronchopathia Osteochondroplastica (TO)

Tracheobronchopathia Osteochondroplastica is an idiopathic rare disease characterized by the presence of submucosal osteocartilaginous nodules in the tracheobronchial tree (Chroneou et al 2008; Jindal Shikha 2013). They consist of hyaline cartilage with areas of lamellar bone or bony nodules with hematopoietic bone marrow (Tajima et al 1997). Those nodule arise from mesenchymal cells in submucosa (Dalgaard 1947) or from the perichondrium (Paaske & Tang

1985). Study by Tajima *et al*. showed an extensive BMP-2 (potent osteoinducer, see chapter I. part 4.2.4.3 and chapter II part 3.3) distribution in mesenchymal cells around the oseocartilagenous nodules in the submucosa (Tajima et al 1997). TO occasionally produces mineralization (Fig.A.D) and narrowing of the airways with a variety of symptoms, such as dry cough, hoarseness, dyspnea, and recurrent respiratory tract infections.

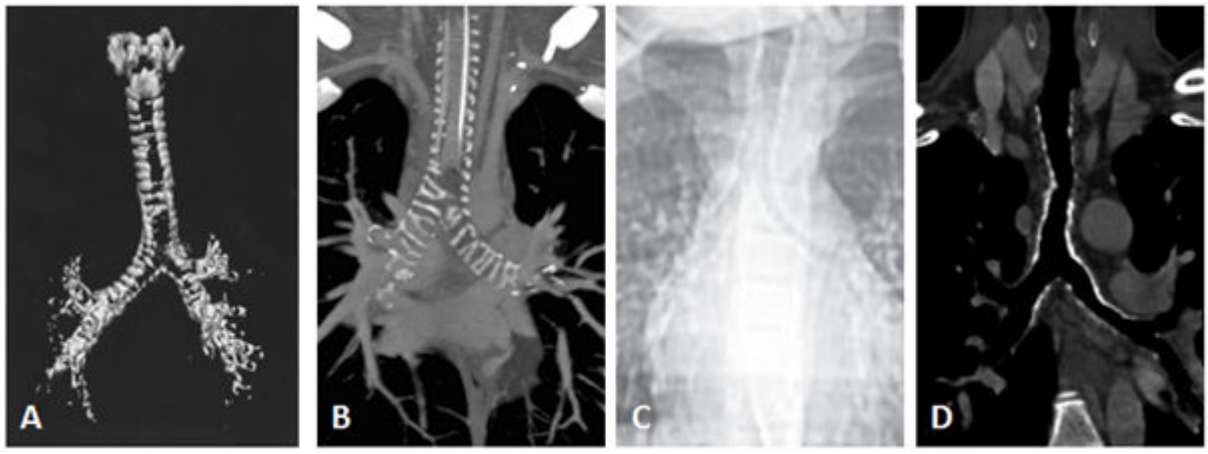

Fig. A. Tracheal mineralization (A, B, C and D) in idiopathic case of 2.5 years old boy, patient treated with warfarin, case of Keutel syndrome, Tracheobronchopathia Osteochondroplastica. From respectively (Ceyhan et al 2008) (Joshi et al 2000) (Ozdemir et al 2006) (Jindal Shikha 2013).

OBJECTIVES OF OUR STUDY

The main objective of this thesis was to understand how, using the mouse as a model, the mineralization of the trachea occurs during aging and possibly established a role of Matrix-Gla Protein (MGP) in this process. For that purpose, we designed:

1. *In vitro* experiments to:

1- Elucidate if chondrocytes and smooth muscle cells of the trachea have both the propensity to mineralize (especially in response to high phosphate levels)

2- Identify the molecular actors responsible for their mineralizing ability

2. *In vivo* experiments to:

1- Elucidate the spatiotemporal pattern of the mineralization process of the trachea

2- Identify the tissues and cells implicated in this process.

3- Decipher the molecular bases behind tracheal mineralization.

OBJECTIFS DE NOTRE ETUDE

L'objectif principal de cette thèse était de comprendre comment, en utilisant la souris comme modèle, la minéralisation de la trachée se produit au cours du vieillissement et d'établir le rôle potentiellement joué par la Matrix-Gla protein (MGP) dans ce processus. Pour cela, il a été réalisé :

1. des expériences *in vitro* pour:

   1- Evaluer si les chondrocytes et les cellules musculaires lisses de la trachée sont capables de minéraliser (en présence de concentrations élevées de phosphate).

   2- Identifier les molécules responsables de la capacité de ces cellules à minéraliser.

2. des expériences *in vivo* pour:

   1- Etablir la progression spatio-temporelle du processus de minéralisation de la trachée.

   2- Identifier les tissus et cellules impliqués dans ce processus.

   3- Caractériser les acteurs moléculaires à l'origine de la minéralisation trachéale et en particulier le rôle de MGP.

CHAPTER III

TRACHEAL MINERALIZATION *IN-VITRO* APPROACH

Etat de l'art

En conditions physiologiques, la minéralisation de la matrice extracellulaire se produit exclusivement dans le squelette et les dents. Cependant, au cours du vieillissement ou de diverses maladies, la minéralisation pathologique peut se produire dans d'autres tissus. Au cours de l'arthrose, la dégradation du cartilage articulaire est associée à une perte de protéoglycanes et un changement phénotypique des chondrocytes articulaires vers une différenciation terminale qui s'accompagne d'une hypertrophie des cellules et une minéralisation de leur matrice extracellulaire. Des événements cellulaires similaires se produisent lors des complications cardiovasculaires de diverses maladies telles que le diabète ou l'insuffisance rénale chronique, où les cellules musculaires lisses vasculaires subissent également un changement phénotypique par transdifférentiation en cellules chondro/ostéoblastiques qui minéralisent par la suite. La minéralisation observée est dûe au dépôt de cristaux contenant du phosphate (Pi) dans la matrice extracellulaire des chondrocytes articulaires ou des cellules musculaires lisses vasculaires. Même si la minéralisation de la trachée a été observée chez des sujets âgés, la capacité de chondrocytes de la trachée et / ou les cellules des muscles lisses de la trachée à minéraliser n'a pas été étudiée.

Objectif

Le but de cette première étude était de déterminer si, comme demontré pour les cellules musculaires lisses vasculaires et les chondrocytes articulaires, les cellules musculaires lisses trachéales et les chondrocytes trachéaux étaient également capables de se minéraliser en réponse à des concentrations élevées de Pi.

Matériel et méthodes

Nous avons mis en place une procédure expérimentale pour isoler simultanément les chondrocytes et les cellules musculaires lisses de la trachée de la souris adulte.

Ces cellules ont ensuite été soumises à différentes concentrations de Pi (1, 3, 5 mM) pendant 7 et 14 jours. La minéralisation a été évaluée par coloration au rouge alizarine, qui identifie les dépôts de calcium. L'expression de gènes permettant de caractériser l'identité phénotypique des cellules et impliqués dans le processus de minéralisation a été évaluée par PCR quantitative en temps réel.

Résultats

Le traitement avec une concentration croissante de Pi induit une minéralisation des deux types cellulaires observable dès 7 jours de culture pour la plus forte concentration de phosphate, mais par des mécanismes de modifications phénotypiques à priori différents.

Ces données qui demandent à être complétées indiquent que, tout comme les chondrocytes articulaires ou les cellules musculaires lisses vasculaires, les chondrocytes et les cellules musculaires vasculaires d'origine trachéale ont la capacité de se minéraliser en conditions hyperphosphatémiques

PHOSPHATE-INDUCED MINERALIZATION OF TRACHEAL SMOOTH MUSCLE AND CARTILAGE CELLS

Lina Tabcheh, Arnaud Bianchi, Alexandra Clément, Jean-Yves Jouzeau and Hervé Kempf

Bio-Medical Materials and Engineering 24 (2014) S37-S45

Bio-Medical Materials and Engineering 24 (2014) S37–S45
DOI 10.3233/BME-140972
IOS Press

Phosphate-induced mineralization of tracheal smooth muscle and cartilage cells

Lina Tabcheh [a,b], Arnaud Bianchi [a,b], Alexandra Clément [a,b], Jean-Yves Jouzeau [a,b] and Hervé Kempf [a,b,*]

[a] *CNRS, UMR 7365, IMoPA, Vandœuvre-lès-Nancy, France*
[b] *Université de Lorraine, UMR 7365, Vandœuvre-lés-Nancy, France*

Abstract.
BACKGROUND: During aging or various diseases, pathologic mineralization may occur in joints or in the vascular wall. This is due to the deposition of phosphate (Pi)-containing crystals into the extracellular matrix of articular chondrocytes or vascular smooth muscle cells. The mineralization ability of chondrocytes and smooth muscle cells of other tissue has not been investigated.
OBJECTIVE: In this context, our work seeks to study the response induced by Pi on cartilage and smooth muscle cells from tracheal origin.
METHODS: We have established a dissection procedure to harvest and isolate chondrocyte and smooth muscle cells from adult mouse trachea. Both cell types were then exposed to different concentrations of Pi (1, 3 or 5 mM) up to 14 days. Mineralization was evaluated by alizarin red staining, which identifies calcium deposition. The expression of genes characterizing the phenotypic identity of the cells and involved in the mineralization process was assessed by RT-qPCR.
RESULTS: Treatment of tracheal chondrocytes and smooth muscle cells with increasing concentrations of Pi (3 and 5 mM) induced mineralization as revealed by positive alizarin red staining as early as 7 days of culture. Moreover, gene expression analysis revealed profound phenotypic changes in both cell types and suggested they mineralize through TNAP-independent or -dependent mechanisms, respectively.
CONCLUSIONS: Our data indicate that, comparably to articular chondrocytes or vascular smooth muscles, chondrocyte and smooth muscle cells from the trachea are prone to mineralize under high-phosphate conditions.

Keywords: Trachea, smooth muscle cell, chondrocyte, mineralization, inorganic phosphate

1. Introduction

Under normal circumstances, mineralization of the extracellular matrix occurs exclusively in the skeleton (bones and teeth). However, during aging or various diseases, pathologic mineralization may happen in other tissues. During osteoarthritis, the most common rheumatic disease, the articular cartilage degradation is associated with a loss of proteoglycans and a phenotypic change of the articular chondrocytes including terminal differentiation, i.e. hypertrophy and mineralization of their surrounding extracellular matrix. Similar cellular events take place during cardiovascular complications of various diseases, such as diabetes or chronic kidney disease, where vascular smooth muscle cells also undergo a drastic

*Address for correspondence: Hervé Kempf, Ingénierie Moléculaire et Physiopathologie Articulaire (IMoPA), UMR 7365 CNRS, Université de Lorraine, Campus biologie-santé, Faculté de Médecine, Biopôle de l'Université de Lorraine, 9 Avenue de la Forêt de Haye – CS 50184, 54505 Vandœuvre-lès-Nancy Cedex, France. Tel.: +33 3 83 685 426; Fax: +33 3 83 685 959; E-mail: herve.kempf@inserm.fr.

phenotypic change by trans-differentiating into chondro/osteoblast-like cells, whose extracellular matrix eventually mineralizes. Interestingly, contrary to former conception, there are now accumulating evidence suggesting that the mineralization that occurs in the joint or the arterial wall is due to an active and regulated deposition of phosphate (Pi)-containing crystals, similar to those found in bone tissues, within the extracellular matrix of articular chondrocytes or vascular smooth muscle cells, respectively.

Moreover, *in vitro* studies and animal models of articular and vascular calcifications suggest that Pi not only participates in hydroxyapatite crystal formation, but also directly induces phenotypic changes and mineralization of the cells. For instance, using the murine ATDC5 chondrogenic cell line, it has been shown that Pi supplementation induces chondrogenic maturation and mineralization [1]. Similarly, numerous reports demonstrated that elevated phosphate induces chondro-osteogenic differentiation and mineralization of vascular smooth muscle cells [2–4].

Aside from the vast body of literature investigating the mineralization of smooth muscle cells from the vasculature and chondrocytes from the skeleton, to our knowledge, there is no report regarding the mineralizing potential of the very same cells from other tissues.

Remarkably, the trachea, also called windpipe, is composed of both smooth muscle and hyaline cartilage cells in juxtaposed tissues that play essential roles in the function of this very complex structure of the respiratory tract. Indeed, for the flawless passage of the air throughout the trachea and its further progression into the bronchi, the trachea needs to be elastic and rigid enough at the same time in order to maintain the right air pressure and prevent the collapse of the tracheal tube, respectively. A band of smooth muscle cells, called trachealis muscle and located dorsally, contributes to the elasticity of the trachea during breathing and fills the gap between ventrally distributed C-shaped cartilaginous rings, made of hyaline cartilage, that allow the tracheal lumen to stay open.

The aim of the present study was to determine whether, as reported for vascular smooth muscle cells and articular chondrocytes, tracheal smooth muscle and cartilage cells were similarly prone to mineralize. For this purpose, we set up an experimental procedure to concurrently isolate both types of cells from murine trachea and investigated the effect of high-phosphate level on tracheal primary cell cultures.

2. Material and methods

2.1. Mouse strain and trachea dissection and preparation

Both male and female C57BL/6 mice (Charles River) were used for experiments. All mice were 1.5 months of age. After the mice were euthanized with CO_2 in an appropriate chamber, the tracheae of the mice were immediately dissected out and either fixed by 4% paraformaldehyde in PBS, dehydrated and embedded in paraffin for *in situ* hybridization experiments ($n = 3$) or further dissected as described below ($n = 8$ for each primary culture).

2.2. In situ Hybridization (*ISH*)

Non-radioactive ISH was performed as previously described [5] on 10 μm-thick paraffin embedded sections of adult mouse trachea specimens mounted on Superforst+ glass slides (Fisher). Mouse digoxigenin-labeled cRNA probes were generated from appropriate plasmids encoding *Collagen II* or *SM*22. Details are available upon request.

2.3. Isolation of smooth muscle cells and chondrocytes from adult mouse trachea

Mucus and epithelial tissues were removed from freshly isolated trachea by friction of tweezers on the lumen wall of the trachea. Then, the muscular layer localized to the dorsal side and positive for the smooth muscle marker *SM*22 was manually separated from the ventral *Collagen II* positive layer made of cartilage rings, which were further dissected (Fig. 1(A)–(D)). Both layers were independently enzymatically digested as described below to eventually obtain primary cultures of smooth muscle cells or chondrocytes (Fig. 1(E) and (F)).

On the one hand, smooth muscle cells were obtained by digestion with 3 mg/ml NBG4 Collagenase (Serva) for at least 3 h at 37°C, with occasional gentle agitation (Fig. 1). On the other hand, chondrocytes were obtained by sequential digestion of the cartilage rings with 0.25% Trypsin (Life Technologies) for 15′, 0.5 mg/ml Hyaluronidase (Sigma) for 30′ and 1 mg/ml Collagenase (Sigma) for 30′. A final 1 mg/ml Collagenase digestion was performed for 3 h at 37°C, with manual pipetting every 15′.

After the digestion procedure, both types of cell suspensions were centrifuged at 1,200*g* for 5'. Cell pellets were washed twice with phosphate buffered saline (PBS) and resuspended in culture medium made of Dulbecco's modified Eagle medium (DMEM; Life Technologies) supplemented with 10% heat-inactivated fetal calf serum (Life Technologies), 100 U/ml penicillin and 100 µg/ml streptomycin (Life Technologies). Finally, the cells were seeded in 24 well plates (Corning) maintained at 37°C in a humidified 5% CO_2 atmosphere. The chondrocytes and smooth muscle cells were only used as primary cultures (passage 0). At 90% confluence, the cells were switched to calcifying conditions (3 or 5 mM Pi), which were obtained by adding 2 or 4 mM of inorganic phosphate to the culture medium (1 mM Pi).

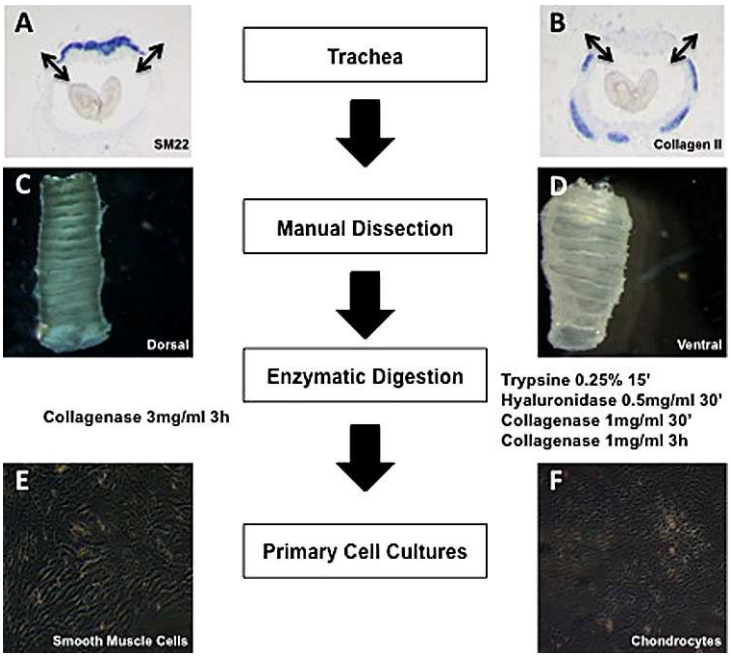

Fig. 1. Schematic diagram of the isolation procedure of murine tracheal cells. *In situ* hybridization experiments clearly authenticated that trachea is made of *SM*22-positive smooth muscle cells located dorsally (A) and Collagen type II-positive cartilage cells located ventrally (B). These two distinct regions were manually dissected out ((C) and (D)) and further digested by different enzymatic treatments to ultimately be grown as primary culture ((E) and (F)). (Colors are visible in the online version of the article; http://dx.doi.org/10.3233/BME-140972.)

2.4. Mineralization study

To assess mineralization, both smooth muscle cells and chondrocytes isolated from adult murine tracheae ($n = 8$ for each experiment) were cultured in the presence of increasing concentration of Pi (1, 3 or 5 mM) for 1, 7 or 14 days. The cells were further stained with 2% alizarin red S (Sigma) in H_2O (pH was adjusted to 4.2 with 0.5% NH_4OH), for 30 min at room temperature. After staining, cultures were washed three times and images were acquired with a Canon EOS 10D digital SLR camera. To quantify the alizarin red staining highlighting the presence of calcium deposits, the cell monolayer was lysed and dissolved mechanically in 400 µl of 10% acetic acid for 30′ at room temperature. The lysate was vortexed, heated to 85°C and then centrifuged at 12,000 g for 10 min. The aqueous phase was recovered and supplemented with 100 µl of 10% ammonium hydroxide. The absorbance at 405 nm was then read on a microplate reader Multiskan EX (Thermo Labsystems).

2.5. RNA Isolation and Real-time quantitative polymerase Chain Reaction (RT-qPCR)

Chondrocyte or smooth muscle cell mRNA levels were determined using SYBR Green-based quantitative PCR. Total RNA was isolated using RNeasyplus mini kit® (Qiagen, France), which allows total removal of genomic DNA with an on-column DNA elimination step. Five hundred ng of total RNA were reverse-transcribed for 90 minutes at 37°C in a 20 µl reaction mixture containing 2.5 mM dNTP, 5 µM random hexamer primers, 1.5 mM $MgCl_2$, and 200U Moloney Murine Leukemia Virus reverse transcriptase (Invitrogen). cDNAs production was performed in a Mastercycler gradient thermocycler (Eppendorf, France).

Next, real time-PCR was performed using the Step One Plus (Applied Biosystems) technology using set of primers specific to the genes of interest (Table 1) and an iTaq SYBRgreen master mix system (Bio-Rad) at the concentrations provided by the manufacturer. Melting curve was performed to determine the melting temperature of the specific PCR products and, after amplification, the product size was checked on a 1% agarose gel stained with 0.5 µg/ml GelRed™ Nucleic Acid Gel Stain (Interchim). Each run included positive and negative reaction controls. The mRNA level of the gene of interest and of S29, chosen as housekeeping gene, was determined in parallel for each sample. Quantification was determined using the $\Delta\Delta^{CT}$ method and the results were expressed as fold change over control.

Table 1
Sequences of primers used for qPCR

Gene	Primer sequences (5′–3′)
RPS29	Forward primer GGAGTCACCCACGGAAGTT
	Reverse primer GCCTATGTCCTTCGCGTACT
SM22	Forward primer CAACAAGGGTCCATCCTACGG
	Reverse primer ATCTGGGCGGCCTACATCA
Coll II	Forward primer GGCCAGGATGTCCAGGAGGC
	Reverse primer GGGCAGATGGGGCAGCACTC
Coll X	Forward primer TGCCCACAGGCATAAAAGGCCC
	Reverse primer TGGTGGTCCAGAAGGACCTGGG
MMP13	Forward primer TGGTGGTGATGAAGATGATTTG
	Reverse primer TCTAAGCCGAAGAAAGACTGC
TNAP	Forward primer CCACGTCTTCACATTTGGTG
	Reverse primer GCAGTGAAGGGCTTCTTGTC

2.6. Statistics

All experiments were repeated at least 3 times. All data are reported as means ± S.E.M. with statistical significance defined as $p < 0.05$ (*), $p < 0.01$ (**) or $p < 0.001$ (***) using two-tailed distribution with equal variance Student's t-test evaluated with Prism 6 software (GraphPad).

3. Results

3.1. Isolation and primary cultures of tracheal smooth muscle cells and chondrocytes

Setting-up a straightforward multi-procedure, we were able, after careful surgical dissection and enzymatic digestion of the *SM*22-positive muscular (Fig. 1(A) and (C)) and *Collagen II*-positive cartilage layers of adult mice tracheae (Fig. 1(B) and (D)), to eventually isolate tracheal cells that display genuine smooth muscle (Fig. 1(E)) or chondrocyte (Fig. 1(F)) morphology, when seeded as primary cultures.

3.2. High-phosphate conditions induced mineralization of both tracheal smooth muscle and cartilage cells

In a first step, as previously reported for smooth muscle cells and chondrocytes of non-tracheal origin, we examined the effects of high-phosphate concentration on the mineralization of tracheal smooth muscle cell and chondrocyte primary cultures at different time points. Calcium deposition was assessed at the macroscopic level by alizarin red staining (Fig. 2(A) and (C)). As expected, in control cultures for both smooth muscle cells and chondrocytes (1 mM Pi), no calcium deposits were formed at any time

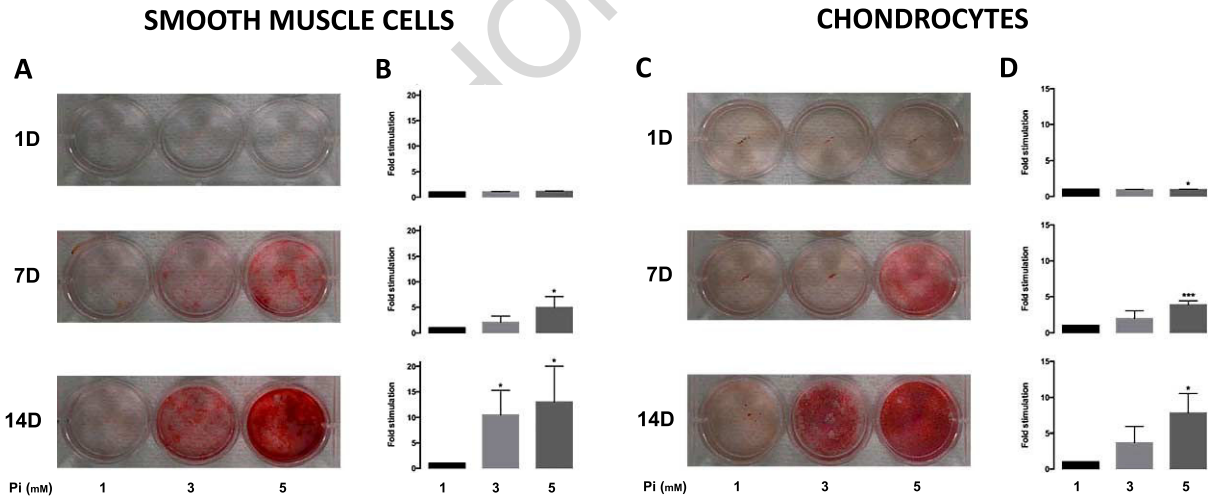

Fig. 2. High-Pi condition induced calcium deposition of cultured tracheal cells in a dose- and time-dependent manner. Representative results of one of three different experiments showing alizarin red staining of tracheal smooth muscle cells (panels in (A)) and chondrocytes (panels in (C)) exposed to 1 mM (control medium), 3 or 5 mM Pi for 1, 7 or 14 days. Calcium content assessed by absorbance at 405 nm of alizarin red stained cultures of smooth muscle cells (histograms in (B)) and chondrocytes (histograms in (D)) incubated in control medium (1 mM) or calcifying medium (3 and 5 mM Pi) for 1, 7 or 14 days. Data show the average ± S.E.M. of three separate experiments. $^{*}p < 0.05$, $^{***}p < 0.001$ compared with the 1 mM control group. (Colors are visible in the online version of the article; http://dx.doi.org/10.3233/BME-140972.)

point (Fig. 2(A) and (C); left wells). In striking contrast, alizarin red staining revealed that incubation with elevated phosphate conditions markedly induced calcium deposits in both tracheal primary smooth muscle cells and chondrocytes (Fig. 2(A) and (C); middle and right wells). Indeed, we observed a dose- and time-dependent response of both cell types with a maximum of staining occurring in cells exposed to the highest dose of Pi for two weeks.

To confirm these results, measurement of calcium deposition was performed by quantifying alizarin red staining through its absorbance at 405 nm. Consistent with the aforementioned qualitative observations, the quantitative assays at 7 or 14 days with Pi showed that Pi supplementation in excess of 1 mM increased calcification of smooth muscle cells (Fig. 2(B)) and chondrocytes (Fig. 2(D)) in a dose- and time-dependent manner.

3.3. Gene expression modifications associated with mineralization of tracheal smooth muscle cells and chondrocytes

To further address the mechanism by which high-Pi induced tracheal cell calcification, we analyzed gene expression variations in normal or calcifying conditions after 7 days of culture, a time point where calcification was already present in both cell cultures (Fig. 2). mRNA levels were measured by real-time PCR using primers (Table 1) to amplify *SM*22 and *Coll II*, as smooth muscle and cartilage specific markers respectively, *Coll X* and *MMP13* as markers of terminal differentiation of hypertrophic chondrocytes, as well as *Tissue non specific alkaline phosphatase (TNAP)*, known to be a hallmark and crucial regulator of mineralization.

To first determine whether smooth muscle cells and chondrocytes undergo phenotypic changes in response to high Pi, we tested the effects of high-Pi on the expression of the smooth muscle marker *SM*22 and cartilage marker *Coll II*. Of note, in addition to our previous morphological observation (Fig. 1(E), (F)), the high expression of these two markers at day one further evidenced that our primary cultures were *bona fide* smooth muscle and cartilage cells (not shown).

After 7 days, the mRNA levels for the smooth muscle marker *SM*22 were significantly decreased by treatment with 3 mM and 5 mM Pi (Fig. 3(A)). In similar fashion, chondrocyte-specific marker *Coll II* expression was slightly reduced when the chondrocytes were cultured with 3 mM Pi and significantly diminished with 5 mM Pi (Fig. 4(A)). In addition, increased *Coll X* mRNA levels were observed in primary chondrocytes cultured under high-phosphate conditions (Fig. 4(B)). These results suggest a phenotypic change of tracheal smooth muscle cells and chondrocytes upon Pi treatment.

Concomitantly, we observed in both cell types a massive dose-dependent increase in the expression of *MMP13* (Figs 3(B) and 4(C)). Interestingly enough, Pi-induced calcification of tracheal cells was associated with up-regulation of *TNAP* expression only in smooth muscle cells (compare Figs 3(C) and 4(D)). Indeed, if 5 mM Pi induced a 4-fold *TNAP* overexpression in these latter cells (Fig. 3(C)), no changes were observed between chondrocytes cultured in control or high-Pi conditions (Fig. 4(D)).

4. Discussion

In this work, we questioned if tracheal chondrocytes and tracheal smooth muscle cells were able to mineralize when challenged with high-Pi conditions. For this purpose, we adapted recently published techniques to harvest either tracheal smooth muscle cells [6] or cartilage cells [7] in order to set up a procedure that allowed us to isolate simultaneously and culture in parallel both type of cells harvested from adult mouse tracheae.

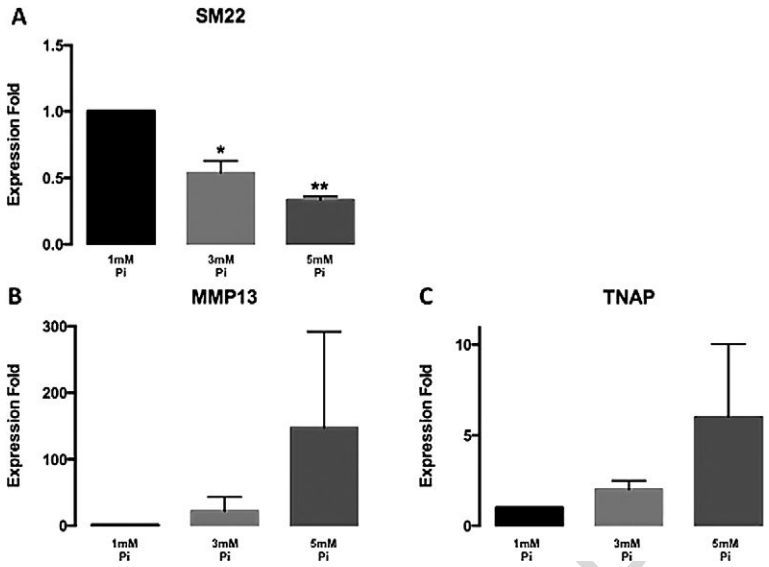

Fig. 3. Effect of Pi on the expression of smooth muscle cell and mineralization markers. Smooth muscle cells were cultured for 7 days with 1, 3 or 5 mM Pi. Gene expression of the smooth muscle specific transgelin or *SM*22 (A), the matrix metallopeptidase 13 or MMP13 (B) and Tissue non-specific alkaline phosphatase or TNAP (C) was analyzed with quantitative real-time PCR. Expression levels were normalized to RP29 and expressed relative to control medium. Data are presented as means ± S.E.M. of three different experiments. $^{*}p < 0.05$, $^{**}p < 0.01$ compared with the 1 mM control group.

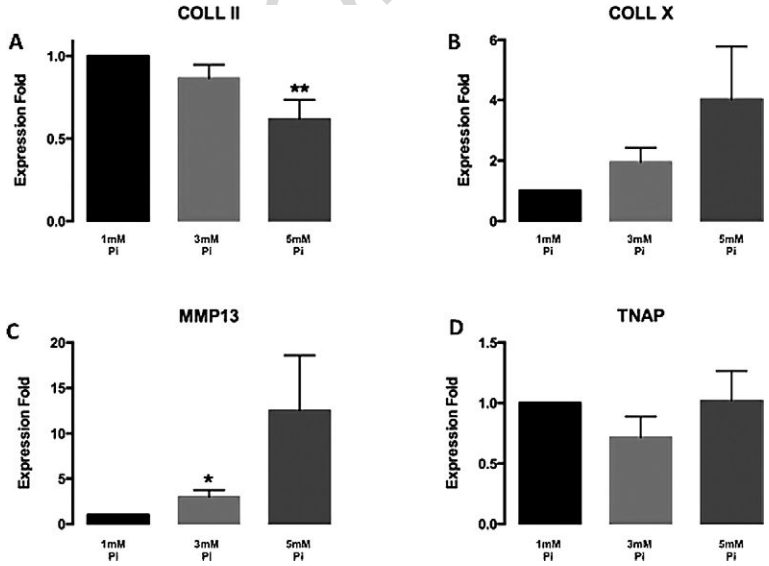

Fig. 4. Effect of Pi on the expression of cartilage and mineralization markers. Chondrocyte were cultured for 7 days with 1, 3 or 5 mM Pi. Gene expression of collagen type II (A), collagen type X (B), MMP13 (C) and TNAP (D) was analyzed with quantitative real-time PCR. Expression levels were normalized to RP29 and expressed relative to control medium. Data are presented as means ± S.E.M. of six different experiments. $^{*}p < 0.05$, $^{**}p < 0.01$ compared with the 1 mM control group.

As previous studies indicated that elevated phosphate could induce mineralization of non-tracheal smooth muscle or cartilage cells, we investigated the effect of high-phosphate levels on the primary tracheal cell cultures. Our results demonstrate that Pi dramatically increased mineralization of both cell types in a dose- and time-dependent manner. Moreover, our gene expression study provides evidence that, the mineralization process is correlated with a change of phenotype in both cases. Indeed, like abundantly reported for their vascular counterparts, our data clearly show that, challenged with high-Pi, tracheal smooth muscle cells lost their differentiated phenotype as determined by the decrease of *SM*22. Similarly, upon Pi challenge, tracheal chondrocytes underwent a phenotypic change towards terminal differentiation as demonstrated by the concomitant loss of *Collagen type II* and gain of *Collagen type X* expression. This is substantiated by the massive induction of *MMP13* expression observed in chondrocytes. Interestingly, *MMP13* is also induced in smooth muscle cells. Although we found no evidence of transdifferentiation of the smooth muscle cells into hypertrophic chondrocytes (not shown), it is possible that smooth muscle cells transdifferentiate into osteoblast-like cells. As a matter of fact, we also showed that *TNAP* expression is induced in smooth muscle cells exposed to high-Pi conditions, whereas its expression is unchanged in chondrocytes. Altogether, the results obtained in this study show that the Pi-induced mineralization process does not involve the same molecular mechanisms in both types of cells. Under hyperphosphatemic conditions, tracheal chondrocytes are likely to terminally differentiate into hypertrophic chondrocytes and eventually mineralize without the involvement of TNAP. In contrast, if tracheal smooth muscle cells also endure profound phenotypic changes and active matrix remodeling, TNAP apparently drives the process of calcification in these cells.

Further work and additional statistical power are undeniably needed to support our preliminary findings and more extensively explore the underpinning mechanisms responsible for the phenotype changes observed in the course of our investigations. Yet, our pilot study provides original and novel evidence that, comparably to articular chondrocytes [1] or vascular smooth muscle cells [2–4], chondrocytes and smooth muscle cells from the trachea are prone to mineralize *in vitro* under high-phosphate conditions.

In vivo, however, mineralization of the trachea has been only scarcely reported. Calcification of the trachea- and proximal bronchi- can be found on chest radiographs in the elderly population [8–10]. Extensive calcification of the airways is a very rare occurrence during pathological conditions. Abnormal tracheobronchial calcification is observed in patients with Keutel syndrome, where extensive mineralization of the airway walls, extending from the trachea to the lung periphery is detected. Keutel syndrome is an extremely rare autosomal genetic disorder due to mutations in the gene coding for matrix gla protein (MGP), a potent inhibitor of calcification, whose activity is vitamin K-dependent [11,12]. Moreover, chest radiographs of patients with long-term anti-vitamin K (warfarin) therapy reveal pronounced and diffuse calcification of the tracheobronchial tree [13]. Altogether, these clinical observations support a major role played by MGP in the pathological mineralization of the trachea in humans. Consistently, mice deficient for *MGP* also display aberrant mineralization of their trachea, together with spontaneous and extensive vascular calcifications that lead to death through arterial rupture and internal hemorrhage [14]. Noteworthy, although MGP is known to be expressed in smooth muscle cells and chondrocytes and trachea is made of both cell types, all the aforementioned human or mouse studies only described calcification of the cartilaginous part of the trachea. Since our *in vitro* findings support that both smooth muscle cells and cartilage cells of the trachea are prone to calcify, further investigations are required to determine whether or not tracheal smooth muscle cells could mineralize *in situ*.

Acknowledgements

This study was funded through grants from the Fondation pour la Recherche Médicale local committee and by the Region Lorraine and Université de Lorraine. Support for Lina Tabcheh was provided by a stipend from the Middle East Institute of Health (Dr Norman Makdissy), Tripoli, Lebanon.

We thank all the members of the team for their technical help and helpful discussions.

Conflict of interest

All authors have no conflict of interest.

References

[1] D. Magne, G. Bluteau, C. Faucheux, G. Palmer, C. Vignes-Colombeix, P. Pilet et al., Phosphate is a specific signal for ATDC5 chondrocyte maturation and apoptosis-associated mineralization: possible implication of apoptosis in the regulation of endochondral ossification, *Journal of Bone and Mineral Research* **18**(8) (2003), 1430–1442.

[2] C.M. Giachelli, M.Y. Speer, X. Li, R.M. Rajachar and H. Yang, Regulation of vascular calcification: roles of phosphate and osteopontin, *Circulation Research* **96**(7) (2005), 717–722.

[3] M. Leroux-Berger, I. Queguiner, T.T. Maciel, A. Ho, F. Relaix and H. Kempf, Pathologic calcification of adult vascular smooth muscle cells differs on their crest or mesodermal embryonic origin, *Journal of Bone and Mineral Research* **26**(7) (2011), 1543–1553.

[4] D.A. Prosdocimo, S.C. Wyler, A.M. Romani, W.C. O'Neill and G.R. Dubyak, Regulation of vascular smooth muscle cell calcification by extracellular pyrophosphate homeostasis: synergistic modulation by cyclic AMP and hyperphosphatemia, *American Journal of Physiology Cell Physiology* **298**(3) (2010), C702–C713.

[5] S. Provot, H. Kempf, L.C. Murtaugh, U.I. Chung, D.W. Kim, J. Chyung et al., Nkx3.2/Bapx1 acts as a negative regulator of chondrocyte maturation, *Development* **133**(4) (2006), 651–662.

[6] J.S. Mohamed, A. Hajira, Z. Li, D. Paulin and A.M. Boriek, Desmin regulates airway smooth muscle hypertrophy through early growth-responsive protein-1 and microRNA-26a, *The Journal of Biological Chemistry* **286**(50) (2011), 43394–43404.

[7] B. Gradus, I. Alon and E. Hornstein, miRNAs control tracheal chondrocyte differentiation, *Developmental Biology* **360**(1) (2011), 58–65.

[8] S.H. Jo, Y.J. Choi, G.Y. Cho, H.S. Kim, K.S. Jung and C.Y. Rhim, Tracheal calcification, *Canadian Medical Association Journal* **179**(3) (2008), 291.

[9] H. Sosnik and K. Sosnik, Investigations into human tracheal cartilage osseocalcineus metaplasia. I. Radiographic findings, *Folia Morphologica* **67**(2) (2008), 143–149.

[10] H. Sosnik and K. Sosnik, Investigations into human tracheal cartilage osseocalcineus metaplasia IV. Morphokinesis of tracheal cartilage retrograde lesions during the process of aging, *Polish Journal of Pathology* **61**(4) (2010), 224–228.

[11] D.J. Hur, G.V. Raymond, S.G. Kahler, D.L. Riegert-Johnson, B.A. Cohen and S.A. Boyadjiev, A novel MGP mutation in a consanguineous family: review of the clinical and molecular characteristics of Keutel syndrome, *American Journal of Medical Genetics Part A* **135**(1) (2005), 36–40.

[12] P.B. Munroe, R.O. Olgunturk, J.P. Fryns, L. Van Maldergem, F. Ziereisen, B. Yuksel et al., Mutations in the gene encoding the human matrix Gla protein cause Keutel syndrome, *Nature Genetics* **21**(1) (1999), 142–144.

[13] H. Taybi and M.A. Capitanio, Tracheobronchial calcification: an observation in three children after mitral valve replacement and warfarin sodium therapy, *Radiology* **176**(3) (1990), 728–730.

[14] G. Luo, P. Ducy, M.D. McKee, G.J. Pinero, E. Loyer, R.R. Behringer et al., Spontaneous calcification of arteries and cartilage in mice lacking matrix GLA protein, *Nature* **386**(6620) (1997), 78–81.

Primary culture of tracheal cells as an in vitro model to study tracheal mineralization

In order to elucidate the mechanism lying behind tracheal mineralization, we set up an isolation procedure of both tracheal cartilage and smooth muscle cells and study their ability to mineralize under high PI conditions.

Our results showed that the mineralization of both type of cells occurs in a time- and dose-dependent manner, and, interestingly, indicated that the mechanisms responsible differ between both cell types even though this requires further investigations

In tracheal smooth muscle cells, mineralization was accompanied with an increased expression of TNAP and a concurrent transdifferentiation of the cells as SM22, a smooth muscle cells marker, decreases with mineralization. This is consistent with numerous studies made on vascular smooth muscle cells, where transdifferentiation into osteogenic lineage has been largely reported (Pai et al 2011; Tanaka et al 2008). TNAP can also be considered as a marker of osteogenic lineage and can be secondary to a transdifferentiation phenomenon as in the case of aortic smooth muscle (Leroux-Berger et al 2011; Rajamannan et al 2003; Speer et al 2009). We did find also an increase in the expression level of MMP13, a collagenase, which is known to play significant role in the degradation of collagens and implicated in the growth plate mineralization (Nishimura et al 2012; Wang et al 2004). Although in the literature there is no clear link between MMP13 and smooth muscle cells mineralization, other MMPs such as MMP-2 and MMP-9 seems to be implicated in this process (Jiang et al 2012; Pai et al 2011).

The mineralization of tracheal chondrocytes seems to be due to terminal differentiation, as chondrocyte shows a progression toward hypertrophic maturation, revealed by the increasing expression of the hypertrophic chondrocytes marker, Coll X and MMP13, and a decrease in the expression of Coll II considered as a marker of hyaline chondrocyte. Yet, Sasano demonstrated that in the mineralized cartilage of tracheal rat, Coll X was not localized in the same region as of hypertrophic and mineralized chondrocytes (Sasano et al 1998).

With regard to MMPs, the expression of MMP2 and MMP9 was solely investigated (Miller et al 2006). It has been reported that the expression of MMP-2 decreases with age accompanied with decrease in the ratio of activated /deactivated MMP2, while MMP9 protein level seems to be constant with predominance in the activated form only in the adult conductive airway. In the same study, the expression level of MMP inhibitors (TIMP) was also evaluated. The expression level of TIMP 2 increased with time, while the TIMP-1 level was stable during aging process. The study did not mention any information concerning mineralization of

tracheal rabbit and, thus, no link between the MMPs and mineralization can be concluded (Miller et al 2006). So, we are here the first to mention the potential implication of MMP (here MMP13) in the mineralization of tracheal cartilage.

Searching for a more physiological model: the ex-vivo explant culture

As isolated primary culture of tracheal smooth muscle and cartilage cells might not totally reflect the physiological conditions, we have tried to develop 3D culture of trachea explants.

Tracheal ex-vivo model was previously used by many authors as Scott (Scott et al 2000) and Park (Park et al 2010a). However, in their studies, the embryonic trachea was used and thus there was no need to maintain an air filled tracheal lumen. As the trachea of young or adult mice was the subject of our study, we tried to create an ex-vivo approach culture model of trachea approaching physiological conditions.

Briefly after death, the thorax of the animal was opened and trachea-surrounding tissues were removed as much as possible. The trachea was separated from the esophagus. An incision was made in the fibrous tissues between the cricoid and the first cartilaginous ring to insert an adequate 0.69 OD (outer diameter) polyethylene catheter. Sutures to close the incision were made with black braided silk 4-0 (ETHICON, Johnson-Johnson). The same steps were made at the other extremity of the trachea, just above the carina. The trachea was then fully excised and transferred into a culture plate punctured on opposite sides to let the catheter pass throughout the plate. Then culture medium was added in the plate which was incubated at 37°C and a humidified 5% CO2 atmosphere.

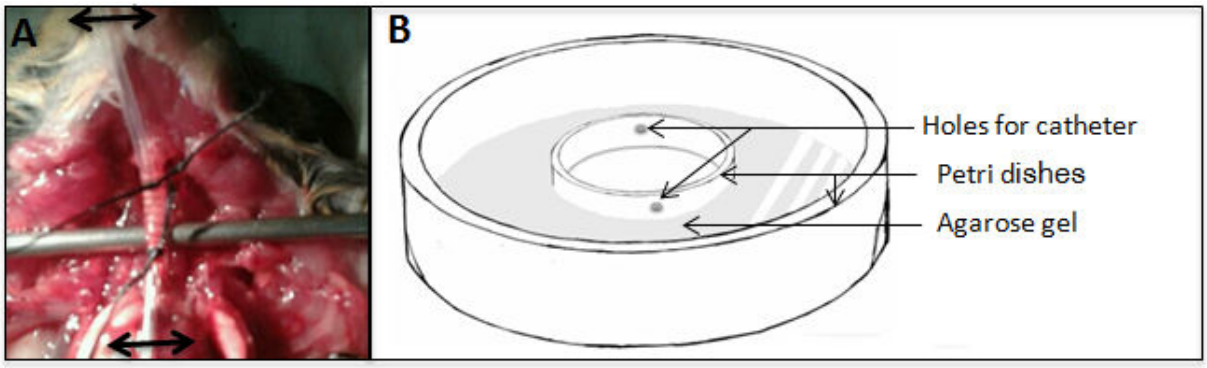

Fig.3. 1. Tracheal dissection for EX-vivo experiment.

(A) Two polyethylene catheter was inserted in both side of the trachea, right under the cricoid and above the carina, catheter then were fixed to the trachea using silk suture, in the fig trachea is still attached to the body through its dorsal part or trachealis. (B) Hand-made device used to culture the dissected trachea is presented.

Using this procedure where the lumen is filled with air instead of medium, trachea explants were cultured in medium containing 1, 3 or 5mM Pi for 7 days. To detect mineralization, double Alcian Blue/Alizarin Red staining was performed. Whereas trachea treated with 1mM of Pi shows no specific red staining (panel A), trachea treated with 3mM (panel B) of Pi or with 5mM of Pi showed increasing level of mineralization in the tracheal rings (panel C). Importantly, if no sign of mineralization in the trachealis smooth muscle was detected with 3mM Pi conditions, most of the tracheal tissues were mineralized when the explant was cultured with 5mM Pi.

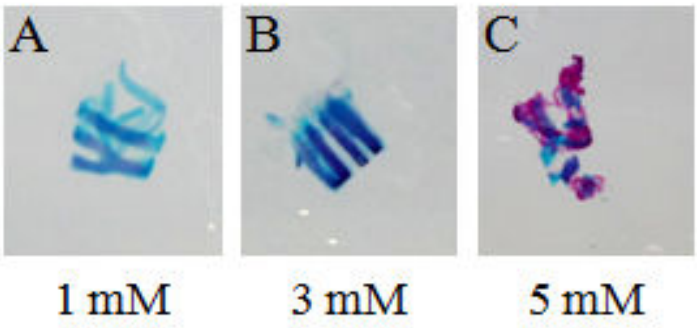

Fig.3.2. Effect of high level of Pi on Ex-vivo cultured trachea.

Alizarin red/ Alcian blue staining of EX-vivo trachea treated with medium of 1, 3 and 5mM Pi shows hardly no mineralization in cartilage rings of the trachea treated with 1mM of Pi (A), while when treated with 3mM Pi containing medium the mineralization was clearly detectable (B). With 5mM Pi, the mineralization was extended to all the tracheal tissues (C).

CHAPTER IV

TRACHEAL MINERALIZATION *IN-VIVO* APPROACH

Etat de l'art

Le cartilage de la trachée, de nature hyaline, a pour fonction essentielle de maintenir un passage libre des gaz respiratoires vers et hors des poumons. Cette fonction est réalisée grâce à un équilibre entre les propriétés de rigidité et d'élasticité de ce cartilage, permettant une adaptation adéquate en réponse au changement de pression extra- et intra-thoracique.
Comme d'autres cartilages hyalins, dont le cartilage articulaire, le cartilage de la trachée subit des modifications liées à l'âge telle que la minéralisation. En effet, chez les personnes âgées, plusieurs études ont rapporté une minéralisation du cartilage de la trachée, qui peut entraîner chez certains patients des dyspnées et/ou des essoufflements sévères.

Objectif

Dans le but de mieux comprendre les mécanismes cellulaires et moléculaires responsables de cette minéralisation trachéale, nous avons étudié la cinétique d'apparition de calcification dans le tissu trachéal de souris au cours du temps, âgées de 0 à 6 mois (la minéralisation étant déjà complète à cet âge).

Matériel et méthodes

Dans ce but, des études morphologiques par une double coloration au bleu alcian et rouge alizarine, couplées à des études histologiques par la double coloration de Von-Kossa et bleu alcian ont été effectuées sur les trachées de souris C57Bl/6 et BALBc de différents âges. L'étude d'expression de gènes impliqués dans la régulation et la caractérisation phénotypique a également été réalisée par la réaction d'amplification en chaîne par polymérase en temps réel et par la technique d'hybridation *in situ*.

Résultats

Nos résultats ont montré que la minéralisation de la trachée des souris commence à un âge plus précoce qu'attendu, puisque les premiers anneaux cartilagineux se calcifient 30 jours après la naissance chez les souris C57Bl/6 et encore plus précocement chez les souris BALB/c. Dans les deux lignées, la minéralisation progresse de façon identique en s'étendant de la partie supérieure vers la partie inférieure de la trachée. L'étude de marqueurs phénotypiques semble indiquer que la minéralisation du cartilage trachéal est due à la différenciation terminale des chondrocytes des anneaux cartilagineux.

Conclusion

Contrairement à ce qui est observé chez l'homme, la minéralisation de la trachée est un phénomène physiologique précoce et d'apparition soudaine chez la souris, qui implique les chondrocytes mais pas les cellules musculaires lisses trachéales.

MINERALIZATION OF THE MOUSE TRACHEA IS A SUDDEN AND EARLY PHYSIOLOGICAL EVENT

Lina Tabcheh, Arnaud Bianchi, Chaohua Deng, Tabea Kraft, Jean-Yves Jouzeau and Hervé Kempf

MINERALIZATION OF THE MOUSE TRACHEA IS A SUDDEN AND EARLY PHYSIOLOGICAL EVENT

Lina Tabcheh, Arnaud Bianchi, Chaohua Deng, Tabea Kraft, Jean-Yves Jouzeau and Hervé Kempf [*]

UMR 7365 CNRS–Université de Lorraine, Laboratoire d'Ingeniérie Moléculaire et Physiopatholgie Articulaire, IMoPA, Faculté de Médecine, Vandoeuvre-lès-Nancy, France

Running Title: Mineralization of the trachea

Authors's email addresses:
ltabcheh@gmail.com
arnaud.bianchi@univ-lorraine.fr
dengchaohua1988@hotmail.com
tabea-kraeft@gmx.de
jean-yves.jouzeau@univ-lorraine.fr
herve.kempf@inserm.fr

[*]Corresponding author: Hervé Kempf
UMR 7365 CNRS-Université de Lorraine, Ingénierie Moléculaire et Physiopathologie Articulaire (IMoPA), Biopôle de l'Université de Lorraine, Campus biologie-santé, Faculté de Médecine
9 Avenue de la Forêt de Haye – CS 50184
54505 Vandœuvre-lès-Nancy Cedex, FRANCE
tel. +33 3 83 685 426; fax. +33 3 83 685 959
e-mail: herve.kempf@inserm.fr

Number of words/characters in abstract : 159/957
in manuscript :4699/25813
Number of Figures : 5 Color Figures/ 2 Supplementary Figures

CONFLICT OF INTEREST

The authors declare that there are no conflicts of interets.

ABSTRACT

Tracheal cartilage is a C-shaped hyaline cartilage known as permanent cartilage. Compliance and elasticity are the two features required for tracheal cartilage in order to fulfill its function in preventing airway collapse. Tracheal mineralization is a rare condition mostly found in the elderly population where the elasticity of the trachea is compromised leading patients to eventually suffer from dyspnea. In that context, we ought to understand the cellular and molecular mechanisms at the origin of tracheal mineralization that has been unexplored so far.

Our morphological and histological studies show an unexpected early mineralization that is detected at only 30 days after birth, and only in the cartilaginous compound. This mineralization extends in rostro-caudal pattern. Our molecular study provides evidence that this mineralization occurs through chondrocytic differentiation.

The present study is the first to describe mouse tracheal calcification and provide evidence that in the mouse, contrary to the typical notion, tracheal cartilage is not a permanent hyaline cartilage throughout life.

KEYWORDS:

Trachea, cartilage, mineralization, mouse, collagen X

INTRODUCTION

The trachea is a very complex structure of the respiratory tract, composed of C-shaped cartilaginous rings, made of hyaline cartilage. In contrast to other intensely studied cartilages such as the ones found in the developing growth plate or in the adult joints, very little information is available on the innate propensity of this structure to mineralize.

Most of the cartilage has a transient phenotype: the chondrocytes first proliferate, then mature into hypertrophic cells, and are finally replaced by osteoblasts during endochondral ossification. However, chondrocytes present in articular cartilage, laryngeal cartilage, tracheal and bronchial rings, nasal septum, costal cartilage, and intervertebral disks do not enter into the maturation process. As a result, these structures persist throughout life and, as such, are viewed as permanent cartilage. However, this definition disregards the fact that, in humans, it has been reported that, on occasion, these 'permanent' cartilages, including that of the windpipe, undergoes mineralization with increasing age.

Tracheal calcification is considered a common finding in elderly patients. Indeed, it is seen almost exclusively in patients aged 40 years and older, especially in woman. Although visually remarkable by standard chest radiography, this is of no clinical significance. Nevertheless, patients can occasionnaly complain from stridor, wheezing and dyspnea because of severe mineralization of the tracheobronchial tree (Jo et al., 2008). A radiologic study including 105 elderly individuals showed that 19% displayed subtle to severe calcifications in the cartilage rings of the trachea and bronchi (Moncada et al., 1992). In the same line, it has been shown that phosphorus and calcium concentration in trachea reach their highest levels at seventieth, while the magnesium concentration remains stable and the sulfur concentration decreases with age (Tohno et al., 2000). This suggested that during aging the calcifications of the trachea are due to the passive deposition of calcium-phosphate crystals, similar to those found in bones or in the vessel wall when patients develop vascular calcifications.

Extensive tracheobronchial mineralization may occur more often and be more severe in patients who have taken long-term anticoagulation therapy, such as Warfarin, after prosthetic heart valve replacement (Thoongsuwan and Stern, 2003). Indeed, the percentage of tracheobronchial calcification is estimated to be 47% in adults receiving warfarin sodium compared to the 19% in age-matched control subjects (Moncada et al., 1992). Noteworthy, although considered a very rare occurrence in young individuals always associated with stridor (Rifkin and Pritzker, 1984), several recent case reports have shown that this is not infrequent in children that underwent valve replacement to treat mitral valvular disease (Golding et al., 2013) or after Fontan surgery for single-ventricle palliation (Eckersley et al., 2014). Patients with Keutel syndrome, a rare autosomal disease with less than 50 cases reported notably from Turkey and the Middle East, present prominent tracheobronchial

calcification, sometimes associated with tracheobronchial stenosis (Meier et al., 2001; Sun and Chen, 2012) leading to distressing dyspnea. Interestingly, altogether these clinical radiographic findings point up the potential role of the potent vitamin K-dependent calcification inhibitor called Matrix Gla Protein (MGP), as the *Mgp* gene is mutated in Keutel Syndrome patients and MGP activity is altered by anti-Vitamin K medication.

Besides these clinical studies in humans, there are hardly no data regarding tracheal mineralization in animal models. To our knowledge, tracheobronchial mineralization in the aged mice has not been studied.

In this study, we thus carried out a thorough anatomical and histological analysis in order to determine the spatiotemporal onset and progression of trachea mineralization during adult development. This extensive and straightforward analysis led to very unanticipated results. Indeed, in contrast to what has been described in humans, our data undeniably demonstrate that, in the mouse, tracheal mineralization initiates in the cartilaginous rings as early as one month after birth and progresses through a rostrocaudal direction throughout the trachea to eventually spread in the bronchi after only 2 months. This process seems to be accompanied by the terminal differenctiation of the chondrocytes of the rings. Notably, this demonstrates that the tracheal cartilage cannot be considered a permanent hyaline cartilage in the windpipe, as it undergoes a maturation similar to that observed in the growth plate.

MATERIAL AND METHODS

Animals

Mice were housed in conventional animal rooms under constant humidity (55 ± 10%) and temperature (22 ± 2ºC) in 12h light-dark cycle conditions. They were fed *ad libitum* with standard food diet (Scientific Animal Food & Engineering, France) and had free access to water. Male and female C57BL6/J and BALB/cJ wild-type mice, originally supplied by Charles River (Charles River, France), were locally inbred. Mice were placed in reproductive conditions whenever necessary in order to maintain the colony or provide the sufficient number of mice for each experiments. For all the following procedures, adult mice were euthanized with CO_2 in an appropriate chamber (Minerva) and newborn or very young animals were euthanized by decapitation. All animal protocols were in accordance with the guideline set by the animal care committee.

Whole-mount Alcian Blue (AB) and Alizarin Red (AR) staining

Euthanized mice were beheaded, skinned, and eviscerated from their internal organs with the exception of their full-length respiratory tract (trachea, bronchi and lungs). The specimens were then fixed in ethanol 95% for at least 2 days till the day of the experiments. Collected specimens were incubated in Alcian Blue 8GX (AB, Sigma A3157) solution (0.03% AB, 80% of 96% EtOH, 20% acetic acid) for approximately 18 hours. AB solution was replaced with 95% EtOH solution for at least 6 hours followed by 2% KOH solution until tissues are cleared out. Specimens were transferred to Alizarin Red S (AR, Sigma A5533) solution (0.003% in KOH 1%) until dark staining of the skeletal bones. Staining was then stopped at the very same time for all specimens in 1% KOH-20% glycerol solution while agitating. To store specimens for long periods of time, they were passed through glycerol/ethanol solutions (50/50, 80/20) and photographed in 100% glycerol solution.

Histology and in situ hybridization

Tracheas were collected promptly after animal euthanasia. They were fixed in sterile 4% paraformaldehyde solution (prepared in RNase-free PBS) overnight at 4° and kept in 70% EtOH for at least 24 hours at 4°C. Specimens were then dehydrated via routine procedures using a Tissue processor (Leica ASP 300S) and embedded in paraffin. Blocks were then sectioned with a manual rotary microtome (Leica RM 2135) and sections where positioned on Superfrost+ glass slides (Fisher, Germany). Images were taken with a Leica DMD 108.

For Von Kossa/Alcian Blue staining, sections were dewaxed and rehydrated through standard procedure. They were incubated for 1 hour in 2% silver nitrate (Normapur, 21572.235) solution (prepared in deionized water) under the light of a 60-Watt lamp, washed twice in deionized water for 3 minutes, once in 1% acetone for 3 minutes, and finally

incubated for 15 minutes in Alcian Blue solution (0.02% Alcian Blue, 70% ethanol, 30 ml acetic acid). They were then washed for 1 minute in 1% acetone, 2 minutes twice in water, dehydrated (3 minutes in 25% EtOH, 3 in 50% EtOH and 3 in 75% EtOH), counterstained with 0.1 % eosine for 30 seconds, destained twice for 3 minutes in ethanol 100%, washed twice with xylene for 5 minutes and mounted using Petrex®.

Non-radioactive ISH was performed on 7µm-thick paraffin embedded longitudinal or transversal sections of C57BL/6J mouse trachea specimens mounted on Superforst + glass slides (Fisher).
Sections were subjected to acid hydrolysis (0.2 N HCl, 15 min), proteinase K treatment (5 µg/ml in PBS, 15 min), postfixation (4% PFA, 5 minutes) and acetylation (0.25% acetic acid, 15 min). Each of these steps was followed by two 5-minute washes with PBS. After the last PBS wash, slides were rinsed with dH2O and air-dried, before a 2-hour prehybridization step, at 65°C, in hybridization solution [50% formamide, 10 mM Tris (pH 7.6), 200 µg/ml Torula yeast RNA, 1xDenhardt's solution, 10% dextran sulfate, 600mM NaCl, 0.25% SDS, 1 mM EDTA (pH 8.0)]. Hybridization with digoxygenin-labeled *CollagenX* RNA probes was performed overnight at 65°C. Posthybridization, slides were rinsed briefly in 5x SSC at 65°C, washed with 1x SSC, 50% formamide (65°C, 30 minutes), subjected to RNase A digestion to reduce nonspecific hybridization, and washed at increasing stringency with SSC buffers (final wash at 55°C with 0.2xSSC). Bound probes were detected with an alkaline phosphatase-conjugated anti-DIG antibody (Roche) and revealed with BM purple substrate (Roche).

RNA extraction and Quantitative-PCR

C57BL/6J mice were sacrificed when they reach the demanded age, then trachea were dissected immediately following their death.
Tracheas were dissected in two parts: the upper part consisting of the first seven cartilage rings and the lower part from the eighth ring to the carina. Dissected parts were rinsed with PBS and directly frozen in liquid nitrogen and conserved at -80°C till the day of RNA extraction procedure.
Total RNA from upper or lower parts of the trachea was isolated using the RNeasy Plus Mini kit (Qiagen) according to manufacturer's instructions. Extracted RNA was reverse transcribed into cDNA by Reverse transcription reaction using the M-MLV enzyme (Invitrogen, 28025-013) and an adequate mix (dNTP, Buffer, random hexaprimer, DTT). cDNAs were then amplified and quantified by Real-time PCR, performed using the StepOne Plus technology (Applied Biosystems) with primers specific to the genes of interest (sequences available upon request) and the iTAQ SYBRgreen master mix (Biorad) according to the manufacturer's instructions.

Melting curve was performed to determine melting temperature of the specific PCR products After amplification, the product size was checked on a 1% agarose gel stained with 0.5µg/ml GelRed™ Nucleic Acid Gel Stain (Interchim). Each run included positive and negative reaction controls. S29 housekeeping gene was determined in parallel for each sample. Quantification was determined using the ΔΔCT method and the results were expressed as fold change over control.

Statistics

All experiments were repeated at least 3 times. All data are reported as means ± S.E.M. with statistical significance defined as $p<0.05$(*), $p<0.01$(**) or $p<0.001$ (***) using two-tailed distribution with equal variance student's t-test evaluated with Prism6 software (GraphPad).

RESULTS

Tracheal mineralization in C57BL/6J mice follows a specific spatiotemporal pattern.

To identify the precise spatio-temporal occurence of mouse tracheal mineralization, we dissected and sequentialy stained with Alcian Blue and Alizarin Red the whole respiratory tract of C57BL/6J mice of different ages.

As anticipated, a broad and initial morphological analysis by the combined Alcian Blue and Alizarin Red staining first revealed that if newborn mice (P0 to P7) displayed no evidence of mineralization in the airway cartilage, the oldest (6-month old) specimens examined displayed strong mineralization along the whole respiratory system (data not shown).

Thus, we undertook a more thorough investigation covering a narrower range of ages between P14 and P60. Alizarin red staining revealed that the thyroid cartilage of the larynx shows the first signs of mineralization at P17 (Fig. 1A). The mineralization spreads to the entire laryngeal cartilage over time (Fig.1B-G) with the cricoid cartilage being one of the last laryngeal structure to be mineralized at P30 (Fig. 1F). With regard to the trachea itself, if occasional and rare spots of AR staining could be found in the very first rings of P29 individuals, extensive mineralization of the trachea spontaneously starts at P30, as the first 5 or 6 cartilage rings display strong to very strong AB staining (Fig.1F), and slowly progresses to adjacent distal rings in a rostro-caudal direction (Fig. 1G) to fully cover the whole trachea and even extend within the two main bronchi after 2 months (Fig. 1H). Noteworthy, there does not seem to exist any sexual dimorphism in the mineralization process of the tracheal structures as we found similar pattern of initiation and progression between individuals, irregardless of their gender (Supplementary Fig. 1). Interestingly, the number of rings affected and their degree of mineralization observed at P30 was virtually uniform between littermates and moderately variable between distinct litters (data not shown).

Altogether, these morphological observations suggest that there is a very short period of time around P30 where tracheal mineralization initiates in C57BL/6J mice.

Tracheal cartilage mineralization comparably happens in mice of different strains.

To confirm that these observations were not specific to the C57BL/6J strain, identical experiments were repeated in mice of a different background: the BALB/cJ mice (Fig. 2). Alcian Blue/Alizarin Red double staining on trachea collected from mice of the BALB/cJ strain revealed a spatiotemporal pattern of occurence and progression similar to that found for the C57BL/6J strain (Fig. 2A-F). However, in contrast to C57BL/6J mice, where the first patches of mineralization appeared at P17 in the larynx and affected the first upper cartilage rings at P30 (Fig. 1), the mineralization of the trachea appeared even earlier in BALB/cJ mice. Indeed, the very first rings are already weakly AR positive at P21 (Fig. 2A) and 5-7 rings are already mineralized as early as P25 (Fig. 2A). The tracheal mineralization is consequently

completed earlier than what has been observed for C57BL/6J mice, as BALB/cJ trachea are already entirely AR positive at P45 (Fig. 2F).

Histo-morphological study of tracheal mineralization:

To validate and strengthen our morphological observations, histological experiments consisting of double staining Von-Kossa/Alcian blue were performed on longitudinal and transversal sections of trachea from C57BL/6J mice of different ages.

The mineralization can be detected in longitudinal section of trachea at the age of P30, were it can only be detected within the core of the first cartilage rings. However rare VonKossa positive stains can be found in the uppermost tracheal rings harvested from P29 mice (data not shown), a stage where the cricoid starts to mineralize (Fig. 3G-L). The thyroid cartilage mineralization can be detected as early as P17 (Fig. 3A) and spreads all over the thyroid cartilage overtime (Fig. 3A-F). Cricoid cartilage mineralization can be detected starting at P29 (Fig. 3I). According to our morphological findings (Fig. 1), trachea mineralization cannot be significantly detected in mice younger than 30-days old, neither in the upper part (Fig. 3M-0) nor in the lower part (Fig.3 S-U). Starting at P30, mineralization can be detected in the upper part of the trachea (Fig.3P) and intensified at P31 and P33 (Fig. 3Q,R). As for the cricoid cartilage, the mineralization is also localized in the upper tracheal cartilage within the core of the rings. No mineralization was detected at the lower part of the trachea from P0 to P33 (Fig. 3S-X).

The mineralization can also be detected in transversal sections as presented in Figure 4. Our results showed as expected a mineralized thyroid cartilage at P29, P30 and P31 (Fig. 4.B-C). With regard to upper tracheal cartilage, mineralization can be detected at P30 and P31 (Fig. 4D,E) but not at P29 (Fig. 4F). In contrast, lower tracheal cartilage showed no sign of mineralization at all stages studied (Fig. 4G,H).

It is important to note that longitudinal and transversal sections also reveal that tracheal chondrocytes become larger with time suggesting that they may undergo hypertrophy.

Chondrocyte terminal differentiation and tracheal mineralization

To further characterize the process of tracheal mineralization, qPCR analysis of various potential genes potentially implicated in terminal chondrocyte differentiation was performed on P20 to P30 samples isolated from upper or lower regions of C57BL/6 trachea.

Among those genes differentially expressed between upper and lower trachea, *Collagen X* (*CollX*) showed a marked difference between the two regions (Fig. 5). Compared to lower region, *CollX* expression started to be significantly up regulated in the upper region at P20 and continued to increase in this region up to P30.

To verify that the *CollX* upregulation observed by qPCR was qualitatively related to an upregulation of the marker in the mineralized region, we looked at its mRNA expression by *in situ* hybridization in the trachea of C57Bl/6J mice at P25 and P30. Interestingly, *CollX* expression can be detected at low level at P25 and strong level at P30 in longitudinal (Fig. 5) and transversal (Supplementary Fig. 2) sections of each region analyzed. Indeed, *CollX* can be detected at P25 in the thyroid region that is mineralized (compare Fig. 5A and 5B), but also in regions that are not yet mineralized such as in the cricoid (Fig. 5E,F) and tracheal rings, even though it is clearly more expressed in upper cartilage rings (Fig. 5I) than in lower cartilage rings (Fig. 5M) in agreement with qPCR analysis. In line with these observations in early individuals, *CollX* is strongly expressed in all the upper respiratory regions analyzed at P30 (Fig. 5 and supplementary Fig.2).

DISCUSSION

To investigate in vivo tracheal mineralization during mouse aging, we performed an extensive and straightforward study to reveal the precise time and location at which mineralization occurs and tried to understand the molecular mechanisms responsible for this process.

Interestingly and surprisingly, we discovered that, in contrast to the current concept that defines tracheal cartilage as a permanent hyaline cartilage, mineralization of the trachea is an early and sudden phenomenon in mice. Indeed, we found that mineralization starts around P30 in C57Bl/6J mice in the upper rings close to the larynx, and through a rostro-caudal progression, spreads into the whole trachea and bronchi that are completely calcified at P60. An identical pattern was also found in BALB/cJ mice, although it initiates even earlier in this strain, as we could detect the mineralization of the first rings as early as P25. Despite an exhaustive scrutiny of the literature, we could not find any tracheal differences reported between these two strains that could explain this difference in timing other than submucus gland distribution (Innes and Dorin, 2001; Widdicombe et al., 2001). Although the implication of this factor in tracheal mineralization is doubtful, we should keep in mind that numerous reports show that defects in one of the components of the trachea can lead to defects in others as in asthma (Jeffery, 2001) and cystic fibrosis (Regamey et al., 2008; Wallace et al., 2013). Thus, although we have absolutely no evidence, we cannot rule out that submucus gland repartition may have a role in the timing variation observed in the occurrence of tracheal mineralization between the two strains studied.

In view of this striking phenotype, it is retrospectively very surprising that, except our current study, there is no report of tracheal mineralization in early individuals in the mouse model. Our data are however in agreement and thus confirm and strengthen rather ancient data obtained in birds and rats. The tendency of the cartilage of avian vocal and respiratory systems to mineralize is well know. In the early 80's, Hogg performed an extensive characterization of the timing and pattern of the mineralization process in syringeal, laryngeal and tracheal cartilages (Hogg, 1982). He showed that the first tracheal ring start to mineralize at 126 days post-hatching. Interestingly, there are some major differences with what we observed in the mouse: i) the process follows a caudo-rostral pattern, ii) it is incomplete as the tracheal rings at the cranial end tend to remain lightly to not mineralized, iii) the mineralization is due to the ossification of the cartilage rings (Hogg, 1982). With regard to the only 3 reports by Bonnuci *et al*. in 1974 (Bonucci et al., 1974) and Sasano *et al.* in the mid-90's (Sasano et al., 1993; Sasano et al., 1998) that studied mineralization in the rat, they all agree that mineralization of the tracheal cartilage can be seen in rather young individuals.

However, they only show Von Kossa staining in 10-week old rats, whereas they clearly show hypertrophic chondrocytes in the central region of the tracheal rings at 4 weeks in postnatal rats. This is rather consistent with our results, although we observed earlier occurrence of Von Kossa (and Alizarin Red) staining since we can detect those in the upper cartilage of P30 mice. So, among rodents, there seem to have a clear shift towards early stages for the physiological mineralization in mice versus rats. However in both case, chondrocyte hypertrophy and calcified cartilage are responsible of the mineralization observed (Sasano et al., 1993; Sasano et al., 1998), which is different than the ossification process noticed in birds (Hogg, 1982). This propensity of tracheal chondrocyte to engage into terminal differentiation is further demonstrate at the molecular level. Indeed, we observed a progressive upregulation of *CollX* mRNA expression in the cartilaginous rings of upper and lower regions, revealed both by qPCR and in situ hybridization. This is to some extent contradictory to previous work (Sasano et al., 1998) performed on rats, where COLLX protein was detected in the developing tracheal ring of rats, but outside of the mineralized or hypertrophic zones, as immunoreactivity was localized in the uncalcified peripheral region of the trachea in all age group included in the study (4,8 and 10 week old rats) (Sasano et al., 1998).

Altogether our results demonstrate a very specific and early timing and pattern of calcification of the trachea in mice that display subtle to very substantial differences with other species (Bonucci et al., 1974; Hogg, 1982; Sasano et al., 1993; Sasano et al., 1998). The most striking dissimilarity is that observed with humans, who in normal conditions display tracheal mineralization solely in very aged people (Jo et al., 2008). Also, if there seems that Matrix Gla Protein likely plays an important role in the precocious abnormal appearance of tracheobronchial calcifications in children with Keutel Syndrome (Meier et al., 2001; Sun and Chen, 2012) or subjected to warfarin therapy (Thoongsuwan and Stern, 2003; Golding et al., 2013; Eckersley et al., 2014), the role that was also potentially attributed in the development of trachea calcification observed in young *Mgp*-deficient mice (Luo et al., 1997) might need to be revisited.

ACKNOWLEDGMENTS

This study was funded through grants from the Fondation pour la Recherche Médicale local committee and by the Region Lorraine, Université de Lorraine and CNRS. Support for Lina Tabcheh was provided by a stipend from the Middle East Institute of Health (Dr Norman Makdissy), Tripoli, Lebanon. Support for Chaohua Deng was provided by the Chinese Government. Tabea Kraft was granted through a studentship from Munster University.

We thank all the members of the team for their technical help and helpful discussions.

REFERENCES

Bonucci, E., Cuicchio, M. and Dearden, L. C. (1974) Investigations of ageing in costal and tracheal cartilage of rats, *Z Zellforsch Mikrosk Anat* 147(4): 505-27.

Eckersley, L., Stirling, J., Occleshaw, C. and Wilson, N. (2014) Two cases of warfarin-induced tracheobronchial calcification after Fontan surgery, *Pediatr Cardiol* 35(6): 954-8.

Golding, L. P., Walsh, M. J., Sumner, T. E. and Nakagawa, T. A. (2013) Tracheobronchial calcifications in children, *Pediatr Radiol* 43(8): 937-40.

Hogg, D. A. (1982) Ossification of the laryngeal, tracheal and syringeal cartilages in the domestic fowl, *J Anat* 134(Pt 1): 57-71.

Innes, B. A. and Dorin, J. R. (2001) Submucosal gland distribution in the mouse has a genetic determination localized on chromosome 9, *Mamm Genome* 12(2): 124-8.

Jeffery, P. K. (2001) Remodeling in asthma and chronic obstructive lung disease, *Am J Respir Crit Care Med* 164(10 Pt 2): S28-38.

Jo, S. H., Choi, Y. J., Cho, G. Y., Kim, H. S., Jung, K. S. and Rhim, C. Y. (2008) Tracheal calcification, *CMAJ* 179(3): 291.

Luo, G., Ducy, P., McKee, M. D., Pinero, G. J., Loyer, E., Behringer, R. R. and Karsenty, G. (1997) Spontaneous calcification of arteries and cartilage in mice lacking matrix GLA protein, *Nature* 386(6620): 78-81.

Meier, M., Weng, L. P., Alexandrakis, E., Ruschoff, J. and Goeckenjan, G. (2001) Tracheobronchial stenosis in Keutel syndrome, *Eur Respir J* 17(3): 566-9.

Moncada, R. M., Venta, L. A., Venta, E. R., Fareed, J., Walenga, J. M. and Messmore, H. L. (1992) Tracheal and bronchial cartilaginous rings: warfarin sodium-induced calcification, *Radiology* 184(2): 437-9.

Regamey, N., Ochs, M., Hilliard, T. N., Muhlfeld, C., Cornish, N., Fleming, L., Saglani, S., Alton, E. W., Bush, A., Jeffery, P. K. et al. (2008) Increased airway smooth muscle mass in children with asthma, cystic fibrosis, and non-cystic fibrosis bronchiectasis, *Am J Respir Crit Care Med* 177(8): 837-43.

Rifkin, M. D. and Pritzker, H. A. (1984) Tracheobronchial cartilage calcification in children. Case reports and review of the literature, *Br J Radiol* 57(676): 293-6.

Sasano, Y., Mizoguchi, I., Furusawa, M., Aiba, N., Ohtani, E., Iwamatsu, Y. and Kagayama, M. (1993) The process of calcification during development of the rat tracheal cartilage characterized by distribution of alkaline phosphatase activity and immunolocalization of types I and II collagens and glycosaminoglycans of proteoglycans, *Anat Embryol (Berl)* 188(1): 31-9.

Sasano, Y., Takahashi, I., Mizoguchi, I., Kagayama, M., Takita, H. and Kuboki, Y. (1998) Type X collagen is not localized in hypertrophic or calcified cartilage in the developing rat trachea, *Anat Embryol (Berl)* 197(5): 399-403.

Sun, L. F. and Chen, X. (2012) Tracheobronchial stenosis in Keutel syndrome, *Indian Pediatr* 49(9): 759.

Thoongsuwan, N. and Stern, E. J. (2003) Warfarin-induced tracheobronchial calcification, *J Thorac Imaging* 18(2): 110-2.

Tohno, S., Takano, Y., Tohno, Y., Moriwake, Y., Minami, T., Utsumi, M., Yamada, M. O. and Yuri, K. (2000) Age-dependent changes of elements in human trachea, *Biol Trace Elem Res* 77(2): 131-8.

Wallace, H. L., Southern, K. W., Connell, M. G., Wray, S. and Burdyga, T. (2013) Abnormal tracheal smooth muscle function in the CF mouse, *Physiol Rep* 1(6): e00138.

Widdicombe, J. H., Chen, L. L., Sporer, H., Choi, H. K., Pecson, I. S. and Bastacky, S. J. (2001) Distribution of tracheal and laryngeal mucous glands in some rodents and the rabbit, *J Anat* 198(Pt 2): 207-21.

FIGURES LEGENDS

Figure 1. Kinetic of tracheal mineralization in the C57BL/6J mouse strain.

Representative Alcian-blue/Alizarin red staining of the trachea of C57BL/6J individuals at P17 (A), P21 (B), P25 (C), P27 (D), P29 (E), P30 (F), P31 (G), and P60 (H). Mineralization of the respiratory tract initiates at P17 in the thyroid cartilage in the laryngeal prominence (A) and progresses over time to cover the whole larynx (A-H). At P30, mineralization appears in the first five rings of the trachea (F). At P60, the trachea and the bronchi are fully mineralized (H).

Figure 2. Tracheal mineralization in BALB/cJ versus C57BL/6J mouse strain

Representative Alcian-blue/Alizarin red staining of the trachea of BALB/cJ individuals at P20 (A), P25 (B), P27 (C), P29 (D), P30 (E), and P45 (F). Mineralization of the larynx is well advanced at P17, a time where faint patches of mineralization can already be observed in the first two tracheal rings (A). At P25, mineralization has progressed in the first seven rings of the trachea (B). At P45, the whole tracheobronchial tree is mineralized (F).

Figure 3. Tracheal longitudinal sections of C57BL6 mice stained with Von-Kossa/ Alcian-blue.

Longitudinal sections of the thyroid cartilage (A-F), the cricoid cartilage (G-L), a representative upper tracheal cartilage ring (M-R) and a lower tracheal cartilage ring at P17 (A,G,M and S), P25 (B,H,N and T), P29 (C,I,O and U), P30 (D,J,P and V), P31 (E,K,Q and W) and P33 (F,L,R and X). All thyroid samples panels are markedly stained with black due to mineralized cartilage (A-F). Cricoid mineralization can be detected at P29 (I) and intensifies with time (J-L). Mineralization in the upper tracheal cartilage can only be seen at P30 onward (P-R). No mineralization was detected at the lower part of the trachea at any time point (S-X).

Figure 4. Von-Kossa/ Alcian-blue staining in transversal section of C57BL6J trachea.

Transversal sections of the thyroid cartilage (A-C), the cricoid cartilage (I), a representative upper tracheal cartilage ring (D-F) and a representative lower tracheal cartilage ring (G-I) at P29 (A,D and G), P30 (B,E and H) and P31 (E,K,Q and W) and P33 (F,L,R and X). At P29 no mineralization can be detected in the upper tracheal cartilage (D), while at P30 (E) and P31 (F) mineralization can be detected in the first cartilage rings of the upper region of the trachea. No mineralization can be detected in the lower tracheal cartilage at any time point. Mineralized cricoid cartilage is mineralized at P31.

Figure 5. Collagen X expression is spatiotemporally expressed throughout the airways
CollX mRNA expression studied by qPCR or *in situ* hybridization (A-P). Expression of *CollX* assesses by qPCR is upregulated in upper versus lower tracheal regions. Longitudinal sections of the thyroid cartilage (A-D), the cricoid cartilage (E-H), a representative upper tracheal cartilage ring (I-L) and a lower tracheal cartilage ring at P25 (A-B,E-F,I-J and M-N) and P30 (C-D,G-H,K-L and O-P). *CollX* expression starts to be visible by in situ hybridization in all P25 samples (A,E,I and M) and is markedly induced at P30 in the larynx (C,G) and the trachea (K,O). Von Kossa staining appears through a time-dependent rostrocaudal pattern.

SUPPLEMENTARY DATA

Supplemental Figure 1. Tracheal mineralization displays no gender difference in C57BL/6J mice.

Alcian blue/alizarin red staining done on trachea of male and female C57BL6mice aged of 30 days shows no difference in the mineralization pattern with sex variation, panel 1 represent the trachea of female mice while in panel 2 the trachea of mal mice is presented, in both trachea the mineralization revealed by red staining are localized in the cartilage of the upper part of the trachea.

Supplemental Figure 2. Collagen X expression in P30 larynx and trachea

Adjacent transversal sections of the thyroid cartilage (A-D), the cricoid cartilage (E-H), a representative upper tracheal cartilage ring (I-L) and a representative lower tracheal cartilage ring (M-P) at P30 hybrized with DIG-labelled CollX-riboprobe or double stained with Alcian Blue and Von Kossa.

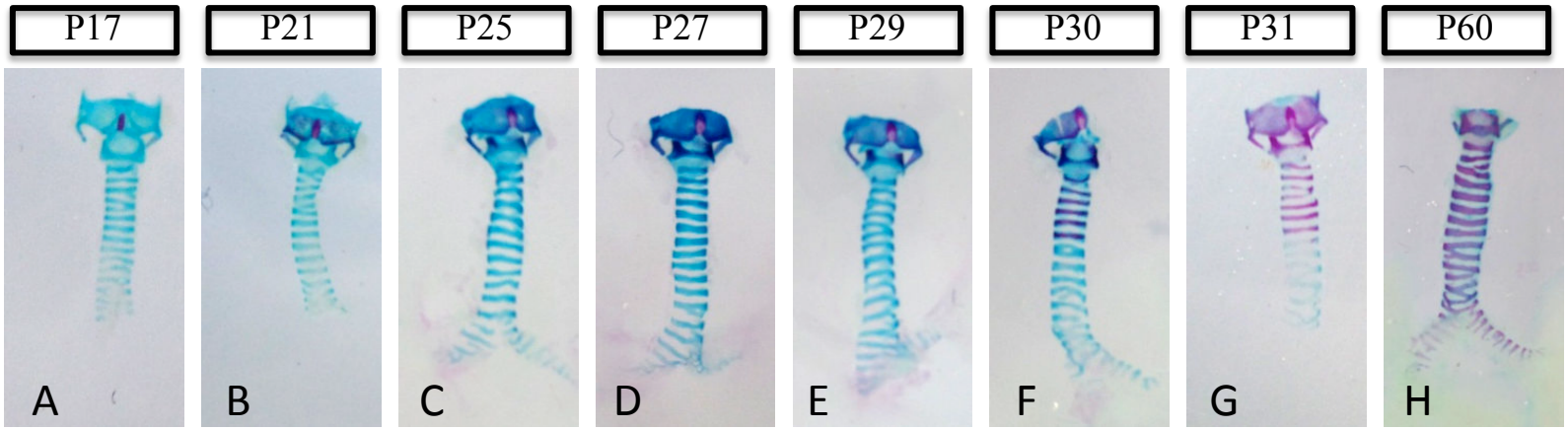

Figure 1

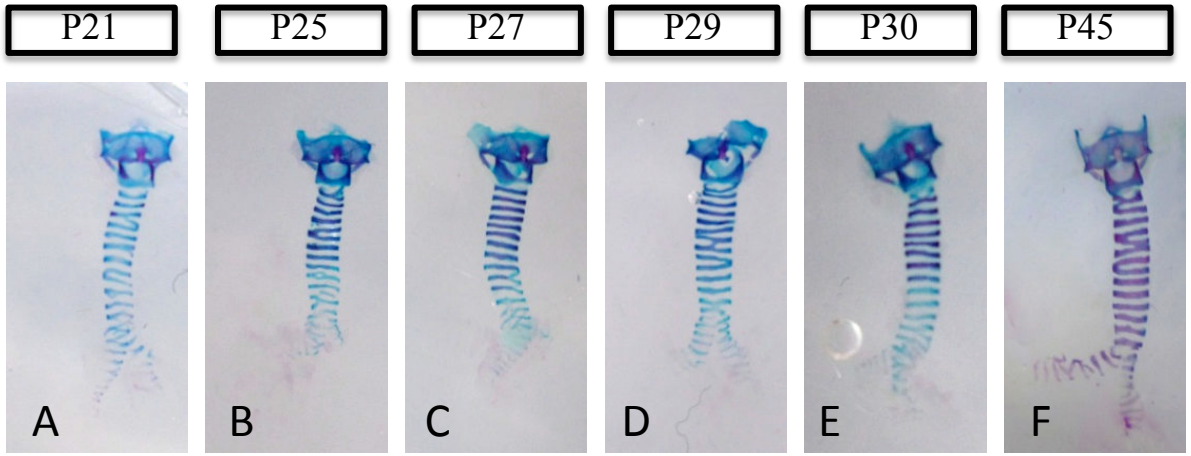

Figure 2

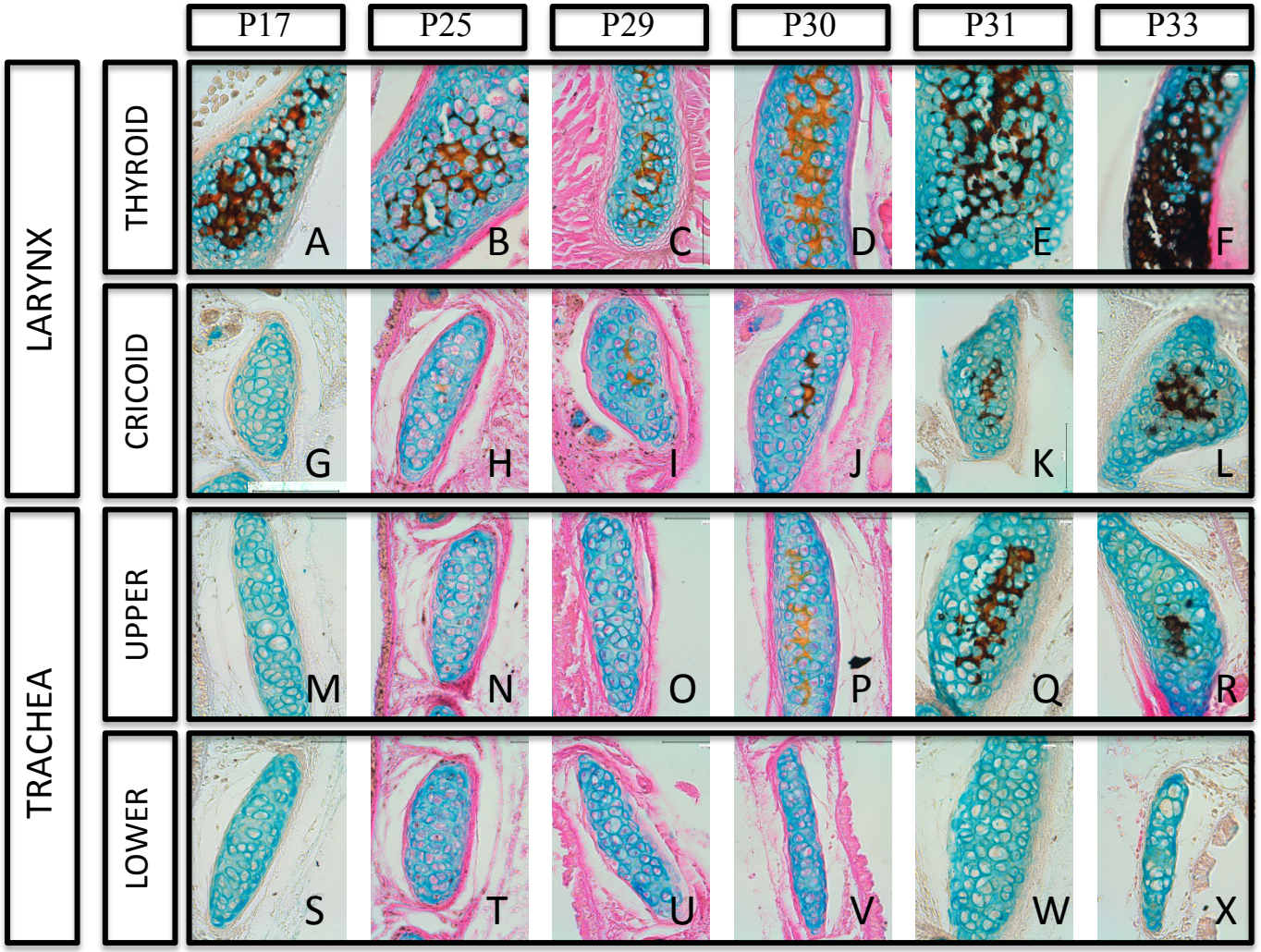
P17
P25
P29
P30
P31
P33
LARYNX
TRACHEA
THYROID
CRICOID
UPPER
LOWER
A
B
C
D
E
F
G
H
I
J
K
L
M
N
O
P
Q
R
S
T
U
V
W
X

Figure 3

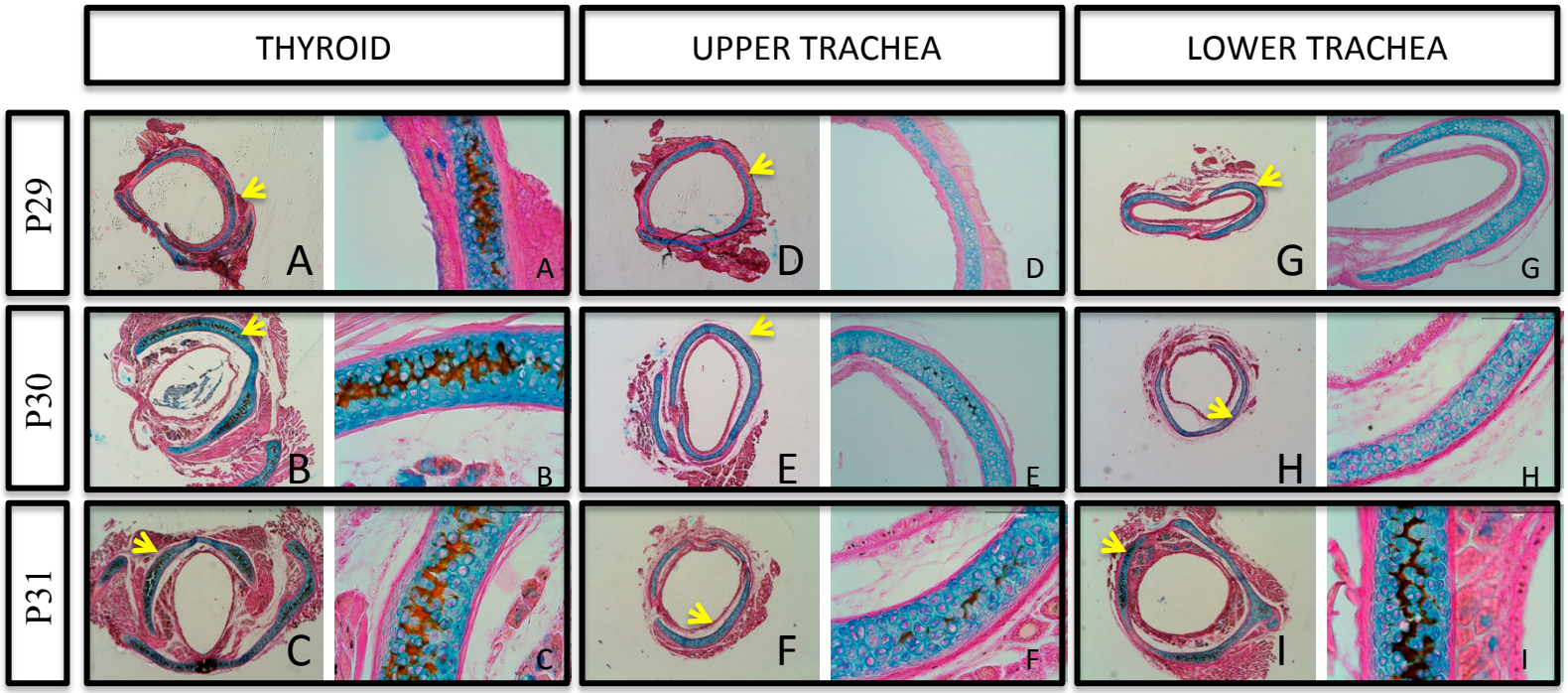
THYROID
UPPER TRACHEA
LOWER TRACHEA
P29
P30
P31
A
A
D
D
G
G
B
B
E
E
H
H
C
C
F
F
I
I

Figure 4

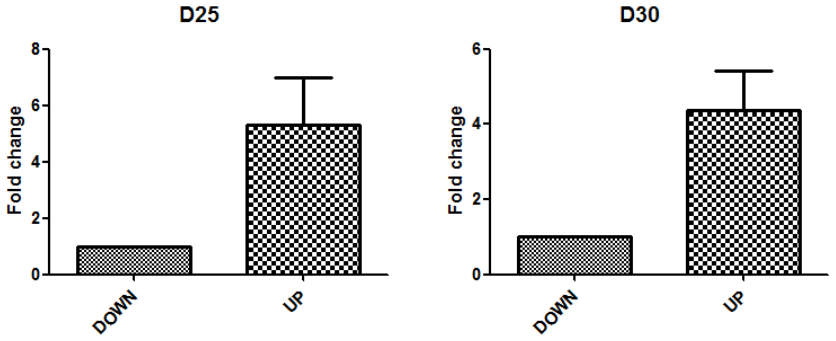
D25
Fold change
8
6
4
2
0
DOWN
UP
D30
Fold change
6
4
2
0
DOWN
UP

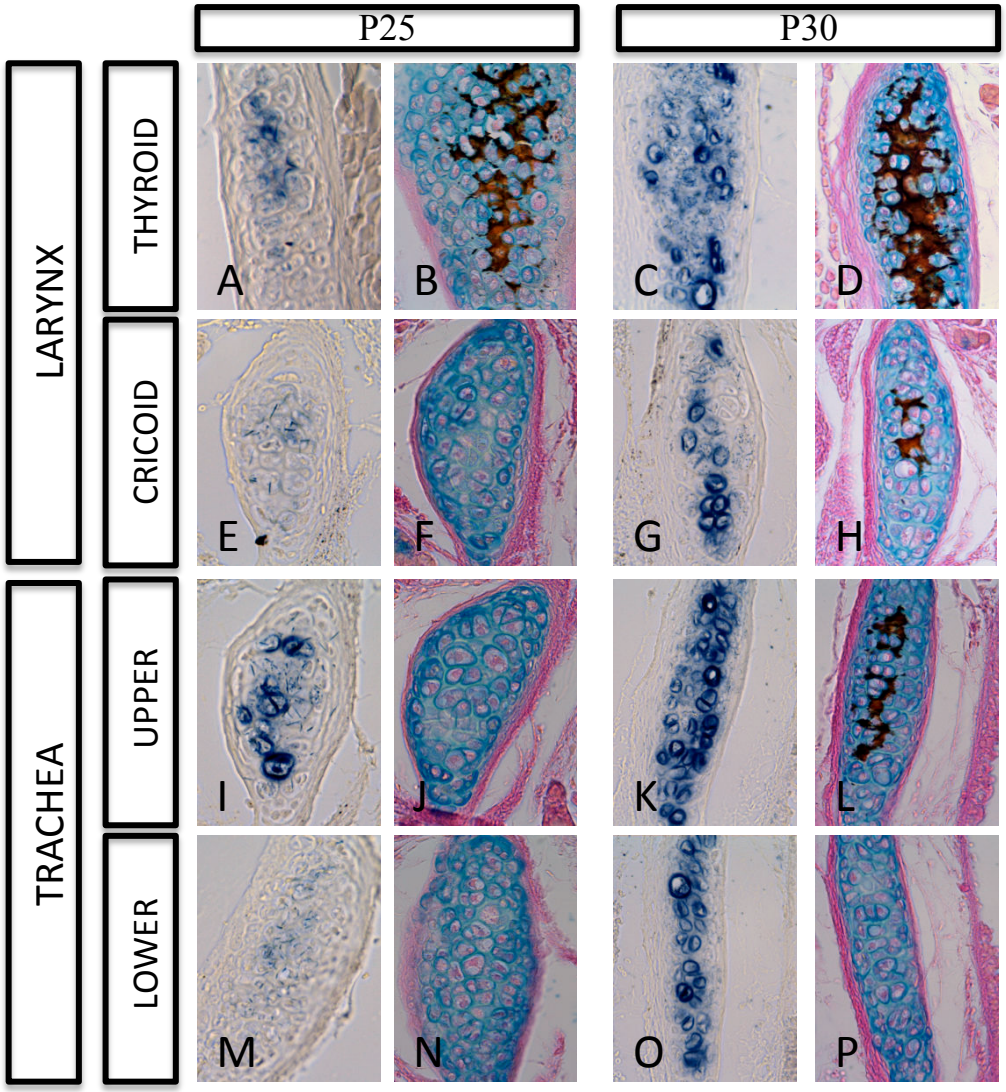
P25
P30
LARYNX
TRACHEA
THYROID
CRICOID
UPPER
LOWER
A
B
C
D
E
F
G
H
I
J
K
L
M
N
O
P

Figure 5

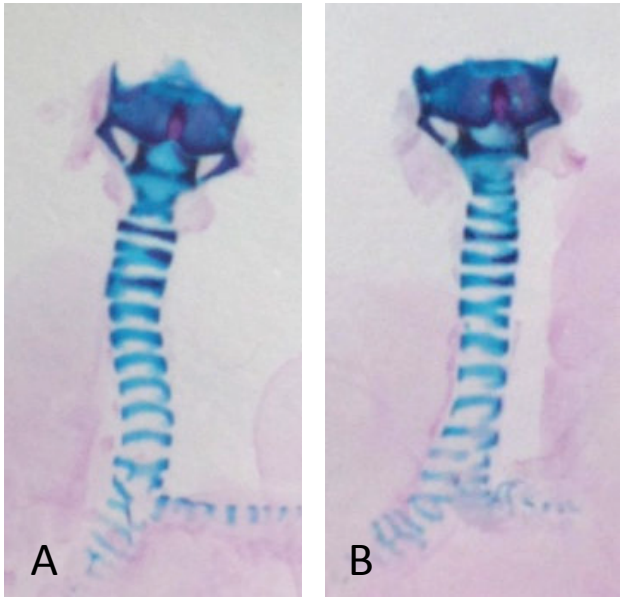

Supplementary Figure 1

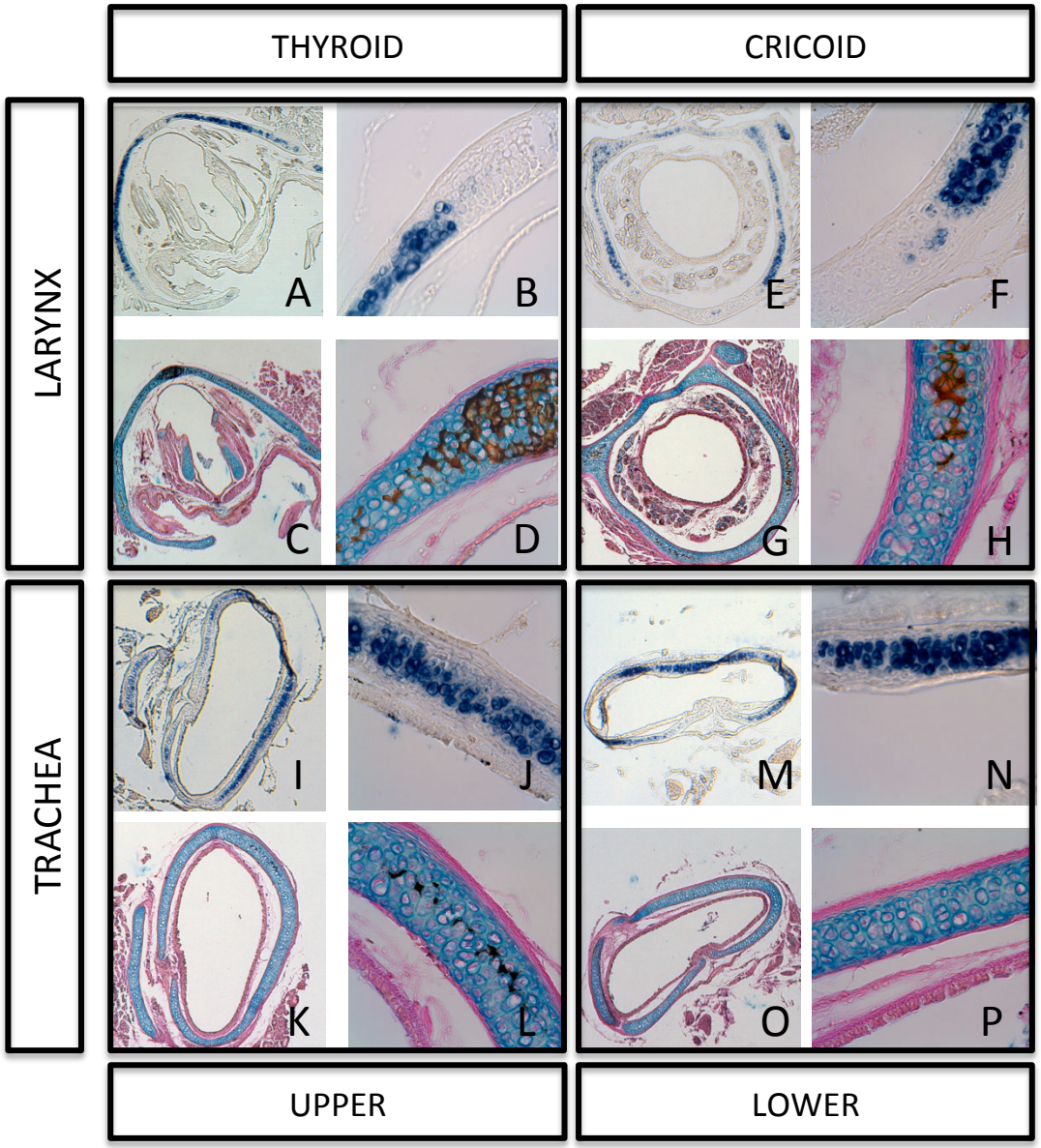

Supplementary Figure 2

Model of tracheal mineralization in the mouse

The trachea is a very complex structure of the respiratory tract, composed of C-shaped cartilaginous rings, made of hyaline cartilage. Although this cartilage does not typically mineralize, tracheal mineralization has been reported in humans in the elderly population and in rare pathological cases involving the Matrix gla protein (Mgp) gene.

In this context, this work seeked to understand the molecular mechanisms regulating tracheal mineralization that has been unexplored so far.

In the course of this study, unanticipated results were obtained as we provide solid morphological, and histological evidence showing that, in mice, in contrast to what has been commonly predicted, the mineralization of the trachea is an early and physiological event. A very schematic model summarizing these findings is presented in Fig.4.1 Further investigations are however needed to finalize the work and bring a more comprehensive understanding of the mechanisms involved in the process.

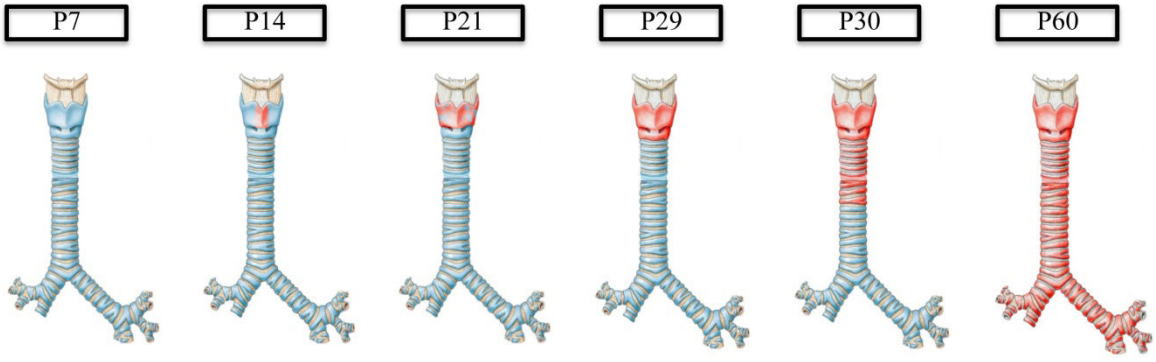

Fig.4.1. Schematic model of tracheobronchial mineralization in C57Bl/6J mouse postnatal development.

The presence of a clear time-shift in the mineralization occurrence between upper and lower regions of the trachea is also a puzzling problem for which we still have no satisfactory explanation. It would be worth investigating if the blood supply of the trachea can be behind this time-shift, as the upper part and the lower part are irrigated by different vessels (Grillo 2004).

Besides the initiation factors potentially involved, we were interested in understanding the molecular mechanism governing the mineralization in the trachea, and comprehending what are the differences between upper and lower tracheal cartilages. In order to do that, we

compared gene expressions in the upper part and lower part of the trachea respectively at different times preceding the onset of mineralization.

Among the data collected, these results show the presence of a peak of Bmp2, Nkx3.2 and CD73 expression at P26 both in the upper and lower parts (Fig.4.2). Sox9 and Runx2 expression pattern show a relative resemblance between the upper and lower parts, with a shift of the highest expression level from P26 for the upper part to P29 to the lower part. MGP was expressed uniformly at all times with a higher expression rate at the lower part of the trachea compared to the upper part.

BMP2 and NKX3.2 are both pro-chondrogenic molecules. BMP2 activates the expression of Sox9 and Nkx3.2 at early stages of chondrogenesis and NKX3.2 acts as a negative regulator of chondrocyte maturation (Zeng et al 2002). BMP2 can also activate Runx2 through the Smad pathway (Hirao et al 2006) and induce terminal differentiation of the chondrocytes.

On the other hand, BMP2 can also play a function in the activation of TNAP through a Wnt/Lrp5 loop (Rawadi et al 2003) and can also activate Runx2 through the Smad pathway (Hirao et al 2006). We did not find any changes in Tnap expression level in accordance with changes found in Bmp2 expression level. In fact Tnap expression fold remain stable with time. Intriguingly, Tnap expression level in the lower part of the trachea was higher from the expression level found in the upper part (where the mineralization begins) at all time; this can be explained by CD73 high expression level observed at two different times (P26 and P29) only in the lower part, where also the expression level of MGP was also more elevated. Indeed, CD73 converts AMP into inorganic phosphate and adenosine, which at high level has been shown to inhibit TNAP activity (St. Hilaire et al 2011).

In these qPCR experiments, we quantified the expression of genes not only in cartilaginous rings, but in all tissues of the upper part and lower part of the trachea, including the muscular and respiratory mucous. Thus, as we did for Coll X (see manuscript #2), to recognize if the expression of these genes reflect the expression in the cartilaginous part, complementary in situ hybridization or immunohistology experiments are needed and are currently ongoing.

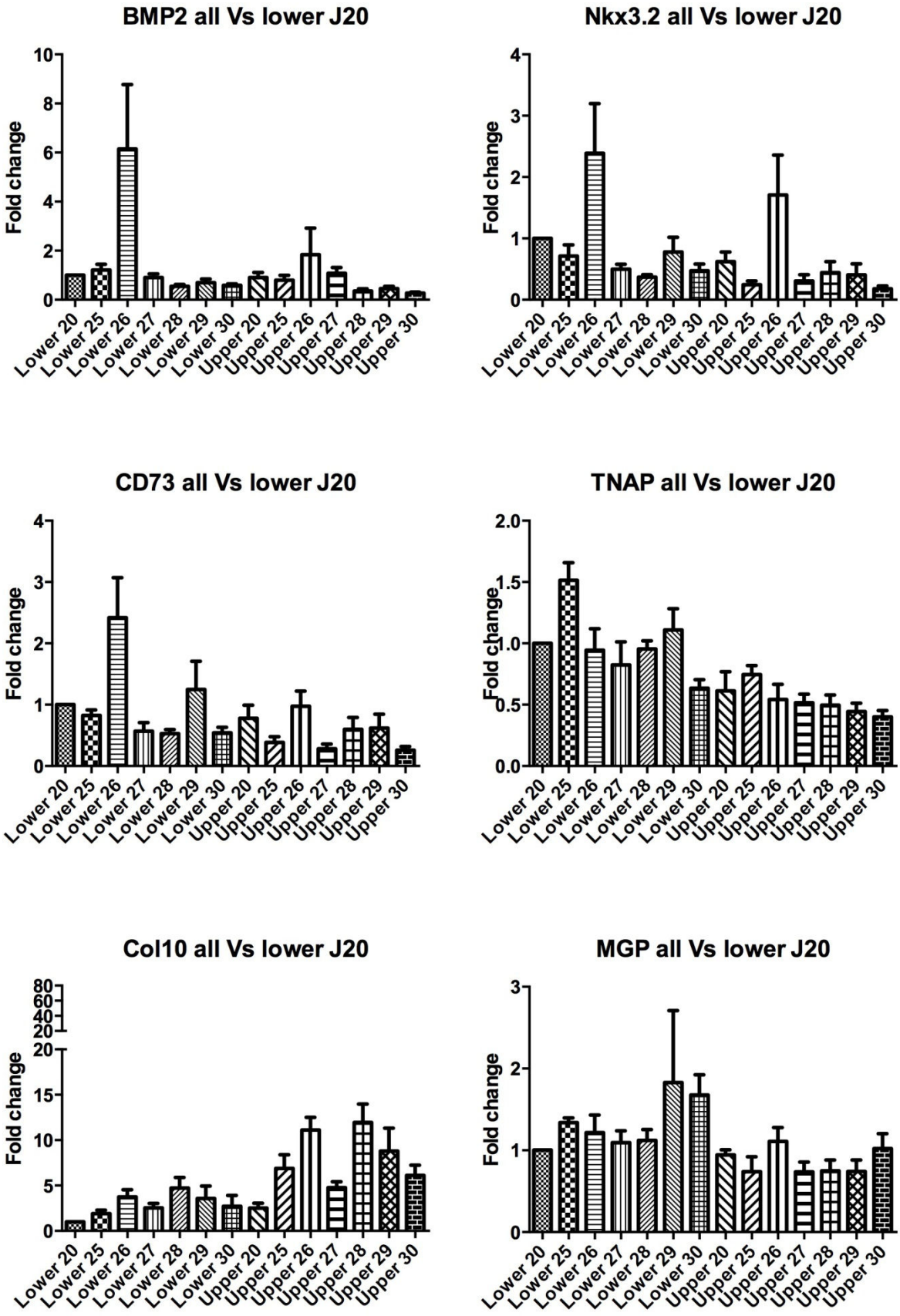

Fig.4.2. qPCR analysis of various genes in lower vs upper regions of mouse trachea between P20 and P30.

Primary culture of tracheal cells before mineralization and from different regions reveals different propensity to respond to Pi

The results we obtained *in vivo* revealed that the experiments done in our *in vitro* approach and published in the manuscript #1 were obtained from tracheal chondrocytes already engaged into a mineralized phenotype. Although the mineralized matrix seems to be lost when primary cultured, we ought to perform the same experiments before these chondrocytes enter the mineralization process. In order to address this question, we started a series of experiments, where we cultured chondrocytes from either the upper or the lower part of the trachea at P20 (Postnatal day 20), i.e. at least 10 days before the tracheal chondrocytes become mineralized.

When visualized under the microscope, primary chondrocytes harvested from the upper part of the trachea seems to be smaller than the chondrocytes harvested from the lower part of the trachea (compare A to B in Fig.4.3). Interestingly, upper and lower primary cultures of chondrocytes show morphology slightly different from that of primary culture of femoral head chondrocytes (panel C).

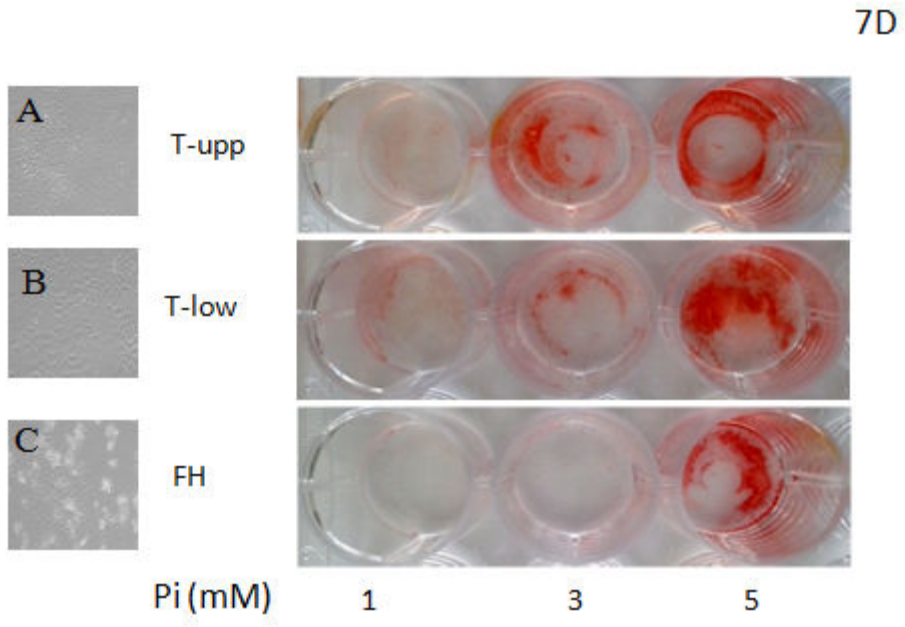

Fig.4.3. Morphological difference between the upper and lower tracheal chondrocytes and the effect of high concentration of Pi on these cells.

Chondrocytes harvested from the upper trachea (T-upp) of P20 mice (panel A) look smaller than chondrocytes harvested from the lower part (T-low) of the trachea (panel B), however both types of chondrocytes have a morphology different than that of femoral head (FH) harvested chondrocytes (C).

Chondrocytes treated at their first passage with 3 different concentrations of Pi (1,3 and 5 mM), after 7 days of treatment. Mineralization was assessed by the amount of calcium deposition revealed by alizarin red staining.

As done previously (manuscript #1), we tested the effect of high concentration of Pi on the cells from the two different regions of the trachea and from femoral head.

In this experiment, chondrocytes from the femoral head, the upper part and the lower part of the trachea were treated separately at first passage by three different concentrations of Pi (1, 3 and 5mM). At day 7, alizarin red staining was performed to detect calcium deposits. Chondrocytes from upper and lower trachea and femoral heads show no mineralization when treated with 1mM Pi. Red staining or mineralization can be detected in the wells containing tracheal chondrocytes when treated with 3mM of Pi. However, a more pronounced staining in the well containing chondrocytes from the upper trachea was observed. In contrast, chondrocytes obtained from femoral head cartilage showed no sign of mineralization when treated with 3mM of Pi. Mineralization was evident in all chondrocyte cultures submitted to 5mM of Pi (Fig.4.3). These results suggest that tracheal chondrocytes might be more prone to mineralization than joint cells, and that chondrocyte harvested from the upper trachea may be more sensitive towards high Pi levels than chondrocyte harvested from the lower part of the trachea. Although these preliminary data need to be confirmed, they seem somehow coherent with what we observed *in vivo*. They also confirm that there are marked differences between hyaline cartilage of distinct origins.

Role of MGP in tracheal mineralization

As previously mentioned, MGP is known as a potent mineralization inhibitor. In addition to the extensive mineralization of their arterial trunk, *Mgp* KO mice were also reported to develop abnormal early tracheal mineralization (Luo et al 1997). Because we found that early tracheal mineralization was a physiological process in mice, we wondered if the absence of *Mgp* in these mice was responsible of the observed mineralization or solely the incorrect interpretation of a normal but unknown process when the initial observation was made.

In order to revisit the potential effect of MGP deficiency in tracheal mineralization, we compared the tracheal phenotype of $Mgp^{+/+}$, $Mgp^{+/-}$ and $Mgp^{-/-}$ C57BL/6 mice using Alcian-blue/Alizarin-red staining. We found that the tracheal phenotype differ from $Mgp^{-/-}$ to their WT ($Mgp^{+/+}$) littermates since mineralization are more pronounced and more extended in the *Mgp*-deficient tracheal cartilage. When no mineralization was detected in the trachea of $Mgp^{+/+}$ mice at P28 postnatal, the trachea of $Mgp^{-/-}$ mice at the same age was already fully mineralized. Surprisingly, at every time studied, an intermediate phenotype was observed in the trachea of $Mgp^{+/-}$ mice, whereas no vascular phenotype can be observed in the heterozygous mice (Fig.4.4)

These morphological results suggest that MGP may play a role in the appearance of tracheal mineralization but this role is more limited than originally thought. This strikingly contrasts

with its major role in humans, since patients with defective MGP expression or activity (Keutel syndrome or warfarin therapy) show enhanced calcification at very early ages. Further molecular analysis of the regulation of the genes potentially involved in the mineralization of the trachea between the three genotypes may help to decipher the role of Mgp in this process. However, we believe its role as a BMP inhibitor is important in the process. If as observed in WT mice, BMP2 peak at P26 is involved in the mineralization process, it is reasonable to think that the partial or complete absence of one of the inhibitor of the BMP signaling in the $Mgp^{+/-}$ and $Mgp^{-/-}$ trachea respectively may accelerate the mineralization process.

Further investigations including crossing BMP2-conditionnal KO mice with $Mgp^{+/+}$, $Mgp^{+/-}$ and $Mgp^{-/-}$ mice would tremendously help understand the initiation of mineralization in the the trachea.

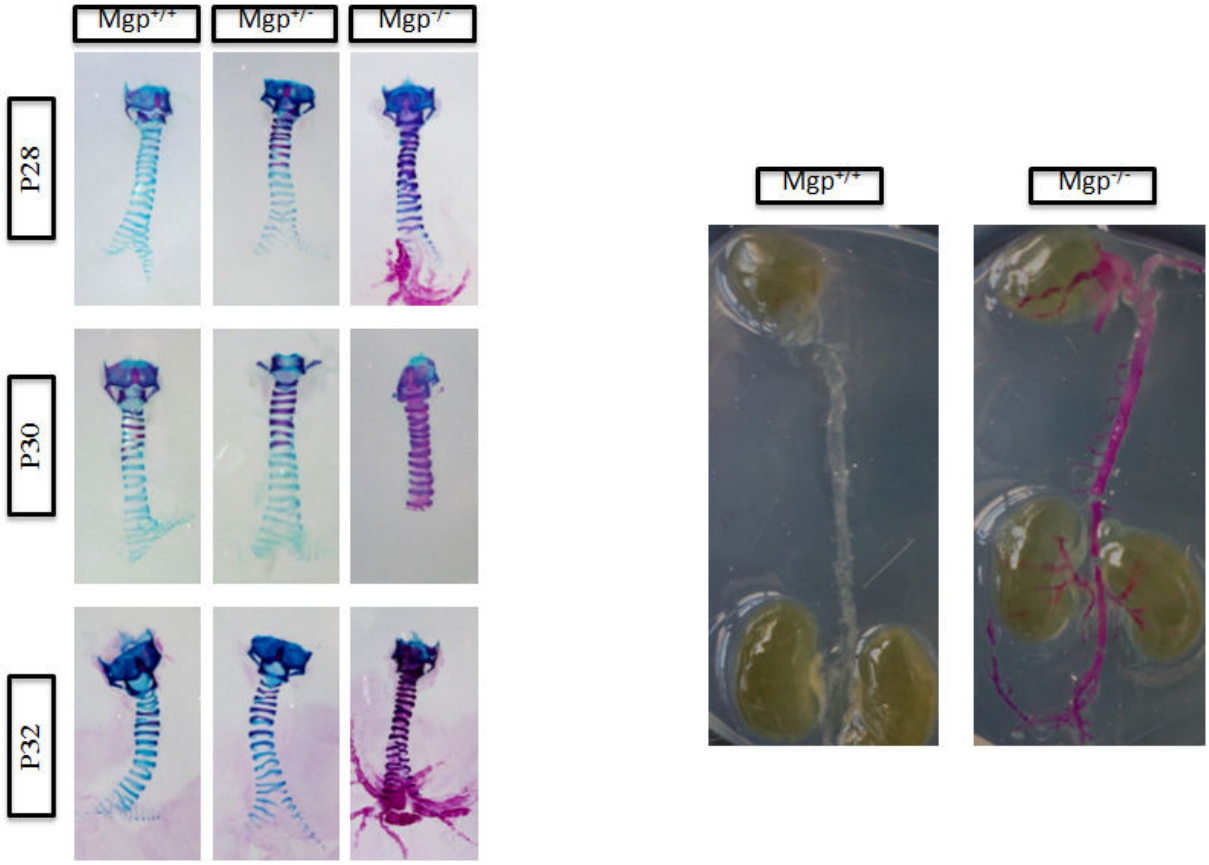

Fig.4.4. The absence of MGP in *Mgp*-deficient mice enhances tracheal mineralization.

The effect of Mgp absence on trachea mineralization was morphologically studied using Alcian blue/Alizarin red staining on trachea harvested from $Mgp^{+/+}$, $Mgp^{+/-}$ and $Mgp^{-/-}$ mice at 3 different ages P28, P30 and P32. As expected at P28, no mineralization was detected in $Mgp^{+/+}$ trachea and at P30 and P32 mineralization at the upper part of the trachea was detectable where the mineralization in $Mgp^{+/+}$ trachea seems to progress transversely in the upper part of the trachea after 30P. $Mgp^{-/-}$ trachea was almost fully mineralized at P28 and is fully mineralized at P30 and P32 where mineralization at main bronchi can also be seen; unexpectedly the trachea of $Mgp^{+/-}$ showed a phenotype at all age.

CHAPTER V

GENERAL CONCLUSION

Le travail expérimental présenté dans cette thèse s'est intéressé à la minéralisation de la trachée. En l'absence de protocoles d'étude spécifiques au tissu trachéal, le développement d'approches originales non disponibles au laboratoire a été nécessaire pour répondre aux questions posées.

Ainsi, la mise en place de culture primaire de cellules cartilagineuses et musculaires provenant de trachée de souris a tout d'abord permis de démontrer la capacité de ces deux types cellulaires à minéraliser en réponse à une hyperphosphatémie (Tabcheh *et al*, Biomed Mater Eng. 2014; 24:37-45). A notre connaissance, ces résultats sont les premiers à étudier les capacités minéralisantes des cellules trachéales cartilagineuses et musculaires. Ils démontrent que ces cellules ont des capacités minéralisantes identiques à celles d'origine articulaire ou vasculaire.

En parallèle, une étude complémentaire a été menée sur la minéralisation trachéale au cours du vieillissement chez la souris afin d'appréhender les mécanismes impliqués dans un processus observé chez certains patients âgés souffrant de dyspnées parfois sévères. Cette étude comportant des analyses morphologiques, histologiques et moléculaires a démontré que la trachée commence à se minéraliser après seulement un mois de vie chez la souris C57Bl/6. Ces données plutôt inattendues (Tabcheh *et al*, en préparation) sur la chronologie d'apparition de la minéralisation trachéale suggèrent que celle-ci est un processus physiologique précoce et soudain chez la souris, alors que chez l'homme elle n'apparaît que chez l'individu âgé ou dans des conditions pathologiques rares.

Ces résultats particulièrement intéressants soulèvent de nombreuses questions dont certaines sont évoquées et partiellement résolues dans les discussions propres à chaque étude *in vitro* (chapitre 3) ou *in vivo* (chapitre 4). Il n'en reste pas moins qu'analysées globalement, nos deux approches révèlent des interrogations supplémentaires auxquelles nous n'avons à ce jour pas de réponses satisfaisantes ou définitives à apporter, mais qui sont intéressantes d'évoquer.

Minéralisation des cellules musculaires lisses trachéales: fait ou fiction?

Les résultats obtenus sur les cultures primaires de cellules musculaires trachéales (manuscrit #1) démontrent sans ambiguïté la capacité de ces cellules à se minéraliser en réponse à des concentrations anormales de Pi. Les expériences obtenues avec la technique de culture d'explants trachéaux confirment ces données bien qu'une plus forte concentration de Pi soit nécessaire pour induire la minéralisation du tissu musculaire trachéal au sein de ces explants.

Notre étude de la minéralisation trachéale chez la souris n'a cependant révélé aucun signe de minéralisation du muscle trachealis. En effet, aucune des données morphologiques et histologiques obtenues au cours de notre deuxième étude, résumées dans la version préliminaire du manuscrit #2, ne permet de conclure à une implication des cellules du muscle de la trachée dans le processus physiologique de minéralisation trachéale. De façon encore plus surprenante, les résultats récemment obtenus avec les souris déficientes en *Mgp* sont en accord avec l'absence de capacité minéralisante du tissu musculaire trachéal *in vivo*. En effet, alors que MGP a été indéniablement impliquée comme un inhibiteur de minéralisation des cellules musculaires du tissu vasculaire dont l'absence entraine une calcification spontanée et importante de la matrice extracellulaire de ces cellules, nous n'avons trouvé aucune trace de minéralisation dans les cellules musculaires lisses d'origine trachéale même en absence de MGP. Même si nous n'avons à l'heure actuelle aucune preuve de l'expression de MGP dans les cellules musculaires trachéales, l'ensemble de ces résultats suggère que les résultats obtenus *in vitro* sont à interpréter avec prudence.

Cependant, ces résultats apparemment contradictoires pourraient s'expliquer par le fait que le stimulus à l'origine de la minéralisation physiologique, chez la souris sauvage ou accélérée chez la souris déficiente en *Mgp*, n'est à l'évidence pas une augmentation locale de la concentration en Pi. Toutefois, dans certains cas, les concentrations élevées de Pi pourraient participer à la minéralisation de la trachée. En effet, chez les patients en insuffisance rénale chronique (chez qui il existe une hyperphosphatémie), il a été observé des calcifications des parois bronchique et trachéale (Alkan et al, 2009). Cependant, les informations disponibles ne permettent pas de distinguer si ces minéralisations restent localisées au tissu cartilagineux ou pourraient également affecter le muscle trachéal.

Bien qu'hypothétique, la possibilité que les cellules musculaires lisses trachéales puissent donc, dans certains cas (hyperphosphatémie, ...), minéraliser *in vivo* comme nous l'avons démontré *in vitro* pourrait peut-être expliquer pourquoi, seulement dans de très rares cas, la minéralisation généralement asymptomatique amène le patient à consulter à cause de

l'apparition de dyspnée ou d'essoufflement. En effet la minéralisation du tissu musculaire en diminuant la propriété élastique de la trachée pourrait expliquer l'évolution symptomatique du patient.

Minéralisation du cartilage trachéal: intérêt et importance?

Les études qui rapportent une minéralisation trachéale proviennent majoritairement d'observations cliniques réalisées chez des individus âgés voire très âgés. Les quelques rares cas observés chez des individus plus jeunes ou des enfants mettaient en avant le rôle probable d'une perte de fonction de la protéine MGP dans cette apparition précoce de la minéralisation trachéale (traitement à la Warfarine ou syndrome de Keutel). Ce rôle de la MGP semblait confirmé dans les souris puisque l'équipe de Gérard Karsenty, dans la publication originale décrivant le phénotype des souris *Mgp*$^{-/-}$, rapportaient une minéralisation anormale et précoce de la trachée (Luo *et al*, 1997), observation également réalisée par des membres de notre équipe chez des souris de 24 jours (Leroux-Berger *et al*, 2011). Le travail de cette thèse était donc de comprendre les mécanismes à l'origine de l'apparition anormale de minéralisation dans la trachée de souris et en particulier le rôle de MGP dans ce processus.
Du fait de la perte accidentelle de la colonie de souris déficientes en *Mgp*, nous avons focalisé notre étude sur la minéralisation trachéale lors du vieillissement de la souris pour mieux comprendre les mécanismes à l'origine de cette minéralisation que l'on retrouve chez l'homme chez des patients âgés soufrant de dyspnées parfois sévères.
Au cours de cette étude, nous avons découvert que la minéralisation chez la souris était un phénomène physiologique précoce et non lié au vieillissement et que le rôle de MGP était de fait beaucoup plus limité qu'initialement envisagé. Ces résultats très inattendus sont révélateurs de l'intérêt plutôt limité porté à la trachée par la communauté scientifique malgré son importance fonctionnelle. Ils soulèvent également la question de l'importance de la minéralisation dans le fonctionnement de cet organe.
Plus généralement, ces résultats pointent également les limites des modèles murins déficients dans la compréhension des mécanismes physiopathologiques.

Les informations pourtant nombreuses exposées dans le chapitre introductif de cette thèse sur la trachée proviennent souvent d'informations très ponctuelles retrouvées dans des articles concernant le système respiratoire en général. Sauf en de très rares exceptions, les

observations concernant les malformations trachéales obtenues chez différentes souris KO et qui ont permis de démontrer un rôle de telle ou telle molécule dans le développement de la trachée sont souvent dissimulées dans des articles sur le développement du poumon. Fort de cet enseignement sur le désintérêt apparent de la communauté sur le tissu trachéal, et au vue des résultats apparemment contradictoires avec la littérature, nous avons entrepris une recherche bibliographique plus poussée qu'une simple recherche par mots clés tels que "mineralization", trachea" and "mice". Bien que compliquée, cette recherche a permis de retrouver seulement 4 articles qui avaient préalablement rapporté une apparition physiologique précoce de la minéralisation trachéale. Un papier publié en 1981 décrivait ainsi l'ossification des cartilages du larynx, du syrinx et de la trachée chez la poule domestique. Trois articles, publiés en 1973 pour le premier, puis en 1993 pour les deux autres, faisaient quant à eux la description d'une minéralisation précoce des anneaux trachéaux chez le Rat. Si ces résultats confortent les résultats obtenus au cours de cette thèse chez la souris ou si, à l'inverse, nous confirmons les résultats préalablement obtenus chez d'autres espèces animales, l'ancienneté de ces études et la difficulté à les mettre à jour démontrent que la minéralisation de la trachée est un phénomène qui a été sous-évalué dans le modèle souris. L'étude attentive de figures de certains papiers montre même que les auteurs ne mentionnent pas cette minéralisation, y compris lorsque celle-ci paraît évidente. Nous espérons que nos résultats qui confirment et complètent les quelques études anciennes sur le sujet puissent enfin mettre fin au dogme qui affirme que le cartilage trachéal est un cartilage hyalin permanent tout au long de la vie.

Notre étude a permis de mette à jour une différence très nette entre le processus de minéralisation trachéale entre la souris et l'homme. Excepté la néoténie souvent décrite chez l'homme qui, de façon purement hypothétique, pourrait être poussée à l'extrême pour la trachée, nous n'avons aucune explication à cette différence entre espèces. Quoiqu'il en soit, il est évident que cette minéralisation précoce chez la souris d'un mois ne perturbe pas la vie de l'animal. La souris poursuit en effet une vie tout à fait normale après l'établissement de la minéralisation de ses anneaux trachéaux. Cette absence de symptôme est, dans la plupart des cas, également retrouvé chez l'homme bien que certains patients consultent suite à des dyspnées ou des essoufflements à l'effort ou au repos. Il est possible que ces symptômes ne soient pas dus à la minéralisation du cartilage trachéal lui même mais à la sténose trachéale associée et/ou, comme évoquée précédemment, à l'atteinte du tissu musculaire, deux conditions que nous n'avons pas observées dans le modèle souris. Enfin, bien qu'aucun élément ne nous permette d'être affirmatif, nous pouvons suggérer que la position debout due

à la bipédie humaine entraine une position de la trachée qui, en cas de minéralisation, induit plus facilement une gêne respiratoire, alors que la quadrupédie de la souris et autres rongeurs pourrait participer à l'absence de manifestation de gêne respiratoire consécutive à une minéralisation prononcée mais physiologique de la trachée.

REFERENCES

Abbott A, Sibert J, Weaver J. 1977. Chondrodysplasia punctata and maternal warfarin treatment. *British Medical Journal* 1:1639

Abedin M, Tintut Y, Demer LL. 2004. Vascular calcification mechanisms and clinical ramifications. *Arteriosclerosis, Thrombosis, and Vascular Biology* 24:1161-70

Abhishek A, Doherty M. 2010. Pathophysiology of articular chondrocalcinosis—role of ANKH. *Nature Reviews Rheumatology* 7:96-104

Acar GO, Yilmaz M, Sekercioglu N, Yuksel A. 2010. Keutel syndrome in a patient presenting with hearing loss. *B Ent* 6:201-4

Adams CS, Mansfield K, Perlot RL, Shapiro IM. 2001. Matrix Regulation of Skeletal Cell Apoptosis role of calcium and phosphate ions. *Journal of Biological Chemistry* 276:20316-22

Addison WN, Azari F, Sørensen ES, Kaartinen MT, McKee MD. 2007. Pyrophosphate inhibits mineralization of osteoblast cultures by binding to mineral, up-regulating osteopontin, and inhibiting alkaline phosphatase activity. *Journal of Biological Chemistry* 282:15872-83

Adeney KL, Siscovick DS, Ix JH, Seliger SL, Shlipak MG, et al. 2009. Association of serum phosphate with vascular and valvular calcification in moderate CKD. *Journal of the American Society of Nephrology* 20:381-7

Akiyama H, Lyons JP, Mori-Akiyama Y, Yang X, Zhang R, et al. 2004. Interactions between Sox9 and β-catenin control chondrocyte differentiation. *Genes & Development* 18:1072-87

Al-Qadi MO, Artenstein AW, Braman SS. 2013. The "forgotten zone": Acquired disorders of the trachea in adults. *Respiratory Medicine* 107:1301-13

Ali S. 1976. Analysis of matrix vesicles and their role in the calcification of epiphyseal cartilage. *Federation Proceedings*, pp. 135-42

Alini M, Carey D, Hirata S, Grynpas MD, Pidoux I, Poole AR. 1994. Cellular and matrix changes before and at the time of calcification in the growth plate studied in vitro: arrest of type X collagen synthesis and net loss of collagen when calcification is initiated. *Journal of Bone and Mineral Research* 9:1077-87

Aliperta A, Mauro G, Saviano G, Bellissimo U, Perna A, Tartufi S. 1977. Proteinosi alveolare, pneumopatia a corpi amilacei e microlitiasi polmonare: Contributo istopatologico. *Arch Monaldi Mal Torace* 31:87-118

Amorós J, Lluberas A. 2013. Tracheobronchial Anatomy. In *Interventions in Pulmonary Medicine*, ed. JP Díaz-Jimenez, AN Rodriguez, pp. 3-11: Springer New York

Anderson HC. 1967. Electron microscopic studies of induced cartilage development and calcification. *The Journal of Cell Biology* 35:81-101

Anderson HC. 1983. Mineralization by matrix vesicles. *Scanning Electron Microscopy*:953-64

Anderson HC, Harmey D, Camacho NP, Garimella R, Sipe JB, et al. 2005. Sustained osteomalacia of long bones despite major improvement in other hypophosphatasia-related mineral deficits in tissue nonspecific alkaline phosphatase/nucleotide pyrophosphatase phosphodiesterase 1 double-deficient mice. *The American Journal of Pathology* 166:1711-20

Andrew L, Brancolini V, Serrano De la Pena L, Devoto M, Caeiro F, et al. 1999. Refinement of the chromosome 5p locus for familial calcium pyrophosphate dihydrate deposition disease. *The American Journal of Human Genetics* 64:136-45

Arden N, Nevitt MC. 2006. Osteoarthritis: epidemiology. *Best Practice & Research Clinical Rheumatology* 20:3-25

Aristotle. 1918 *Parts of Animals* Cambridge: MA: Harvard University Press

Arora R, Metzger RJ, Papaioannou VE. 2012. Multiple roles and interactions of Tbx4 and Tbx5 in development of the respiratory system. *PLoS Genet* 8:2

Arsenis C. 1972. Role of mitochondria in calcification. Mitochondrial activity distribution in the epiphyseal plate and accumulation of calcium and phosphate ions by chondrocyte mitochondria. *Biochemical and Biophysical Research Communications* 46:1928-35

Arsic D, Keenan J, Quan QB, Beasley S. 2003. Differences in the levels of Sonic hedgehog protein during early foregut development caused by exposure to Adriamycin give clues to the role of the Shh gene in oesophageal atresia. *Pediatric Surgery International* 19:463-6

Ascenzi A, Bonucci E, Steve Bocciarelli D. 1965. An electron microscope study of osteon calcification. *Journal of Ultrastructure Research* 12:287-303

Atala A, Kasper FK, Mikos AG. 2012. Engineering complex tissues. *Science Translational Medicine* 4:3004890

Aubin J, Davy A, Soriano P. 2004. In vivo convergence of BMP and MAPK signaling pathways: impact of differential Smad1 phosphorylation on development and homeostasis. *Genes & Development* 18:1482-94

Aubin J, Lemieux M, Tremblay M, Berard J, Jeannotte L. 1997a. Early postnatal lethality in Hoxa-5 mutant mice is attributable to respiratory tract defects. *Developmental Biology* 192:432-45

Aubin J, Lemieux M, Tremblay M, Bérard J, Jeannotte L. 1997b. Early Postnatal Lethality inHoxa-5Mutant Mice Is Attributable to Respiratory Tract Defects. *Developmental Biology* 192:432-45

Austin J, Ali T. 2003. Tracheomalacia and bronchomalacia in children: pathophysiology, assessment, treatment and anaesthesia management. *Paediatric Anaesthesia* 13:3-11

Ayers M, Jeffery PK. 1982. Cell division and differentiation in bronchial epithelium. In *Cellular Biology of the Lung*, pp. 33-59: Springer

Bach AM, Hann LE, Hadar O, Shi W, Yoo H-H, et al. 2001. Testicular Microlithiasis: What Is Its Association with Testicular Cancer? *Radiology* 220:70-5

Badylak SF, Gilbert TW. 2008. Immune response to biologic scaffold materials. *Seminars in Immunology*, pp. 109-16: Elsevier

Baer GA, Terho M, Tiensuu T. 1987. Morphologic study of the adult trachea at the 7th and 12th ring. A study on specimens from 205 autopsies. *Surgical and Radiologic Anatomy* 9:169-72

Bai X-Y, Miao D, Goltzman D, Karaplis AC. 2003. The autosomal dominant hypophosphatemic rickets R176Q mutation in fibroblast growth factor 23 resists proteolytic cleavage and enhances in vivo biological potency. *Journal of Biological Chemistry* 278:9843-9

Baldwin JC, Karthikeyan AS, Raghothama KG. 2001. LEPS2, a phosphorus starvation-induced novel acid phosphatase from tomato. *Plant Physiology* 125:728-37

Baum M, Schiavi S, Dwarakanath V, Quigley R. 2005. Effect of fibroblast growth factor-23 on phosphate transport in proximal tubules. *Kidney International* 68:1148-53

Baylink D, Wergedal J, Stauffer M. 1971. Formation, mineralization, and resorption of bone in hypophosphatemic rats. *Journal of Clinical Investigation* 50:2519

Beasley S, Myers N. 1988. The diagnosis of congenital tracheoesophageal fistula. *Journal of Pediatric Surgery* 23:415-7

Beck GR, Sullivan EC, Moran E, Zerler B. 1998. Relationship between alkaline phosphatase levels, osteopontin expression, and mineralization in differentiating MC3T3-E1 osteoblasts. *Journal of Cellular Biochemistry* 68:269-80

Beck GR, Zerler B, Moran E. 2000. Phosphate is a specific signal for induction of osteopontin gene expression. *Proceedings of the National Academy of Sciences* 97:8352-7

Beck Jr GR, Moran E, Knecht N. 2003. Inorganic phosphate regulates multiple genes during osteoblast differentiation, including Nrf2. *Experimental Cell Research* 288:288-300

Bell SM, Schreiner CM, Wert SE, Mucenski ML, Scott WJ, Whitsett JA. 2008. R-spondin 2 is required for normal laryngeal-tracheal, lung and limb morphogenesis. *Development* 135:1049-58

Belli SI, Mercuri FA, Sali A, Goding JW. 1995. Autophosphorylation of PC-1 (Alkaline Phosphodiesterase I/Nucleotide Pyrophosphatase) and Analysis of the Active Site. *European Journal of Biochemistry* 228:669-76

Belli SI, van Driel IR, Goding JW. 1993. Identification and characterization of a soluble form of the plasma cell membrane glycoprotein PC-1 (5'-nucleotide phosphodiesterase). *European Journal of Biochemistry* 217:421-8

Bellows C, Heersche J, Aubin J. 1992. Inorganic phosphate added exogenously or released from β-glycerophosphate initiates mineralization of osteoid nodules in vitro. *Bone and Mineral* 17:15-29

Benet-Pagès A, Orlik P, Strom TM, Lorenz-Depiereux B. 2005. An FGF23 missense mutation causes familial tumoral calcinosis with hyperphosphatemia. *Human Molecular Genetics* 14:385-90

Bi W, Huang W, Whitworth DJ, Deng JM, Zhang Z, et al. 2001. Haploinsufficiency of Sox9 results in defective cartilage primordia and premature skeletal mineralization. *Proceedings of the National Academy of Sciences* 98:6698-703

Bianchine J, Stambler A, Harrison H. 1971. Familial hypophosphatemic rickets showing autosomal dominant inheritance. *Birth Defects original article series* 7:287

Bieger RC, Passarge E, McADAMS AJ. 1965. Testicular intratubular bodies. *The Journal of Clinical Endocrinology & Metabolism* 25:1340-6

Bielenberg DR, D'Amore PA. 2013. All Vessels Are Not Created Equal. *The American Journal of Pathology* 182:1087-91

Biology al. http://163.16.28.248/bio/activelearner/44/ch44c3.html

Birk DE, Linsenmayer TF. 1994. Collagen fibril assembly, deposition, and organization into tissue-specific matrices. *Extracellular Matrix Assembly and Structure*:91-128

Blume C, Felix A, Shushakova N, Gueler F, Falk CS, et al. 2012. Autoimmunity in CD73/Ecto-5'-nucleotidase deficient mice induces renal injury. *PloS one* 7:29

Bobryshev YV. 2005. Transdifferentiation of smooth muscle cells into chondrocytes in atherosclerotic arteries in situ: implications for diffuse intimal calcification. *The Journal of Pathology* 205:641-50

Bochukova EG, Roscioli T, Hedges DJ, Taylor IB, Johnson D, et al. 2009. Rare mutations of FGFR2 causing apert syndrome: identification of the first partial gene deletion, and an Alu element insertion from a new subfamily. *Human Mutation* 30:204-11

Boers JE, Ambergen AW, Thunnissen FB. 1998. Number and proliferation of basal and parabasal cells in normal human airway epithelium. *American Journal of Respiratory and Critical Care Medicine* 157:2000-6

Bollen M, Gijsbers R, Ceulemans H, Stalmans W, Stefan C. 2000. Nucleotide pyrophosphatases/phosphodiesterases on the move. *Critical Reviews in Biochemistry and Molecular Biology* 35:393-432

Bonucci E. 1967. Fine structure of early cartilage calcification. *Journal of Ultrastructure Research* 20:33-50

Bonucci E, Cuicchio M, Dearden LC. 1974. Investigations of ageing in costal and tracheal cartilage of rats. *Zeitschrift fur Zellforschung und mikroskopische Anatomie* 147:505-27

Bonucci E, Silvestrini G, Bianco P. 1992. Extracellular alkaline phosphatase activity in mineralizing matrices of cartilage and bone: ultrastructural localization using a cerium-based method. *Histochemistry* 97:323-7

Boskey A, Bullough P, Posner A. 1982. Calcium-acidic phospholipid-phosphate complexes in diseased and normal human bone. *Metabolic Bone Disease and Related Research* 4:151-6

Boskey A, Maresca M, Ullrich W, Doty S, Butler W, Prince C. 1993. Osteopontin-hydroxyapatite interactions in vitro: inhibition of hydroxyapatite formation and growth in a gelatin-gel. *Bone and Mineral* 22:147-59

Boskey A, Posner A, Lane J, Goldberg M, Cordella D. 1980. Distribution of lipids associated with mineralization in the bovine epiphyseal growth plate. *Archives of Biochemistry and Biophysics* 199:305-11

Boskey A, Spevak L, Paschalis E, Doty S, McKee M. 2002. Osteopontin deficiency increases mineral content and mineral crystallinity in mouse bone. *Calcified Tissue International* 71:145-54

Boskey AL. 1992. Mineral-matrix interactions in bone and cartilage. *Clinical Orthopaedics and Related Research* 281:244-74

Boskey AL. 1995. Osteopontin and Related Phosphorylated Sialoproteins: Effects on Mineralizationa. *Annals of the New York Academy of Sciences* 760:249-56

Bouchard S, Johnson MP, Flake AW, Howell LJ, Myers LB, et al. 2002. The EXIT procedure: experience and outcome in 31 cases. *Journal of Pediatric Surgery* 37:418-26

Boucherat O, Montaron S, Bérubé-Simard F-A, Aubin J, Philippidou P, et al. 2013. Partial functional redundancy between Hoxa5 and Hoxb5 paralog genes during lung morphogenesis. *American Journal of Physiology Lung Cell Molecular Physiology* 304:L817-L30 pp.

Boyan BD, Schwartz Z, Swain LD, Khare A. 1989. Role of lipids in calcification of cartilage. *The Anatomical Record* 224:211-9

Breeze RG, Wheeldon EB. 1977. The cells of the pulmonary airways. *The American Review of Respiratory Disease* 116:705-77

Breuer R, Zajicek G, Christensen T, Lucey E, Snider G. 1990. Cell kinetics of normal adult hamster bronchial epithelium in the steady state. *American Journal of Respiratory Cell and Molecular Biology* 2:51-8

Brocks JJ, Logan GA, Buick R, Summons RE. 1999. Archean molecular fossils and the early rise of eukaryotes. *Science* 285:1033-6

Burger E, Matthews J. 1978. Cellular calcium distribution in fetal bones studied with K-pyroantimonate. *Calcified Tissue Research* 26:181-90

Carlyle RF. 1962. A note on the isolated nerve sternotrachealis preparation of the chicken. *British Journal of Pharmacology and Chemotherapy* 18:612-6

Carr G, Moochhala SH, Eley L, Vandewalle A, Simmons NL, Sayer JA. 2009. The pyrophosphate transporter ANKH is expressed in kidney and bone cells and colocalises to the primary cilium/basal body complex. *Cellular Physiology and Biochemistry* 24:595-604

Carroll DK, Carroll JS, Leong CO, Cheng F, Brown M, et al. 2006. p63 regulates an adhesion programme and cell survival in epithelial cells. *Nature Cell Biology* 8:551-61

Castellana G, Lamorgese V. 2003. Pulmonary Alveolar Microlithiasis. *Respiration* 70:549-55

Caversaccio MD, Becker M, Zbaren P. 1998. Tracheal diverticulum presenting with recurrent laryngeal nerve paralysis. *Annals of Otology, Rhinology and Laryngology* 107:362-4

Cecil DL, Rose DM, Terkeltaub R, Liu-Bryan R. 2005. Role of interleukin-8 in PiT-1 expression and CXCR1-mediated inorganic phosphate uptake in chondrocytes. *Arthritis & Rheumatism* 52:144-54

Ceyhan M, Nural MS, Elmali M, Bayrak IK. 2008. Idiopathic isolated laryngotracheobronchial cartilage calcification in a child. *Clinical Imaging* 32:51-3

Chapman DL, Garvey N, Hancock S, Alexiou M, Agulnik SI, et al. 1996. Expression of the T-box family genes, Tbx1-Tbx5, during early mouse development. *Developmental Dynamics* 206:379-90

Chen G, Korfhagen TR, Xu Y, Kitzmiller J, Wert SE, et al. 2009. SPDEF is required for mouse pulmonary goblet cell differentiation and regulates a network of genes associated with mucus production. *Journal of Clinical Investigation* 119:2914-24

Chen JC, Holinger LD. 1994. Congenital tracheal anomalies: pathology study using serial macrosections and review of the literature. *Pediatric Pathology* 14:513-37

Chen NX, D O'Neill K, Duan D, Moe SM. 2002. Phosphorus and uremic serum up-regulate osteopontin expression in vascular smooth muscle cells. *Kidney International* 62:1724-31

Cheung HS, Sallis JD, Demadis KD, Wierzbicki A. 2006. Phosphocitrate blocks calcification-induced articular joint degeneration in a guinea pig model. *Arthritis & Rheumatism* 54:2452-61

Chiang C-H, Gabella G. 1986. Quantitative study of the ganglion neurons of the mouse trachea. *Cell Tissue Research.* 246:243-52

Chiu Y-W, Adler SG, Budoff MJ, Takasu J, Ashai J, Mehrotra R. 2010. Coronary artery calcification and mortality in diabetic patients with proteinuria. *Kidney International* 77:1107-14

Cho H-J, Cho H-J, Kim H-S. 2009. Osteopontin: a multifunctional protein at the crossroads of inflammation, atherosclerosis, and vascular calcification. *Current Atherosclerosis Reports* 11:206-13

Choo EM, Seaman JC, Musani AI. 2013. Tracheomalacia/Tracheobronchomalacia and hyperdynamic airway collapse. *Immunology and Allergy Clinics of North America* 33:23-34

Chroneou A, Zias N, Gonzalez AV, Beamis JF, Jr. 2008. Tracheobronchopathia osteochondroplastica. An underrecognized entity? *Monaldi Archives for Chest Disease* 69:65-9

Chuck AJ, Pattrick MG, Hamilton E, Wilson R, Doherty M. 1989. Crystal deposition in hypophosphatasia: a reappraisal. *Annals of the Rheumatic Diseases* 48:571-6

Ciccarese F, Poerio A, Stagni S, Attinà D, Fasano L, et al. 2014. Saber-sheath trachea as a marker of severe airflow obstruction in chronic obstructive pulmonary disease. *Radiologia Medica* 119:90-6

Cohen MM, Jr., Kreiborg S. 1992. Upper and lower airway compromise in the Apert syndrome. *American Journal of Medical Genetics* 44:90-3

Cohen MM, Jr., Kreiborg S. 1993. Visceral anomalies in the Apert syndrome. *American Journal of Medical Genetics* 45:758-60

Collins J, Bai L, Ghishan F. 2004. The SLC20 family of proteins: dual functions as sodium-phosphate cotransporters and viral receptors. *Pflugers Arch - European Journal of Physiology* 447:647-52

Colvin JS, White AC, Pratt SJ, Ornitz DM. 2001. Lung hypoplasia and neonatal death in Fgf9-null mice identify this gene as an essential regulator of lung mesenchyme. *Development* 128:2095-106

Conrads KA, Yi M, Simpson KA, Lucas DA, Camalier CE, et al. 2005. A combined proteome and microarray investigation of inorganic phosphate-induced pre-osteoblast cells. *Molecular & Cellular Proteomics* 4:1284-96

Conrads KA, Yu LR, Lucas DA, Zhou M, Chan KC, et al. 2004. Quantitative proteomic analysis of inorganic phosphate-induced murine MC3T3-E1 osteoblast cells. *Electrophoresis* 25:1342-52

Corner GW. 1929. *A well-preserved human embryo of 10 somites*: Carnegie Institution of Washington

Cotrufo M, De Feo M, De Santo LS, Romano G, Della Corte A, et al. 2002. Risk of Warfarin During Pregnancy With Mechanical Valve Prostheses. *Obstetrics & Gynecology* 99:35-40

Cox R, Hernandez-Santana A, Ramdass S, McMahon G, Harmey J, Morgan M. 2012. Microcalcifications in breast cancer: novel insights into the molecular mechanism and functional consequence of mammary mineralisation. *British Journal of Cancer* 106:525-37

Cranenburg E, VAN SPAENDONCK-ZWARTS K, Bonafe L, Mittaz Crettol L, Rödiger L, et al. 2011. Circulating matrix γ-carboxyglutamate protein (MGP) species are refractory to vitamin K treatment in a new case of Keutel syndrome. *Journal of Thrombosis and Haemostasis* 9:1225-35

Croteau JR, Cook CD. 1961. Volume-pressure and length-tension measurements in human tracheal and bronchial segments. *Journal of Applied Physiology* 16:170-2

Dalgaard JB. 1947. Tracheopathia chondro-osteoplastica. A case elucidating the problems concerning development and ossification of elastic cartilage. *Acta Pathologica Microbiologica Scandinavica* 24:118-34

Daniely Y, Liao G, Dixon D, Linnoila RI, Lori A, et al. 2004. Critical role of p63 in the development of a normal esophageal and tracheobronchial epithelium. *American Journal of Physiology Cell Physiology* 287:C171-81

de Bernard B, Bianco P, Bonucci E, Costantini M, Lunazzi GC, et al. 1986. Biochemical and immunohistochemical evidence that in cartilage an alkaline phosphatase is a Ca2+-binding glycoprotein. *The Journal of Cell Biology* 103:1615-23

de Frutos CA, Vega S, Manzanares M, Flores JM, Huertas H, et al. 2007. Snail1 is a transcriptional effector of FGFR3 signaling during chondrogenesis and achondroplasias. *Developmental Cell* 13:872-83

deftstudios. http://www.deftstudios.com/bioweb/images/bimg43sm.jpg

Demirel G, Oguz SS, Celik IH, Erdeve O, Uras N, Dilmen U. 2012. A case of Keutel syndrome diagnosed in the neonatal period: associated with Binder phenotype. *Genetic Counseling* 23:25-30

Denhardt DT, Guo X. 1993. Osteopontin: a protein with diverse functions. *The FASEB Journal* 7:1475-82

Dhingra R, Gona P, Benjamin EJ, Wang TJ, Aragam J, et al. 2010. Relations of serum phosphorus levels to echocardiographic left ventricular mass and incidence of heart failure in the community. *European Journal of Heart Failure* 12:812-8

Doherty M, Hamilton E, Henderson J, Misra H, Dixey J. 1991. Familial chondrocalcinosis due to calcium pyrophosphate dihydrate crystal deposition in English families. *Rheumatology* 30:10-5

Donnelly GM, Haack D, Heird CS. 1982. Tracheal epithelium: cell kinetics and differentiation in normal rat tissue. *Cell Proliferation* 15:119-30

Donoghue PC, Forey PL, Aldridge RJ. 2000. Conodont affinity and chordate phylogeny. *Biological Reviews* 75:191-251

Dony C, Gruss P. 1987. Specific expression of the Hox 1.3 homeo box gene in murine embryonic structures originating from or induced by the mesoderm. *Embo Journal* 6:2965-75

Drezner MK, Harrelson JM. 1979. Newer knowledge of vitamin D and its metabolites in health and disease. *Clinical Orthopaedics and Related Research* 139:206-31

Ducy P, Karsenty G. 2000. The family of bone morphogenetic proteins. *Kidney International* 57:2207-14

Duncker HR. 1972. Structure of avian lungs. *Respiration Physiology* 14:44-63

Ea H-K, Liote F. 2009. Advances in understanding calcium-containing crystal disease. *Current Opinion in Rheumatology* 21:150-7

Ea H-K, Uzan B, Rey C, Lioté F. 2005. Octacalcium phosphate crystals directly stimulate expression of inducible nitric oxide synthase through p38 and JNK mitogen-activated protein kinases in articular chondrocytes. *Arthritis Research & Therapy* 7:R915

Early EK, Bothwell MR. 2002. Congenital tracheal diverticulum. *Otolaryngology Head and Neck Surgery* 127:119-21

Econs MJ, McEnery PT. 1997. Autosomal dominant hypophosphatemic rickets/osteomalacia: clinical characterization of a novel renal phosphate-wasting disorder. *Journal of Clinical Endocrinology & Metabolism* 82:674-81

Ekser B, Ezzelarab M, Hara H, van der Windt DJ, Wijkstrom M, et al. 2012. Clinical xenotransplantation: the next medical revolution? *The Lancet* 379:672-83

El-Abbadi MM, Pai AS, Leaf EM, Yang H-Y, Bartley BA, et al. 2009. Phosphate feeding induces arterial medial calcification in uremic mice: role of serum phosphorus, fibroblast growth factor-23, and osteopontin. *Kidney International* 75:1297-307

El-Maadawy S, Kaartinen M, Schinke T, Murshed M, Karsenty G, McKee M. 2003. Cartilage formation and calcification in arteries of mice lacking matrix Gla protein. *Connective Tissue Research* 44:272-8

Ellefsen P, Tos M. 1972. Goblet cells in the human trachea: quantitative studies of a pathological biopsy material. *Archives of Otolaryngology—Head & Neck Surgery* 95:547

Elluru RG, Thompson F, Reece A. 2009. Fibroblast growth factor 18 gives growth and directional cues to airway cartilage. *The Laryngoscope* 119:1153-65

Elluru RG, Whitsett JA. 2004. Potential role of Sox9 in patterning tracheal cartilage ring formation in an embryonic mouse model. *Archives of Otolaryngology–Head & Neck Surgery* 130:732-6

Emery JL, Haddadin AJ. 1971. Squamous epithelium in respiratory tract of children with tracheo-oesophageal fistula. *Archives of disease in childhood* 46:236-42

Emoto M, Mori K, Lee E, Kawano N, Yamazaki Y, et al. 2010. Fetuin-A and atherosclerotic calcified plaque in patients with type 2 diabetes mellitus. *Metabolism* 59:873-8

Evans JA, Greenberg CR, Erdile L. 1999. Tracheal agenesis revisited: analysis of associated anomalies. *American Journal of Medical Genetics* 82:415-22

Evans M, Shami S, Cabral-Anderson L, Dekker N. 1986. Role of nonciliated cells in renewal of the bronchial epithelium of rats exposed to NO2. *The American Journal of Pathology* 123:126

Evans MJ, Moller PC. 1991. Biology of airway basal cells. *Experimental Lung Research* 17:513-31

Evans TRJ, Kaye SB. 1999. Retinoids: present role and future potential. *British journal of cancer* 80:1-8

F.Perry S. 1988. Functional morphology of the lungs of the nile crocodile, *crocodylus niloticus* : non-respiratory parameters. *Experimental Biology* 99-117

Fam AG, Morava-Protzner I, Purcell C, Young BD, Bunting PS, Lewis AJ. 1995. Acceleration of experimental lapine osteoarthritis by calcium pyrophosphate microcrystalline synovitis. *Arthritis & Rheumatism* 38:201-10

Fanous N, Husain SA, Ruzmetov M, Rodefeld MD, Turrentine MW, Brown JW. 2010. Anterior pericardial tracheoplasty for long-segment tracheal stenosis: long-term outcomes. *The Journal of Thoracic and Cardiovascular Surgery* 139:18-25

Faro RS, Goodwin CD, Organ CH, Jr., Hall RT, Holder TM, et al. 1979. Tracheal agenesis. *The Annals of Thoracic Surgery* 28:295-9

Farwell DG, Birchall MA, Macchiarini P, Luu QC, Mattos AM, et al. 2013. Laryngotracheal transplantation. *The Laryngoscope* 123:2502-8

Fayoux P, Marciniak B, Devisme L, Storme L. 2008. Prenatal and early postnatal morphogenesis and growth of human laryngotracheal structures. *Journal of Anatomy* 213:86-92

Fedde KN, Blair L, Silverstein J, Coburn SP, Ryan LM, et al. 1999. Alkaline phosphatase knock-out mice recapitulate the metabolic and skeletal defects of infantile hypophosphatasia. *Journal of Bone and Mineral Research* 14:2015-26

Felix J, Keijzer R, Van Dooren M, Rottier R, Tibboel D. 2004. Genetics and developmental biology of oesophageal atresia and tracheo-oesophageal fistula: lessons from mice relevant for paediatric surgeons. *Pediatric Surgery International* 20:731-6

Felix JF, van Looij MAJ, Pruijsten RV, de Krijger RR, de Klein A, et al. 2006. Agenesis of the trachea: Phenotypic expression of a rare cause of fatal neonatal respiratory insufficiency in six patients. *International Journal of Pediatric Otorhinolaryngology* 70:365-70

Felson D, Anderson J, Naimark A, Kannel W, Meenan R. 1989. The prevalence of chondrocalcinosis in the elderly and its association with knee osteoarthritis: the Framingham Study. *The Journal of Rheumatology* 16:1241-5

Felson DT, Naimark A, Anderson J, Kazis L, Castelli W, Meenan RF. 1987. The prevalence of knee osteoarthritis in the elderly. the framingham osteoarthritis study. *Arthritis & Rheumatism* 30:914-8

Fernandes DJ, McConville JF, Stewart AG, Kalinichenko V, Solway J. 2004. Can we differentiate between airway and vascular smooth muscle? *Clinical and Experimental Pharmacology and Physiology* 31:805-10

Feteih R, Tassinari MS, Lian JB. 1990. Effect of sodium warfarin on vitamin K-dependent proteins and skeletal development in the rat fetus. *Journal of Bone and Mineral Research* 5:885-94

Fisher A. 1962. The trachealis muscle. *Journal of Anatomy* 139-40

Fisher L, Torchia D, Fohr B, Young M, Fedarko N. 2001. Flexible structures of SIBLING proteins, bone sialoprotein, and osteopontin. *Biochemical and Biophysical Research Communications* 280:460-5

Fishman JM, De Coppi P, Elliott MJ, Atala A, Birchall MA, Macchiarini P. 2011. Airway tissue engineering. *Expert Opinion on Biological Therapy* 11:1623-35

Fishman JM, Lowdell M, Birchall MA. 2014. Stem cell-based organ replacements-airway and lung tissue engineering. *Seminars in Pediatric Surgery*

Fishman JM, Tyraskis A, Maghsoudlou P, Urbani L, Totonelli G, et al. 2013. Skeletal muscle tissue engineering: which cell to use? *Tissue Engineering Part B Reviews* 19:503-15

Fitzpatrick L, Severson A, Edwards W, Ingram R. 1994. Diffuse calcification in human coronary arteries. Association of osteopontin with atherosclerosis. *Journal of Clinical Investigation* 94:1597

Fleisch H, Russell R, Straumann F. 1966. Effect of pyrophosphate on hydroxyapatite and its implications in calcium homeostasis.

Flik KR, Verma N, Cole BJ, Bach Jr BR. 2007. Articular cartilage. In *Cartilage Repair Strategies*, pp. 1-12: Springer

Floyd J, Campbell DC, Jr., Dominy DE. 1962. Agenesis of the trachea. *American Review on Respiratory Disease* 86:557-60

Foley RN, Parfrey PS, Sarnak MJ. 1998. Clinical epidemiology of cardiovascular disease in chronic renal disease. *American Journal of Kidney Diseases* 32:S112-S9

Frappart L, Boudeulle M, Boumendil J, Lin HC, Martinon I, et al. 1984. Structure and composition of microcalcifications in benign and malignant lesions of the breast: study by light microscopy, transmission and scanning electron microscopy, microprobe analysis, and X-ray diffraction. *Human Pathology* 15:880-9

Freiman A, Tessler O, Barankin B. 2006. Apert syndrome. *International Journal of Dermatology* 45:1341-3

Fuerst M, Bertrand J, Lammers L, Dreier R, Echtermeyer F, et al. 2009a. Calcification of articular cartilage in human osteoarthritis. *Arthritis & Rheumatism* 60:2694-703

Fuerst M, Niggemeyer O, Lammers L, Schäfer F, Lohmann C, Rüther W. 2009b. Articular cartilage mineralization in osteoarthritis of the hip. *BMC Musculoskeletal Disorders* 10:166

Fujita T, Meguro T, Izumo N, Yasutomi C, Fukuyama R, et al. 2001. Phosphate stimulates differentiation and mineralization of the chondroprogenitor clone ATDC5. *Japanese Journal of Pharmacology* 85:278-81

Furie B, Furie BC. 1988. The molecular basis of blood coagulation. *Cell* 53:505-18

Gallo G, Zwaveling S, Groen H, Van der Zee D, Hulscher J. 2012. Long-gap esophageal atresia: a meta-analysis of jejunal interposition, colon interposition, and gastric pull-up. *European Journal of Pediatric Surgery* 22:420

Gatz RN, Crawford EC, Jr., Piiper J. 1974. Respiratory properties of the blood of a lungless and gill-less salamander, Desmognathus fuscus. *Respiration Physiology* 20:33-41

Gaunt SJ, Sharpe PT, Duboule D. 1988. Spatially restricted domains of homeo-gene transcripts in mouse embryos: relation to a segmented body plan. *Development* 104:169-79

Gavin BJ, McMahon JA, McMahon AP. 1990. Expression of multiple novel Wnt-1/int-1-related genes during fetal and adult mouse development. *Genes & Development* 4:2319-32

Gea J. 2008. [The evolution of the human species: a long journey for the respiratory system]. *Archivos de Bronconeumologia* 44:263-70

Geisler JD, Smevik B. 2009. Tracheal agenesis - a report of two cases. *Journal of Radiology Case Reports* 3:11-6

Gerstenfeld LC. 1999. Osteopontin in skeletal tissue homeostasis: an emerging picture of the autocrine/paracrine functions of the extracellular matrix. *Journal of Bone and Mineral Research* 14:850-5

Giachelli CM, Bae N, Almeida M, Denhardt DT, Alpers CE, Schwartz SM. 1993. Osteopontin is elevated during neointima formation in rat arteries and is a novel component of human atherosclerotic plaques. *Journal of Clinical Investigation* 92:1686

Giachelli CM, Speer MY, Li X, Rajachar RM, Yang H. 2005. Regulation of vascular calcification roles of phosphate and osteopontin. *Circulation Research* 96:717-22

Gibson G, Lin DL, Francki K, Caterson B, Foster B. 1996. Type X collagen is colocalized with a proteoglycan epitope to form distinct morphological structures in bovine growth cartilage. *Bone* 19:307-15

Gilbert SF, Opitz JM, Raff RA. 1996. Resynthesizing Evolutionary and Developmental Biology. *Developmental Biology* 173:357-72

Glaser JH, Conrad HE. 1981. Formation of matrix vesicles by cultured chick embryo chondrocytes. *Journal of Biological Chemistry* 256:12607-11

Glaser RL, Jiang W, Boyadjiev SA, Tran AK, Zachary AA, et al. 2000. Paternal origin of FGFR2 mutations in sporadic cases of Crouzon syndrome and Pfeiffer syndrome. *American Journal of Human Genetics* 66:768-77

Glimcher MJ, Krane SM. 1968. The organization and structure of bone, and the mechanism of calcification. *Treatise on Collagen* 2:67-251

Goding JW, Terkeltaub R, Maurice M, Deterre P, Sali A, Belli SI. 1998. Ecto-phosphodiesterase/pyrophosphatase of lymphocytes and non-lymphoid cells: Structure and function of the PC-1 family. *Immunological Reviews* 161:11-26

Golub EE. 2011. Biomineralization and matrix vesicles in biology and pathology. *Seminars in Immunopathology* 409-17

Gonfiotti A, Jaus MO, Barale D, Baiguera S, Comin C, et al. 2014. The first tissue-engineered airway transplantation: 5-year follow-up results. *Lancet* 383:238-44

Goo JM, Im JG, Ahn JM, Moon WK, Chung JW, et al. 1999. Right paratracheal air cysts in the thoracic inlet: clinical and radiologic significance. *American Journal of Roentgenology* 173:65-70

Goodman WG, Goldin J, Kuizon BD, Yoon C, Gales B, et al. 2000. Coronary-artery calcification in young adults with end-stage renal disease who are undergoing dialysis. *New England Journal of Medicine* 342:1478-83

Gosney J, Sissons M, Allibone R. 1988. Neuroendocrine cell populations in normal human lungs: a quantitative study. *Thorax* 43:878-82

Goss AM, Tian Y, Cheng L, Yang J, Zhou D, et al. 2011. Wnt2 signaling is necessary and sufficient to activate the airway smooth muscle program in the lung by regulating myocardin/Mrtf-B and Fgf10 expression. *Developmental Biology* 356:541-52

Gould BS. 1963. Collagen formation and fibrogenesis with special reference to the role of ascorbic acid. *International Review of Cytology* 15:301

Gradus B, Alon I, Hornstein E. 2011. miRNAs control tracheal chondrocyte differentiation. *Developmental Biology* 360:58-65

Greene R. 1978. "Saber-sheath" trachea: relation to chronic obstructive pulmonary disease. *American Journal of Roentgenology* 130:441-5

Grillo HC. 2004. *Surgery of the trachea and bronchi*: PMPH-USA

Griscom NT, Wohl ME. 1986. Dimensions of the growing trachea related to age and gender. *American Journal of Roentgenology* 146:233-7

Gross M-L, Meyer H-P, Ziebart H, Rieger P, Wenzel U, et al. 2007. Calcification of coronary intima and media: immunohistochemistry, backscatter imaging, and x-ray analysis in renal and nonrenal patients. *Clinical Journal of the American Society of Nephrology* 2:121-34

Grosser O. 1912. The development of respiratory apparatus. *Manual of Human Embryology* 473–497

Gualeni B, Facchini M, De Leonardis F, Tenni R, Cetta G, et al. 2010. Defective proteoglycan sulfation of the growth plate zones causes reduced chondrocyte proliferation via an altered Indian hedgehog signalling. *Matrix Biology* 29:453-60

Guo S, Lim D, Dong Z, Saunders TL, Ma PX, et al. 2014. Dentin Sialophosphoprotein: A Regulatory Protein for Dental Pulp Stem Cell Identity and Fate. *Stem Cells Development* 21:21

Guseh JS, Bores SA, Stanger BZ, Zhou Q, Anderson WJ, et al. 2009. Notch signaling promotes airway mucous metaplasia and inhibits alveolar development. *Development* 136:1751-9

Hajihosseini MK, Duarte R, Pegrum J, Donjacour A, Lana-Elola E, et al. 2009. Evidence that Fgf10 contributes to the skeletal and visceral defects of an Apert syndrome mouse model. *Developmental Dynamics* 238:376-85

Haka AS, Shafer-Peltier KE, Fitzmaurice M, Crowe J, Dasari RR, Feld MS. 2002. Identifying microcalcifications in benign and malignant breast lesions by probing differences in their chemical composition using Raman spectroscopy. *Cancer Research* 62:5375-80

Hale JE, Fraser JD, Price PA. 1988. The identification of matrix Gla protein in cartilage. *Journal of Biological Chemistry* 263:5820-4

Hall BK. 2005. Chapter 3 - Cartilage. In *Bones and Cartilage*, ed. BK Hall, pp. 33-47. San Diego: Academic Press

Hamburger V, Hamilton HL. 1992. A series of normal stages in the development of the chick embryo. 1951. *Developmental Dynamics* 195:231-72

Hammerschmidt M, Brook A, McMahon AP. 1997. The world according to hedgehog. *Trends in Genetics* 13:14-21

Harahap AR, Goding J. 1988. Distribution of the murine plasma cell antigen PC-1 in non-lymphoid tissues. *The Journal of Immunology* 141:2317-20

Harjeet SD, Jit I. 2004. Development of the Human Trachea. *Journal of the Anatomical Society of India* 53

Hashimoto S, Ochs RL, Rosen F, Quach J, McCabe G, et al. 1998. Chondrocyte-derived apoptotic bodies and calcification of articular cartilage. *Proceedings of the National Academy of Sciences USA* 95:3094-9

Hauschka PV, Lian JB, Cole DE, Gundberg CM. 1989. Osteocalcin and matrix Gla protein: vitamin K-dependent proteins in bone. *Physiological Reviews* 69:990-1047

Haussler MR, McCain TA. 1977. Basic and clinical concepts related to vitamin D metabolism and action, Pt. iI. *New England Journal of Medicine*

Haussler MR, Whitfield GK, Haussler CA, Hsieh JC, Thompson PD, et al. 1998. The nuclear vitamin D receptor: biological and molecular regulatory properties revealed. *Journal of Bone and Mineral Research* 13:325-49

Haynes T, Gutierrez C, Aycinena JC, Tsonis PA, Del Rio-Tsonis K. 2007. BMP signaling mediates stem/progenitor cell-induced retina regeneration. *Proceedings of the National Academy of Sciences U S A* 104:20380-5

Hedrick HL. 2003. Ex utero intrapartum therapy. *Seminars in Pediatric Surgery* 190-5

Helleday R, Huberman D, Blomberg A, Stjernberg N, Sandstrom T. 1995. Nitrogen dioxide exposure impairs the frequency of the mucociliary activity in healthy subjects. *European Respiratory Journal* 8:1664-8

Henderson JH, Welter JF, Mansour JM, Niyibizi C, Caplan AI, Dennis JE. 2007. Cartilage tissue engineering for laryngotracheal reconstruction: comparison of chondrocytes from three anatomic locations in the rabbit. *Tissue Engineering* 13:843-53

Hetz SK, Bradley TJ. 2005. Insects breathe discontinuously to avoid oxygen toxicity. *Nature* 433:516-9

Higo T, Duronio V, Tudan C, Burt HM, Jackson JK. 2010. Calcium pyrophosphate dihydrate crystal-induced inhibition of neutrophil apoptosis: involvement of Bcl-2 family members. *Inflammation Research* 59:71-81

Hines EA, Jones M-KN, Verheyden JM, Harvey JF, Sun X. 2013. Establishment of smooth muscle and cartilage juxtaposition in the developing mouse upper airways. *Proceedings of the National Academy of Sciences* 110:19444-9

Hirao M, Tamai N, Tsumaki N, Yoshikawa H, Myoui A. 2006. Oxygen tension regulates chondrocyte differentiation and function during endochondral ossification. *Journal of Biological Chemistry* 281:31079-92

Ho AM, Johnson MD, Kingsley DM. 2000. Role of the mouse ank gene in control of tissue calcification and arthritis. *Science* 289:265-70

Höbarth K, Susani M, Szabo N, Kratzik C. 1992. Incidence of testicular microlithiasis. *Urology* 40:464-7

Hockstein NG, McDonald-McGinn D, Zackai E, Bartlett S, Huff DS, Jacobs IN. 2004. Tracheal anomalies in Pfeiffer syndrome. *Archives of Otolaryngology Head and Neck Surgery* 130:1298-302

Hogg D. 1982. Ossification of the laryngeal, tracheal and syringeal cartilages in the domestic fowl. *Journal of Anatomy* 134:57

Hoggatt AM, Simon GM, Herring BP. 2002. Cell-specific regulatory modules control expression of genes in vascular and visceral smooth muscle tissues. *Circulation Research* 91:1151-9

Hollister SJ, Green GE. 2013. Porous Bidirectional Bellowed Tracheal Reconstruction Device. Google Patents

Hong S, Derfoul A, Pereira-Mouries L, Hall DJ. 2009. A novel domain in histone deacetylase 1 and 2 mediates repression of cartilage-specific genes in human chondrocytes. *Faseb Journal* 23:3539-52

Hopke P, Wang Z. 2012. Particle Deposition in the Human Respiratory Tract. In *Fine Particles in Medicine and Pharmacy*, ed. E Matijević, pp. 223-40: Springer US

Houston B, Stewart AJ, Farquharson C. 2004. PHOSPHO1—A novel phosphatase specifically expressed at sites of mineralisation in bone and cartilage. *Bone* 34:629-37

Howell DS, Carlson L. 1968. Alterations in the composition of growth cartilage septa during calcification studied by microscopic x-ray elemental analysis. *Experimental Cell Research* 51:185-95

Howell DS, Pita JC, Marquez JF, Gatter RA. 1969. Demonstration of macromolecular inhibitor (s) of calcification and nucleational factor (s) in fluid from calcifying sites in cartilage. *Journal of Clinical Investigation* 48:630

Hsia CC, Schmitz A, Lambertz M, Perry SF, Maina JN. 2013. Evolution of air breathing: oxygen homeostasis and the transitions from water to land and sky. *Comprehensive Physiology*

Huang X, Godfrey TE, Gooding WE, McCarty KS, Jr., Gollin SM. 2006. Comprehensive genome and transcriptome analysis of the 11q13 amplicon in human oral cancer and synteny to the 7F5 amplicon in murine oral carcinoma. *Genes Chromosomes Cancer* 45:1058-69

Hughes AE, McGibbon D, Woodward E, Dixey J, Doherty M. 1995. Localisation of a gene for chondrocalcinosis to chromosome 5p. *Human Molecular Genetics* 4:1225-8

Hughes GM, Morgan M. 1973. The structure of fish gills in relation to their respiratory function. *Biological Reviews* 48:419-75

Hui M, Tenenbaum HC. 1998. New face of an old enzyme: alkaline phosphatase may contribute to human tissue aging by inducing tissue hardening and calcification. *The Anatomical Record* 253:91-4

Hunter DJ, Felson DT. 2006. Osteoarthritis. *British Medical Journal* 332:639

Hunter G, Hauschka P, Poole A, Rosenberg L, Goldberg H. 1996. Nucleation and inhibition of hydroxyapatite formation by mineralized tissue proteins. *Biochemical Journal* 317:59-64

Hur DJ, Raymond GV, Kahler SG, Riegert-Johnson DL, Cohen BA, Boyadjiev SA. 2005. A novel MGP mutation in a consanguineous family: review of the clinical and molecular characteristics of Keutel syndrome. *American Journal of Medical Genetics Part A* 135:36-40

Hutson Jr LR, Young E, Guarisco L. 2007. Tracheal anomalies complicating ventilation of an infant with Apert syndrome. *Journal of Clinical Anesthesia* 19:551-4

Hynes R. 1981. Fibronectin and Its Relation to Cellular Structure and Behavior. In *Cell Biology of Extracellular Matrix*, ed. E Hay, pp. 295-334: Springer US

Iablons'ka SV, Rybal'chenko VK. 2010. [Ecto-nucleotidases of ectonucleoside triphosphate diphosphohydrolase family: structure, localization and functional significance]. *Ukr Biokhim Zh* 82:5-17

Ikinger U, Wurster K, Terwey B, Möhring K. 1982. Microcalcifications in testicular malignancy Diagnostic tool in occult tumor? *Urology* 19:525-8

Ioannides AS, Massa V, Ferraro E, Cecconi F, Spitz L, et al. 2010. Foregut separation and tracheo-oesophageal malformations: The role of tracheal outgrowth, dorso-ventral patterning and programmed cell death. *Developmental Biology* 337:351-62

Jacobs IJ, Que J. 2013. Genetic and cellular mechanisms of the formation of esophageal atresia and tracheoesophageal fistula. *Diseases of the Esophagus* 26:356-8

Jacobs JP, Quintessenza JA, Andrews T, Burke RP, Spektor Z, et al. 1999. Tracheal allograft reconstruction: the total North American and worldwide pediatric experiences. *The Annals of Thoracic Surgery* 68:1043-51

Jeannotte L, Lemieux M, Charron J, Poirier F, Robertson EJ. 1993. Specification of axial identity in the mouse: role of the Hoxa-5 (Hox1.3) gene. *Genes & Development* 7:2085-96

Jeffery P. 1983. Morphologic features of airway surface epithelial cells and glands. *The American Review of Respiratory Disease* 128:S14

Jeffery PK. 2001. Remodeling in asthma and chronic obstructive lung disease. *American Journal of Respiratory and Critical Care Medicine* 164:S28-S38

Jiang L, Zhang J, Monticone RE, Telljohann R, Wu J, et al. 2012. Calpain-1 regulation of matrix metalloproteinase 2 activity in vascular smooth muscle cells facilitates age-associated aortic wall calcification and fibrosis. *Hypertension* 60:1192-9

Jin-Hua P, Goding JW, Nakamura H, Sano K. 1997. Molecular Cloning and Chromosomal Localization of PD-Iβ (< i> PDNP3</i>), a New Member of the Human Phosphodiesterase I Genes. *Genomics* 45:412-5

Jindal Shikha NA, Neyaz Zafar , Jaiswal Sushila 2013. Tracheobronchopathia Osteochondroplastica - A rare or an overlooked entity? *PMC*

Johnson K, Goding J, Van Etten D, Sali A, Hu SI, et al. 2003. Linked Deficiencies in Extracellular PPi and Osteopontin Mediate Pathologic Calcification Associated With Defective PC-1 and ANK Expression. *Journal of Bone and Mineral Research* 18:994-1004

Johnson K, Moffa A, Chen Y, Pritzker K, Goding J, Terkeltaub R. 1999a. Matrix Vesicle Plasma Cell Membrane Glycoprotein-1 Regulates Mineralization by Murine Osteoblastic MC3T3 Cells. *Journal of Bone and Mineral Research* 14:883-92

Johnson K, Polewski M, van Etten D, Terkeltaub R. 2005. Chondrogenesis mediated by PPi depletion promotes spontaneous aortic calcification in NPP1−/− mice. *Arteriosclerosis, Thrombosis, and Vascular Biology* 25:686-91

Johnson K, Pritzker K, Goding J, Terkeltaub R. 2001. The nucleoside triphosphate pyrophosphohydrolase isozyme PC-1 directly promotes cartilage calcification through chondrocyte apoptosis and increased calcium precipitation by mineralizing vesicles. *The Journal of Rheumatology* 28:2681-91

Johnson K, Vaingankar S, Chen Y, Moffa A, Goldring MB, et al. 1999b. Differential mechanisms of inorganic pyrophosphate production by plasma cell membrane glycoprotein-1 and B10 in chondrocytes. *Arthritis & Rheumatism* 42:1986-97

Jono S, McKee MD, Murry CE, Shioi A, Nishizawa Y, et al. 2000a. Phosphate regulation of vascular smooth muscle cell calcification. *Circulation Research* 87:e10-e7

Jono S, Peinado C, Giachelli CM. 2000b. Phosphorylation of osteopontin is required for inhibition of vascular smooth muscle cell calcification. *Journal of Biological Chemistry* 275:20197-203

Joshi A, Berdon WE, Ruzal-Shapiro C, Barst RJ. 2000. CT detection of tracheobronchial calcification in an 18-year-old on maintenance warfarin sodium therapy: cause and effect? *American Journal of Roentgenology* 175:921-2

Kamel KS, Beckert LE, Stringer MD. 2009. Novel insights into the elastic and muscular components of the human trachea. *Clinical Anatomy* 22:689-97

Kanatani M, Sugimoto T, Kano J, Chihara K. 2002. IGF-I mediates the stimulatory effect of high phosphate concentration on osteoblastic cell proliferation. *Journal of Cellular Physiology* 190:306-12

Katz I, Levine M, Herman P. 1962. Tracheobronchiomegaly. The Mounier-Kuhn syndrome. *American Journal of Roentgenology, Radium Therapy and Nuclear Medicine* 88:1084-94

Kaufman MH, Bard J. 1999. *Anatomical Basis of Mouse Development*: Academic

Kazanskaya O, Glinka A, del Barco Barrantes I, Stannek P, Niehrs C, Wu W. 2004. R-Spondin2 is a secreted activator of Wnt/beta-catenin signaling and is required for Xenopus myogenesis. *Developmental Cell* 7:525-34

Keith A. 1904. Respiration in frog. *Nature*

Kempson G, Muir H, Swanson S, Freeman M. 1970. Correlations between stiffness and the chemical constituents of cartilage on the human femoral head. *Biochimica et Biophysica Acta (BBA)-General Subjects* 215:70-7

Kendall SE, Battelli C, Irwin S, Mitchell JG, Glackin CA, Verdi JM. 2005. NRAGE mediates p38 activation and neural progenitor apoptosis via the bone morphogenetic protein signaling cascade. *Molecular and Cellular Biology* 25:7711-24

Kent M, Myers N, Beasley S. 1991. Tracheo-oesophageal fistula: The 'H'fistula. In *Oesophageal Atresia*, pp. 193-207: Springer

Ketteler M, Bongartz P, Westenfeld R, Wildberger JE, Mahnken AH, et al. 2003. Association of low fetuin-A (AHSG) concentrations in serum with cardiovascular mortality in patients on dialysis: a cross-sectional study. *The Lancet* 361:827-33

Kim H. 1998. Stenting therapy for stenosing airway disease. *Respirology* 3:221-8

Kim HJ, Minashima T, McCarthy EF, Winkles JA, Kirsch T. 2010. Progressive ankylosis protein (ANK) in osteoblasts and osteoclasts controls bone formation and bone remodeling. *Journal of Bone and Mineral Research* 25:1771-83

Kim J, Kim P, Hui CC. 2001. The VACTERL association: lessons from the Sonic hedgehog pathway. *Clinical Genetics* 59:306-15

Kirsch T. 2006. Determinants of pathological mineralization. *Current Opinion in Rheumatology* 18:174-80

Kirsch T, Harrison G, Golub EE, Nah HD. 2000. The roles of annexins and types II and X collagen in matrix vesicle-mediated mineralization of growth plate cartilage. *Journal of Biological Chemistry* 275:35577-83

Kluth D, Fiegel H. 2003. The embryology of the foregut. *Seminars in Pediatric Surgery* 12:3-9

Kojima K, Bonassar LJ, Ignotz RA, Syed K, Cortiella J, Vacanti CA. 2003. Comparison of tracheal and nasal chondrocytes for tissue engineering of the trachea. *The Annals of Thoracic Surgery* 76:1884-8

Koleganova N, Piecha G, Ritz E, Schirmacher P, Müller A, et al. 2009. Arterial calcification in patients with chronic kidney disease. *Nephrology Dialysis Transplantation* 24:2488-96

Krumlauf R. 1994. Hox genes in vertebrate development. *Cell* 78:191-201

Kuehne B. 2000. Histology of the trachea and lung of Siphonops annulatus (Amphibiiia, Gymnophiona). *Revista Brasileira de Biologia*:167-72

Kump LR. 2008. The rise of atmospheric oxygen. *Nature* 451:277-8

Kvam BJ, Pollesello P, Vittur F, Paoletti S. 1992. 31P NMR studies of resting zone cartilage from growth plate. *Magnetic Resonance in Medicine* 25:355-61

Lasiewski RC. 1962. The energetics of migrating hummingbirds

Lauing KL, Cortes M, Domowicz MS, Henry JG, Baria AT, Schwartz NB. Aggrecan is required for growth plate cytoarchitecture and differentiation. *Developmental Biology*

Lawson KA, Meneses JJ, Pedersen RA. 1991. Clonal analysis of epiblast fate during germ layer formation in the mouse embryo. *Development* 113:891-911

Leborgne R. 1951. Diagnosis of tumors of the breast by simple roentgenography; calcifications in carcinomas. *The American Journal of Roentgenology and Radium therapy* 65:1

Lees S, Prostak K, Ingle V, Kjoller K. 1994. The loci of mineral in turkey leg tendon as seen by atomic force microscope and electron microscopy. *Calcified Tissue International* 55:180-9

Leroux-Berger M, Queguiner I, Maciel TT, Ho A, Relaix F, Kempf H. 2011. Pathologic calcification of adult vascular smooth muscle cells differs on their crest or mesodermal embryonic origin. *Journal of Bone and Mineral Research* 26:1543-53

Lewis PM, Dunn MP, McMahon JA, Logan M, Martin JF, et al. 2001. Cholesterol modification of sonic hedgehog is required for long-range signaling activity and effective modulation of signaling by Ptc1. *Cell* 105:599-612

Lewis SL, Tam PP. 2006a. Definitive endoderm of the mouse embryo: formation, cell fates, and morphogenetic function. *Developmental Dynamics* 235:2315-29

Lewis SL, Tam PPL. 2006b. Definitive endoderm of the mouse embryo: Formation, cell fates, and morphogenetic function. *Developmental Dynamics* 235:2315-29

Li C, Xiao J, Hormi K, Borok Z, Minoo P. 2002. Wnt5a participates in distal lung morphogenesis. *Developmental Biology* 248:68-81

Li L, Miano JM, Mercer B, Olson EN. 1996. Expression of the SM22alpha promoter in transgenic mice provides evidence for distinct transcriptional regulatory programs in vascular and visceral smooth muscle cells. *Journal of Cell Biology* 132:849-59

Li Q, Price TP, Sundberg JP, Uitto J. 2014a. Juxta-articular joint-capsule mineralization in CD73-deficient mice: Similarities to patients with NT5E mutations. *Cell Cycle* 13:0--1

Li Y, Gordon J, Manley NR, Litingtung Y, Chiang C. 2008. Bmp4 is required for tracheal formation: a novel mouse model for tracheal agenesis. *Developmental Biology* 322:145-55

Li Y, Peng A, Yang X, Xiao Z, Wu W, Wang Q. 2014b. Clinical manifestation and management of primary malignant tumors of the cervical trachea. *European Archives of Otorhinolaryngology* 271:225-35

Li Z, Wu G, Sher RB, Khavandgar Z, Hermansson M, et al. 2014c. Choline kinase beta is required for normal endochondral bone formation. *Biochimica et Biophysica Acta (BBA) - General Subjects* 1840:2112-22

Li Z, Wu G, van der Veen JN, Hermansson M, Vance DE. 2014d. Phosphatidylcholine metabolism and choline kinase in human osteoblasts. *Biochimica et Biophysica Acta (BBA) - Molecular and Cell Biology of Lipids* 1841:859-67

Liebermann-Meffert D, Huber W, Häberle B, Wurzinger LJ, Siewert JR. 1993. Relationship Between the Esophagus, Trachea, and Pleura. In *Recent Advances in Diseases of the Esophagus*, ed. K-i Nabeya, T Hanaoka, H Nogami, pp. 1045-9: Springer Japan

Liechty KW. 2010. Ex-utero intrapartum therapy. *Seminars in Fetal and Neonatal Medicine*, pp. 34-9: Elsevier

Lin S-S, Tzeng B-H, Lee K-R, Smith RJ, Campbell KP, Chen C-C. 2014. Cav3. 2 T-type calcium channel is required for the NFAT-dependent Sox9 expression in tracheal cartilage. *Proceedings of the National Academy of Sciences* 111:E1990-E8

Linde A, Goldberg M. 1993. Dentinogenesis. *Critical Reviews in Oral Biology & Medicine* 4:679-728

Linde A, Lussi A, Crenshaw MA. 1989. Mineral induction by immobilized polyanionic proteins. *Calcified Tissue International* 44:286-95

Lioté F, Ea H-K. 2007. Recent developments in crystal-induced inflammation pathogenesis and management. *Current Rheumatology Reports* 9:243-50

Litingtung Y, Lei L, Westphal H, Chiang C. 1998. Sonic hedgehog is essential to foregut development. *Nature Genetics* 20:58-61

Liu X, Engelhardt JF. 2008. The glandular stem/progenitor cell niche in airway development and repair. *Proc Am Thorac Soc* 5:682-8

Liu Y, Pathak N, Kramer-Zucker A, Drummond IA. 2007. Notch signaling controls the differentiation of transporting epithelia and multiciliated cells in the zebrafish pronephros. *Development* 134:1111-22

Lohmander S, Hjerpe A. 1975. Proteoglycans of mineralizing rib and epiphyseal cartilage. *Biochimica et Biophysica Acta (BBA) - General Subjects* 404:93-109

Lohnes D, Mark M, Mendelsohn C, Dolle P, Dierich A, et al. 1994. Function of the retinoic acid receptors (RARs) during development (I). Craniofacial and skeletal abnormalities in RAR double mutants. *Development* 120:2723-48

London GM, Guérin AP, Marchais SJ, Métivier F, Pannier B, Adda H. 2003. Arterial media calcification in end-stage renal disease: impact on all-cause and cardiovascular mortality. *Nephrology Dialysis Transplantation* 18:1731-40

Lopez-Areal L, Zumarraga R, Gil-Turner C, Martin-Granizo I, Vara-Cuadrado F, Duque-Fraile J. 1965. Microlitiasis alveolar pulmonar familiar e infantil. *Revista Clinica Espanola*

Lotz M, RoSEN F, McCabe G, Quach J, Blanco F, et al. 1995. Interleukin 1 beta suppresses transforming growth factor-induced inorganic pyrophosphate (PPi) production and expression of the PPi-generating enzyme PC-1 in human chondrocytes. *Proceedings of the National Academy of Sciences* 92:10364-8

Lowenstam H, Weiner S. On biomineralization, 1989. *Chapter* 5:74-87

Lowenstam HA, Weiner S. 1989. *On biomineralization*: Oxford University Press

Lumaka A, Mubungu G, Mukaba P, Mutantu P, Luyeye G, et al. 2014. A novel heterozygous mutation of three consecutive nucleotides causing Apert syndrome in a Congolese family. *European Journal of Medical Genetics* 57:169-73

Luo G, D'Souza R, Hogue D, Karsenty G. 1995. The matrix Gla protein gene is a marker of the chondrogenesis cell lineage during mouse development. *Journal of Bone and Mineral Research* 10:325-34

Luo G, Ducy P, McKee MD, Pinero GJ, Loyer E, et al. 1997. Spontaneous calcification of arteries and cartilage in mice lacking matrix GLA protein. *Nature*

Macchiarini P, Jungebluth P, Go T, Asnaghi MA, Rees LE, et al. 2008. Clinical transplantation of a tissue-engineered airway. *Lancet* 372:2023-30

MacKenzie CF, McAslan TC, Shin B, Schellinger D, Helrich M. 1978. The shape of the human adult trachea. *Anesthesiology* 49:48-50

Mackenzie NC, Huesa C, Rutsch F, MacRae VE. 2012. New insights into NPP1 function: lessons from clinical and animal studies. *Bone* 51:961-8

MacRae VE, Davey MG, McTeir L, Narisawa S, Yadav MC, et al. 2010. Inhibition of PHOSPHO1 activity results in impaired skeletal mineralization during limb development of the chick. *Bone* 46:1146-55

Magne D, Bluteau G, Faucheux C, Palmer G, Vignes-Colombeix C, et al. 2003. Phosphate Is a Specific Signal for ATDC5 Chondrocyte Maturation and Apoptosis-Associated Mineralization: Possible Implication of Apoptosis in the Regulation of Endochondral Ossification. *Journal of Bone and Mineral Research* 18:1430-42

Mahlapuu M, Enerback S, Carlsson P. 2001. Haploinsufficiency of the forkhead gene Foxf1, a target for sonic hedgehog signaling, causes lung and foregut malformations. *Development* 128:2397-406

Mailleux AA, Kelly R, Veltmaat JM, De Langhe SP, Zaffran S, et al. 2005. Fgf10 expression identifies parabronchial smooth muscle cell progenitors and is required for their entry into the smooth muscle cell lineage. *Development* 132:2157-66

Maina JN. 2002. Structure, function and evolution of the gas exchangers: comparative perspectives. *Journal of Anatomy* 201:281-304

Mair EA, Parsons DS. 1992. Pediatric tracheobronchomalacia and major airway collapse. *Ann Otol Rhinol Laryngol* 101:300-9

Malvè M, Pérez del Palomar A, Trabelsi O, López-Villalobos JL, Ginel A, Doblaré M. 2011. Modeling of the fluid structure interaction of a human trachea under different ventilation conditions. *International Communications in Heat and Mass Transfer* 38:10-5

Mansfield K, Rajpurohit R, Shapiro IM. 1999. Extracellular phosphate ions cause apoptosis of terminally differentiated epiphyseal chondrocytes. *Journal of Cellular Physiology* 179:276-86

Mansfield K, Teixeira C, Adams C, Shapiro I. 2001. Phosphate ions mediate chondrocyte apoptosis through a plasma membrane transporter mechanism. *Bone* 28:1-8

Mariotta S, Guidi L, Papale M, Ricci A, Bisetti A. 1997. Pulmonary alveolar microlithiasis: Review of Italian reports. *European Journal of Epidemiology* 13:587-90

Markello TC, Pak LK, St Hilaire C, Dorward H, Ziegler SG, et al. 2011. Vascular pathology of medial arterial calcifications in NT5E deficiency: implications for the role of adenosine in pseudoxanthoma elasticum. *Mol Genetics and Metabolism* 103:44-50

Matsui H, Randell SH, Peretti SW, Davis CW, Boucher RC. 1998. Coordinated clearance of periciliary liquid and mucus from airway surfaces. *Journal of Clinical Investigation* 102:1125

Mauer ER. 1964. AN atlas of vascular rings and related malformation of the aortic arch system. by james r. stewart, owings w. kingaid and jesse e. edwards, charles c thomas, springfield, illinois, 1964, 171 pages, 216 illustrations, *CHEST Journal* 46:245-

Mayne R, von der Mark K. 1983. Collagens of cartilage. *Cartilage* 1:181-214

McCance R, Fairweather D, Barrett A, Morrison A. 1956. Genetic, clinical, biochemical, and pathological features of hypophosphatasia Based on the Study of a Family. *QJM* 25:523-38

McCarthy GM, Cheung HS. 2009. Point: Hydroxyapatite crystal deposition is intimately involved in the pathogenesis and progression of human osteoarthritis. *Current Rheumatology Reports* 11:141-7

McCutcheon FH. 1964. Organ systems in adaptation: the respiratory system. *Handbook of Physiology* 4:167-91

McHugh KM. 1995. Molecular analysis of smooth muscle development in the mouse. *Developmental Dynamics* 204:278-90

McKay DG, Adams EC, Hertig AT, Danziger S. 1956. Histochemical horizons in human embryos: II. 6 and 7 millimeter embryos — Streeter horizon XIV. *The Anatomical Record* 126:433-63

McKee MD, Nanci A. 1996. Osteopontin: an interfacial extracellular matrix protein in mineralized tissues. *Connective Tissue Research* 35:197-205

Meier M, Weng LP, Alexandrakis E, Ruschoff J, Goeckenjan G. 2001. Tracheobronchial stenosis in Keutel syndrome. *European Respiratory Journal* 17:566-9

Meleti Z, Shapiro I, Adams C. 2000. Inorganic phosphate induces apoptosis of osteoblast-like cells in culture. *Bone* 27:359-66

Mendelsohn C, Lohnes D, Decimo D, Lufkin T, LeMeur M, et al. 1994. Function of the retinoic acid receptors (RARs) during development (II). Multiple abnormalities at various stages of organogenesis in RAR double mutants. *Development* 120:2749-71

Menéndez I, Mancha D, Fitch G. 2011. Fourth branchial arch defects in full-siblings treated with a partial arytenoidectomy. *Equine Veterinary Education*

Mercer RR, Russell ML, Roggli VL, Crapo JD. 1994. Cell number and distribution in human and rat airways. *American Journal of Respiratory Cell and Molecular Biology* 10:613-24

Merx MW, Schäfer C, Westenfeld R, Brandenburg V, Hidajat S, et al. 2005. Myocardial stiffness, cardiac remodeling, and diastolic dysfunction in calcification-prone fetuin-A–deficient mice. *Journal of the American Society of Nephrology* 16:3357-64

Metzger R, Wachowiak R, Kluth D. 2011. Embryology of the early foregut. *Seminars in Pediatric Surgery* 20:136-44

Metzger RJ, Klein OD, Martin GR, Krasnow MA. 2008. The branching programme of mouse lung development. *Nature* 453:745-50

Meyer JL, Nancollas GH. 1973. The influence of multidentate organic phosphonates on the crystal growth of hydroxyapatite. *Calcified Tissue Research* 13:295-303

Miano JM, Cserjesi P, Ligon KL, Periasamy M, Olson EN. 1994. Smooth muscle myosin heavy chain exclusively marks the smooth muscle lineage during mouse embryogenesis. *Circulation Research* 75:803-12

Miller LA, Wert SE, Clark JC, Xu Y, Perl AK, Whitsett JA. 2004. Role of Sonic hedgehog in patterning of tracheal-bronchial cartilage and the peripheral lung. *Developmental Dynamics* 231:57-71

Miller LA, Wert SE, Whitsett JA. 2001. Immunolocalization of sonic hedgehog (Shh) in developing mouse lung. *Journal of Histochemistry and Cytochemistry* 49:1593-604

Miller TL, Touch SM, Singhaus CJ, Ramesh Babu PB, Chidekel A, Shaffer T. 2006. Expression of matrix metalloproteinases 2, 7 and 9, and their tissue inhibitors 1 and 2, in developing rabbit tracheae. *Neonatology* 89:236-43

Minagawa M, Yasuda T, Watanabe T, Minamitani K, Takahashi Y, et al. 2002. Association between AAAG repeat polymorphism in the P3 promoter of the human parathyroid hormone (PTH)/PTH-related peptide receptor gene and adult height, urinary pyridinoline excretion, and promoter activity. *Journal of Clinical Endocrinology & Metabolism* 87:1791-6

Minoo P, Su G, Drum H, Bringas P, Kimura S. 1999. Defects in tracheoesophageal and lung morphogenesis in Nkx2.1(-/-) mouse embryos. *Developmental Biology* 209:60-71

Mitchell H, Sparrow M, Tagliaferri R. 1990. Inhibitory and excitatory responses to field stimulation in fetal and adult pig airway. *Pediatric Research* 28:69-70

Mizobuchi M, Towler D, Slatopolsky E. 2009. Vascular calcification: the killer of patients with chronic kidney disease. *Journal of the American Society of Nephrology* 20:1453-64

Moe SM, D O'Neill K, Duan D, Ahmed S, Chen NX, et al. 2002. Medial artery calcification in ESRD patients is associated with deposition of bone matrix proteins. *Kidney International* 61:638-47

Moe SM, Reslerova M, Ketteler M, O'Neill K, Duan D, et al. 2005. Role of calcification inhibitors in the pathogenesis of vascular calcification in chronic kidney disease (CKD). *Kidney International* 67:2295-304

Moessler H, Mericskay M, Li Z, Nagl S, Paulin D, Small JV. 1996. The SM 22 promoter directs tissue-specific expression in arterial but not in venous or visceral smooth muscle cells in transgenic mice. *Development* 122:2415-25

Moncada RM, Venta LA, Venta ER, Fareed J, Walenga JM, Messmore HL. 1992. Tracheal and bronchial cartilaginous rings: warfarin sodium-induced calcification. *Radiology* 184:437-9

Moore C, Moore M, Trumble S, Niemeyer M, Lentell B, et al. 2014. A comparative analysis of marine mammal tracheas. *The Journal of Experimental Biology* 217:1154-66

Moreno E, Aoba T. 1987. Calcium binding in enamel fluid and driving force for enamel mineralization in the secretory stage of amelogenesis. *Advances in Dental Research* 1:245-51

Morimoto M, Liu Z, Cheng HT, Winters N, Bader D, Kopan R. 2010. Canonical Notch signaling in the developing lung is required for determination of arterial smooth muscle cells and selection of Clara versus ciliated cell fate. *Journal of Cell Science* 123:213-24

Moss D, Eaton RH, Smith J, Whitby L. 1967. Association of inorganic-pyrophosphatase activity with human alkaline-phosphatase preparations. *Biochemical Journal* 102:53-7

Motoyama J, Liu J, Mo R, Ding Q, Post M, Hui CC. 1998. Essential function of Gli2 and Gli3 in the formation of lung, trachea and oesophagus. *Nature Genetics* 20:54-7

Mucenski ML, Wert SE, Nation JM, Loudy DE, Huelsken J, et al. 2003. β-catenin is required for specification of proximal/distal cell fate during lung morphogenesis. *Journal of Biological Chemistry* 278:40231-8

Muglia LJ, Bae DS, Brown TT, Vogt SK, Alvarez JG, et al. 1999. Proliferation and differentiation defects during lung development in corticotropin-releasing hormone-deficient mice. *American Journal of Respiratory Cell and Molecular Biology* 20:181-8

Munroe PB, Olgunturk RO, Fryns J-P, Van Maldergem L, Ziereisen F, et al. 1999. Mutations in the gene encoding the human matrix Gla protein cause Keutel syndrome. *Nature Genetics* 21:142-4

Murer H, Hernando N, Forster I, Biber J. 2000. Proximal tubular phosphate reabsorption: molecular mechanisms. *Physiological Reviews* 80:1373-409

Murphy SV, Atala A. 2014. 3D bioprinting of tissues and organs. *Nature Biotechnology* 32:773-85

Murshed M, Harmey D, Millán JL, McKee MD, Karsenty G. 2005. Unique coexpression in osteoblasts of broadly expressed genes accounts for the spatial restriction of ECM mineralization to bone. *Genes & Development* 19:1093-104

Murshed M, Schinke T, McKee MD, Karsenty G. 2004. Extracellular matrix mineralization is regulated locally; different roles of two gla-containing proteins. *Journal of Cell Biology* 165:625-30

Mychaliska GB, Bealer JF, Graf JL, Rosen MA, Adzick NS, Harrison MR. 1997. Operating on placental support: The ex utero intrapartum treatment procedure. *Journal of Pediatric Surgery* 32:227-31

Naiche LA, Harrelson Z, Kelly RG, Papaioannou VE. 2005. T-box genes in vertebrate development. *Annual Review of Genetics* 39:219-39

Nakamura S, Ishibashi-Ueda H, Niizuma S, Yoshihara F, Horio T, Kawano Y. 2009. Coronary calcification in patients with chronic kidney disease and coronary artery disease. *Clinical Journal of the American Society of Nephrology* 4:1892-900

Nam JS, Turcotte TJ, Smith PF, Choi S, Yoon JK. 2006. Mouse cristin/R-spondin family proteins are novel ligands for the Frizzled 8 and LRP6 receptors and activate beta-catenin-dependent gene expression. *Journal of Biological Chemistry* 281:13247-57

Narisawa S, Frohlander N, Millan JL. 1997a. Inactivation of two mouse alkaline phosphatase genes and establishment of a model of infantile hypophosphatasia. *Developmental Dynamics* 208:432-46

Narisawa S, Fröhlander N, Millán JL. 1997b. Inactivation of two mouse alkaline phosphatase genes and establishment of a model of infantile hypophosphatasia. *Developmental Dynamics* 208:432-46

Naviglio S, Spina A, Chiosi E, Fusco A, Illiano F, et al. 2006. Inorganic phosphate inhibits growth of human osteosarcoma U2OS cells via adenylate cyclase/cAMP pathway. *Journal of Cellular Biochemistry* 98:1584-96

Netter P, Bardin T, Bianchi A, Richette P, Loeuille D. 2004. The< i> ANKH</i> gene and familial calcium pyrophosphate dihydrate deposition disease. *Joint Bone Spine* 71:365-8

Nishimura R, Wakabayashi M, Hata K, Matsubara T, Honma S, et al. 2012. Osterix regulates calcification and degradation of chondrogenic matrices through matrix metalloproteinase 13 (MMP13) expression in association with transcription factor Runx2 during endochondral ossification. *Journal of Biological Chemistry* 287:33179-90

Nistal M, Martínez-García C, Paniagua R. 1995. The origin of testicular microliths. *International Journal of Andrology* 18:221-9

Nusse R, Fuerer C, Ching W, Harnish K, Logan C, et al. 2008. Wnt signaling and stem cell control. *Cold Spring Harbor symposia on quantitative biology*, pp. 59-66: Cold Spring Harbor Laboratory Press

O'Rahilly R, Boyden E. 1973. The timing and sequence of events in the development of the human respiratory system during the embryonic period proper. *Z. Anat. Entwickl. Gesch.* 141:237-50

O'Rahilly R, Muller F. 1984. Chevalier Jackson lecture. Respiratory and alimentary relations in staged human embryos. New embryological data and congenital anomalies. *Annals of Otology, Rhinology & Laryngology* 93:421-9

O'Neill WC, Sigrist MK, McIntyre CW. 2010. Plasma pyrophosphate and vascular calcification in chronic kidney disease. *Nephrology Dialysis Transplantation* 25:187-91

Oh J, Wunsch R, Turzer M, Bahner M, Raggi P, et al. 2002. Advanced coronary and carotid arteriopathy in young adults with childhood-onset chronic renal failure. *Circulation* 106:100-5

Okahata S, Yamamoto R, Yamakoshi Y, Fukae M. 2011. A Large Chondroitin Sulfate Proteoglycan, Versican, in Porcine Predentin. *Journal of Oral Biosciences* 53:72-81

Oldak M, Grzela T, Lazarczyk M, Malejczyk J, Skopinski P. 2001. Clinical aspects of disrupted Hedgehog signaling. *International Journal of Molecular Medecine* 8:445-52

Op den Kamp J. 1979. Lipid asymmetry in membranes. *Annual review of biochemistry* 48:47-71

Ornitology ArB. http://people.eku.edu/ritchisong/birdrespiration.html

Ozdemir N, Ersu R, Akalin F, Karadag B, Kut A, et al. 2006. Tracheobronchial calcification associated with Keutel syndrome. *Turkish Journal of Pediatrics* 48:357-61

Paaske PB, Tang E. 1985. Tracheopathia osteoplastica in the larynx. *Journal of Laryngology & Otology* 99:305-10

Pace JM, Corrado M, Missero C, Byers PH. 2003. Identification, characterization and expression analysis of a new fibrillar collagen gene, COL27A1. *Matrix Biology* 22:3-14

Packer AI, Mailutha KG, Ambrozewicz LA, Wolgemuth DJ. 2000. Regulation of the Hoxa4 and Hoxa5 genes in the embryonic mouse lung by retinoic acid and TGFβ1: Implications for lung development and patterning. *Developmental Dynamics* 217:62-74

Pai A, Leaf EM, El-Abbadi M, Giachelli CM. 2011. Elastin Degradation and Vascular Smooth Muscle Cell Phenotype Change Precede Cell Loss and Arterial Medial Calcification in a Uremic Mouse Model of Chronic Kidney Disease. *The American Journal of Pathology* 178:764-73

Palombini B, da Silva Porto N, Wallau C, Camargo J. 1981. Bronchopulmonary lavage in alveolar microlithiasis. *CHEST Journal* 80:242-3

Park J, Zhang JJ, Choi R, Trinh I, Kim PC. 2010a. A simple in vitro culture system for tracheal cartilage development. *In Vitro Cellular & Developmental Biology-Animal* 46:92-6

Park J, Zhang JJ, Moro A, Kushida M, Wegner M, Kim PC. 2010b. Regulation of Sox9 by Sonic Hedgehog (Shh) is essential for patterning and formation of tracheal cartilage. *Dev Dyn* 239:514-26

Park KS, Korfhagen TR, Bruno MD, Kitzmiller JA, Wan H, et al. 2007. SPDEF regulates goblet cell hyperplasia in the airway epithelium. *J Clin Invest* 117:978-88

Parmar H, Blaser S, Unger S, Yoo S-J, Papsin B. 2006. Petrified ears in a patient with Keutel syndrome: temporal bone CT findings. *Pediatric Radiology* 36:241-3

Parr BA, McMahon AP. 1995. Dorsalizing signal Wnt-7a required for normal polarity of D–V and A–P axes of mouse limb. *Nature* 374:350-3

Payne W. 1900. Congenital absence of the trachea. *Brooklyn Medical Journal* 14:568

Peacock C, Given-Wilson R, Duffy S. 2004. Mammographic casting-type calcification associated with small screen-detected invasive breast cancers: is this a reliable prognostic indicator? *Clinical rRadiology* 59:165-70

Pedersen KO. 1944. Fetuin, a new globulin isolated from serum. *Nature* 154:575

Pendleton A, Johnson MD, Hughes A, Gurley KA, Ho AM, et al. 2002. Mutations in< i> ANKH</i> Cause Chondrocalcinosis. *The American Journal of Human Genetics* 71:933-40

Pepicelli CV, Lewis PM, McMahon AP. 1998. Sonic hedgehog regulates branching morphogenesis in the mammalian lung. *Current Biology* 8:1083-6

Perelman M, Koroleva N. 1980. Surgery of the trachea. *World Journal of Surgery* 4:583-91

Perl AK, Wert SE, Nagy A, Lobe CG, Whitsett JA. 2002. Early restriction of peripheral and proximal cell lineages during formation of the lung. *Proceedings of the National Academy of Sciences U S A* 99:10482-7

Poole AR, Pidoux I, Rosenberg L. 1982. Role of proteoglycans in endochondral ossification: immunofluorescent localization of link protein and proteoglycan monomer in bovine fetal epiphyseal growth plate. *The Journal of Cell Biology* 92:249-60

Price P, Williamson M, Otawara Y, Butler W. 1985. The Chemistry and Biology of Mineralized Tissue. *Birmingham, AL: EBSCO Media*

Price PA, Urist MR, Otawara Y. 1983. Matrix Gla protein, a new γ-carboxyglutamic acid-containing protein which is associated with the organic matrix of bone. *Biochemical and Biophysical Research Communications* 117:765-71

Price PA, Williamson MK. 1985. Primary structure of bovine matrix Gla protein, a new vitamin K-dependent bone protein. *Journal of Biological Chemistry* 260:14971-5

Price PA, Williamson MK, Haba T, Dell RB, Jee W. 1982. Excessive mineralization with growth plate closure in rats on chronic warfarin treatment. *Proceedings of the National Academy of Sciences* 79:7734-8

Prince CW, Rahemtulla F, Butler WT. 1983. Metabolism of rat bone proteoglycans in vivo. *Biochemical Journal* 216:589-96

Pritzker KP. 2009. Counterpoint: Hydroxyapatite crystal deposition is not intimately involved in the pathogenesis and progression of human osteoarthritis. *Current Rheumatology Reports* 11:148-53

Que J, Choi M, Ziel JW, Klingensmith J, Hogan BL. 2006. Morphogenesis of the trachea and esophagus: current players and new roles for noggin and Bmps. *Differentiation* 74:422-37

Que J, Luo X, Schwartz RJ, Hogan BL. 2009. Multiple roles for Sox2 in the developing and adult mouse trachea. *Development* 136:1899-907

Que J, Okubo T, Goldenring JR, Nam KT, Kurotani R, et al. 2007. Multiple dose-dependent roles for Sox2 in the patterning and differentiation of anterior foregut endoderm. *Development* 134:2521-31

Rabinovitch A, Anderson HC. 1976. Biogenesis of matrix vesicles in cartilage growth plates. *Federation proceedings*, pp. 112-6

Rachow JW, Ryan L. 1988. Inorganic pyrophosphate metabolism in arthritis. *Rheumatic Diseases Clinics of North America* 14:289-302

Radtke F, Raj K. 2003. The role of Notch in tumorigenesis: oncogene or tumour suppressor? *Nature Reviews Cancer* 3:756-67

Raggi P, Boulay A, Chasan-Taber S, Amin N, Dillon M, et al. 2002. Cardiac calcification in adult hemodialysis patientsA link between end-stage renal disease and cardiovascular disease? *Journal of the American College of Cardiology* 39:695-701

Raggio C, Boyan B, Boskey AL. 1986. In vivo hydroxyapatite formation induced by lipids. *Journal of Bone and Mineral Research* 1:409-15

Rajamannan NM, Subramaniam M, Rickard D, Stock SR, Donovan J, et al. 2003. Human aortic valve calcification is associated with an osteoblast phenotype. *Circulation* 107:2181-4

Ramalho-Santos M, Melton DA, McMahon AP. 2000. Hedgehog signals regulate multiple aspects of gastrointestinal development. *Development* 127:2763-72

Rashid HH, Cos LR, Weinberg E, Messing EM. 2004. Testicular microlithiasis: A review and its association with testicular cancer. *Urologic Oncology: Seminars and Original Investigations* 22:285-9

Ratjen F. 2009. Update in cystic fibrosis 2008. *American Journal of Respiratory and Critical Care Medicine* 179:445-8

Rawadi G, Vayssière B, Dunn F, Baron R, Roman-Roman S. 2003. BMP-2 controls alkaline phosphatase expression and osteoblast mineralization by a Wnt autocrine loop. *Journal of Bone and Mineral Research* 18:1842-53

Reese AM. 1926. The occlusion of the oesophagus and trachea in crocodilia and snakes. *American Journal of Anatomy* 37:195-212

Regamey N, Ochs M, Hilliard TN, Mühlfeld C, Cornish N, et al. 2008. Increased airway smooth muscle mass in children with asthma, cystic fibrosis, and non-cystic fibrosis bronchiectasis. *American Journal of Respiratory and Critical Care Medicine* 177:837-43

Régnier CH, Masson R, Kedinger V, Textoris J, Stoll I, et al. 2002. Impaired neural tube closure, axial skeleton malformations, and tracheal ring disruption in TRAF4-deficient mice. *Proceedings of the National Academy of Sciences* 99:5585-90

Reynolds CC, Martinez SA, Furr A, Cunningham M, Bumpous JM, et al. 2006. Risk acceptance in laryngeal transplantation. *The Laryngoscope* 116:1770-5

Riazulhaq M, Elhassan E. 2012. Early recognition of h-type tracheoesophageal fistula. *APSP journal of case reports* 3:4

Riordan JF. 1979. Arginyl residues and anion binding sites in proteins. *Molecular and cellular Biochemistry* 26:71-92

Rittling SR, Matsumoto HN, Mckee MD, Nanci A, An XR, et al. 1998. Mice lacking osteopontin show normal development and bone structure but display altered osteoclast formation in vitro. *Journal of Bone and Mineral Research* 13:1101-11

Roberts CR, Rains JK, Paré PD, Walker DC, Wiggs B, Bert JL. 1997. Ultrastructure and tensile properties of human tracheal cartilage. *Journal of Biomechanics* 31:81-6

Roberts S, Narisawa S, Harmey D, Millán JL, Farquharson C. 2007. Functional involvement of PHOSPHO1 in matrix vesicle–mediated skeletal mineralization. *Journal of Bone and Mineral Research* 22:617-27

Roberts S, Stewart A, Sadler P, Farquharson C. 2004. Human PHOSPHO1 exhibits high specific phosphoethanolamine and phosphocholine phosphatase activities. *Biochemical Journal* 382:59-65

Rock JR, Futtner CR, Harfe BD. 2008. The transmembrane protein TMEM16A is required for normal development of the murine trachea. *Developmental Biology* 321:141-9

Rock JR, Randell SH, Hogan BL. 2010. Airway basal stem cells: a perspective on their roles in epithelial homeostasis and remodeling. *Disease Models & Mechanisms* 3:545-56

Rosenthal AH. 1931. Congenital atresia of the esophagus with tracheo-esophageal fistula. Report of eight cases. *Archives of Pathology* 12:756-72

Roughley P, Dickson I. 1980. Factors influencing proteoglycan size in rachitic-chick growth cartilage. *Biochemical Journal* 185:33-9

Roy S. 2009. The motile cilium in development and disease: emerging new insights. *Bioessays* 31:694-9

Rubin B. 2014. Secretion properties, clearance, and therapy in airway disease. *Transl Respir Med* 2:1-7

Russell R. 1976. Metabolism of inorganic pyrophosphate (PPi). *Arthritis & Rheumatism* 19:465-78

Russell RG, Bisaz S, Donath A, Morgan DB, Fleisch H. 1971. Inorganic pyrophosphate in plasma in normal persons and in patients with hypophosphatasia, osteogenesis imperfecta, and other disorders of bone. *Journal of Clinical Investigation* 50:961-9

Rutsch F, Ruf N, Vaingankar S, Toliat MR, Suk A, et al. 2003. Mutations in ENPP1 are associated with'idiopathic'infantile arterial calcification. *Nature Genetics* 34:379-81

Ryu K, Iriuchishima T, Oshida M, Kato Y, Saito A, et al. 2014. The prevalence of and factors related to calcium pyrophosphate dihydrate crystal deposition in the knee joint. *Osteoarthritis Cartilage* 22:975-9

Sagehashi N. 1992. An infant with Crouzon's syndrome with a cartilaginous trachea and a human tail. *Journal of Craniomaxillofacial Surgery* 20:21-3

Sala FG, Del Moral PM, Tiozzo C, Alam DA, Warburton D, et al. 2011. FGF10 controls the patterning of the tracheal cartilage rings via Shh. *Development* 138:273-82

Sasano Y, Mizoguchi I, Furusawa M, Aiba N, Ohtani E, et al. 1993. The process of calcification during development of the rat tracheal cartilage characterized by distribution of alkaline phosphatase activity and immunolocalization of types I and II collagens and glycosaminoglycans of proteoglycans. *Anatomy and Embryology* 188:31-9

Sasano Y, Takahashi I, Mizoguchi I, Kagayama M, Takita H, Kuboki Y. 1998. Type X collagen is not localized in hypertrophic or calcified cartilage in the developing rat trachea. *Anatomy and Embryology* 197:399-403

Schaefer L, Schaefer R. 2010. Proteoglycans: from structural compounds to signaling molecules. *Cell and Tissue Research* 339:237-46

Schäfer C, Heiss A, Schwarz A, Westenfeld R, Ketteler M, et al. 2003a. The serum protein α2–Heremans-Schmid glycoprotein/fetuin-A is a systemically acting inhibitor of ectopic calcification. *Journal of Clinical Investigation* 112:357-66

Schäfer C, Heiss A, Schwarz A, Westenfeld R, Ketteler M, et al. 2003b. The serum protein α 2–Heremans-Schmid glycoprotein/fetuin-A is a systemically acting inhibitor of ectopic calcification. *The Journal of Clinical Investigation* 112:357-66

Schipani E, Kruse K, Juppner H. 1995. A constitutively active mutant PTH-PTHrP receptor in Jansen-type metaphyseal chondrodysplasia. *Science* 268:98-100

Schittny JC, Miserocchi G, Sparrow MP. 2000. Spontaneous peristaltic airway contractions propel lung liquid through the bronchial tree of intact and fetal lung explants. *American Journal of Respiratory Cell and Molecular Biology* 23:11-8

Schurgers L, Spronk H, Skepper J, Hackeng T, Shanahan C, et al. 2007. Post-translational modifications regulate matrix Gla protein function: importance for inhibition of vascular smooth muscle cell calcification. *Journal of Thrombosis and Haemostasis* 5:2503-11

Schurgers LJ, Barreto DV, Barreto FC, Liabeuf S, Renard C, et al. 2010. The circulating inactive form of matrix gla protein is a surrogate marker for vascular calcification in chronic kidney disease: a preliminary report. *Clinical Journal of the American Society of Nephrology* 5:568-75

Schurgers LJ, Joosen IA, Laufer EM, Chatrou ML, Herfs M, et al. 2012. Vitamin k-antagonists accelerate atherosclerotic calcification and induce a vulnerable plaque phenotype. *PloS One* 7:e43229

Schwarzbauer JE. 1991. Identification of the fibronectin sequences required for assembly of a fibrillar matrix. *Journal of Cell Biology* 113:1463-73

Scott E, Goddard C, Wiseman J, Evans M, Colledge W. 2000. A murine tracheal culture system to investigate parameters affecting gene therapy for cystic fibrosis. *Gene therapy* 7

Seery JP, Watt FM. 2000. Asymmetric stem-cell divisions define the architecture of human oesophageal epithelium. *Current Biology* 10:1447-50

Seki K, Fujimori T, Savagner P, Hata A, Aikawa T, et al. 2003. Mouse Snail family transcription repressors regulate chondrocyte, extracellular matrix, type II collagen, and aggrecan. *Journal of Biological Chemistry* 278:41862-70

Sekine K, Ohuchi H, Fujiwara M, Yamasaki M, Yoshizawa T, et al. 1999. Fgf10 is essential for limb and lung formation. *Nature Genetics* 21:138-41

Serafini SM, Michaelson ED. 1977. Length and distribution of cilia in human and canine airways. *Bulletin Européen de Physiopathologie Respiratoire* 13:551-9

Shadmehr MB, Farzanegan R, Graili P, Javaherzadeh M, Arab M, et al. 2011. Primary major airway tumors; management and results. *European Journal of Cardio-Thoracic Surgery* 39:749-54

Shanahan CM, Cary NR, Salisbury JR, Proudfoot D, Weissberg PL, Edmonds ME. 1999. Medial Localization of Mineralization-Regulating Proteins in Association With Mönckeberg's Sclerosis Evidence for Smooth Muscle Cell–Mediated Vascular Calcification. *Circulation* 100:2168-76

Shannon JM. 1994. Induction of alveolar type II cell differentiation in fetal tracheal epithelium by grafted distal lung mesenchyme. *Developmental Biology* 166:600-14

Shannon JM, Nielsen LD, Gebb SA, Randell SH. 1998. Mesenchyme specifies epithelial differentiation in reciprocal recombinants of embryonic lung and trachea. *Developmental Dynamics* 212:482-94

Shao Y, Alicknavitch M, Farach-Carson MC. 2005. Expression of voltage sensitive calcium channel (VSCC) L-type Cav1. 2 (α1C) and T-type Cav3. 2 (α1H) subunits during mouse bone development. *Developmental Dynamics* 234:54-62

Shapiro IM, Greenspan JS. 1969. Are mitochondria directly involved in biological mineralisation? *Calcified Tissue International* 3:100-2

Shebani E, Shahana S, Janson C, Roomans GM. 2005. Attachment of columnar airway epithelial cells in asthma. *Tissue and Cell* 37:145-52

Shiels H, Li X, Schumacker PT, Maltepe E, Padrid PA, et al. 2000. TRAF4 deficiency leads to tracheal malformation with resulting alterations in air flow to the lungs. *American Journal of Pathol*ogy157:679-88

Shimada T, Hasegawa H, Yamazaki Y, Muto T, Hino R, et al. 2004a. FGF-23 is a potent regulator of vitamin D metabolism and phosphate homeostasis. *Journal of Bone and Mineral Research* 19:429-35

Shimada T, Kakitani M, Yamazaki Y, Hasegawa H, Takeuchi Y, et al. 2004b. Targeted ablation of Fgf23 demonstrates an essential physiological role of FGF23 in phosphate and vitamin D metabolism. *The Journal of Clinical Investigation* 113:561-8

Shu W, Jiang YQ, Lu MM, Morrisey EE. 2002. Wnt7b regulates mesenchymal proliferation and vascular development in the lung. *Development* 129:4831-42

Simon M, Vremaroiu P, Andrei F. 2014. Mounier-kuhn syndrome. *Journal of Bronchology & Interventional Pulmonology* 21:145-9

Smith EI. 1957. *The early development of the trachea and esophagus in relation to atresia of the esophagus and tracheoesophageal fistula*: Carnegie Inst.

Snouwaert JN, Brigman KK, Latour AM, Malouf NN, Boucher RC, et al. 1992. An animal model for cystic fibrosis made by gene targeting. *Science* 257:1083-8

Sodek K, Tupy J, Sodek J, Grynpas M. 2000. Relationships between bone protein and mineral in developing porcine long bone and calvaria. *Bone* 26:189-98

Solmyo ASA. 1994. Signal transduction and regulation in smooth muscle. *Nature*:231-6

Sondo E, Caci E, Galietta LJ. 2014. The TMEM16A chloride channel as an alternative therapeutic target in cystic fibrosis. *The International Journal of Biochemistry & Cell Biology* 52:73-6

Sparrow MP, Lamb JP. 2003. Ontogeny of airway smooth muscle: structure, innervation, myogenesis and function in the fetal lung. *Respiratory Physiology & Neurobiology* 137:361-72

Sparrow MP, Weichselbaum M, McCray PB. 1999. Development of the innervation and airway smooth muscle in human fetal lung. *American Journal of Respiratory Cell and Molecular Biology* 20:550-60

Speer MY, Yang H-Y, Brabb T, Leaf E, Look A, et al. 2009. Smooth muscle cells give rise to osteochondrogenic precursors and chondrocytes in calcifying arteries. *Circulation Research* 104:733-41

Springer J, Groneberg DA, Pregla R, Fischer A. 2005. Inflammatory cells as source of tachykinin-induced mucus secretion in chronic bronchitis. *Regulatory Peptides* 124:195-201

Srivastava A, Guitron J, Williams VA. 2014. Tracheal diverticulum: An atypical presentation. *The Journal of Thoracic and Cardiovascular Surgery*

St. Hilaire C, Ziegler SG, Markello TC, Brusco A, Groden C, et al. 2011. NT5E mutations and arterial calcifications. *New England Journal of Medicine* 364:432-42

Standardnote. http://standardnote.blogspot.fr/2012/12/respiratory-system-of-frog.html

Stary H. 2000. Natural history of calcium deposits in atherosclerosis progression and regression. *Zeitschrift für Kardiologie* 89:S028-S35

Stefan C, Jansen S, Bollen M. 2006. Modulation of purinergic signaling by NPP-type ectophosphodiesterases. *Purinergic Signal* 2:361-70

Stein S, Fritsch R, Lemaire L, Kessel M. 1996. Checklist: Vertebrate homeobox genes. *Mechanisms of Development* 55:91-108

Stewart AJ, Roberts SJ, Seawright E, Davey MG, Fleming RH, Farquharson C. 2006. The presence of PHOSPHO1 in matrix vesicles and its developmental expression prior to skeletal mineralization. *Bone* 39:1000-7

Stewart JR, Kincaid OW, Titus JL. 1966. Right aortic arch: plain film diagnosis and significance. *Am J Roentgenol Radium Ther Nucl Med* 97:377-89

Stone P, Trevenen CL, Mitchell I, Rudd N. 1990. Congenital tracheal stenosis in Pfeiffer syndrome. *Clinical Genetics* 38:145-8

Stracke ML, Clair T, Liotta LA. 1997. Autotaxin, tumor motility-stimulating exophosphodiesterase. *Advances in Enzyme Regulation* 37:135-44

Streeter GL. 1945. *Developmental horizons in human embryos: Description of age group XIII, embryos about 4 or 5 millimeters long, and age group XIV, period of indentation of the lens vesicle*: Carnegie Institution of Washington

Streiter A. 1951. *Ein menschlicher Keimling mit 7 Urwirbelpaaren (Keimling Ludwig)*: Arbeitsgemeinschaft med. Verlag

Strife JL, Matsumoto J, Bisset GS, III, Martin R. 1989. The position of the trachea in infants and children with right aortic arch. *Pediatric Radiology* 19:226-9

StudyBlue. http://www.studyblue.com/notes/note/n/bio-106-study-guide-2013-14-cousinslee/deck/10683368

Sweatt A, Sane D, Hutson S, Wallin R. 2003. Matrix Gla protein (MGP) and bone morphogenetic protein-2 in aortic calcified lesions of aging rats. *Journal of Thrombosis and Haemostasis* 1:178-85

Szpinda M, Daroszewski M, Szpinda A, WoŸniak A, Wiśniewski M, et al. 2012a. New quantitative patterns of the growing trachea in human fetuses. *Medical science monitor: international medical journal of experimental and clinical research* 18:PH63

Szpinda M, Daroszewski M, Szpinda A, Woźniak A, Mila-Kierzenkowska C, et al. 2012b. The normal growth of the tracheal wall in human foetuses. *Archives of Medical Science*

Szpinda M, Daroszewski M, Woźniak A, Szpinda A, Mila-Kierzenkowska C. 2012c. Tracheal dimensions in human fetuses: an anatomical, digital and statistical study. *Surgical and Radiologic Anatomy* 34:317-23

Szweras M, Liu D, Partridge EA, Pawling J, Sukhu B, et al. 2002. α2-HS glycoprotein/fetuin, a transforming growth factor-β/bone morphogenetic protein antagonist, regulates postnatal bone growth and remodeling. *Journal of Biological Chemistry* 277:19991-7

Tabar L, Tony Chen HH, Amy Yen M, Tot T, Tung TH, et al. 2004. Mammographic tumor features can predict long-term outcomes reliably in women with 1–14-mm invasive breast carcinoma. *Cancer* 101:1745-59

Tajima K, Yamakawa M, Katagiri T, Sasaki H. 1997. Immunohistochemical detection of bone morphogenetic protein-2 and transforming growth factor beta-1 in tracheopathia osteochondroplastica. *Virchows Arch* 431:359-63

Takechi M, Itakura C. 1995. Ultrastructural studies of the epiphyseal plate of chicks fed a vitamin D-deficient and low-calcium diet. *Journal of Comparative Pathology* 113:101-11

Tam PP, Beddington RS. 1992. Establishment and organization of germ layers in the gastrulating mouse embryo. *Ciba Found Symp* 165:27-41

Tanaka T, Sato H, Doi H, Yoshida CA, Shimizu T, et al. 2008. Runx2 represses myocardin-mediated differentiation and facilitates osteogenic conversion of vascular smooth muscle cells. *Molecular and Cellular Biology* 28:1147-60

Tanaka Y, DeLuca H. 1973. The control of 25-hydroxyvitamin D metabolism by inorganic phosphorus. *Archives of Biochemistry and Biophysics* 154:566-74

Tarran R, Grubb BR, Gatzy JT, Davis CW, Boucher RC. 2001. The relative roles of passive surface forces and active ion transport in the modulation of airway surface liquid volume and composition. *Journal of General Physiology* 118:223-36

Tchetina EV, Squires G, Poole AR. 2005. Increased type II collagen degradation and very early focal cartilage degeneration is associated with upregulation of chondrocyte differentiation related genes in early human articular cartilage lesions. *The Journal of Rheumatology* 32:876-86

Teixeira CC, Mansfield K, Hertkorn C, Ischiropoulos H, Shapiro IM. 2001. Phosphate-induced chondrocyte apoptosis is linked to nitric oxide generation. *American Journal of Physiology-Cell Physiology* 281:C833-C9

Teng Z, Ochoa I, Li Z, Doblare M. 2009. Study of tracheal collapsibility, compliance and stress by considering its asymmetric geometry. *Medical Engineering & Physics* 31:328-36

Teng Z, Ochoa I, Li Z, Lin Y, Rodriguez JF, et al. 2008. Nonlinear mechanical property of tracheal cartilage: A theoretical and experimental study. *Journal of Biomechanics* 41:1995-2002

Terkeltaub R. 2006. Physiologic and pathologic functions of the NPP nucleotide pyrophosphatase/phosphodiesterase family focusing on NPP1 in calcification. *Purinergic Signal* 2:371-7

Terkeltaub RA. 2001. Inorganic pyrophosphate generation and disposition in pathophysiology. *American Journal of Physiology-Cell Physiology* 281:C1-C11

Thomas D, Vlachopapadopoulou E, Papadakis V, Sklavou R, Stefanaki K, et al. 2008. Testicular microlithiasis in siblings: clinical implications. *Pediatric Radiology* 38:688-90

Thompson E, Baylink D, Wergedal J. 1975. Increases in Number and Size of Osteoclasts in Response to Calcium or Phosphorus Deficiency in the Rat 1. *Endocrinology* 97:283-9

Thorek P. 1985. Trachea and Extrapulmonary Bronchi. In *Anatomy in Surgery*, pp. 314-7: Springer New York

Tiozzo C, De Langhe S, Carraro G, Al Alam D, Nagy A, et al. 2009. Fibroblast growth factor 10 plays a causative role in the tracheal cartilage defects in a mouse model of Apert syndrome. *Pediatric Research* 66:386-90

Tollet J, Everett AW, Sparrow MP. 2001. Spatial and temporal distribution of nerves, ganglia, and smooth muscle during the early pseudoglandular stage of fetal mouse lung development. *Developmental Dynamics* 221:48-60

Tos M. 1966. Development of the tracheal glands in man; number, density, structure, shape, and distribution of mucous glands elucidated by quantitative studies of whole mounts.

Toskala E, Smiley-Jewell SM, Wong VJ, King D, Plopper CG. 2005. Temporal and spatial distribution of ciliogenesis in the tracheobronchial airways of mice. *Am J Physiol Lung Cell Mol Physiol* 289:6

Towler DA, Bidder M, Latifi T, Coleman T, Semenkovich CF. 1998. Diet-induced diabetes activates an osteogenic gene regulatory program in the aortas of low density lipoprotein receptor-deficient mice. *Journal of Biological Chemistry* 273:30427-34

Trabelsi O, del Palomar AP, López-villalobos JL, Ginel A, Doblaré M. 2010. Experimental characterization and constitutive modeling of the mechanical behavior of the human trachea. *Medical Engineering & Physics* 32:76-82

Tremblay KD, Zaret KS. 2005. Distinct populations of endoderm cells converge to generate the embryonic liver bud and ventral foregut tissues. *Developmental Biology* 280:87-99

Truchot JP. Gas Transfer in Vertebrates. *eLS*

Tsao PN, Vasconcelos M, Izvolsky KI, Qian J, Lu J, Cardoso WV. 2009. Notch signaling controls the balance of ciliated and secretory cell fates in developing airways. *Development* 136:2297-307

Tsao TC, Shieh WB. 1994. Intrathoracic tracheal dimensions and shape changes in chronic obstructive pulmonary disease. *Journal of the Formosan Medical Association* 93:30-4

Tseng H-T, Shah R, Jamrich M. 2004. Function and regulation of FoxF1 during Xenopus gut development. *Development* 131:3637-47

Tudan C, Jackson JK, Blanis L, Pelech SL, Burt HM. 2000. Inhibition of TNF-α-induced neutrophil apoptosis by crystals of calcium pyrophosphate dihydrate is mediated by the extracellular signal-regulated kinase and phosphatidylinositol 3-kinase/Akt pathways up-stream of caspase 3. *The Journal of Immunology* 165:5798-806

Turcatel G, Rubin N, Menke DB, Martin G, Shi W, Warburton D. 2013. Lung mesenchymal expression of Sox9 plays a critical role in tracheal development. *BMC Biology* 11:1741-7007

Tyson KL, Reynolds JL, McNair R, Zhang Q, Weissberg PL, Shanahan CM. 2003. Osteo/chondrocytic transcription factors and their target genes exhibit distinct patterns of expression in human arterial calcification. *Arteriosclerosis, Thrombosis, and Vascular Biology* 23:489-94

Umezu H, Tamura M, Kobayashi S, Sawabata N, Honma K, Miyoshi S. 2008. Tracheal chondrosarcoma. *General Thoracic and Cardiovascular Surgery* 56:199-202

Unbekandt M, del Moral PM, Sala FG, Bellusci S, Warburton D, Fleury V. 2008. Tracheal occlusion increases the rate of epithelial branching of embryonic mouse lung via the FGF10-FGFR2b-Sprouty2 pathway. *Mechanisms and Development* 125:314-24

Urist M, Huo Y, Brownell A, Hohl W, Buyske J, et al. 1984. Purification of bovine bone morphogenetic protein by hydroxyapatite chromatography. *Proceedings of the National Academy of Sciences* 81:371-5

van der Hoeven F, Zákány J, Duboule D. 1996. Gene Transpositions in the HoxD Complex Reveal a Hierarchy of Regulatory Controls. *Cell* 85:1025-35

van der Rest M, Garrone R. 1991. Collagen family of proteins. *The FASEB Journal* 5:2814-23

van Ravenswaaij-Arts CM, van den Ouweland AM, Hoogeboom AJ, Herbergs J, Pals G. 2002. [From gene to disease; craniosynostosis syndromes due to FGFR2-mutation]. *Ned Tijdschr Geneeskd* 146:63-6

Vanpeperstraete F. 1973. The Tracheal Bifurcation. In *The Cartilaginous Skeleton of the Bronchial Tree*, pp. 22-8: Springer Berlin Heidelberg

Vegni-Talluri M, Bigliardi E, Vanni M, Tota G. 1980. Testicular microliths: their origin and structure. *The Journal of Urology* 124:105-7

Veis A. 2003. Mineralization in organic matrix frameworks. *Reviews in Mineralogy and Geochemistry* 54:249-89

Veis A, Perry A. 1967. The Phosphoprotein of the Dentin Matrix*. *Biochemistry* 6:2409-16

Verkman AS, Song Y, Thiagarajah JR. 2003. Role of airway surface liquid and submucosal glands in cystic fibrosis lung disease. *American Journal of Physiology Cell Physiology* 284:C2-15

Viegas CS, Simes DC, Laizé V, Williamson MK, Price PA, Cancela ML. 2008. Gla-rich protein (GRP), a new vitamin K-dependent protein identified from sturgeon cartilage and highly conserved in vertebrates. *Journal of Biological Chemistry* 283:36655-64

Villarreal-Ramirez E, Garduno-Juarez R, Gericke A, Boskey A. 2014. The role of phosphorylation in dentin phosphoprotein peptide absorption to hydroxyapatite surfaces: a molecular dynamics study. *Connective Tissue Research* 1:134-7

Villavicencio EH, Walterhouse DO, Iannaccone PM. 2000. The sonic hedgehog-patched-gli pathway in human development and disease. *American Journal of Human Genetics* 67:1047-54

Voynow JA, Rubin BK. 2009. Mucins, mucus, and sputum. *Chest* 135:505-12

Waddington RJ, Hall RC, Embery G, Lloyd DM. 2003. Changing profiles of proteoglycans in the transition of predentine to dentine. *Matrix Biology* 22:153-61

Wailoo M, Emery JL. 1980. Structure of the membranous trachea in children. *Acta Anat* 106:254-61

Wailoo MP, Emery JL. 1979. The trachea in children with tracheo-oesophageal fistula. *Histopathology* 3:329-38

Wajant H, Grell M, Scheurich P. 1999. TNF receptor associated factors in cytokine signaling. *Cytokine & Growth Factor Reviews* 10:15-26

Wajih N, Borras T, Xue W, Hutson SM, Wallin R. 2004. Processing and Transport of Matrix γ-Carboxyglutamic Acid Protein and Bone Morphogenetic Protein-2 in Cultured Human Vascular Smooth Muscle Cells Evidence For An Uptake Mechanism For Serum Fetuin. *Journal of Biological Chemistry* 279:43052-60

Walker HK, Hall WD, Hurst JW, Bansal VK. 1990. Serum Inorganic Phosphorus.

Wan H, Dingle S, Xu Y, Besnard V, Kaestner KH, et al. 2005. Compensatory roles of Foxa1 and Foxa2 during lung morphogenesis. *Journal of Biological Chemistry* 280:13809-16

Wang AY-M, Woo J, Lam CW-K, Wang M, Chan IH-S, et al. 2005. Associations of serum fetuin-A with malnutrition, inflammation, atherosclerosis and valvular calcification syndrome and outcome in peritoneal dialysis patients. *Nephrology Dialysis Transplantation* 20:1676-85

Wang D, Canaff L, Davidson D, Corluka A, Liu H, et al. 2001. Alterations in the sensing and transport of phosphate and calcium by differentiating chondrocytes. *Journal of Biological Chemistry* 276:33995-4005

Wang H, Zhang M, Soda K, Sama A, Tracey KJ. 1997. Fetuin protects the fetus from TNF. *The Lancet* 350:861-2

Wang Y, Middleton F, Horton JA, Reichel L, Farnum CE, Damron TA. 2004. Microarray analysis of proliferative and hypertrophic growth plate zones identifies differentiation markers and signal pathways. *Bone* 35:1273-93

Weaver M, Batts L, Hogan BL. 2003. Tissue interactions pattern the mesenchyme of the embryonic mouse lung. *Developmental Biology* 258:169-84

Weaver M, Yingling JM, Dunn NR, Bellusci S, Hogan BL. 1999. Bmp signaling regulates proximal-distal differentiation of endoderm in mouse lung development. *Development* 126:4005-15

Weibel ER. 1984. *The pathway for oxygen*: Harvard university press 425 pp.

Weichselbaum M, Sparrow MP, Hamilton EJ, Thompson PJ, Knight DA. 2005. A confocal microscopic study of solitary pulmonary neuroendocrine cells in human airway epithelium. *Respiratory Research* 6:115

Weidenbecher M, Tucker HM, Awadallah A, Dennis JE. 2008. Fabrication of a neotrachea using engineered cartilage. *Laryngoscope* 118:593-8

Weidenfeld J, Shu W, Zhang L, Millar SE, Morrisey EE. 2002. The WNT7b promoter is regulated by TTF-1, GATA6, and Foxa2 in lung epithelium. *Journal of Biological Chemistry* 277:21061-70

Wessells NK. 1970. Mammalian lung development: interactions in formation and morphogenesis of tracheal buds. *Journal of Experimental Zoology* 175:455-66

West RB, Corless CL, Chen X, Rubin BP, Subramanian S, et al. 2004. The novel marker, DOG1, is expressed ubiquitously in gastrointestinal stromal tumors irrespective of KIT or PDGFRA mutation status. *American Journal of Pathology* 165:107-13

Westneat MW, Betz O, Blob RW, Fezzaa K, Cooper WJ, Lee WK. 2003. Tracheal respiration in insects visualized with synchrotron x-ray imaging. *Science* 299:558-60

Whimster W. 1985. Number and mean volume of individual submucous glands in the human tracheobronchial tree. *Applied Pathology* 4:24-32

White KE, Carn G, Lorenz-Depiereux B, Benet-Pages A, Strom TM, Econs MJ. 2001a. Autosomal-dominant hypophosphatemic rickets (ADHR) mutations stabilize FGF-23. *Kidney International* 60:2079-86

White KE, Jonsson KB, Carn G, Hampson G, Spector TD, et al. 2001b. The autosomal dominant hypophosphatemic rickets (ADHR) gene is a secreted polypeptide overexpressed by tumors that cause phosphate wasting. *Journal of Clinical Endocrinology & Metabolism* 86:497-500

Whitsett JA, Haitchi HM, Maeda Y. 2011. Intersections between pulmonary development and disease. *American Journal of Respiratory and Critical Care Medecine* 184:401-6

Whyte MP. 1994. Hypophosphatasia and the Role of Alkaline Phosphatase in Skeletal Mineralization*. *Endocrine Reviews* 15:439-61

Whyte MP. 2000. Hypophosphatasia. In *The Genetics of Osteoporosis and Metabolic Bone Disease*, pp. 335-56: Springer

Williams CJ, Pendleton A, Bonavita G, Reginato AJ, Hughes AE, et al. 2003. Mutations in the amino terminus of ANKH in two US families with calcium pyrophosphate dihydrate crystal deposition disease. *Arthritis & Rheumatism* 48:2627-31

Wilt FH, Killian CE, Livingston BT. 2003. Development of calcareous skeletal elements in invertebrates. *Differentiation* 71:237-50

Wittrant Y, Bourgine A, Khoshniat S, Alliot-Licht B, Masson M, et al. 2009. Inorganic phosphate regulates Glvr-1 and-2 expression: role of calcium and ERK1/2. *Biochemical and Biophysical Research Communications* 381:259-63

Wurtz A, Porte H, Conti M, Desbordes J, Copin MC, et al. 2006. Tracheal replacement with aortic allografts. *New England Journal of Medicine* 355:1938-40

Wuthier R. 1976. Lipids of matrix vesicles. *Federation proceedings*, pp. 117-21

Wuthier R, Majeska R, Collins GM. 1977. Biosynthesis of matrix vesicles in epiphyseal cartilage. *Calcified Tissue Research* 23:135-9

Wuthier RE. 1989. Mechanism of de novo mineral formation by matrix vesicles. *Connective Tissue Research* 22:653-9

Yadav MC, Simao AM, Narisawa S, Huesa C, McKee MD, et al. 2011. Loss of skeletal mineralization by the simultaneous ablation of PHOSPHO1 and alkaline phosphatase function: a unified model of the mechanisms of initiation of skeletal calcification. *Journal of Bone and Mineral Research* 26:286-97

Yamada S, Samtani RR, Lee ES, Lockett E, Uwabe C, et al. 2010. Developmental atlas of the early first trimester human embryo. *Developmental Dynamics* 239:1585-95

Yang Y, Palmer KC, Relan N, Diglio C, Schuger L. 1998. Role of laminin polymerization at the epithelial mesenchymal interface in bronchial myogenesis. *Development* 125:2621-9

Yao Y, Shahbazian A, Boström KI. 2008. Proline and γ-carboxylated glutamate residues in matrix Gla protein are critical for binding of bone morphogenetic protein-4. *Circulation Research* 102:1065-74

Yao Y, Zebboudj AF, Shao E, Perez M, Boström K. 2006. Regulation of bone morphogenetic protein-4 by matrix GLA protein in vascular endothelial cells involves activin-like kinase receptor 1. *Journal of Biological Chemistry* 281:33921-30

Yates AJ, Oreffo RO, Mayor K, Mundy GR. 1991. Inhibition of bone resorption by inorganic phosphate is mediated by both reduced osteoclast formation and decreased activity of mature osteoclasts. *Journal of Bone and Mineral Research* 6:473-8

Yin J, Xia Y. 2014. Proteoglycan concentrations in healthy and diseased articular cartilage by Fourier transform infrared imaging and principal component regression. *Spectrochimica Acta Part A: Molecular and Biomolecular Spectroscopy* 133:825-30

Yoshiko Y, Candeliere GA, Maeda N, Aubin JE. 2007. Osteoblast autonomous Pi regulation via Pit1 plays a role in bone mineralization. *Molecular and Cellular Biology* 27:4465-74

Young B, Lowe, J.S., Stevens, A., Heath, J.W. 2006. *Wheater's Functional Histology A text and Colour Atlas* Churchill Livingstone, Philadelphia, USA.

Yuan B, Li C, Kimura S, Engelhardt RT, Smith BR, Minoo P. 2000. Inhibition of distal lung morphogenesis in Nkx2.1(-/-) embryos. *Developmental Dynamics* 217:180-90

Zackai EH, McDonald-McGinn DM, Stolle C, Huff DS. Craniosynostosis with tracheal sleeve: a patient with Pfeiffer syndrome, tracheal sleeve and additional malformations in whom an FGFR2 mutation was found. *Clinical Dysmorphology* 2003 Jul;12(3):209.

Zaka R, Stokes D, Dion AS, Kusnierz A, Han F, Williams CJ. 2006. P5L mutation in Ank results in an increase in extracellular inorganic pyrophosphate during proliferation and nonmineralizing hypertrophy in stably transduced ATDC5 cells. *Arthritis Research & Therapy* 8:R164

Zaka R, Williams CJ. 2005. Genetics of chondrocalcinosis. *Osteoarthritis and Cartilage* 13:745-50

Zaw-Tun HA. 1982. The tracheo-esophageal septum--fact or fantasy? Origin and development of the respiratory primordium and esophagus. *Acta Anatomica* 114:1-21

Zebboudj AF, Imura M, Boström K. 2002. Matrix GLA protein, a regulatory protein for bone morphogenetic protein-2. *Journal of Biological Chemistry* 277:4388-94

Zeng L, Kempf H, Murtaugh LC, Sato ME, Lassar AB. 2002. Shh establishes an Nkx3.2/Sox9 autoregulatory loop that is maintained by BMP signals to induce somitic chondrogenesis. *Genes and Development* 16:1990-2005

Zhang DW, Burton-Wurster N, Lust G. 1995. Alternative splicing of ED-A and ED-B sequences of fibronectin pre-mRNA differs in chondrocytes from different cartilaginous tissues and can be modulated by biological factors. *Journal of Biological Chemistry* 270:1817-22

Zimmermann H. 1992. 5'-Nucleotidase: molecular structure and functional aspects. *Biochemical Journal* 285:345

Zopf DA, Flanagan CL, Wheeler M, Hollister SJ, Green GE. 2014. TReatment of severe porcine tracheomalacia with a 3-dimensionally printed, bioresorbable, external airway splint. *JAMA Otolaryngology–Head & Neck Surgery* 140:66-71

Zur K. 2014. Congenital Malformations of the Trachea. In *Congenital Malformations of the Head and Neck*, ed. LM Elden, KB Zur, pp. 141-57: Springer New York

OPEN ACCESS Freely available online

PLOS ONE

Simultaneous Characterization of Metabolic, Cardiac, Vascular and Renal Phenotypes of Lean and Obese SHHF Rats

Gina Youcef[1,2,3,4], Arnaud Olivier[1,2,3,5,6], Clément P. J. L'Huillier[1,2,3], Carlos Labat[1,2,3], Renaud Fay[5,6], Lina Tabcheh[2,3,7], Simon Toupance[1,2,3,5,6], Rosa-Maria Rodriguez-Guéant[2,3,5,8], Damien Bergerot[9], Frédéric Jaisser[5,6], Patrick Lacolley[1,2,3,5], Faiez Zannad[1,2,3,5,6], Laurent Vallar[4], Anne Pizard[1,2,3,6]*

1 UMRS U1116 Inserm, Vandoeuvre-lès-Nancy, France, **2** Fédération de Recherche 3209, Nancy, France, **3** Université de Lorraine, Nancy, France, **4** Genomics Research Unit, Centre de Recherche Public de la Santé, Strassen, Luxembourg, **5** CHU Nancy, Nancy, France, **6** CIC 1433, Pierre Drouin, Vandoeuvre-lès-Nancy, France, **7** UMR 7365 CNRS, Vandoeuvre-lès-Nancy, France, **8** U954 Inserm, Vandoeuvre-lès-Nancy, France, **9** CIC 9201, PARCC, HEGP, Paris, France

Abstract

Individuals with metabolic syndrome (MetS) are prone to develop heart failure (HF). However, the deleterious effects of MetS on the continuum of events leading to cardiac remodeling and subsequently to HF are not fully understood. This study characterized simultaneously MetS and cardiac, vascular and renal phenotypes in aging Spontaneously Hypertensive Heart Failure lean ($SHHF^{+/?}$ regrouping $^{+/+}$ and $^{+/cp}$ rats) and obese ($SHHF^{cp/cp}$, "cp" defective mutant allele of the leptin receptor gene) rats. We aimed to refine the milestones and their onset during the progression from MetS to HF in this experimental model. We found that $SHHF^{cp/cp}$ but not $SHHF^{+/?}$ rats developed dyslipidemia, as early as 1.5 months of age. This early alteration in the lipidic profile was detectable concomitantly to impaired renal function (polyuria, proteinuria but no glycosuria) and reduced carotid distensibility as compared to $SHHF^{+/?}$ rats. By 3 months of age $SHHF^{cp/cp}$ animals developed severe obesity associated with dislipidemia and hypertension defining the onset of MetS. From 6 months of age, $SHHF^{+/?}$ rats developed concentric left ventricular hypertrophy (LVH) while $SHHF^{cp/cp}$ rats developed eccentric LVH apparent from progressive dilation of the LV dimensions. By 14 months of age only $SHHF^{cp/cp}$ rats showed significantly higher central systolic blood pressure and a reduced ejection fraction resulting in systolic dysfunction as compared to $SHHF^{+/?}$. In summary, the metabolic and hemodynamic mechanisms participating in the faster decline of cardiac functions in $SHHF^{cp/cp}$ rats are established long before their physiological consequences are detectable. Our results suggest that the molecular mechanisms triggered within the first three months after birth of $SHHF^{cp/cp}$ rats should be targeted preferentially by therapeutic interventions in order to mitigate the later HF development.

Citation: Youcef G, Olivier A, L'Huillier CPJ, Labat C, Fay R, et al. (2014) Simultaneous Characterization of Metabolic, Cardiac, Vascular and Renal Phenotypes of Lean and Obese SHHF Rats. PLoS ONE 9(5): e96452. doi:10.1371/journal.pone.0096452

Editor: Mihai Covasa, INRA, France

Received August 18, 2013; **Accepted** April 7, 2014; **Published** May 15, 2014

Funding: Dr A. Pizard acknowledges Inserm, Région Lorraine, the « Comité Lorrain » of the « Fondation pour la Recherche Médicale » and FP7-HEALTH-2010 # 261409 MEDIA program for their financial supports to carry this project. G. Youcef is supported by a salary fellowship from AFR PhD grants, Luxembourg. The funders had no role in study design, data collection and analysis, decision to publish or preparation of the manuscript.

Competing Interests: The authors have declared that no competing interests exist.

* E-mail: anne.pizard@inserm.fr

Introduction

Chronic heart failure (HF) is of heterogeneous etiology but it usually occurs in the elderly [1] and unlike other cardiovascular problems its prevalence is increasing. Several studies demonstrated that patients affected by metabolic syndrome (MetS) -defined as the simultaneous occurrence of at least three of the five following risk factors: obesity, hypertension, dyslipidemia, type 2 diabetes and insulin resistance- have a higher risk of developing HF [2,3,4,5]. Indeed, it has been described that long-lasting hypertension induces left ventricular hypertrophy (LVH) and later dilatation of the LV internal cavity [6]. Diabetes as well as insulin resistance have been also associated with ventricular dysfunction and increased heart mass [7]. Furthermore, the risk of developing chronic HF has been demonstrated to be higher in obese patients and more specifically so, in those presenting abdominal obesity, a fundamental feature of MetS [8,9,10]. Thus, metabolic risk appears to be critical for the development of HF suggesting that the rising incidence of HF over the last decade probably mirrors the concurrent epidemics of obesity. Identifying and managing the patients at risk of HF prior to the onset of symptoms may be an effective approach to prolong active life by delaying or preventing the onset of HF in those patients [11]. For this attractive preventive strategy to be effective, a deep understanding of the continuum of events underpinning the transition from obesity/MetS to HF is required. Furthermore a better characterization of risk factors for the transition to HF is likely to provide new preventive therapeutic opportunities.

To study the influence of MetS on the cardiac, renal and vascular remodeling leading to the development of HF, an experimental animal model such as the Spontaneously Hypertensive rats prone to HF (SHHF/MccGmiCrl- $Lepr^{cp}$, SHHF) might be particularly relevant [12,13].

Obtained from the seventh backcross between SHR/N-cp obese and SHR/N rats (Spontaneously hypertensive) [14], the SHHF rat model is of great interest in our study since it mimics the same pathophysiology of human MetS and HF [12,13,15,16,17,18].

To our knowledge, it represents the only available model that could progressively and spontaneously develop HF with earlier onset when rats are homozygous for the mutant allele of the leptin receptor gene $Lepr^{cp}$, a genotype that renders them hyperphagic and obese [19]. Interestingly, the onset of HF varies accordingly to the $Lepr^{cp}$ allele dosage and consequently obese homozygous mutant animals $SHHF^{cp/cp}$ die before the lean littermates (heterozygous, $SHHF^{+/cp}$ and wild type, $SHHF^{+/+}$ later referred to as $SHHF^{+/?}$) [12].

Although some studies have been published using the SHHF rat model, the data are too scattered to draw clear-cut conclusions on the continuum of events leading to HF. Indeed, if reports have focused either on the SHHF cardiac [15,20,21] or renal features [22] and the combination of both is rarely addressed. As they are not based on the concurrent observation of obese versus lean animals in similar conditions (sex, diet, analyzed parameters), conclusions from these studies are difficult to combine in order to get a unified model. Furthermore, the vascular phenotypes of the obese and their control lean SHHF rats have not yet been evaluated.

The present study has been therefore designed to provide an integrated status of the metabolic, cardiac and vascular phenotypes of the SHHF obese as compared to lean rats in order to fully appreciate the impact of MetS on the progression towards HF.

Materials and Methods

Animal model

Male 1 month-old lean (homozygous wild type $SHHF^{+/+}$ and heterozygous $SHHF^{+/cp}$, hereafter referred to as $SHHF^{+/?}$, n = 23) and obese ($SHHF^{cp/cp}$, n = 21) Spontaneously Hypertensive Heart Failure rats (SHHF/MccGmiCrl-$Lepr^{cp}$) were purchased from Charles River Laboratories (L'Arbresle, France). Animals were maintained on a 12:12-h light-dark cycle with *ad libitum* access to tap water and modestly enriched fatty diet (Purina 5008, Charles River, France) as recommended by the supplier. The composition of the diet by weight was 23% protein, 58.5% carbohydrate, 6.5% fat (as compared to 3.15% in standard diet; M20 SDS)), 4.0% fiber and 8.0% ash. Delivery of calories from each component was: approximately 16.7% from fat, 26.8% from proteins and 56.4% from carbohydrates. After a 2-week-period of acclimation, fourteen 1.5 month-old $SHHF^{+/?}$ and twelve $SHHF^{cp/cp}$ underwent detailed metabolic, cardiac, renal and vascular phenotyping before being euthanized by exsanguination leading to cardiac arrest. The remaining animals were monitored regularly over a period of 12.5 months in order to evaluate their metabolic, cardiac, renal and vascular status over time. Experimental protocols were carried out according to the institutional animal care and use committee of Inserm in order to minimize animal suffering. This protocol was reviewed and the experiments were monitored by the staff of the animal facility, which was authorized (agreement # B54-547-17) by the Ministry and local authorities.

Three $SHHF^{cp/cp}$ rats died while none of the $SHHF^{+/?}$ did during the confinement at 37°C required for the phethymography blood pressure measuring experiment. One $SHHF^{cp/cp}$ rat was found dead in his cage while no confounding behaviour warned us of such a potential event. Although those sudden deaths suggest a fragility of the $SHHF^{cp/cp}$ rats as compared to their lean counterparts it seemed inappropriate to draw a Kaplan Meier curve while most of the deaths occurring within the group of obese rats intervened during their phenotyping. Thus, the end point of our study (month 14) was determined by the number of $SHHF^{cp/cp}$ rats still alive that had to be sufficient to allow statistical comparison with the $SHHF^{+/?}$ group of rats.

Metabolic cages

All animals were individually transferred into siliconed metabolic cages (Silicone Solution in Isopropanol, SERVA; Tecniplast, France) where they were given ad libitum access to water and powdered food (Purina 5008, Charles River). Animals were followed during three consecutive days with daily monitoring of their water and food consumption as well as collection of fecal and urinary excretion. The intakes and excretions were estimated during the 3-day follow-up by averaging daily measurements to mitigate the possible changes linked to rat acclimation to the metabolic cages. Urine samples were collected on a daily basis and centrifuged at 4,500 rpm for 10 min at RT in order to discard cell debris and other solid materials before being stored at −20°C for further biochemical analysis. Urinary osmolality, ionogram, enzymatic creatinine and aldosterone levels were determined in urine samples collected on the third day since it corresponds to a physiological steady state of the rats. Osmolality was assayed using a freezing point osmometer (Roebling, Germany) whereas creatinine and aldosterone were measured with commercial kits according to the manufacturer's recommendations (OSR61204, Beckman Coulter and Siemens 06615154 Coat-A-Count RIA Aldosterone Kit, respectively).

To evaluate renal performance and activity, glomerular filtration rate (eGFR) was estimated in ml/24h and calculated as follows:

eGFR (ml/24 h) = [(Urinary creatinine concentration (mmol/L) × Urinary daily volume (mL/24 h))/serum creatinine concentration (mmol/L)].

Echocardiography

Transthoracic echocardiography was performed on anesthetized rats (Isoflurane 5% initial, 3% maintenance, in 1.5 L/min dioxygen) at different time points: 1.5, 3, 6, 9, 12 and 14 months in the left decubitus position using a 12 MHz pediatric transducer connected to a Sonos 5500 Ultrasound System (Philips, France). Short axis M-mode echocardiograms were obtained for measurement of Left Ventricle (LV) Internal Diameters at end diastole (LVIDd) and end systole (LVIDs), LV Fractional Shortening (FS), Ejection Fraction (EF), Septal (Septum) and Posterior Wall thickness (PWT). Doppler flow velocities were taken at the level of the mitral valve in the apical four-chamber view with the Doppler probe placed at the edge of the mitral leaflets where the peak of early (E) and late filling waves (A) as well as E wave deceleration time (EDT) were measured. Measurements and calculations used were as follows:

(i) **FS** (%) = [(LVIDd – LVIDs)/LVIDd] ×100.

(ii) **EF** (%) = [(EDV- ESV)/EDV] ×100 where EDV and ESV referred to End-diastolic and End-systolic volumes respectively.

(iii) **LV mass** (mg) = 1.04× [(PWT+Septum+LVIDd)^3-(LVIDd)^3] where 1.04 is the specific gravity of the myocardium.

All echocardiographic parameters were calculated by averaging results from three to four consecutive cardiac cycles for each rat at each time point.

Blood Pressure measurements

Peripheric Systolic blood pressure (SBP) as well as HR were monitored at different time points in conscious animals using the tail-cuff method (Visitech BP-2000 Systems, France). After the placement of the rats in a warmed chamber to allow caudal vein dilatation, the tail-cuff computerized non-invasive method was set to measure 10 preliminary cycles followed by 10 effective measurements. To prevent bias in data due to animal anxiety, all rats were familiarized with the procedure for at least one week before measurements.

Invasive Blood pressure and Arterial stiffness measurements

Arterial diameter (right carotid artery) and central blood pressure (diastolic, systolic and pressure pulse (PP) on left carotid artery) were simultaneously recorded in isoflurane-anesthetized rats (3% of isoflurane in 1.5 L/min dioxygen). Internal arterial diameter was measured using a 17 MHz ultrasonic echo-tracking device (NIUS-01; Asulab SA, Marin, Switzerland). 1.5- and 14-month-old rats were characterized for their carotid distensibility and compliance as well as the incremental elastic modulus (Einc) and circumferential wall stress (σ) as described previously [23].

Histology

After arterial hemodynamic property evaluation, anesthetized animals were euthanized by exsanguination leading to cardiac arrest and organs were rapidly dissected and weighted. Organs and tissue specimens were washed in physiological saline, fixed in formalin for 24 h, and then preserved in 70% ethanol before being paraffin-embedded. Histological slides for heart, kidney, liver and peri-renal visceral adipose tissue were prepared from 5 µm thick sections of the paraffin blocks and stained using Sirius Red or hematoxylin-eosin. Myocardial fibrosis was determined on Sirius red stained heart sections by measuring the percentage of fibrotic area to whole heart section area using Image J software. Paraffin-embedded carotid sections underwent Weigert's staining in order to measure the carotid mean cross sectional area (MCSA) as previously described [23]. Glomerular surface area was traced manually on different places on the kidney section and measured by using NIS-element software (Nikon). Results were the average of up to 50 glomeruli per animal of each group.

Blood collection and Biochemical assays

Arterial blood samples were collected at 1.5 months and 14 months of age through a catheter implanted in the carotid of the anesthetized rats. Venous blood samples were collected from the jugular vein puncture at several time points taking advantage of the anaesthesia of the rats that underwent echocardiographic examination. Plasma samples were collected in presence of sodium citrate (1:10 v:v of blood) to separate plasma after immediate centrifugation at 3,000 rpm for 10 min at room temperature (RT).

Plasma samples from 1.5 and 14 months old rats were used to evaluate Brain Natriuretic Peptide 45 (BNP 45) using a BNP 45 Rat ELISA Kit (Abcam, ab108816) according to manufacturer's instructions.

Serum samples were collected after 20 min sedimentation at RT and subsequent 2,300-rpm centrifugation for 15 min. Serum samples from 16 h-fasted rats at 1.5 and 14 months of age were used to evaluate total cholesterol, triglycerides, free fatty acids, creatinine and glucose concentrations by routine enzymatic methods on an automatic biochemical analyzer, sodium and potassium (Na^+, K^+) by a standardized indirect potentiometry technique. Adiponectin and Insulin levels were measured using commercially available kits according to manufacturer's instructions of the Adiponectin Rat ELISA Kit (Abcam, #ab108784) and Insulin Human ELISA kit (Abcam, #ab100578) respectively.

Insulin resistance (IR) was evaluated in rats using the homeostasis model assessment (HOMA) by calculating the HOMA-IR index as follows:

HOMA-IR = [fasting glucose concentration (mmol/L) × fasting insulin concentration (µIU/mL)]/22.5.

Statistics

All results are presented as mean ± sem. Statistical analysis of data was performed using unpaired Student's t test to compare the genotypes and ages respectively with *$p<0.05$, **$p<0.01$, ***$p<0.001$ and $^{\S}p<0.05$, $^{\S\S}p<0.01$, $^{\S\S\S}p<0.001$ to be considered statistically significant. Non-parametric ANOVA analysis with two factors allowed the evaluation of interaction between aging and genotypes.

Results

Early Metabolic disorders in SHHF$^{cp/cp}$ rats

While no differences were observed at 1.5 months of age, SHHF$^{cp/cp}$ gained significantly more weight during the following 3 months than their SHHF$^{+/?}$ littermates as animals underwent a rapid growth phase (Figure 1A). Then, both groups of rats showed a slower and almost parallel growth phase. At 14 months of age, SHHF$^{cp/cp}$ and SHHF$^{+/?}$ rat weight increased by about 6- and 4-fold, respectively (Figure 1A). Histological analysis of peri-renal visceral fat revealed the presence of very large adipocytes and evidence of fibrosis in SHHF$^{cp/cp}$ rats as compared to that of SHHF$^{+/?}$ rats (Figure 1B).

Altered plasma metabolic profiles were detectable in SHHF$^{cp/cp}$ rats as early as 1.5 months of age. These included higher levels of total cholesterol, HDL cholesterol, free fatty acids (FFA) and triglycerides (TG) (Table 1). The overall increase in blood lipid concentration in the SHHF$^{cp/cp}$ rats was significantly maintained over the time leading to major dyslipidemia at 14 months of age (Table 1). While the fasting glycemia levels were not modified either over time or between genotypes, fasting insulin levels increased significantly in animal of both genotypes but more dramatically in the SHHF$^{cp/cp}$ group indicating the development of an insulin resistance (IR) (Table 1). The IR development was confirmed by the HOMA-IR index, that discriminated the SHHF$^{cp/cp}$ rats from the SHHF$^{+/?}$ as early as 1.5 months of age. Adiponectin levels were higher as early as 1.5 months of age in the homozygous mutant group. At both ages, plasma BNP concentrations were not different between genotypes but significantly increased over time in SHHF$^{cp/cp}$ and SHHF$^{+/?}$ rats. No differences were recorded in serum sodium and potassium levels between SHHF$^{cp/cp}$ and SHHF$^{+/?}$ rats throughout the follow-up (Table 1). Hepatic steatosis was detected only at 14 months of age in livers dissected from SHHF$^{cp/cp}$ rats (Figure 1C).

Worsening of the renal function associated with $^{cp/cp}$ genotype

Average water intake (Table 2) and urine excretion (Figure 2A) estimated over three consecutive days indicated that SHHF$^{cp/cp}$ rats developed polyuria as early as 1.5 months of age before showing evidence of polydipsia. Up to 12 months of age volumes of water consumed and urinary excretion were greater in SHHF$^{cp/cp}$ rats as compared to SHHF$^{+/?}$ animals (Table 2 and Figure 2A, respectively). This occurred concomitantly with a progressive decrease in urine osmolality and creatinine (Table 2), and in parallel with a progressive increase in proteinuria over the

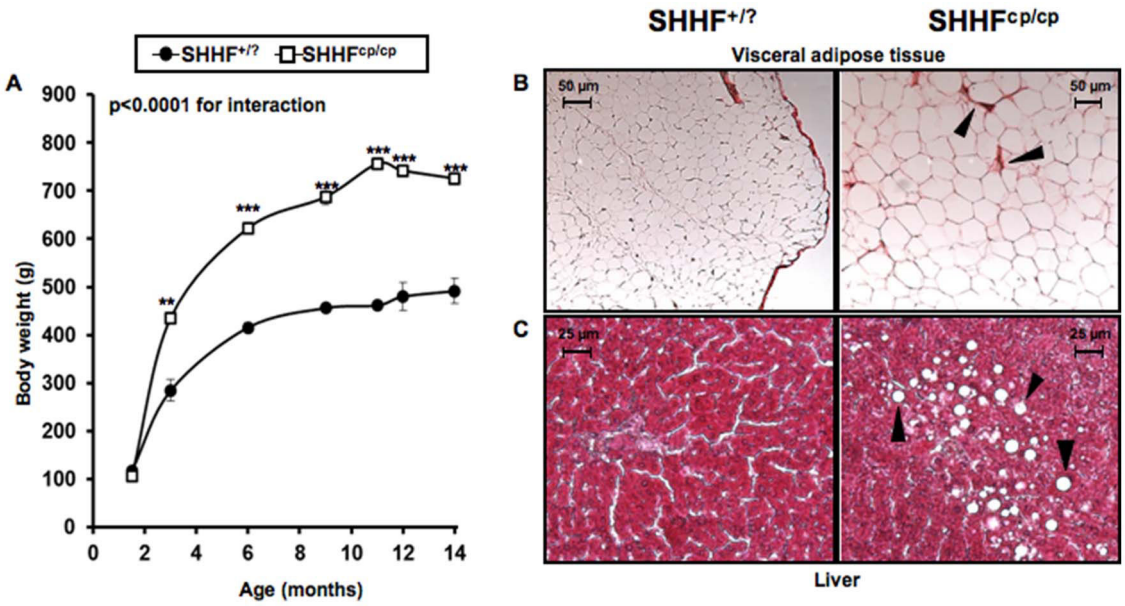

Figure 1. Metabolic follow-up. A- The monitoring of body weight shows that the onset of obesity occurs during the first three months after birth of SHHF$^{cp/cp}$ rats. Progressively, the SHHF$^{cp/cp}$ rats continue to gain weight accentuating their differences with the SHHF$^{+/?}$ (n = 5 to 14 rats per genotype). (**B–C**) Paraffin embedded tissues dissected from SHHF$^{cp/cp}$ and SHHF$^{+/?}$ rats at 14 months of age showing metabolic disorder related-tissue alterations **B**- Peri-renal visceral fat of SHHF$^{cp/cp}$ rats stained with Sirius red exhibited marked fibrosis (arrows) and hypertrophic adipocytes. **C**- Hemaetoxylin & Eosin staining shows the deposition of lipid droplets (arrows) in the liver dissected from SHHF$^{cp/cp}$ rats suggesting the development of non-alcoholic hepatic steatosis. Pictures are representative of each analyzed group (n = 5 to 7 rats per genotype). Values are mean ± sem. Non-parametric ANOVA analysis with two factors allowed the evaluation of an interaction between aging and genotype. * $p<0.05$, ** $p<0.01$, *** $p<0.001$ for comparing SHHF$^{cp/cp}$ vs. SHHF$^{+/?}$ at the same time point.
doi:10.1371/journal.pone.0096452.g001

animals lifetime measured in the urine obtained on the third day in the metabolic cages (Figure 2B). Interestingly, while showing higher daily sodium and potassium excretions at 1.5 months of age, SHHF $^{cp/cp}$ rats reduced their excretions over time to concentrations similar to those of the SHHF$^{+/?}$ rats (Table 2). It is noteworthy that the significantly smaller sodium to potassium ratio in SHHF$^{cp/cp}$ at 1.5 months of age was observed while a higher urinary excretion of aldosterone was detected in those rats as compared to the SHHF$^{+/?}$ animals (Table 2).

The kidney weight-to-tibia length ratio was greater in the SHHF$^{cp/cp}$ rats than in the SHHF$^{+/?}$ rats (Table 2). However, histology and tissue architecture of the kidney of the obese rats did not appear altered at 1.5 months of age (Figure 2C). In contrast, abnormal architecture of the kidney was observed in 14 month-old in SHHF$^{cp/cp}$ rats compared to SHHF$^{+/?}$. Renal lesions in obese rats included increases in glomerular surface area (Figure 2C and Table 2, respectively) associated with massive protein casts in the Bowman's space and tubular lumens in both kidney cortex and medulla. In SHHF$^{+/?}$ rats, tissue alterations were restricted mostly to the cortex. At 14 months of age, the abnormal histological modifications were observed simultaneously with a significant reduction of the estimated glomerular filtration rate (eGFR) in the SHHF$^{cp/cp}$ group thus reflecting significantly reduced kidney function (Table 2).

Exacerbated cardiac remodeling in SHHF$^{cp/cp}$ rats

At 1.5 months of age, heart weight-to-tibia length ratios were significantly increased in the SHHF$^{cp/cp}$ group as compared to the SHHF$^{+/?}$ group (Table 3). Cardiac hypertrophy was not associated with gross histological modifications of the heart structure or with functional impairment at that age (Figures 3A–E at 1.5 months of age). By contrast, at 14 months of age, Sirius red staining revealed massive cardiac fibrosis in the SHHF$^{cp/cp}$ rats (Figure 3E; 14 months and table 3; % fibrotic area) which was less apparent in SHHF$^{+/?}$ animals. In the former group of rats, this was observed concomitantly with dramatically altered cardiac function parameters together with elevated HW/tibia length (Table 3).

Echocardiographic monitoring from 1.5 to 14 months of age demonstrated the development of worsened and faster cardiac remodeling in the SHHF$^{cp/cp}$ group (Table 3 and Figure 3) as compared to the SHHF$^{+/?}$ rats. Indeed, while showing indistinguishable echocardiographic parameters at 1.5 months of age, the two groups of rats developed progressively distinctive features from 6 months of age. The measured cardiac remodeling was indicative of alterations of the cardiac systolic function in the SHHF$^{cp/cp}$ group only (Table 3 and Figure 3A–B). Diastolic function was not different between lean and obese rats at 14 months of age (Table 3; LV Diastolic function).

Interestingly, a significantly heavier mass of the left ventricle (LV) of the SHHF$^{cp/cp}$ was observed as early as 6 months of age, a difference that was sustained through to 9 months of age (Figure 3C). A thinning of the LV wall (Table 3; septum and posterior wall thickness) was present in the SHHF$^{cp/cp}$ that led to dilation as early as 3 months of age (Figure 3D) and the decline by 14 months of age of the left ventricular systolic function (Figure 3A–B). Over the whole period of monitoring, the observed hypertrophic remodeling was of the eccentric type in the SHHF$^{cp/cp}$ animals since their LV dilated and their LV walls had firstly thickened before becoming thinner at 14 months of age (Figure 3C). Meanwhile the SHHF$^{+/?}$ rats developed concentric hypertrophic remodeling as their cardiac LV wall continued to thicken (Table 3; septum and posterior wall thickness and Figure 3C).

Table 1. Blood parameters.

Genotype	$SHHF^{+/?}$	$SHHF^{cp/cp}$	$SHHF^{+/?}$	$SHHF^{cp/cp}$		ANOVA	
Parameters							
Age, month	**1.5**	**1.5**	**14**	**14**	**Genotype**	**Age**	**Interaction**
N	7–12	5–10	7	5			
Ionogram, mmol/l							
Na^+	140.8±0.5	141.4±0.6	143.7±0.7§§§	143.0±0.8	ns	0.0003	ns
K^+	4.8±0.2	4.9±0.2	5.3±0.2	4.7±0.2	ns	ns	ns
Na^+/K^+ ratio	29.8±0.9	28.8±1.0	28.1±1.2	30.3±1.4	ns	ns	ns
Lipidic profil, g/l							
Total Cholesterol	0.7±0.2	0.9±0.3***	0.8±0.3	4.6±0.4***§§§	<0.0001	<0.0001	<0.0001
HDL	0.2±0.0	0.3±0.0**	0.2±0.0	0.4±0.0***§§§	<0.0001	<0.0001	<0.0001
LDL	0.4±0.1	0.5±0.1	0.4±0.1	1.3±0.2§	0.0026	0.0045	0.0141
FFA	1.1±0.4	1.7±0.5*	1.1±0.5	5.2±0.6*§	<0.0001	0.0045	0.0023
TG	0.3±0.7	0.8±0.0*	0.5±0.1	14.6±1.1***§§§	<0.0001	<0.0001	<0.0001
Fasting glycemia, mg/dl	83±5	100±12	107±5	92±9	ns	ns	ns
Fasting insulin, µIU/ml	12±2	25±4	16±4§§	226±92***§§§	0.007	0.004	0.009
HOMA-IR index	0.9±0.3	2.6±0.8***	2.0±0.3§§§	14.6±5.9***§§	0.004	0.007	0.022
Creatinine, mmol/l	2.13±0.60	1.88±0.69**	4.60±0.79§§§	8.00±0.93***§§§	0.0489	<0.0001	0.0244
BNP, pg/ml	117±18	116±24	212±29§§	207±29§§	ns	0.0013	ns
Adiponectin, µg/ml	6.4±0.5	19.7±0.8***	5.3±0.7§	12.8±0.8***§§§	<0.0001	<0.0001	0.0007

Na^+, sodium, **K^+**, potassium; **HDL**, High Density Lipoprotein; **LDL**, Low density Lipoprotein; **FFA**, Free Fatty Acids; **TG**, triglyceride; **BNP**, Brain Natriuretic Peptide. Values are the mean±sem. Non-parametric ANOVAs analysis with two factors allowed the evaluation of interaction between aging and genotype. Student's T test * $p<0.05$; ** $p<0.01$, *** $p<0.001$ to compare $SHHF^{cp/cp}$ *vs.* $SHHF^{+/?}$ at same time point; § $p<0.05$; §§$p<0.01$, §§§ $p<0.001$ to compare T14-mo *vs* T1.5-mo for a same genotype; **N** stands for the number of samples; **ns** stands for not significant.

doi:10.1371/journal.pone.0096452.t001

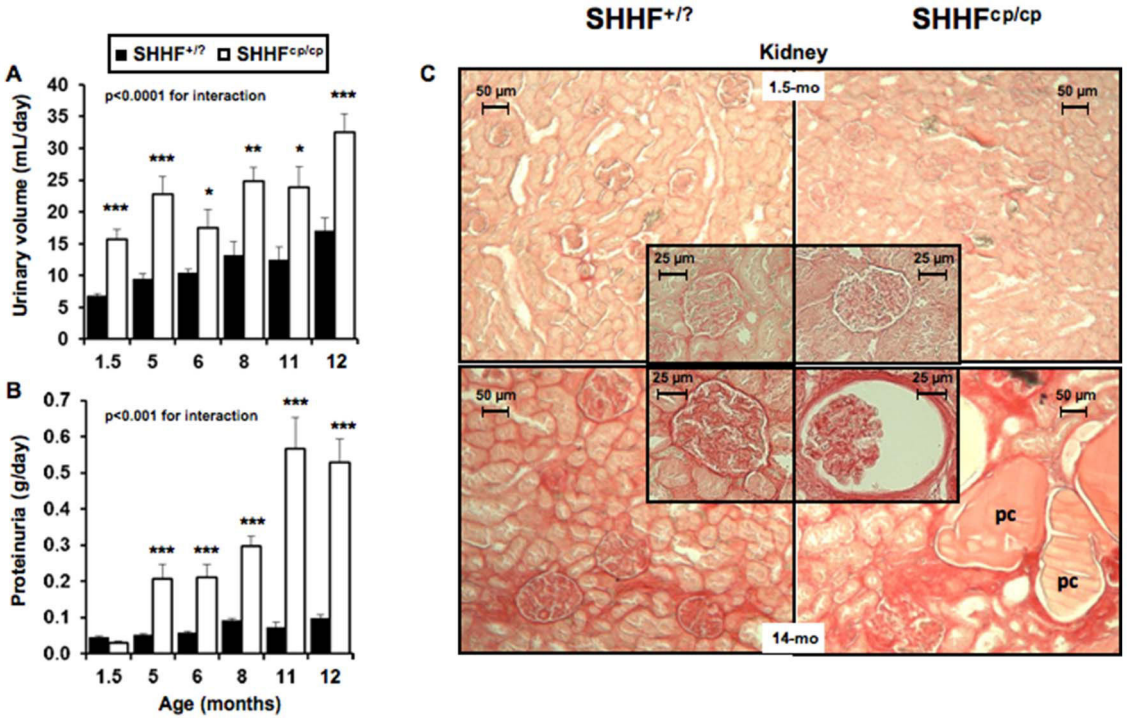

Figure 2. Renal function follow-up. The worsening of renal function associated with the $^{cp/cp}$ genotype was evaluated while rats were placed individually in metabolic cages for 3 consecutive days (n = 5 to 10 rats per genotype). The alteration of renal function observed in SHHF$^{cp/cp}$ rats is shown by **A**- increased urine excretion as early as 1.5 months of age, **B**- increased proteinuria and **C**- by major deteriorations of renal histological ultrastructure at 14 months for SHHF$^{cp/cp}$ rats ie. massive protein casts (pc), fibrosis, tubular atrophy and enlarged glomerular surfaces (insert in the bottom right panel). Pictures are representative of each analyzed group (n = 5 to 14 rats per genotype); 5-fold magnification for the global kidney picture and 20-fold for the glomeruli (inserts). Values are mean ± sem. Non-parametric ANOVA analysis with two factors allowed the evaluation of an interaction between aging and genotype. * $p<0.05$, ** $p<0.01$, *** $p<0.001$ for comparing SHHF$^{cp/cp}$ vs. SHHF$^{+/?}$ at the same time point.
doi:10.1371/journal.pone.0096452.g002

Higher Systolic and pulse pressures in SHHF$^{cp/cp}$ rats

Blood pressure measurement was performed either invasively in anesthetized animals at the earliest and latest ages (Table 4) or in conscious rats by plethysmography at different time points (Table 5). We observed that rats of both genotypes presented comparable values of systolic, diastolic and pulse blood pressure (SBP, DBP and PP respectively) at 1.5 months of age, indicating a similar pre-hypertensive state (Figure 4A). The progression towards severe hypertension was monitored in both SHHF$^{+/?}$ and SHHF$^{cp/cp}$ groups of vigil rats by repeated measures of blood pressure using noninvasive phlethysmography (Table 5). Further hemodynamic evaluation using invasive technique on anesthetized rats showed that the central SBP and PP became significantly higher at 14 months of age only for the SHHF$^{cp/cp}$ rats as compared to their SHHF$^{+/?}$ counterparts (Figure 4A).

Age related arterial stiffening in SHHF rats

No differences in the arterial diameters at systole, diastole and mean BP were detected between the two rat groups either in younger or in older animals (Table 4). The distensibility-pressure curve at 14 months of age for SHHF$^{+/?}$ rats was shifted down words as compared to that of the SHHF$^{+/?}$ animals at 1.5 months of age reflecting stiffening of the carotid during aging (Figure 4B). Similarly, the distensibility-BP curve of the 14-month-old SHHF$^{cp/cp}$ rats was shifted down words but as well to the right in the prolongation of the curve observed in the aged-matched SHHF$^{+/?}$ attesting of higher systolic blood pressure in SHHF$^{cp/cp}$ rats (Figure 4A). Interestingly, at both studied time-points, the values of distensibility at the MBP for the SHHF$^{cp/cp}$ group were significantly decreased as compared to SHHF$^{+/?}$ rats (Table 4, $p<0.05$) suggesting an altered functionality of the carotid occurring as early as 1.5 months of age. The Einc values were slightly higher in 1.5 month-old SHHF$^{cp/cp}$ animals and significantly increased at 14 months of age (Table 4). Furthermore, the intrinsic mechanical behavior of the wall material evaluated by the wall stress/Einc curve (Figure 4C) and of the wall stress at fixed 600 kPa Einc were decreased with age in all animals but were not significantly different between the two rat groups at any time (Figure 4D). Similarly, the influence of age was detected in the MCSA values (increasing from 1.5 to 14 months of age, $p<0.00001$), but no association with the genotype could be revealed at any of the two studied time points (Table 4). Overall, the decreased distensibility observed systematically in SHHF$^{cp/cp}$ rats was not associated with dramatic remodeling of their carotid wall over time that could distinguish them from the SHHF$^{+/?}$ rats.

Discussion

It is now well established that metabolic disorders may dramatically affect heart disease manifestation, especially in the context of a metabolic syndrome when multiple disorders such as obesity, diabetes and dyslipidemia occur simultaneously [2,3,16]. There is growing evidence that alterations associated with obesity are not restricted to adipose tissue, but also affect other organs such as brain, liver, and skeletal muscle, resulting in systemic insulin resistance, inflammation, and oxidative stress [9] eventually leading to endothelial and cardiac dysfunction.

Table 2. Renal parameters.

Genotype	SHHF$^{+/?}$	SHHF$^{cp/cp}$	SHHF$^{+/?}$	SHHF$^{cp/cp}$		ANOVA	
Parameters							
Age, month	**1.5**	**1.5**	**12**	**12**	**Genotype**	**Age**	**Interaction**
N	5–10	6–10	7	5			
KW, g	0.64±0.03	0.69±0.01*	1.69±0.04§§§	1.97±0.05*§§§	0.0007	<0.0001	0.0114
KW/Tibia length, g/cm	0.27±0.01	0.32±0.01**	0.39±0.02§§§	0.49±0.02**§§§	<0.0001	<0.0001	0.0459
Glomerular surface area, μm^2	6179±777	7527±905	14969±1095§§	18864±1347*§§§	ns	<0.0001	ns
Water intake, ml/24h	21.5±1.8	22.5±1.8	30.7±3.2§	41.5±2.9**§§§	ns	<0.0001	0.019
Osmolality, mOsmol/kg H_2O	2583±103	1630±120	2268±103§§§	986±126**§§§	0.002	<0.0001	ns
Ionogram, mmol/24h							
Na^+	1668±191	2639±177***	1065±81§§	1136±93§§§	0.001	<0.0001	0.014
K^+	2965±321	5685±298***	2907±267	2886±289§§§	0.0001	0.0009	0.001
Na^+/K^+ ratio	0.57±0.02	0.46±0.01**	0.38±0.03§§	0.38±0.03§	0.046	<0.0001	0.012
Urine Creatinine, mmol//24h	72.8±5.5	81.0±5.2***	115.2±4.7§§	66.4±5.1§	0.0001	0.0434	0.0005
Aldosterone, ng/24h	3.66±1.51	14.02±1.78*	9.40±0.88§§§	7.18±1.01§§§	0.0195	ns	0.0002
eGFR, mL/24h	35±4	25±2	42±2§	11±2***§§§	ns	<0.0001	0.0004

KW, Kidney Weight; **Na^+**, sodium, **K^+**, potassium, **eGFR**, estimated Glomerular filtration rate; Values are the mean±sem. Non-parametric ANOVAs analysis with two factors allowed the evaluation of interaction between aging and genotype. Student's T test *, ** and *** $p<0.01$, $p<0.001$ and $p<0.0001$ respectively when comparing SHHF $^{+/?}$ *vs.* SHHF$^{cp/cp}$ at same time point; § $p<0.05$, §§ $p<0.01$ and §§§ $p<0.001$ to compare T14-mo *vs* T1.5-mo for a same genotype; **N** stands for the number of samples; **ns** stands for not significant.

doi:10.1371/journal.pone.0096452.t002

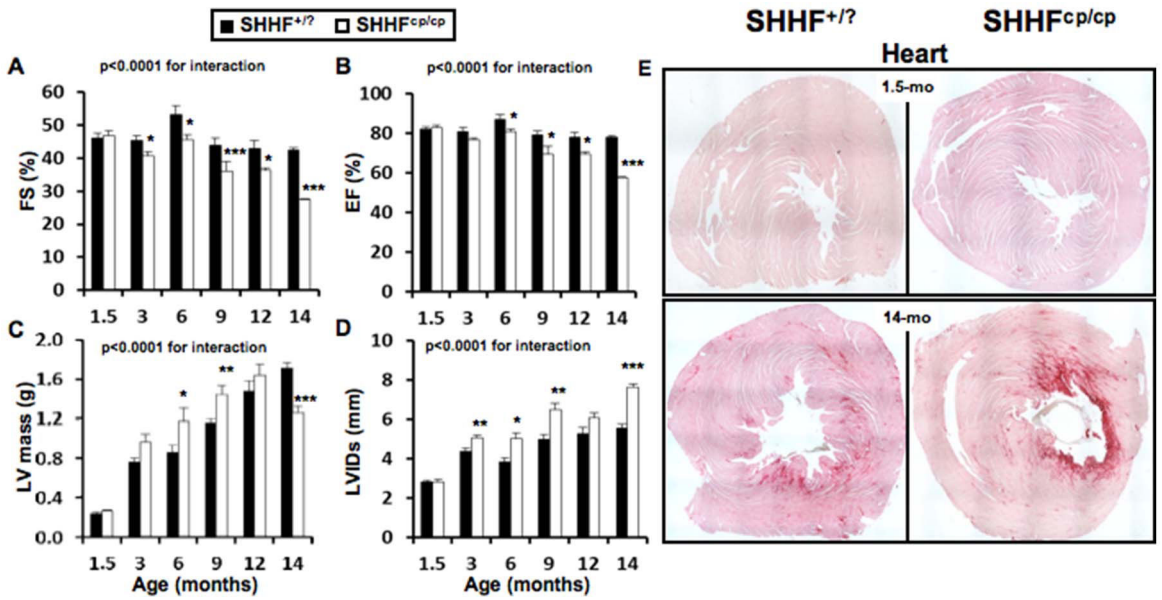

Figure 3. Cardiac follow-up. Transthoracic echocardiograms were performed on isoflurane-anesthetized SHHF at different time points throughout the protocol (1.5; 6; 9 and 14 months of age, n = 5 to 10 rats per genotype). **A**- Fractional Shortening (FS) and **B**- Ejection Fraction (EF) showed the progressive but faster decline of heart systolic function in SHHF$^{cp/cp}$ rats compared to SHHF$^{+/?}$ controls. **C**- LV mass as well as **D**- Left Ventricular (LV) Internal Diameters at end systole (LVIDs) were significantly higher in the SHHF$^{cp/cp}$ group from 6 months and continued to rise till 12 and 14 months of age respectively demonstrating LV hypertrophy and dilation **E**- Red Sirius staining performed on heart sections obtained from SHHF$^{+/?}$ and SHHF$^{cp/cp}$ rats at 1.5 and 14 months of age showed greater myocardial fibrosis in 14-month-old SHHF$^{cp/cp}$ rats compared to SHHF$^{+/?}$ from the same age (n = 5 to 7 rats per genotype). Mean ± sem. Non-parametric ANOVAs analysis with two factors allowed the evaluation of an interaction between aging and genotype. * $p<0.05$, ** $p<0.01$, *** $p<0.001$ for comparing SHHF$^{cp/cp}$ *vs.* SHHF$^{+/?}$ at the same age.
doi:10.1371/journal.pone.0096452.g003

Interestingly, different strains of rat develop abnormalities quite similar to those present in patients with MetS and/or obesity [24]. Among them, the SHHF rat is a particularly interesting study model since it spontaneously develops HF either in the presence or absence of MetS [12,21] unlike other similar animal models described so far [13]. With the aim to investigate in-depth the impact of MetS on the progression towards cardiac remodeling and subsequent failure, we performed a comprehensive analysis of the SHHF$^{+/?}$ and SHHF$^{cp/cp}$ rats phenotypes at cardiac, renal and vascular levels. The concomitant phenotyping of both lean and obese rats helped us refine the physiopathological status of the model during development of HF and clarify discrepancies reported previously for the SHHF model. The side-by-side comparison for a period of 12.5 months (1.5 to 14 months of age) of the SHHF$^{cp/cp}$ and SHHF$^{+/?}$ rats allowed us to characterize the sequence of events leading towards the faster development of heart failure in the obese rats.

If phenotypically barely distinguishable at 1.5 month-old, the SHHF$^{+/?}$ and SHHF$^{cp/cp}$ rats develop very distinctive phenotypes with age. As reported previously SHHF$^{cp/cp}$ rats have a shorter life expectancy than their SHHF$^{+/?}$ littermates (data not shown). This might be explained by the development of severe metabolic disorders that is exclusively present in the obese rats and consequently affected pejoratively their cardiac and renal functions.

Interestingly, altered serum lipidic profiles, presence of insulin resistance and higher adiponectin levels accompanied with hyperaldosteronism were found in young SHHF$^{cp/cp}$ animals (1.5 month-old). The contribution of each of these metabolic factors in obesity and/or MetS development is well known [25,26], and it is conceivable that their alteration with ageing together with the hyperphagia resulting from the leptin receptor inactivation, participates in the development of the massive obesity and non-alcoholic hepatic steatosis found in SHHF$^{cp/cp}$ rats. Since the metabolic disorders arise at 1.5 months of age when cardiac function and blood pressure were not different between the genotypes, it is likely that these deregulations may have participated in the faster cardiac function decline observed in the SHHF$^{cp/cp}$ rats.

In discordance with reports indicating that the obese SHHF rats are affected by diabetes [13,27] we monitored glucose concentrations in blood and urine during aging in both groups of rats and never observed fasting hyperglycemia or glycosuria. However, high levels of fasting serum insulin in the SHHF$^{cp/cp}$ rats reflecting the development of an insulin resistance, rather than type 2 diabetes were detected as early as 1.5 months of age. Although SHHF$^{cp/cp}$ rats did not develop diabetes, they presented polydipsia and polyuria that were not associated with dramatic histological alteration of the kidney at the earliest studied age. Despite the absence of glycosuria, interestingly renal histological analysis of 14 month-old SHHF$^{cp/cp}$ rats showed renal lesions similar to those described for diabetes, i.e. hypercellularity, glomerular sclerosis, and increased glomerular surface. The massive proteinuria observed at 5 months of age in SHHF$^{cp/cp}$ rats was consistent with previous reports [17]. Thus, our data suggest that the SHHF$^{cp/cp}$ rats exhibit pre-diabetic features rather than diabetic type 2 trademarks. Since the SHHF strain originates from the breeding of SHR/N-cp rats themselves derived from the original Koletsky rat colony, with SHR-N rats [14] they are likely to share unidentified protective genes that may protect against the onset of Type 2 diabetes in the face of extreme obesity and insulin resistance proposed to be also present in the SHROB genetic background. Indeed, diabetes is not an intrinsic function of the cp mutation itself but likely requires polygenic interaction with

Table 3. Cardiac parameters.

Genotype	SHHF$^{+/?}$	SHHF$^{cp/cp}$	SHHF$^{+/?}$	SHHF$^{cp/cp}$		ANOVA	
Parameters							
Age, month	**1.5**	**1.5**	**14**	**14**	**Genotype**	**Age**	**Interaction**
N	10	10	7	5			
Cardiac Morphometry							
HW, g	0.75±0.03	0.77±0.04	1.95±0.04§§§	2.08±0.05***§§§	ns	<0.0001	ns
Tibia length, cm	2.30±0.03	2.13±0.03*	4.31±0.04§§	3.98±0.05***§§	<0.0001	<0.0001	0.0538
HW/Tibia, g/cm	0.32±0.01	0.36±0.01**	0.45±0.01§	0.52±0.01*§	0.0004	<0.0001	ns
Cardiac Remodeling, mm							
LVIDd	5.6±0.2	5.4±0.1	9.6±.01§§	10.7±0.2***§§§	0.013	<0.0001	0.002
Septum Thickness	1.2±0.0	1.1±0.0*	2.4±0.0§§§	1.6±0.1***§§§	<0.0001	<0.0001	<0.0001
Posterior Wall Thickness	0.9±0.0	1.0±0.0	1.6±0.0§§§	1.1±0.0***§§§	<0.0001	<0.0001	<0.0001
% myocardial fibrosis	0.10±0.01	0.12±0.02	1.14±0.56	4.75±1.02*§	0.0005	0.0013	0.0372
LV Diastolic function							
A, mm/s	31±4	24±2	41±7	92±25	ns	ns	ns
E, mm/s	96±5	108±6	101±2	124±7	ns	ns	ns
E/A	3.2±0.4	4.0±0.9	2.9±0.4	1.5±0.4	ns	ns	ns
EDT, ms	14±1	14±1	32±1§§	20±5***§	<0.0001	<0.0001	<0.0001

HW, Heart Weight; **LV**, Left Ventricle; **LVIDd**, Left Ventricle Internal Diameters at diastole; **E** and **A**, early and late filling waves; **EDT**, E-vel Deceleration Time. These echocardiographic parameters are the mean ± sem of the average of three to four consecutive cardiac cycles for each rat. % of Myocardial fibrosis was determined on Sirius red stained heart sections by measuring the percentage of fibrotic area to whole heart section area using Image J software. Non-parametric ANOVAs analysis with two factors allowed the evaluation of interaction between aging and genotype. Student's T test * $p<0.05$; ** $p<0.01$, *** $p<0.001$ to compare SHHF$^{+/?}$ *vs.* SHHF$^{cp/cp}$ at same time point; ; § $p<0.05$, §§ $p<0.01$ and §§§ $p<0.001$ to compare T14-mo *vs* T1.5-mo for a same genotype; **N** stands for the number of rats; **ns** stands for not significant.

doi:10.1371/journal.pone.0096452.t003

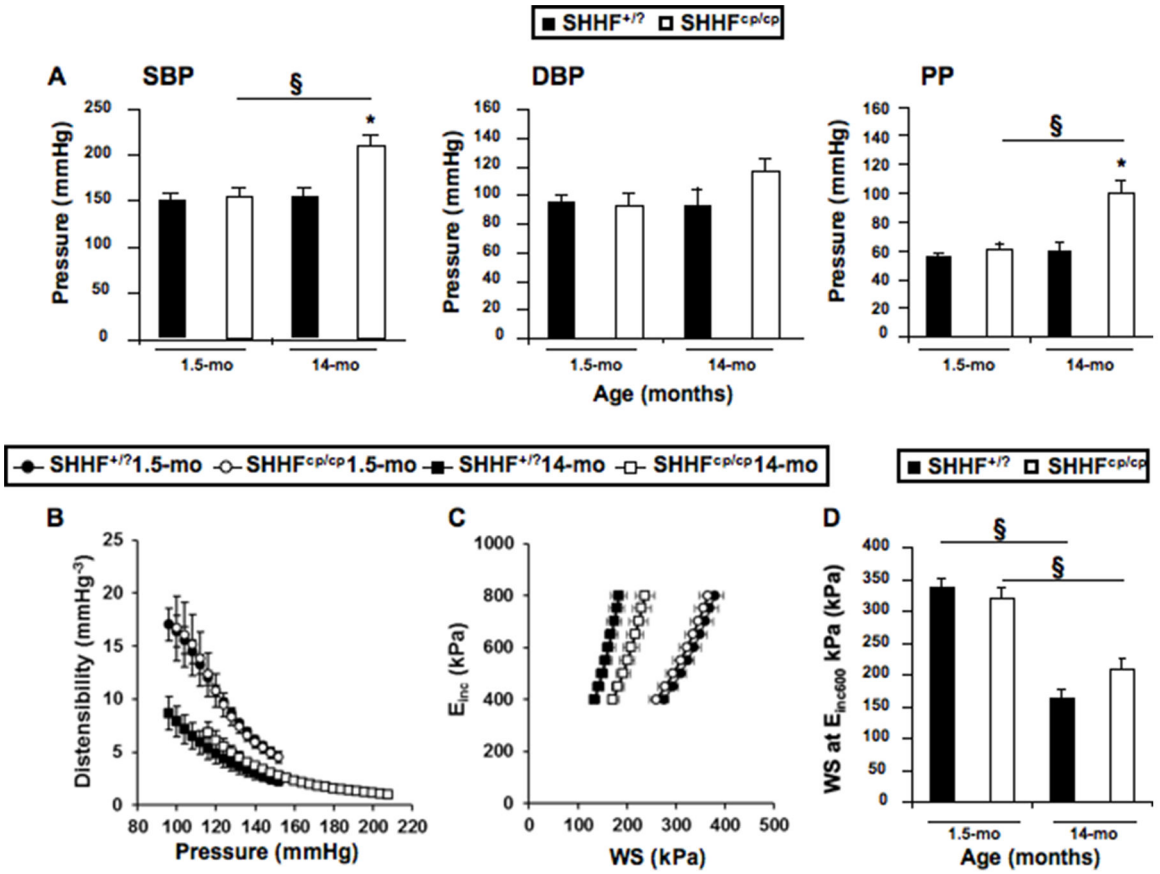

Figure 4. Hemodynamic phenotyping. Invasive blood pressure measurements were obtained on anesthetized rats during vascular phenotyping of the animals. **A**- Systolic (SBP), Diastolic (DBP) Blood Pressures and Pulse Pressure (PP) were measured at both the earliest and latest ages. Results showed that over time only SHHF$^{cp/cp}$ rats increased their SBP and PP becoming significantly higher at 14 months of age compared to SHHF$^{+/?}$ animals. **B**- Distensibility, **C**- Incremental Elastic modulus (E_{inc}) to Wall Stress (WS) curves and **D**- WS at Einc 600 kPa were recorded. Values are mean ± sem of 5 to 14 measurements depending on the genotype and age. Fisher's LSD Multiple-Comparison Test * $p<0.05$ for comparing of SHHF$^{cp/cp}$ *vs.* SHHF$^{+/?}$ rats at the same age; § $p<0.05$ for comparison of 14 month-old *vs.* 1.5-month-old rats of the same genotype.
doi:10.1371/journal.pone.0096452.g004

other diabetogenic modifier genes present in the background of other strains [28]. Of note, SHHF$^{cp/cp}$ rats did not reach end-stage renal disease causing the reduction of urine volume by the time our protocol ended i.e. at 14 months of age. It is noteworthy that, like dyslipidemia, alterations in the kidney function have been described as risk factors favoring the development of HF, rendering the SHHF strain an adequate model to study the implication of MetS in the decline of the cardiac function. While the discrepancies regarding the diabetic status of SHHF rats requires further analysis, the combination of hyperlipidemia and a pre-hypertensive state as early as 1.5-months of age in the SHHF$^{cp/cp}$ rats nevertheless demonstrates two critical hallmarks of MetS. By 5 months of age the obesity was established in SHHF$^{cp/cp}$ determining the onset of the MetS only in this genotype.

The concurrent comparison of cardiac remodeling between the SHHF$^{+/?}$ and SHHF$^{cp/cp}$ groups of rats allowed us to confirm data from previous reports [15,20,21] and extend further the knowledge about the consequences of metabolic disorders on the heart.

At 1.5 months of age, the echocardiographic phenotyping could not distinguish the two rat strains but the simultaneous evaluation of cardiac function in both SHHF$^{+/?}$ and SHHF$^{cp/cp}$ rats during aging indicated that animals differ by the type of cardiac remodeling they develop. The left ventricular wall remodeling is hypertrophic in both groups but is eccentric in SHHF$^{cp/cp}$ while it is concentric in SHHF$^{+/?}$ rats at 14 months of age. Indeed the LV diastolic diameter is greater in SHHF$^{cp/cp}$ rats from 6 months to 14 months of age when the LV internal cavity expands dramatically. Together with the differential modulation of E and A velocity waves between the genotypes over time, cardiac remodeling observed in the SHHF$^{cp/cp}$ group is characteristic of cardiac diastolic dysfunction.

The premature sudden deaths observed during the phenotyping of the SHHF$^{cp/cp}$ group (4 deaths out of 9 SHHF$^{cp/cp}$ rats involved in the follow-up protocol) precluded the observation of a fully declined systolic function at 14 months of age. However, the systolic function evaluation throughout the follow-up of ejection and shortening fractions indicated that those parameters were significantly lower in SHHF$^{cp/cp}$ than in SHHF$^{+/?}$ rats. Moreover, this difference increased significantly after 6 months of SHHF$^{cp/cp}$ rat survival, reflecting the onset of a cardiac decompensation state. By 14 months, SHHF$^{cp/cp}$ animals exhibited dilation of their LV, concomitantly with depletion of the walls and a drop in EF and FS values. Unlike previous reports [13,18], we did not observe any congestion in the heart of SHHF$^{cp/cp}$ animals, neither during the compensatory cardiac remodeling phase (before 6 months) nor during the decompensate phase (after 6 months of age). However, a massive congestion was observed in 22 month-old lean SHHF

Table 4. Mechanical properties of the carotid artery.

Genotype	$SHHF^{+/?}$	$SHHF^{cp/cp}$	$SHHF^{+/?}$	$SHHF^{cp/cp}$		ANOVA	
Parameters							
Age, month	**1.5**	**1.5**	**14**	**14**	**Genotype**	**Age**	**Interaction**
N	14	12	7	5			
Diameter, mm							
Diastolic	0.78±0.02	0.80±0.05	083±0.05	0.96±0.04§	ns	0.03	ns
Systolic	1.01±0.02	0.99±0.05	1.01±0.03	1.13±0.05	ns	ns	ns
Mean Blood Pressure, mmHg	113±5	113±8	114±13	150±9	0.046	0.045	0.047
Values at the MBP							
Diameter, mm	0.88±0.03	0.88±0.05	0.92±0.04	1.05±0.04§	ns	0.046	ns
Compliance, $mm^2/mmHg^{-1}.10^3$	5.88±0.29	4.15±0.26*	4.45±0.53§	2.79±0.40*§	0.0002	0.002	ns
Distensibility, $mm.Hg^{-3}$	9.98±0.71	7.33±0.73*	7.25±1.26§	2.95±0.38*§	0.002	0.002	ns
Einc, kPa	388±58	577±110	421±125	1004±133*	0.002	0.049	0.08
WS, kPa	234±28	245±40	142±26	242±35	ns	ns	ns
MCSA, mm^2	0.084±0.013	0.087±0.019	0.149±0.014§	0.132±0.060§	ns	<0.00001	ns

MBP, Mean Blood Pressure; **Einc**, Incremental Elastic-modulus; **WS**, Wall Stress; **MCSA**, Mean Cross Sectional Area. Values are mean ± sem. Non-parametric ANOVAs analysis with two factors allowed the evaluation of interaction between aging and genotype. Fisher's LSD Multiple-Comparison Test * $p<0.05$ to compare $SHHF^{cp/cp}$ *vs.* $SHHF^{+/?}$ at the same age; § $p<0.05$ to compare of 14 month-old vs. 1.5-month-old rats of the same genotype; **N** stands for the number of rats; **ns** stands for not significant.

doi:10.1371/journal.pone.0096452.t004

Table 5. Blood pressure follow-up in conscious SHHF rats.

Genotype	$SHHF^{+/?}$				$SHHF^{cp/cp}$				ANOVA		
Age, month	**2.5**	**5**	**13**	**14**	**2.5**	**5**	**13**	**14**	**Genotype**	**Age**	**Interaction**
N	8	8	7	7	9	9	6	5			
SBP, mmHg	176±4	182±12	187±6	195±8	150±8	163±14	182±7	207±9	ns	<0.0001	ns
HR, bpm	397±5	383±12	466±13	460±6	368±10*	390±6	401±20*	412±18*	<0.0001	<0.0001	0.0020

SBP, Systolic Blood Pressure; **HR**, Heart Rate; **bpm**, beats per minute. Values are mean ± sem. Non-parametric ANOVAs analysis with two factors allowed the evaluation of interaction between aging and genotype. **N** stands for the number of rats; **ns** stands for not significant. Student's T test * $p<0.05$ to compare $SHHF^{cp/cp}$ *vs.* $SHHF^{+/?}$ at same age.

doi:10.1371/journal.pone.0096452.t005

rats from an unrelated series of animals (not shown). Altogether our results show that SHHF rat strains exhibit rather specific features stressing the importance and relevance of studying the signaling pathways specifically stimulated or muted during the development of heart failure phenotype associated with each etiology.

Arterial stiffening resulting from metabolic injury or natural aging is a mechanism that might accelerate cardiac remodeling [29,30]. The deleterious implication of the metabolic disorders in altering hemodynamic parameters was also suggested in other experimental models. Among others, Sloboda et al [31] demonstrated that in old obese Zucker rats had elevated plasma free fatty acid levels alter arterial stiffness was a result of endothelial dysfunction and higher systolic arterial pressure. Based on those data, it is conceivable that the early increase in FFA observed in $SHHF^{cp/cp}$ rats might participate in the impairment of carotid distensibility and compliance in these animals while no difference in the echocardiographic parameters could yet be detected. $SHHF^{cp/cp}$ rats exhibited higher FFA than that of $SHHF^{+/?}$ counterparts but also developed higher blood pressure overtime. For the first time, we evaluated the mechanical properties of the carotid artery in $SHHF^{cp/cp}$ as compared with $SHHF^{+/?}$ rats when only few metabolic disorders were established (1.5 month), and during the decline of cardiac function (14 months of age). Altogether, the significant alteration of carotid distensibility observed in $SHHF^{cp/cp}$ rats suggested that dyslipidemia together with hypertension conjointly affected the mechanical properties of the arteries as early as 1.5 months of age.

While our findings were obtained from a longitudinal study design, they are based on a relatively small sample size that did not allow the sacrifice of animals at intermediary time points. However, the $SHHF^{cp/cp}$ rats still alive at 14 months of age certainly showed the less severe symptomatology as compared to the rats which died prematurely. This probably introduced a bias in our data analysis by minimizing the significance of the differences observed between the $SHHF^{+/?}$ and $SHHF^{cp/cp}$ groups.

As it is not yet clear whether diastolic heart failure progresses towards systolic heart failure or if both, diastolic and systolic dysfunctions are two distinct manifestations of the large clinical spectrum of this disease, there is a clear interest for experimental models such as the SHHF rat. Because alterations of the filling and of the contraction of the myocardium were observed in the SHHF rats, a further refined comparison of the myocardial signal pathways between obese and lean could help discriminating the common physiopathological mechanisms from the specific ones. The echographic manifestation of telediastolic elevation of left ventricular pressure (lower IVRT and increase of E/e' ratio) reflects the altered balance between the preload and afterload of the heart, which are a paraclinical early signs of congestion. These measurements and evaluation are routinely performed during the follow-up of HF human patients.

Several clinical manifestations described in congestive heart failure patients were not observed in the $SHHF^{cp/cp}$ rats but it is likely that the massive obesity in these animals modified profoundly their appearance that might have hidden the manifestation of oedema. Nevertheless, the hyperaldosteronism is in favour of the development of hydrosodic retention in this experimental model. A phenotypic evaluation of older rats might have allowed the observations of fully developed congestive heart failure as it has been reported by others, knowing that congestion is one of the latest clinical phenotypes appearing in humans. The high levels of hormone secretions such as aldosterone are known also in humans to affect the myocardium by causing at least

fibrotic remodelling over the long term. The hyperaldosteronism developed by the SHHF rats makes this model appropriate to study the influence of the renin angiotensin aldosterone system on heart failure progression.

Furthermore, the SHHF$^{cp/cp}$ rat allows the study of comorbid conditions like renal dysfunction, insulin resistance, obesity, dyslipidaemia, hypertension that have been pinpointed as major determinants of outcomes in patients with HF. The apparent conflicting results demonstrating that unlike Zucker and Koletsky rats, obese SHHF$^{cp/cp}$ rats develop elevated serum adiponectin levels, which might in fact reinforce the pathophysiological pertinence of this latter strain from a cardiovascular point of view. Recent studies in human have described that in contrast with patients « solely » at risk of cardiovascular disease, circulating adiponectin levels are increased in patients with chronic heart failure, and this finding is associated with adverse outcomes [32]. Furthermore a concept has emerged of functional skeletal muscle adiponectin resistance that has been suggested to explain the compensatory elevated adiponectin levels observed in chronic heart failure [33]. Contrary to Zucker and Kolestky rats which develop mainly hypertension-induced heart dysfunction rather than heart failure, SHHF rats have the advantage to develop spontaneously HF with elevated serum adiponectin levels. Although a more detailed comparison of all these animal models is required, SHHF strains seem more appropriate to study HF than the other strains as they better mimic the human heart failure condition.

Altogether, our results reinforce and complete those obtained by others that conclude on the pertinence of the SHHF rat model in studying the impact of MetS on HF [13,15,24,34,35,36]. The SHHF model is an instrumental model to address those issues first, because the metabolic alterations appear in the animals at a very early stage (1.5 months of age); second, because all the rats develop cardiac remodeling, and third, because the severity of the cardiac phenotypes mirror the worsening of metabolic parameters. Importantly, and unlike other animal disease models developing a MetS *per se* (Obese prone rat, SHROB for example) the SHHF strain does develop HF spontaneously [24]. Even though some other strains like the ZSF1 strain [37] could be interesting to study cardiovascular complications of MetS, they develop such dramatic renal injury that the animals die from kidney failure or urinary track pathologies before the establishment of HF features. This is a clear advantage of the SHHF strain over others for studying the biological mechanisms underlying the progression from MetS-induced metabolic disorders to cardiac remodeling.

Here we describe several non-mutually exclusive physiological alterations (dyslipidemia, obesity, renal dysfunction, hypertension, arterial stiffness) that individually, but concomitantly, participate to the adverse cardiac effects of MetS. Since these alterations are established long before their cardiac consequences are detectable in SHHF$^{cp/cp}$ rats, the first trimester of the rat's life appears as an optimal time window for evaluating preventive treatment strategies in these animals.

As suggested in the present study, the pathological molecular programming of cardiac and vascular remodeling had to occur before the detection of their consequences on the phenotypes. An early intervention on MetS-associated disorders may have the potential to prevent, delay or mitigate the renal and vascular alterations as well as cardiac remodeling that appear later.

Acknowledgments

The authors wish to thank Dr H. Kempf, Pr L. Monassier, Pr S. Thornton, A-L. Leblanc, D. Meng, and Z. Lamiral for their helpful discussions and technical help during the completion of the study.

Author Contributions

Conceived and designed the experiments: AP FZ FJ PL. Performed the experiments: GY AO C. L'Huillier LT ST RMRG DB AP. Analyzed the data: GY AO C. L'Huillier C. Labat RF FZ PL AP. Wrote the paper: AP PL FJ LV GY.

References

1. Lazzarini V, Mentz RJ, Fiuzat M, Metra M, O'Connor CM (2013) Heart failure in elderly patients: distinctive features and unresolved issues. Eur J Heart Fail.
2. Aroor AR, Madavia CH, Sowers JR (2012) Insulin resistance and heart failure: molecular mechanisms. Heart Fail Clin 8: 609–617.
3. Bui AL, Horwich TB, Fonarow GC (2011) Epidemiology and risk profile of heart failure. Nat Rev Cardiol 8: 30–41.
4. De Pergola G, Nardecchia A, Giagulli VA, Triggiani V, Guastamacchia E, et al. (2013) Obesity and Heart Failure. Endocr Metab Immune Disord Drug Targets.
5. Ebong IA, Goff DC Jr, Rodriguez CJ, Chen H, Bluemke DA, et al. (2013) The relationship between measures of obesity and incident heart failure: The multi-ethnic study of atherosclerosis. Obesity (Silver Spring).
6. Bountiouskos M, Schinkel A, BAx J, Lampropoulos S, Poldermans D (2006) The impact of hypertension on systolic and diastolic left ventricular function. A tissue Doppler echocardiographic study. American Heart Journal 151.
7. Ingelsson E, Arnlov J, Sundstrom J, Zethelius B, Vessby B, et al. (2005) Novel metabolic risk factors for heart failure. J Am Coll Cardiol 46: 2054–2060.
8. Aspelund T, Gudnason V, Magnusdottir BT, Andersen K, Sigurdsson G, et al. (2010) Analysing the large decline in coronary heart disease mortality in the Icelandic population aged 25–74 between the years 1981 and 2006. PLoS One 5: e13957.
9. Horwich TB, Fonarow GC (2010) Glucose, obesity, metabolic syndrome, and diabetes relevance to incidence of heart failure. J Am Coll Cardiol 55: 283–293.
10. Simpson CR, Buckley BS, McLernon DJ, Sheikh A, Murphy A, et al. (2011) Five-year prognosis in an incident cohort of people presenting with acute myocardial infarction. PLoS One 6: e26573.
11. Ardehali H, Sabbah HN, Burke MA, Sarma S, Liu PP, et al. (2012) Targeting myocardial substrate metabolism in heart failure: potential for new therapies. Eur J Heart Fail 14: 120–129.
12. Altschuld RA, Holycross BJ, Radin MJ, McCune SA (2003) The failing SHHF Rat heart. Cardiac remodeling and failure: 67–75.
13. McCune SA, Baker PB, Stills Jr HF (1990) SHHF/Mcc-cp Rat: Model of obesity, Non-insulin-dependant Diabetes, and Congestive Heart Failure. ILAR News 32: 23–27.
14. Greenhouse DD, Michaelis IV OE, McCune SA (1990) Development of corpulent rat strains. Frontiers in diabetes research Lessons from animal diabetes III VIII: 375–377.
15. Heyen JR, Blasi ER, Nikula K, Rocha R, Daust HA, et al. (2002) Structural, functional, and molecular characterization of the SHHF model of heart failure. Am J Physiol Heart Circ Physiol 283: H1775–1784.
16. Hoversland RC (1992) Onset of obesity and puberty in genetically obese SHHF/Mcc-cp rats. Int J Obes Relat Metab Disord 16: 977–984.
17. McCune SA, Jenkins JE, Stills Jr HJ, Park S, Radin MJ, et al. (1990) Renal and heart functions in the SHHF/Mcc-cp rat. Frontiers in diabetes research Lessons from animal diabetes III VIII.6.: 397–401.
18. McCune SA, Radin MJ, Jenkins JE, CHU Y-Y, Park S, et al. (1995) SHHF/Mcc-facp rat model: effects of gender and genotype on age of expression of metabolic complications and congestive heart failure and on response to drug therapy. Leesons from animal diabetes: 255–270.
19. Meier DA, Hennes MM, McCune SA, Kissebah AH (1995) Effects of obesity and gender on insulin receptor expression in liver of SHHF/Mcc-FAcp rats. Obes Res 3: 465–470.
20. Haas GJ, McCune SA, Brown DM, Cody RJ (1995) Echocardiographic characterization of left ventricular adaptation in a genetically determined heart failure rat model. Am Heart J 130: 806–811.
21. Reffelmann T, Kloner RA (2003) Transthoracic echocardiography in rats. Evalution of commonly used indices of left ventricular dimensions, contractile performance, and hypertrophy in a genetic model of hypertrophic heart failure (SHHF-Mcc-facp-Rats) in comparison with Wistar rats during aging. Basic Res Cardiol 98: 275–284.
22. Radin MJ, Jenkins JE, McCune SA, Jurin RR, Hamlin RL (1992) Effects of enalapril and clonidine on glomerular structure, function, and atrial natriuretic peptide receptors in SHHF/Mcc-cp rats. J Cardiovasc Pharmacol 19: 464–472.
23. Lacolley P, Labat C, Pujol A, Delcayre C, Benetos A, et al. (2002) Increased carotid wall elastic modulus and fibronectin in aldosterone-salt-treated rats: effects of eplerenone. Circulation 106: 2848–2853.

24. Fellmann L, Nascimento AR, Tibirica E, Bousquet P (2012) Murine models for pharmacological studies of the metabolic syndrome. Pharmacol Ther 137: 331–340.
25. Caprio M, Antelmi A, Chetrite G, Muscat A, Mammi C, et al. (2011) Antiadipogenic effects of the mineralocorticoid receptor antagonist drospirenone: potential implications for the treatment of metabolic syndrome. Endocrinology 152: 113–125.
26. Caprio M, Feve B, Claes A, Viengchareun S, Lombes M, et al. (2007) Pivotal role of the mineralocorticoid receptor in corticosteroid-induced adipogenesis. FASEB J 21: 2185–2194.
27. Kim SH, Chu YK, Kwon OW, McCune SA, Davidorf FH (1998) Morphologic studies of the retina in a new diabetic model; SHR/N:Mcc-cp rat. Yonsei Med J 39: 453–462.
28. Friedman JE, Ferrara CM, Aulak KS, Hatzoglou M, McCune SA, et al. (1997) Exercise training down-regulates ob gene expression in the genetically obese SHHF/Mcc-fa(cp) rat. Horm Metab Res 29: 214–219.
29. Benetos A, Waeber B, Izzo J, Mitchell G, Resnick L, et al. (2002) Influence of age, risk factors, and cardiovascular and renal disease on arterial stiffness: clinical applications. Am J Hypertens 15: 1101–1108.
30. Marti CN, Gheorghiade M, Kalogeropoulos AP, Georgiopoulou VV, Quyyumi AA, et al. (2012) Endothelial dysfunction, arterial stiffness, and heart failure. J Am Coll Cardiol 60: 1455–1469.
31. Sloboda N, Feve B, Thornton SN, Nzietchueng R, Regnault V, et al. (2012) Fatty acids impair endothelium-dependent vasorelaxation: a link between obesity and arterial stiffness in very old Zucker rats. J Gerontol A Biol Sci Med Sci 67: 927–938.
32. Masson S, Gori F, Latini R, Milani V, Flyvbjerg A, et al (2011) Adiponectin in chronic heart failure: influence of diabetes and genetic variants. Eur J Clin Invest. 41: 1330–8.
33. Van Berendoncks AM, Conraads VM (2011) Functional adiponectin resistance and exercise intolerance in heart failure. Curr Heart Fail Rep. 8: 113–22.
34. Holycross BJ, Summers BM, Dunn RB, McCune SA (1997) Plasma renin activity in heart failure-prone SHHF/Mcc-facp rats. Am J Physiol 273: H228–233.
35. Przybylski R, McCune S, Hollis B, Simpson RU (2010) Vitamin D deficiency in the spontaneously hypertensive heart failure [SHHF] prone rat. Nutr Metab Cardiovasc Dis 20: 641–646.
36. Radin MJ, Holycross BJ, Hoepf TM, McCune SA (2003) Increased salt sensitivity secondary to leptin resistance in SHHF rats is mediated by endothelin. Mol Cell Biochem 242: 57–63.
37. Griffin KA, Abu-Naser M, Abu-Amarah I, Picken M, Williamson GA, et al. (2007) Dynamic blood pressure load and nephropathy in the ZSF1 (fa/fa cp) model of type 2 diabetes. Am J Physiol Renal Physiol 293: F1605–1613.

La minéralisation de la trachée: mécanismes cellulaires et moléculaires dans le modèle souris

La trachée est une structure très complexe des voies respiratoires, qui est composée d'anneaux cartilagineux, fait de cartilage hyalin, et de bandes musculaires, formées de cellules musculaires lisses, dont l'architecture confère à la fois rigidité et souplesse au canal trachéen. Contrairement à d'autres cartilages, tels que ceux trouvés dans la plaque de croissance en développement et dans les articulations adultes, ou aux cellules musculaires lisses des vaisseaux, très peu d'informations sont disponibles sur le développement du cartilage et du tissu musculaire trachéal et sur leur capacité à se minéraliser, bien que la calcification de la trachée soit un événement commun dans la population âgée et plus rare dans certaines pathologies.

Dans ce contexte, ce travail de thèse a cherché dans le modèle souris à mieux caractériser le cartilage et le tissu musculaire lisse de la trachée et également comprendre les mécanismes moléculaires jusqu'alors inexplorés, régulant la minéralisation de la trachée.

Grâce à une nouvelle technique de culture de cellules provenant de la trachée, nous avons démontré que les chondrocytes et les cellules musculaires lisses trachéaux sont tous deux capables de minéraliser lorsqu'ils sont traités avec un haut niveau de Pi, mais via des mécanismes moléculaires différents. En parallèle, une étude in vivo nous a permis de démontrer que la minéralisation de la trachée se produit uniquement dans les anneaux cartilagineux dès 30 jours après la naissance. Des analyses histologiques et moléculaires ont permis d'affiner ces résultats et de proposer un modèle de minéralisation de la trachée via une progression rostro-caudale dépendante de BMP2.

Mots-Clés : Trachée, Minéralisation, Phosphate, Cartilage, Matrix Gla Protein.

Tracheal mineralization: cellular and molecular mechanisms in mice

The trachea is a very complex structure of the respiratory tract, composed of C-shaped cartilaginous rings, made of hyaline cartilage, and muscular bands, made of smooth muscle cells, conferring rigidity and compliance to the windpipe, respectively. In contrast to other intensely studied cartilages such as the ones found in the developing growth plate and in the adult joints or smooth muscle cells from the vasculature, very little information is available on the development of the tracheal cartilage and smooth muscle tissues and on their innate propensity to mineralize, although calcification of the trachea is a common finding in the elderly population and also a rare manifestation of pathologic conditions.

In this context, this PhD work sought to better characterized the poorly studied tracheal cartilage and smooth muscle tissue and understand the molecular mechanisms regulating tracheal mineralization that has been unexplored so far.

We tackle these questions in the mouse model. Setting up a novel in-vitro culture of tracheal cells, we demonstrated that tracheal chondrocytes and smooth muscles cells are prone to mineralize when treated with high level of Pi, through different molecular mechanisms. In parallel, we found that in vivo mineralization of the trachea only happens in the cartilaginous rings, as early as 30 days after birth. Histological and molecular evidence suggest that tracheal mineralization occurs through a BMP-dependent rostro-caudal progression.

Key-Words: Trachea, Mineralization, Phosphate, Cartilage, Matrix Gla Protein.